Stony Brook University

Spin and QCD Instanton & Stringy Pomeron

A Dissertation presented

by

Yachao Qian

to

The Graduate School

in Partial Fulfillment of the

Requirements

for the Degree of

Doctor of Philosophy

in

Physics

Stony Brook University

May 2017

Stony Brook University

The Graduate School

Yachao Qian

We, the dissertation committee for the above candidate for the

Doctor of Philosophy degree, hereby recommend

acceptance of this dissertation

Ismail Zahed
Professor, Department of Physics and Astronomy

Edward Shuryak
Distinguished Professor, Department of Physics and Astronomy

Xu Du
Associate Professor, Department of Physics and Astronomy

Robert Pisarski
Senior Scientist, Department of Physics, Brookhaven National Laboratory

Charles Taber
Dean of the Graduate School

Abstract of the Dissertation

Spin and QCD Instanton & Stringy Pomeron

by

Yachao Qian

Doctor of Philosophy

in

Physics

Stony Brook University

2017

We summarize some of the works on understanding the nonperturbative effects in QCD.

In the first part of the thesis, we review some aspects of spin physics where QCD instantons play an important role. In particular, their large contributions in semi-inclusive deep-inelastic scattering and polarized proton on proton scattering. We also review their possible contribution in the $\mathcal{P}$-odd pion azimuthal charge correlations in peripheral AA scattering at collider energies. The QCD vacuum is dominated by large instanton and anti-instanton fluctuations in the infrared, which are largely responsible for the spontaneous breaking of chiral symmetry and the anomalously large mass. The QCD instanton intrinsic spin-color polarization makes them ideal for generating non-perturbative and large spin asymmetries in deep inelastic scattering using polarized proton targets and polarized proton on proton scattering. The large spin asymmetries observed experimentally are triggered by T-odd contributions in the scattering amplitude. Since perturbative QCD does not accommodate these effects, it was initially suggested that these $\mathcal{T}$-odd contributions are either induced in the initial state (Sivers effect) or in the fragmentation function (Collins effect) thereby preserving the integrity of QCD perturbation theory and factorization. QCD instantons offer a natural

mechanism for generating T-odd amplitudes that is fully rooted in QCD and beyond perturbation theory.

In the second part, we show that a single closed string exchange contribution to the eikonalized dipole-dipole scattering amplitude yields a Regge behavior of the elastic amplitude. The overall dipole-dipole scattering amplitude in the soft pomeron kinematics is shown to be sensitive to the extrinsic curvature of the string for finite momentum transfer. The characteristics of the diffractive peak in the differential elastic pp scattering are affected by a small extrinsic curvature of the string. After discretizing the string in N string bits, we analyze its length, mass and spatial distribution for large N and away from its Hagedorn point. The string bit distribution shows sizable asymmetries in the transverse plane that may translate to azimuthal asymmetries in primordial particle production in the Pomeron kinematics, and the flow moments in minimum bias pp and pA events. We also analyze the length, mass and spatial distribution of a discretized transverse string near its Hagedorn temperature. We suggest that such a string may dominate the (holographic) Pomeron kinematics for dipole-dipole scattering at intermediate and small impact parameters. Attractive self-string interactions cause the transverse string size to contract away from its diffusive size, a mechanism reminiscent of the string-black-hole transmutation. The string shows sizable asymmetries in the transverse plane that translate to primordial azimuthal asymmetries in the stringy particle production in the Pomeron kinematics for current pp and pA collisions at collider energies.

Dedicated to my family.

Table of Contents

List of Figures

List of Tables

Acknowledgements

I would like to thank my Ph.D. advisor, Dr. Ismail Zahed, for his guidance, support and help. His patience and encouragement not only help me through research but also shows me the wisdom of the life.

I would like to thank Dr. Edward Shuryak, who shared with me his excitement of doing theoretical research and taught an excellent class which prepared me for my research.

I would like to thank Dr. Alexandre G. Abanov, who taught me many wonderful classes and patiently answered my questions for hours a day in several semesters.

I would like to thank my friends at Stony Brook, Scott Mills for proofreading many of my works and sharing his excellent Mathematic and programming knowledge with me; Yiming Zhong for answering my questions about particle physics and teaching me how to use Mathematica; Mao Zeng for teaching me the advanced skills of calculating Feynman diagrams; Jun Nian for working with me on a difficult project for years and sharing his profound understanding of physics with me; Moshe Kellerstein for teaching me English and for his wonderful salad.

Finally, I would like to thank my family. I met my wife Nan Li when we were in college and we have been together since then for 10 years. We have shared our happiness, sadness, excitement and disappointments everyday of our lives. Life has ups and downs and we move from east to west, but our love always warms one another and keep us moving forward. My daughter, Madison Qian, is three years old now. Though she always keeps her dad busy and away from work, without her our lives will never be complete.

Publications

1. *"Spin Physics through QCD Instantons,"*
   Y. Qian and I. Zahed,
   Annals Phys. **374**, 314 (2016)

2. *"Streched String with Self-Interaction at the Hagedorn Point: Spatial Sizes and Black Hole,"*
   Y. Qian and I. Zahed,
   Phys. Rev. D **92**, 105001 (2015)

3. *"A Stringy (Holographic) Pomeron with Extrinsic Curvature,"*
   Y. Qian and I. Zahed,
   Phys. Rev. D **92**, 085012 (2015)

4. *"Stretched String with Self-Interaction at High Resolution: Spatial Sizes and Saturation,"*
   Y. Qian and I. Zahed,
   Phys. Rev. D **91**, 125032 (2015)

5. *"$\mathcal{P}$-Odd Pion Azimuthal Charge Correlations in Heavy Ion Collisions,"*
   Y. Qian and I. Zahed,
   Nucl. Phys. A **940**, 227 (2015)

6. *"Double Spin Asymmetries through QCD Instantons,"*
   Y. Qian and I. Zahed,
   Phys. Rev. D **90**, 114012 (2014)

7. *"Single Spin Asymmetry through QCD Instantons,"*
   Y. Qian and I. Zahed,
   Phys. Rev. D **86**, 014033 (2012) [Erratum-ibid. D **86**, 059902 (2012)]

8. *"Quantum fluctuations of one-dimensional free fermions and Fisher–Hartwig formula for Toeplitz determinants,"* [1]
   A. G. Abanov, D. A. Ivanov, and **Y. Qian**,
   J. Phys. A: Math. Theor. **44**, 485001 (2011)

[1] The contents of this paper will not be dicussed in the dissertation.

Chapter 1

Introduction

1.1 Instantons

1.1.1 Single (anti-)instanton solution

Yang-Mills theory [9] has a central position in modern theoretical physics. The successful standard model of particle physics [10, 11, 12] was formulated in the language of Yang-Mills theory. Historically, each step in understanding the structure and the dynamics of Yang-Mills theory has helped us formulate quantum field theory, which in turn widens and deepens our knowledge of nature. One important discovery is instanton, which plays a central role in the spontaneous breaking of chiral symmetry in the QCD vacuum. Though, nowadays the calculations and analysis of the instantons are usually implemented through 't hooft symbols [13], it is still worthy reviewing the discovery of instanton and the physics behind it [14].

Before the discovery of instantons, a static sourceless gauge field for SU(2) in 3-Euclidean space solution has been found by Wu & Yang [15]:

$$A_{\mu,a} = -\epsilon_{\mu a\nu}\frac{(x-x_0)_\nu}{(x-x_0)^2}\,, \tag{1.1}$$

where we do not distinguish the upper and the lower indices for the Eulidean space. The ansatz of the solution can be easily written down since both the spinor indices μ and color indices a running from 1 to 3, which is natural because both the lorentz group and color group are $SU(2)$. According to group theory:

$$3 \otimes 3 \doteq 5 \oplus 3 \oplus 1\,, \tag{1.2}$$

and we can specify (for $A_{\mu,a}$):

- 5
$$\frac{1}{x^3}\left(x_\mu x_a - \delta_{\mu a}x^2\right) . \tag{1.3}$$
- 3
$$\frac{1}{x^2}\left(\epsilon_{\mu a\nu}x_\nu\right) . \tag{1.4}$$
- 1
$$\frac{1}{x}\delta_{\mu a} . \tag{1.5}$$

It is not the same for $SU(2)$ Yang-Mills theory in 4-Euclidean space because the Lorentz group now is $SO(4)$. In other words, for $A_{\mu,a}$ the indices μ run from 1 to 4 while the indices a run from 1 to 3. There are two ways out, we can either decompose the lorentz $SO(4)$ group as $SU(2)\times SU(2)$, or we can extend the color group $SU(2)$ to $SO(4)$. The first case correspond to the use of 't hooft symbols and the second case was how the instanton had originally been found [14]. First, we extend the $SU(2)$ color group to $SO(4)$

$$A^a_\mu \xrightarrow{\text{extend}} A^{\alpha\beta}_\mu . \tag{1.6}$$

This step is important because when we find the classical solution in forms of $A^{\alpha\beta}_\mu$ for $SO(4)$ Yang-Mills theory we can write down the classical solution in forms of A^a_μ for $SU(2)$ Yang-Mills theory. The key here is $SO(4)\simeq SU(2)\times SU(2)$. In simple words, if we can find a classical solution in forms of $A^{\alpha\beta}_\mu$, then we can obtain the classical solution A^a_μ by

$$A^a_\mu = \frac{1}{2}\left(A^{4a}_\mu \pm \frac{1}{2}\epsilon_{a\beta\gamma}A^{\beta\gamma}_\mu\right) . \tag{1.7}$$

Therefore, to search for the solution, one can easily write down the ansatz

$$A^{\alpha\beta}_\mu = f(x^2)(x_\alpha\delta_{\mu\beta} - x_\beta\delta_{\mu\alpha}) , \tag{1.8}$$

where $f(x^2)$ is an analytical function. In fact, one can write it down as $O_{\mu\nu}x_\nu$ where $O_{\mu\nu}$ is the $SO(4)$ generators. In one of author's paper, this ansatz has been derived rigorously by considering the form invariance condition [16]. The step above doesn't just give us a compact ansatz to search for the solutions of Yang-Mills equation. It also reveals many important properties that

instanton have. For example, the symmetries between the lorentz group and color group are related. Because of this reason, in fact the instanton solution has a simple topological interpretation. Another important property of (anti-)instanton is that it satisfies the (anti-)selfdual equation:

$$F^a_{\mu\nu} = \pm\frac{1}{2}\epsilon_{\mu\nu\rho\sigma}F^a_{\rho\sigma}\,. \tag{1.9}$$

Or we can write it as

$$\epsilon_{\alpha\beta\alpha'\beta'}F^{\alpha'\beta'}_{\mu\nu} = \pm\epsilon_{\mu\nu\mu'\nu'}F^{\alpha\beta}_{\mu'\nu'}\,. \tag{1.10}$$

First, the equation above clearly shows the relations between the symmetries in lorentz group and the symmetries in color group. The relation above can also used to prove that instanton is not just the solution of Yang-Mills equation, but is also the ground state. One can solve the equation of motion and obtain the (anti-)instanton when $f = 1/(x^2+\rho^2)$. We then find

$$A_\mu \xrightarrow{|x|\longrightarrow\infty} U^{-1}\partial_\mu U\,, \tag{1.11}$$

where U is a $SU(2)$ group element. In sec-2.2, we will show that the topological nature of the instanton is the winding number for one S^3 sphere warping around another S^3 sphere. Besides the topological nature that instanton contains, the instanton background also results in zero mode. A zero mode is a solution of the linearized field equations for the fluctuations which is normalizable. There are many important properties of zero mode: first, the zero mode is nonperturbative, and thus the effects induced from the zero modes cannot be obtained by perturbative QCD. Second, the zero mode contribute to the path integral differently from the non-zero modes. The measure of the zero modes in path integral is important in QCD vacuum [13]. Third, the zero mode spontaneously break the chiral symmetry [17]. Fourth, the color indices and spinor indices of the fermionic zero modes are mixed, and therefore the imaginary phase due to the soft gluon exchange will result in single spin asymmetry in instanton background.

1.1.2 Instanton liquid model and spin physics

The physical interpretation of an instanton is a tunneling event between degenerate classical vacuua [18, 19, 20]. In the instanton liquid model [21], the

QCD vacuum is populated with interacting instantons and anti-instantons with a mean instanton density $n \approx 1$ fm^{-4} and an average instanton size of $\rho = 1/3$ fm. The classical configurations of instanton and anti-instantons have been observed in lattice simulations using cooling methods. A typical distribution of the topological charge $G\widetilde{G}$ with quantum noise is shown in Fig. 1.1 (left) and after 25 cooling sweeps in Fig. 1.1 (right) [22].

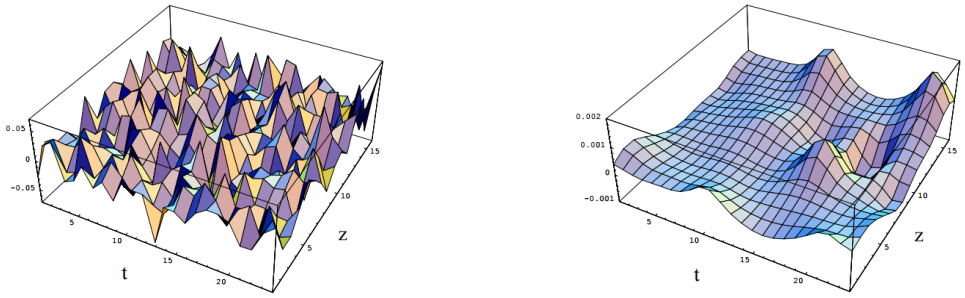

Figure 1.1: Left: typical fluctuations of $G\widetilde{G}$ in a lattice simulation with a lattice unit of 0.16 fm. Right: the same fluctuations of $G\widetilde{G}$ after 25 cooling sweeps with a lattice unit of 0.14 fm.

The instanton ensemble is dilute with a diluteness factor $n\rho^4 \approx 0.01$. The latter provides a natural order parameter when evaluating the various contributions in collision processes induced by instantons to be detailed below. Instantons provide an important mechanism for the spontaneous breaking of chiral symmetry and the resolution of the axial $U(1)$ problem through the emergence and delocalization of the light quarks zero modes.

A number of important vacuum expectations values, e.g.

$$\left\langle \bar{\psi}\psi \right\rangle , \quad \left\langle \bar{\psi}\gamma^5\psi \right\rangle \quad \text{and} \quad \left\langle G_{\mu\nu}G_{\mu\nu} \right\rangle . \tag{1.12}$$

have been reproduced in the instanton liquid model of the QCD vacuum, in support of the underlying semi-classical gauge and fermionic degrees of freedom. Also many mesonic correlation functions of the type $\langle j(x)\, j(0)\rangle$, with j a local operator with the quantum numbers of a mesonic state, e.g.

$$j_\pi = \bar{q}\tau^a\gamma^5 q\,, \quad j_\rho = \frac{1}{2}\bar{q}\tau^a\gamma_\mu q \quad \text{and} \qquad j_\eta = \bar{q}\gamma^5 q\,. \tag{1.13}$$

have led to detailed agreements with lattice simulations after cooling [22]. These correlation functions are important in understanding the QCD vac-

uum, hadrons and mesons. In particular, the heavy η' mass is related to the $U(1)_A$ anomaly [17].

Though instanton does not account for confinement of static charges. Recently, it was noted that twisted instantons and anti-instantons with finite Polyakov lines preserve most of the features of the instanton liquid model and do account for confinement. QCD instantons may contribute substantially to small angle hadron-hadron scattering [23, 24, 25, 26, 27] and possibly gluon saturation at HERA [28, 29], as evidenced by recent lattice investigations [30, 31].

A number of semi-inclusive DIS experiments carried by the CLAS and HERMES collaborations [32, 1, 33], and more recently with polarized protons on protons by the STAR and PHENIX collaborations [34, 35, 36], have revealed large spin asymmetries in polarized lepton-hadron and hadron-hadron collisions at collider energies. These effects are triggered by $\mathcal{T}$-odd contributions in the scattering amplitude. Perturbative QCD does not support the $\mathcal{T}$-odd contributions, which are usually parametrized in the initial state (Sivers effect) [37, 38] or the final state (Collins effect) [39, 40]. Non-perturbative QCD with instantons allow for large spin asymmetries as discussed by Kochelev and others [41, 42, 43, 44, 2]. In [41] a particularly large Pauli form factor was noted, with an important contribution to the Single Spin Asymmetry (SSA) in polarized proton on proton scattering.

In author's papers [44, 45, 46, 47], we showed some recent developments regarding our understanding of spin physics in the instanton liquid model. Assuming that the vacuum is populated by semi-classical but interacting instantons and anti-instantons, with the vacuum parameters fixed by the spontaneous breaking of chiral symmetry in bulk, we explicit their effects on semi-inclusive DIS processes as well as singly polarized pp scattering. In both cases, uncorrelated instantons or anti-instantons are at work. We show that the effects of correlations between instantons and anti-instantons through fluctuations are also important in both doubly polarized pp scattering as well as through $\mathcal{P}$-odd effects in peripheral AA scattering.

1.2 Stringy pomeron

The high energy proton on proton (anti-proton) cross sections are dominated by Pomeron exchange, an effective object corresponding to the highest Regge trajectory. The slowly rising cross sections are described by the soft Pomeron

with intercept $\alpha_P(0) - 1 \approx 0.08$ and vacuum quantum numbers. Reggeon exchanges have smaller intercepts and are therefore subleading. Reggeon theory for hadron-hadron scattering with large rapidity intervals provide an effective explanation for the transverse growth of the cross sections [48].

The transverse growth of the proton with rapidity χ follows from the BFKL ladders [49, 50, 51, 52, 53] at weak coupling in QCD. Collinear gluon bremsstrahlung is large even when the coupling is weak and requires resummation. The ensuing BFKL hard Pomeron carries a large intercept and zero slope. The intercept is slightly improved by higher order perturbative corrections to the BFKL ladder.

The soft Pomeron kinematics suggests an altogether non-perturbative approach. Through duality arguments, Veneziano suggested long ago that the soft Pomeron is a closed string exchange [54]. In QCD the closed string world-sheet can be thought as the surface spanned by planar gluon diagrams or fish-nets [55]. The quantum theory of planar diagrams in supersymmetric gauge theories is tractable in the double limit of a large number of colors N_c and $'$ t Hooft coupling $\lambda = g^2 N_c$ using the AdS/CFT holographic approach [56].

In the past decade there have been several attempts at describing the soft pomeron using holographic QCD [57, 58, 59, 60, 61, 62, 63, 64, 65, 66, 67, 68, 69, 70, 71, 72, 73, 74, 75, 76, 77, 78, 79]. In [80] we follow the work in [70, 71, 72, 73] and describe the soft pomeron as an effective string with extrinsic curvature in 5-dimensions. This is inherently a bottom-up approach with the holographic or 5th direction playing the role of the scale dimension for the closed string. The geometry is that of AdS_5 with a wall. In the UV AdS_5 enforces conformality which is a property of QCD-BFKL-kernels, while in the IR the wall enforces confinement a generic feature of QCD.

Also, many descriptions of the soft Pomeron in holographic duals to QCD have been suggested recently without supersymmetry [57, 58, 59, 60, 81, 61, 62, 63, 64, 65, 66, 67, 68, 69, 70, 71, 72, 73, 74, 75]. A simple version is a stringy exchange in AdS_5 with a wall with $D_\perp = 3$ dimensions, that reproduces a number of features of diffractive scattering, production and low-x DIS [76].

The Pomeron as a string exchange in holography can be thought as a chain of closed but confined gluons, some sort of non-perturbative Weizacker-Williams field tying two colorless dipoles separated by a large rapidity interval χ. In this spirit, lepton on proton scattering in DIS at low-x can be described through a holographic string exchange with the identification $\chi \approx \ln(1/x)$.

In the proton rest frame, the leptonic dipole of size $1/Q$ acts as a small probe dipole scattering off the larger dipole composing the proton at a fixed impact parameter b. DIS experiments are always averaged over this impact parameter when measuring gluonic densities in structure functions. However, the dominant contribution in the averaging stems from large b [71, 72, 73]. More exclusive experiments could be done in future electron-Ion-Colliders to unravel the impact parameter dependence at low-x as well.

Low-x physics translates to a large $N = 1/x$ resolution of the holographic string as we detail below. This is achieved for long strings by discretizing the transverse Polyakov scalar action in N string bits and initially ignoring the stringy interactions (free string) and the curvature of AdS_5. String bits have been identified with wee (gluonic) partons by Thorn [82, 83]. The slow logarithmic growth of the free string transverse area translates to an anomalously large transverse string bit density at low-x. Repulsive string interactions can cause the transverse density to conform with the maximum Bekenstein bound for a black-hole as argued by Susskind for wee gravitons [81, 84, 85]. However, such a growth appears to be at odd with the Froissart bound [86].

A high string bit density at low-x points towards a liquid of string bits, a priori resolving the string. However, the underlying presence of the string is still paramount to maintain the (Gribov) diffusion of the string bits in the transverse plane. Recall that the diffusion constant $\mathbf{D} = l_s^2/2$ is dimensional and ties with the squared string length. Also, a highly resolved string provides an optimal description of low-x saturation in QCD as wee partons reaching the Bekenstein bound [87, 88, 89, 90, 91, 77, 78, 79]. In this work we will show that the bound is reached in two stages in flat $D_\perp = 3$. First a dilute pre-saturation stage where the string transverse area undergoes a first order transition from a large diffusive growth to a small but fixed size set by the string scale for relatively weak string self-interactions. Second a dense saturation stage at very low-x whereby the transverse string bit density saturates the Bekenstein bound of one bit per transverse Planck area. To assess the role of the AdS curvature on our results we suggest the use of an effective transverse dimension for the string bit interactions. The result is a smoothening of the transition to the Bekenstein bound.

Our pre-saturation condition in [76] is overall consistent with the saturation condition following from the stringy dipole-dipole cross section analysis derived in [71, 72, 73]. In some ways, the stringy description of saturation can be regarded as the dual of the weak coupling description of gluon saturation in QCD based on the color glass condensate [92, 93, 94, 95, 96,

97, 98, 99, 100, 101, 102, 103, 104] and is variant in the impact parameter space [105, 106, 107]. The exponential rise of the string density of states with its mass provides the most efficient way of scrambling information and reaching the Bekenstein bound and thus the saturation point as we will show below.

In [76], we obtain number of new results:

- A detailed numerical spatial shape analysis of an open and free string in flat $D_\perp = 3$ dimensions for increasing resolution.
- A variational analysis of the effects of two-body interactions on the string shape as a function of the resolution.
- A contraction of the string to a black-hole-like configuration under attraction and an expansion of the string shape under repulsion.
- A physical interpretation of the contracted string at high resolution with saturation in DIS dipole-dipole scattering in curved $D_\perp(\lambda) < 3$.
- A prompt transverse azimuthal asymmetry in dipole-dipole scattering.

One of the most remarkable feature of free strings is the exponential growth with their mass of the degeneracy in their spectra, which translates to a constant entropy to mass ratio [108, 109]. Excited strings offer a very efficient way to scramble information and create entropy. A competing mechanism for scrambling information appears in the opposite realm of the physical spectrum in the form of black-holes. Bekenstein noticed that the black-hole entropy grows in proportion to its area therefore to its mass to a power larger than 1 in any dimension [87, 88, 89]. This has led Susskind and others [81, 84, 85, 110, 111] to suggest that fundamental interacting single strings reduce to black-holes at sufficiently strong self-coupling.

Recently the paper [75] has suggested that the transmutation of strings to black-holes under self-interaction maybe revealed in hadron-hadron collisions at high energy when probing small impact parameters. The idea is that the standard Pomeron as a string exchange in pp collisions dominates the cross section for typical impact parameters $\mathbf{b} \approx 1.5$ fm. However, at smaller impact parameters, the string gets highly excited with a rapid buildup of entropy. This translates to a high multiplicity event possibly at the origin of the ridge observed recently at the LHC [112, 113, 114]. In author's paper[115], the length, mass and spatial distribution of a discretized transverse string

in $D_\perp$ dimensions with fixed end-points near its Hagedorn temperature are discussed.

1.3 Organization of the thesis

This thesis includes my work during the last five years. It includes the Spin Physics & QCD instantons and stringy pomeron. My research is closely related to the current and future experiment. The thesis is organized in the following:

- **Chapter 2: Instanton Solution**

  We introduce the 't hooft symbols and review the instanton solution in different gauges. The topological nature of the instanton is also discussed.

- **Chapter 3: Instanton Background**

  The zero modes and non-zero modes in instanton background should be analyzed separately. We calculate the bosonic zero modes and fermionic zero modes in single instanton background. We also derive the non-zero modes with spin 0 and with spin 1/2. Since the zero mode has its own measure in path integral, the measure of the zero modes is discussed.

- **Chapter 4: Spin effects through one instanton**

  We derive the Pauli form factor induced by single QCD instanton. By inserting the effective vertex into the perturbative diagrams, we explicit the QCD instantons effects on semi-inclusive DIS processes as well as singly polarized pp scattering.

- **Chapter 5: Spin effects through two instantons**

  We show that the effects of correlations between instantons and anti-instantons through fluctuations in both doubly polarized pp scattering as well as through $\mathcal{P}$-odd effects in peripheral AA scattering.

- **Chapter 6: Stringy pomeron I**

  We model the soft pomeron in QCD using a scalar Polyakov string in the bottom-up approach of holographic QCD. The effects of the extrinsic curvature in Polyakov string is also discussed.

- **Chapter 7: Stringy pomeron II**

  We discretize a long and stretched (fixed impact parameter) transverse quantum string in flat $D_\perp = 3$ dimensions. Its length, mass and spatial distribution are discussed respectively when it is away from its Hagedorn point and is near its Hagedorn point.

Chapter 2

Instanton Solution

2.1 Classical solution

In this section, we will briefly review the instanton solution, which is a classical solution to the Yang-Mills equation. We consider the $SU(2)$ gauge group in 4-dimensional Euclidean space here and will embed the $SU(2)$ group into the larger $SU(3)$ color gauge group in the next section.

2.1.1 SO(4) group and Euclidean space

In this subsection we will review the SO(4) group and Euclidean Space. The convention here is consistent with [16]. First, the Lie algebra $\mathfrak{so}(4)$ has the generators given by

$$(M_{\mu\nu})_{mn} \equiv \delta_{\mu m}\delta_{\nu n} - \delta_{\mu n}\delta_{\nu m}\,, \tag{2.1}$$

satisfying

$$[M_{\mu\nu},\, M_{\rho\sigma}] = \delta_{\nu\rho}M_{\mu\sigma} + \delta_{\mu\sigma}M_{\nu\rho} - \delta_{\mu\rho}M_{\nu\sigma} - \delta_{\nu\sigma}M_{\mu\rho}\,. \tag{2.2}$$

Let us write down the generators in fundamental representations:

$$M_{23} = \begin{pmatrix} 0 & 0 & 0 & 0 \\ 0 & 0 & 1 & 0 \\ 0 & -1 & 0 & 0 \\ 0 & 0 & 0 & 0 \end{pmatrix} \equiv J_1\,, \quad M_{14} = \begin{pmatrix} 0 & 0 & 0 & 1 \\ 0 & 0 & 0 & 0 \\ 0 & 0 & 0 & 0 \\ -1 & 0 & 0 & 0 \end{pmatrix} \equiv K_1\,,$$

$$M_{31} = \begin{pmatrix} 0 & 0 & -1 & 0 \\ 0 & 0 & 0 & 0 \\ 1 & 0 & 0 & 0 \\ 0 & 0 & 0 & 0 \end{pmatrix} \equiv J_2\,, \quad M_{24} = \begin{pmatrix} 0 & 0 & 0 & 0 \\ 0 & 0 & 0 & 1 \\ 0 & 0 & 0 & 0 \\ 0 & -1 & 0 & 0 \end{pmatrix} \equiv K_2\,,$$
$$M_{12} = \begin{pmatrix} 0 & 1 & 0 & 0 \\ -1 & 0 & 0 & 0 \\ 0 & 0 & 0 & 0 \\ 0 & 0 & 0 & 0 \end{pmatrix} \equiv J_3\,, \quad M_{34} = \begin{pmatrix} 0 & 0 & 0 & 0 \\ 0 & 0 & 0 & 0 \\ 0 & 0 & 0 & 1 \\ 0 & 0 & -1 & 0 \end{pmatrix} \equiv K_3\,, \tag{2.3}$$

where we have

$$[J_i,\, J_j] = -\epsilon_{ijk} J_k\,, \quad [K_i,\, K_j] = -\epsilon_{ijk} J_k\,, \quad [K_i,\, J_j] = -\epsilon_{ijk} K_k\,. \tag{2.4}$$

For convenience, we define

$$M_i \equiv \frac{1}{2}(J_i + K_i)\,, \quad N_i \equiv \frac{1}{2}(J_i - K_i)\,. \tag{2.5}$$

The (anti-)commutation relations are given by

$$[M_i,\, M_j] = -\epsilon_{ijk} M_k\,, \quad [N_i,\, N_j] = -\epsilon_{ijk} N_k\,, \quad [M_i,\, N_j] = 0\,, \tag{2.6}$$

$$\{M_i,\, M_j\} = -\frac{1}{2}\delta_{ij}\,, \quad \{N_i,\, N_j\} = -\frac{1}{2}\delta_{ij}\,. \tag{2.7}$$

M_i and N_i together form a complete basis of $\mathfrak{so}(4)$ algebra. We expand $M_{\mu\nu}$ as

$$M_{\mu\nu} \equiv \eta_{i\mu\nu} M_i + \bar{\eta}_{i\mu\nu} N_i\,, \tag{2.8}$$

where η and $\bar{\eta}$ are 't Hooft symbols, which read

$$\begin{aligned} \eta_{i\mu\nu} &= -\mathrm{tr}\,(M_i M_{\mu\nu}) = -(M_i)_{mn}(M_{\mu\nu})_{nm} = 2(M_i)_{\mu\nu} = (\epsilon_{i\mu\nu 4} + \delta_{i\mu}\delta_{\nu 4} - \delta_{i\nu}\delta_{\mu 4})\,, \\ \bar{\eta}_{i\mu\nu} &= -\mathrm{tr}\,(N_i M_{\mu\nu}) = -(N_i)_{mn}(M_{\mu\nu})_{nm} = 2(N_i)_{\mu\nu} = (\epsilon_{i\mu\nu 4} - \delta_{i\mu}\delta_{\nu 4} + \delta_{i\nu}\delta_{\mu 4})\,, \end{aligned} \tag{2.9}$$

where we used

$$\mathrm{tr}\,(M_i M_j) = -\delta_{ij}\,, \quad \mathrm{tr}\,(N_i N_j) = -\delta_{ij}\,, \quad \mathrm{tr}\,(M_i N_j) = 0\,. \tag{2.10}$$

Some important properties are

$$\frac{1}{2}\epsilon_{\mu\nu\rho\sigma}\eta_{i\rho\sigma} = \eta_{i\mu\nu}\,, \quad \frac{1}{2}\epsilon_{\mu\nu\rho\sigma}\bar{\eta}_{i\rho\sigma} = -\bar{\eta}_{i\mu\nu}\,. \tag{2.11}$$

For convenience, we will also use the spinor representations:

$$\begin{aligned} \sigma_{\mu\nu} &\equiv \frac{1}{2}\left(\sigma_\mu\bar{\sigma}_\nu - \sigma_\nu\bar{\sigma}_\mu\right) , \\ \bar{\sigma}_{\mu\nu} &\equiv \frac{1}{2}\left(\bar{\sigma}_\mu\sigma_\nu - \bar{\sigma}_\nu\sigma_\mu\right) , \end{aligned} \tag{2.12}$$

where

$$\sigma_\mu \equiv (\tau^a, i) \quad \text{and} \quad \bar{\sigma}_\mu \equiv (\tau^a, -i) . \tag{2.13}$$

τ^a is pauli matrices. Since $\sigma_{\mu\nu}$ is the spinor representation of the $SO(4)$ group, we have

$$[\sigma_{\mu\rho}, \sigma_{\nu\sigma}] = 2\delta_{\mu\sigma}\sigma_{\rho\nu} + 2\delta_{\rho\nu}\sigma_{\mu\sigma} - 2\delta_{\mu\nu}\sigma_{\rho\sigma} - 2\delta_{\rho\sigma}\sigma_{\mu\nu} . \tag{2.14}$$

It is easy to show that the Clifford algebra is satisfied:

$$\sigma_\mu\bar{\sigma}_\nu + \sigma_\nu\bar{\sigma}_\mu = 2\delta_{\mu\nu} . \tag{2.15}$$

The following properties are also important:

$$\bar{\sigma}_{\mu\nu} = i\eta_{a\mu\nu}\tau^a \quad \text{and} \quad \sigma_{\mu\nu} = i\bar{\eta}_{a\mu\nu}\tau^a . \tag{2.16}$$

2.1.2 (Anti-)selfdual equation

The Yang-Mills equation reads

$$D_\mu F_{\mu\nu} = 0 , \tag{2.17}$$

where

$$D_\mu \equiv \partial_\mu + A_\mu , \tag{2.18}$$

and

$$F_{\mu\nu} \equiv [D_\mu, D_\nu] . \tag{2.19}$$

Notice, we do not distinguish the upper and the lower indices for the Eulidean space. Eq. (2.17) in general is difficult to solve. Instead, we consider the (anti-)selfdual equation:

$$\widetilde{F}_{\mu\nu} = \begin{cases} +F_{\mu\nu} & \text{selfdual;} \\ -F_{\mu\nu} & \text{anti-selfdual,} \end{cases} \tag{2.20}$$

where

$$\widetilde{F}_{\mu\nu} \equiv \frac{1}{2}\epsilon_{\mu\nu\rho\sigma}F_{\rho\sigma}\,. \tag{2.21}$$

It is easy to show that Eq. (2.20) naturally satisfies Eq. (2.17):

$$\begin{aligned} D_\mu F_{\mu\nu} &= \pm D_\mu \widetilde{F}_{\mu\nu} \\ &= \mp\frac{1}{2}\epsilon_{\mu\nu\rho\sigma}D_\nu F_{\rho\sigma} \\ &= \mp\epsilon_{\mu\nu\rho\sigma}D_\nu D_\rho D_\sigma \\ &= 0\,. \end{aligned} \tag{2.22}$$

where we used the Bianchi identity [116]. The solution to the (anti-)selfdual equation is usually referred as (anti-)instanton solutions.

2.1.3 Classical solutions

Though the (anti-)selfdual equation (Eq. (2.20)) suffice our purpose in this section, we will still show some simple steps to solve the spherically symmetric Yang-Mills equations because we will also obtain Meron solution, which does not satisfy the (anti-)selfdual equation, but is still very important in QCD vacuum [117, 118].

The derivatives here are similar to the author's paper [16]. Let us start with

$$A_\mu = A^a_\mu\, T_a\,, \tag{2.23}$$

where

$$T_a = \frac{\sigma_a}{2i}\,. \tag{2.24}$$

Hence

$$F^a_{\mu\nu} = \partial_\mu A^a_\nu - \partial_\nu A^a_\mu + \epsilon_{abc}A^b_\mu A^c_\nu\,. \tag{2.25}$$

The ansatz is then given by:

$$A_{\mu,a} = 2\,\frac{p(\tau)}{\tau}\,\eta_{a\mu\nu}(x-x_0)_\nu\,, \tag{2.26}$$

where $\eta_{a\mu\nu}$ is the 't hooft symbol, $p(\tau)$ stands for arbitrary analytical function of τ and

$$\tau \equiv \sum_{i=1}^{4}(x-x_0)^i(x-x_0)^i\,, \tag{2.27}$$

where x_0 is the center of the solution. For simplicity, we chose the coordinate centering at x_0 in this section. In fact, the ansatz Eq. (2.26) can be derived through a general way: the ansatz should satisfy certain geometric symmetries and topological boundary conditions to be stable. We will not review the details in this thesis. For more details, see [16].

We obtain

$$F^a_{\mu\nu} = 4\eta_{a\mu\nu}\left(\frac{p^2}{\tau} - \frac{p}{\tau}\right) + 4x_\rho(x_\mu\eta_{a\nu\rho} - x_\nu\eta_{a\mu\rho})\left[\left(\frac{p}{\tau}\right)' + \frac{p^2}{\tau^2}\right], \tag{2.28}$$

where the prime denotes the derivative with respect to τ

$$(\cdots)' \doteq \frac{\partial(\cdots)}{\partial\tau}. \tag{2.29}$$

The Yang-Mills equation reads

$$(D_\mu F_{\mu\nu})^a = 8\,\frac{\eta_{a\nu\rho}x_\rho}{\tau^2}\,(-p + 3p^2 - 2p^3 + \tau p' + \tau^2 p'') = 0\,, \tag{2.30}$$

and we only need to solve the differential equation

$$-p + 3p^2 - 2p^3 + \tau p' + \tau^2 p'' = 0\,. \tag{2.31}$$

As we explained in paper [16], the boundary values of p should be fixed by the topological charges and can not be divergent. Hence, we can expand p near the boundaries, which for the spherically symmetric case are just $\tau = 0$ and $\tau = \infty$. The series is given as follows:

$$p(\tau) = \begin{cases} a_0^{\tau=0} + \sum_{n=1}^{\infty} a_n^{\tau=0}\,\tau^n\,, & \text{for small } \tau\,; \\ a_0^{\tau=\infty} + \sum_{n=1}^{\infty} a_n^{\tau=\infty}/\tau^n\,, & \text{for large } \tau\,. \end{cases}$$

Plugging these expressions into Eq. (2.31), at the leading order they both lead to

$$a_0^{\tau=0,\infty} = 0 \text{ or } \frac{1}{2} \text{ or } 1\,. \tag{2.32}$$

It is simple to show that there are five solutions that satify the Yang-Mills equation:

1. 4D meron solution:

   $a_0^{\tau=0} = \frac{1}{2}\,, \quad a_0^{\tau=\infty} = \frac{1}{2}$. We obtain

   $$p = a_0 = \frac{1}{2} \tag{2.33}$$

2. Instanton solution in regular gauge:
   $a_0^{\tau=0} = 0\,, \quad a_0^{\tau=\infty} = 1$. We obtain

$$a_n^{\tau=\infty} = (a_1^{\tau=\infty})^n\,, \tag{2.34}$$

   which leads to

$$p(\tau) = 1 + \sum_{n=1}^{\infty} \frac{(a_1^{\tau=\infty})^n}{\tau^n} = \frac{\tau}{\tau+\rho^2}\,, \tag{2.35}$$

   where we denote $-a_1^{\tau=\infty} \to \rho^2$.

3. Pure Gauge solution:
   $a_0^{\tau=0} = 1\,, \quad a_0^{\tau=\infty} = 1$:
   We obtain

$$a_1^{\tau=\infty} = 0\,. \tag{2.36}$$

   and

$$a_n^{\tau=\infty} = 0 \quad \text{for} \quad n \geq 1\,. \tag{2.37}$$

   Therefore

$$p(\tau) = 1\,. \tag{2.38}$$

4. Anti-instanton solution in singular gauge:
   $a_0^{\tau=0} = 1\,, \quad a_0^{\tau=\infty} = 0$. We obtain

$$a_n^{\tau=\infty} = (-1)^{n-1}(a_1^{\tau=\infty})^n\,. \tag{2.39}$$

   and

$$p(\tau) = \sum_{n=1}^{\infty}(-1)^{n-1}\frac{(a_1^{\tau=\infty})^n}{\tau^n} = \frac{\rho^2}{\tau+\rho^2}\,, \tag{2.40}$$

   where we denote $a_1^{\tau=\infty} \to \rho^2$.

5. Trivial vacuum:
   $a_0^{\tau=0} = 0\,, \quad a_0^{\tau=\infty} = 0$. This case is the trivial solution with

$$a_1^{\tau=\infty} = 0\,, \tag{2.41}$$

   and

$$a_n^{\tau=\infty} = 0 \quad \text{for} \quad n \geq 1\,. \tag{2.42}$$

   Therefore

$$p(\tau) = 0\,. \tag{2.43}$$

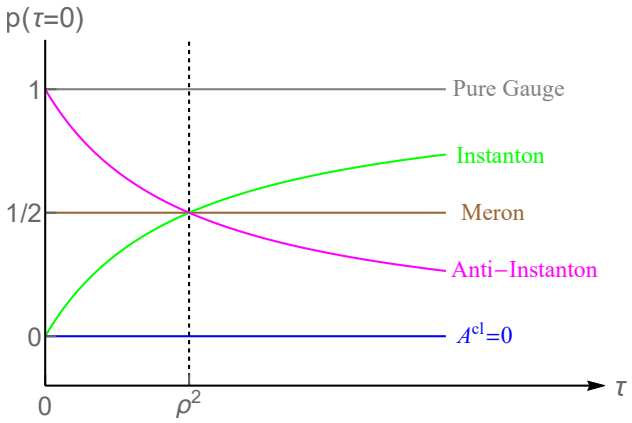

Figure 2.1: Classical solutions in the regular coordinate.

We summarize the classical solutions obtained above in Fig. 2.1.

In fact, as we have shown in the author's paper [16], all these five solutions can be expected from the topological properties. To illustrate this point, we can adopt a new coordinate introduced by the conformal transformation

$$\zeta = \frac{1}{2}\frac{\tau - \rho^2}{\tau + \rho^2}\,, \tag{2.44}$$

then all the solutions displayed in Fig. 2.1 are replotted in the new coordinate in Fig. 2.2.

2.1.4 (Anti-)instanton solutions

Let us continue the discussion with the instanton solution we obtained in last subsection. First, we need to check that it indeed satisfies the selfdual equation

$$F_{\mu\nu} = \widetilde{F}_{\mu\nu}\,. \tag{2.45}$$

The ansatz Eq. (2.26) we used in last subsection is

$$A_{\mu,a} = 2\,\frac{p(\tau)}{\tau}\,\eta_{a\mu\rho}x_\rho\,. \tag{2.46}$$

From the ansatz Eq. (2.46), we have

$$F^a_{\mu\nu} = 4\eta_{a\mu\nu}\left(\frac{p^2}{\tau} - \frac{p}{\tau}\right) + 4x_\rho(x_\mu\eta_{a\nu\rho} - x_\nu\eta_{a\mu\rho})\left[\left(\frac{p}{\tau}\right)' + \frac{p^2}{\tau^2}\right]\,. \tag{2.47}$$

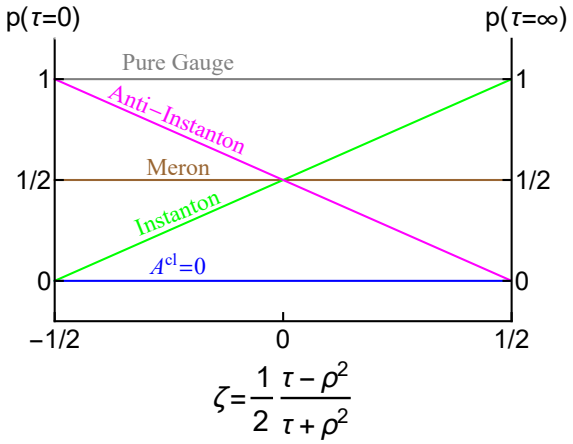

Figure 2.2: Classical solutions in a conformal coordinate.

Plugging

$$p(\tau) = \frac{\tau}{\tau + \rho^2} \tag{2.48}$$

into Eq. (2.47), we obtain

$$F^a_{\mu\nu} = -4\eta_{a\mu\nu}\frac{\rho^2}{(\rho^2+\tau)^2}\,. \tag{2.49}$$

Recalling the important properties of the 't hooft symbol

$$\frac{1}{2}\epsilon_{\mu\nu\rho\sigma}\eta_{a\rho\sigma} = \eta_{a\mu\nu}\,, \tag{2.50}$$

we obtain

$$\widetilde{F}_{\mu\nu} = F_{\mu\nu}\,, \tag{2.51}$$

which is the selfdual equation. Also notice, in the paper we emphasize that it is in the regular gauge, the reason is the following: A_μ is divergent at $\tau \sim 0$ yet is the pure gauge at $\tau \sim \infty$. To illustrate it, let us rewrite it as

$$\begin{aligned} A_\mu &= \frac{2}{\tau+\rho^2}\,\eta_{a\mu\rho}x_\rho\,T_a \\ &= -\frac{1}{\tau+\rho^2}\,(i\eta_{a\mu\rho}\sigma_a)\,x_\nu \\ &= \frac{\tau}{\tau+\rho^2}\left(-\frac{\bar{\sigma}_{\mu\nu}\,x_\nu}{\tau}\right)\,, \end{aligned} \tag{2.52}$$

where we used

$$\bar{\sigma}_{\mu\nu} = i\eta_{a\mu\nu}\tau^a \,. \tag{2.53}$$

It is easy to check

$$-\frac{\bar{\sigma}_{\mu\nu}\, x_\nu}{\tau} = U^{-1}\partial_\mu U \,, \tag{2.54}$$

where

$$U = \frac{i\bar{\sigma}_\mu x_\mu}{|x|} \quad \text{and} \quad U^{-1} = -\frac{i\sigma_\mu x_\mu}{|x|} \,. \tag{2.55}$$

Now we can rewrite instanton solution in regular gauge as

$$A_\mu = \frac{\tau}{\tau+\rho^2}\left(U^{-1}\partial_\mu U\right) \,. \tag{2.56}$$

We have

- $\tau \longrightarrow 0$

$$A_\mu \longrightarrow 0 \,. \tag{2.57}$$

- $\tau \longrightarrow \infty$

$$A_\mu \longrightarrow U^{-1}\partial_\mu U \,. \tag{2.58}$$

If we perform a gauge transformation

$$A_\mu^{\text{singular}} = U A_\mu^{\text{regular}} U^{-1} + U\partial_\mu U^{-1} \,, \tag{2.59}$$

we obtain

$$A_\mu^{\text{singular}} = \frac{\rho^2}{\tau+\rho^2}\left(U\partial_\mu U^{-1}\right) \,. \tag{2.60}$$

The discussion above is about instanton. The same analysis also applies to anti-instanton. Recalling the anti-instanton solution in singular gauge we obtained in last section:

$$\begin{aligned} A_\mu &= \frac{2\rho^2}{\tau(\tau+\rho^2)}\,\eta_{a\mu\rho}x_\rho\, T_a \\ &= \frac{\rho^2}{\tau+\rho^2}\left(-\frac{\bar{\sigma}_{\mu\nu}\, x_\nu}{\tau}\right) \\ &= \frac{\rho^2}{\tau+\rho^2}\left(U^{-1}\partial_\mu U\right) \,. \end{aligned} \tag{2.61}$$

The anti-instanton solution in regular can be obtained by

$$\begin{aligned} A_\mu^{\text{regular}} &= U A_\mu^{\text{singular}} U^{-1} + U\partial_\mu U^{-1} \\ &= \frac{\tau}{\tau+\rho^2}\left(U\partial_\mu U^{-1}\right) \\ &= -\frac{\sigma_{\mu\nu}x_\nu}{\tau+\rho^2}\,. \end{aligned} \tag{2.62}$$

We can also calculate

$$F_{\mu\nu} = 2\sigma_{\mu\nu}\frac{\rho^2}{(\tau+\rho^2)^2}\,, \tag{2.63}$$

and check

$$\widetilde{F}_{\mu\nu} = -F_{\mu\nu}\,, \tag{2.64}$$

where we used

$$\frac{1}{2}\epsilon_{\mu\nu\rho\sigma}\sigma_{\rho\sigma} = -\sigma_{\mu\nu}\,. \tag{2.65}$$

2.2 Winding number

In 4-dimensional Euclidean space, we introduce the topological term

$$S \equiv i2\pi k\,, \tag{2.66}$$

with the winding number

$$\begin{aligned} k &= -\frac{1}{16\pi^2}\int d^4x\,\mathrm{Tr}\left[F^{\mu\nu}(\widetilde{F}_{\mu\nu})\right] \\ &= -\frac{1}{8\pi^2}\int d^4x\,\partial_\mu\epsilon^{\mu\nu\rho\sigma}\,\mathrm{Tr}\left[A_\nu\partial_\rho A_\sigma + \frac{2}{3}A_\nu A_\rho A_\rho\right]\,. \end{aligned} \tag{2.67}$$

Let us derive the second line by rewriting the A_μ as 1-form

$$A \equiv A_\mu\, dx^\mu\,. \tag{2.68}$$

Then

$$F = dA + A^2\,, \tag{2.69}$$

where

$$A^2 \doteq A\wedge A\,, \tag{2.70}$$

and

$$\begin{aligned} F \wedge F &= (dA + A^2)(dA + A^2) \\ &= (dA)(dA) + 2A^2 dA \,, \end{aligned} \tag{2.71}$$

where we dropped A^4. We also notice

$$(dA)(dA) = d(AdA) \,, \tag{2.72}$$

because

$$d(dA) = 0 \,. \tag{2.73}$$

In sum

$$F^2 = d\left(AdA + \frac{2}{3}A^3\right) \,. \tag{2.74}$$

According to Stokes' theorem, we have

$$k = -\frac{1}{16\pi^2}\int_{S^3 \text{ space}} d\Omega_\mu \, \epsilon^{\mu\nu\rho\sigma} \,\mathrm{Tr}\left[A_\nu \partial_\rho A_\sigma + \frac{2}{3}A_\nu A_\rho A_\sigma\right] \,, \tag{2.75}$$

where the integral is over S^3 surface. Notice that A_μ does not have singular point and therefore there are only two surface: around $\tau \sim 0$ and around $\tau \sim \infty$. In this subsection, we adopt the solution in regular gauge, take instanton for example

$$A_\mu \xrightarrow{\tau\sim 0} 0 \,. \tag{2.76}$$

and

$$A_\mu \xrightarrow{\tau\sim\infty} U^{-1}\partial_\mu U \,. \tag{2.77}$$

As we can see, only one surface would contribute to the integral

$$\begin{aligned} k = \frac{-1}{8\pi^2}\int_{S^3\ (\tau\sim\infty)} d\Omega_\mu \, \epsilon^{\mu\nu\rho\sigma} \,\mathrm{Tr} \quad &\Big[\quad (U^{-1}\partial_\nu U)\partial_\rho(U^{-1}\partial_\sigma U) \\ &+ \quad \frac{2}{3}(U^{-1}\partial_\nu U)(U^{-1}\partial_\rho U)(U^{-1}\partial_\sigma U)\Big] \\ &. \end{aligned} \tag{2.78}$$

After simple algebra, we obtain

$$k = \frac{1}{24\pi^2}\int_{S^3\ (\tau\sim\infty)} d\Omega_\mu \, \epsilon^{\mu\nu\rho\sigma} \,\mathrm{Tr}\left[(U^{-1}\partial_\nu U)(U^{-1}\partial_\rho U)(U^{-1}\partial_\sigma U)\right] \,. \tag{2.79}$$

Now let us use x^μ and $\xi^i(x)$ $(i = 1, 2, 3)$ to denote the spacetime coordinates and the group coordinates respectively [16]. Using

$$\begin{aligned} & \mathrm{Tr}\left[(U^{-1}\partial_\nu U)\,(U^{-1}\partial_\rho U)\,(U^{-1}\partial_\sigma U)\right] \\ = \quad & \frac{\partial\xi^i}{\partial x^\nu}\frac{\partial\xi^j}{\partial x^\rho}\frac{\partial\xi^k}{\partial x^\sigma}\,\mathrm{Tr}\left[(U^{-1}\partial_i U)\,(U^{-1}\partial_j U)\,(U^{-1}\partial_k U)\right]\,, \end{aligned} \tag{2.80}$$

and the volume element is given by

$$d\Omega_\mu = \frac{1}{6}\epsilon_{\mu\alpha\beta\gamma}\,dx_\alpha\,dx_\beta\,dx_\gamma\,. \tag{2.81}$$

The Integrand on the surface S^3 around $\tau \sim \infty$ reads

$$\begin{aligned} dk &= \frac{1}{24\pi^2}\epsilon^{ijk}\,\mathrm{Tr}\left[(U^{-1}\partial_i U)(U^{-1}\partial_j U)(U^{-1}\partial_k U)\right]\,d^3\xi \\ &= \frac{1}{24\pi^2}\,(\det e)\,\mathrm{Tr}\left(\epsilon^{abc}T_aT_bT_c\right)d^3\xi \\ &= \frac{1}{16\pi^2}\,(\det e)\,d^3\xi\,, \end{aligned} \tag{2.82}$$

where we write

$$U^{-1}\partial_i U = e_i^a(\xi)\,T_a\,, \tag{2.83}$$

and $(\det e)d^3\xi$ is the Haar measure on the group manifold. Hence,

$$k = \int dk = 1 \tag{2.84}$$

takes values in $\mathbb{Z}$ and in this case 1 since it is 1-instanton.

The derivative above shows the geometric meaning of the instanton. One can also calculate the winding number by using

$$F^a_{\mu\nu} = -4\eta_{a\mu\nu}\frac{\rho^2}{(\rho^2+\tau)^2}\,. \tag{2.85}$$

$$\frac{1}{2}\epsilon_{\mu\nu\rho\sigma}F^a_{\mu\nu}F^a_{\rho\sigma} = 16\eta_{a\mu\nu}\eta_{a\mu\nu}\frac{\rho^4}{(\rho^2+\tau)^4}\,. \tag{2.86}$$

It is easy to check

$$\eta_{a\mu\nu}\eta_{a\mu\nu} = 12\,. \tag{2.87}$$

Obtain

$$\begin{aligned} k &= -\frac{1}{16\pi^2}\int d^4x\,\mathrm{Tr}\left[F^{\mu\nu}(\widetilde{F}_{\mu\nu})\right] \\ &= -\frac{1}{16\pi^2}\times 16\times 12\times 2\times\frac{1}{(2i)^2}\int d^4x\,\frac{\rho^4}{(\rho^2+x^2)^4} \\ &= 1\,. \end{aligned} \tag{2.88}$$

Instead of instanton, if we use anti-instanton, there is a negative sign due to

$$\widetilde{F}_{\mu\nu} = -F_{\mu\nu}\,. \tag{2.89}$$

It is clear that the instanton is topologically stable because it has integer winding number. Now we also want to show here that instanton is the extrema of the action

$$\begin{aligned} \int d^4x\,F_{\mu\nu}F_{\mu\nu} &= \frac{1}{2}\int d^4x\,\left(F_{\mu\nu}\pm\widetilde{F}_{\mu\nu}\right)^2 \mp\int d^4x\,F_{\mu\nu}\widetilde{F}_{\mu\nu} \\ &\geq \mp\int d^4x\,F_{\mu\nu}\widetilde{F}_{\mu\nu}\,, \end{aligned} \tag{2.90}$$

where the equality is true if and only if the field strength $F_{\mu\nu}$ is (anti-)selfdual.

Chapter 3

Instanton Background

3.1 Zero mode

3.1.1 Bosonic zero mode

What is a zero mode?

A zero mode is a normalizable solution of the linearized field equations for the quantum fluctuations.

To illustrate the point, we write [16]

$$A_\mu = A_\mu^{\rm cl} + Q_\mu \,, \tag{3.1}$$

where $A_\mu^{\rm cl}$ is the classical background and Q_μ is the quantum fluctuations. The full field strength is then given by

$$\mathcal{F}_{\mu\nu} = [D_\mu + Q_\mu,\, D_\nu + Q_\nu] \,, \tag{3.2}$$

and one can also define a field strength of the classical background as

$$F_{\mu\nu} = [D_\mu,\, D_\nu] \,, \tag{3.3}$$

where

$$D_\mu \equiv \partial_\mu + A_\mu^{\rm cl} \,. \tag{3.4}$$

The field strength now reads

$$\mathcal{F}_{\mu\nu} = F_{\mu\nu} + D_\mu Q_\nu - D_\nu Q_\mu + [Q_\mu,\, Q_\nu] \,, \tag{3.5}$$

where $F_{\mu\nu}$ is the field strength of the background Yang-Mills field. The Yang-Mills Lagrangian is given by

$$\begin{aligned}\mathcal{L}_{\rm YM} &\equiv -\frac{1}{2}\,{\rm Tr}\,(\mathcal{F}_{\mu\nu}\mathcal{F}_{\mu\nu}) \\ &= -{\rm Tr}\left(\frac{1}{2}F_{\mu\nu}F_{\mu\nu} + 2Q_\mu\,(D_\nu F_{\mu\nu}) - Q_\mu\mathcal{M}_{\mu\nu}Q_\nu + \mathcal{O}(Q^3)\right)\,, \end{aligned} \tag{3.6}$$

where

$$\mathcal{M}_{\mu\nu} \equiv D^2\delta_{\mu\nu} + F_{\mu\nu} - D_\nu D_\mu\,, \tag{3.7}$$

and we dropped the higher order of Q_μ. In a full analysis, the higher orders could be important. For more details, it is discussed in author's paper [16]. To quantize the theory, we need to fix the gauge of quantum mode [16, 116]:

$$D_\mu Q_\mu = 0\,, \tag{3.8}$$

which could be done by introducing the gauge fixing term

$$\mathcal{L}_{\rm fix} = -{\rm Tr}\left[(D_\mu Q_\mu)^2\right]\,. \tag{3.9}$$

Combining everything above, we have

$$\begin{aligned}\mathcal{L} &= \mathcal{L}_{\rm YM} + \mathcal{L}_{\rm fix} \\ &= -{\rm Tr}\left(\frac{1}{2}F_{\mu\nu}F_{\mu\nu} + 2Q_\mu\,(D_\nu F_{\mu\nu}) - Q_\mu M_{\mu\nu}Q_\nu + \mathcal{O}(Q^3)\right)\,, \end{aligned} \tag{3.10}$$

where

$$M_{\mu\nu} \equiv \mathcal{M}_{\mu\nu} + D_\mu D_\nu = D^2\delta_{\mu\nu} + 2F_{\mu\nu}. \tag{3.11}$$

Therefore, a zero mode Z_μ by definition is the solution to $M_{\mu\nu}$

$$M_{\mu\nu}Z_\nu = 0\,. \tag{3.12}$$

Bosonic zero modes

Our goal is to find the solutions to the equations

$$M_{\mu\nu}Z_\nu = 0\,. \tag{3.13}$$

But before we proceed, we still need to fix the gauge of the zero mode. In fact, in almost all the works, the gauge is fixed as

$$D_\mu Z_\mu = 0\,, \tag{3.14}$$

where

$$D_\mu = \partial_\mu + A^{\rm cl}_\mu \,. \tag{3.15}$$

There are two reasons: first, later we will obtain a propagator containing both zero mode and quantum mode, it is convenient to analyze it if both the zero mode and quantum mode satify the same gauge fixing condition; second and probably the more important reason is that we want to find the mode that is perpendicular to the gauge transformation. To illustrate the second point, we write down the "perpendicular" condition

$$\int d^D x \, (D_\mu \Lambda) \, Z_\mu = 0 \,. \tag{3.16}$$

In order for the equation above is true for any gauge, we have

$$D_\mu Z_\mu = 0 \,. \tag{3.17}$$

Well, now we have all the equations to solve the zero mode

$$M_{\mu\nu} Z_\nu = 0 \quad \text{and} \quad D_\mu Z_\mu = 0 \,. \tag{3.18}$$

In fact, this problem can become simpler. The classical solution by definition satisfy

$$\frac{\delta S^{\rm cl}}{\delta A^{\rm cl}_\mu} = 0 \,, \tag{3.19}$$

where $S^{\rm cl}$ is the action. We also have

$$\frac{\delta \left(\frac{\delta S^{\rm cl}}{\delta A^{\rm cl}_\mu} \right)}{\delta \gamma^{(i)}} = 0 \,, \tag{3.20}$$

where $\gamma^{(i)}$ is the free parameter in the classical solution. We obtain the important equation:

$$\frac{\delta^2 S^{\rm cl}}{\delta A^{\rm cl}_\nu \, \delta A^{\rm cl}_\mu} \partial_{\gamma^i} A^{\rm cl}_\mu = 0 \,, \tag{3.21}$$

where

$$\frac{\delta^2 S^{\rm cl}}{\delta A^{\rm cl}_\nu \, \delta A^{\rm cl}_\mu} \longrightarrow M_{\mu\nu} \,. \tag{3.22}$$

The solution is still a solution up to a gauge transformation, therefore we can writen down the zero mode as

$$Z^{(i)}_\mu = \frac{\partial A^{\rm cl}_\mu}{\partial \gamma^{(i)}} + D_\mu \Lambda^{(i)} \,, \tag{3.23}$$

where $\Lambda^{(i)}$ should be fixed by

$$D_\mu Z_\mu = 0\,. \tag{3.24}$$

To show how to calculate the zero modes, we take anti-instanton as an example:

$$A^a_\mu = 2\frac{\rho^2}{\tau(\tau+\rho^2)}\,\eta_{a\mu\nu}(x-x_0)_\nu\,. \tag{3.25}$$

First, the solution has a parameter x_0, which is the center of the anti-instanton. Second, the solution has a size parameter ρ. Third, the solution is still a solution up to a gauge transformation, so we can write

$$A_\mu \longrightarrow U^{-1}A_\mu U + U^{-1}\partial_\mu U\,, \tag{3.26}$$

where

$$U = \exp\left(\theta^\alpha T_\alpha\right) \tag{3.27}$$

and thus θ^α is a parameter. In fact, when we analyze the QCD instanton, there are more freedoms, due to different ways to embed the $SU(2)$ subgroup into the larger $SU(3)$ group. The last point is out of the scope of this paper, but let us consider the first three cases: (see [16])

- Translational ($\gamma^{(\nu)} = x_0^\nu$):

$$\begin{aligned} \frac{\partial A^{\rm cl}_\mu}{\partial x_0^\nu} &= -\partial_\nu A^{\rm cl}_\mu\,, \\ \text{choose} \qquad \Lambda_\nu &= A^{\rm cl}_\nu\,, \\ Z^{(\nu)}_\mu &= F^{\rm cl}_{\mu\nu}\,, \\ \text{check} \qquad D_\mu Z^{(\nu)}_\mu &= D_\mu F^{\rm cl}_{\mu\nu} = 0\,. \end{aligned} \tag{3.28}$$

- Gauge orientation ($\gamma^{(\alpha)} = \theta^\alpha$):

$$\begin{aligned} \left.\frac{\partial A^{\rm cl}_\mu}{\partial\theta^\alpha}\right|_{\theta^\alpha=0} &= \delta_{\alpha a}[A^{\rm cl}_\mu, T^a]\,, \\ \text{choose} \qquad \Lambda_\nu &= -\delta_{\alpha a}\frac{\rho^2}{\tau+\rho^2}T_a\,, \\ Z^{(\alpha)}_\mu &= \delta_{\alpha a}D_\mu\left(\frac{\tau}{\tau+\rho^2}T_a\right)\,, \\ \text{check} \qquad D_\mu Z^{(\alpha)}_\mu &= D^2\left(\frac{\tau}{\tau+\rho^2}T_\alpha\right) = 0\,. \end{aligned} \tag{3.29}$$

- Dilatational (size ρ):

$$\begin{aligned} \frac{\partial A_\mu^{\rm cl}}{\partial \rho} &= \frac{2\rho\tau}{(\tau+\rho^2)^2}\left(\frac{2}{\tau}\eta_{a\mu\nu}(x-x_0)_\nu T_a\right), \\ \text{choose} \qquad \Lambda_\nu &= 0\,, \\ Z_\mu^\rho &= \frac{2\rho\tau}{(\tau+\rho^2)^2}\left(\frac{2}{\tau}\eta_{a\mu\nu}(x-x_0)_\nu T_a\right), \\ \text{check} \qquad D_\mu Z_\mu^\rho &= 0\,. \end{aligned} \tag{3.30}$$

We have obtained all the zero modes due to translational invariance, gauge orientation equivalence, and dilatational invariance. As we will see later, these modes will become important because they contribute to the Jacobian in the path integral nontrivially.

3.1.2 Fermionic zero mode

Because of the presence of the (anti-)instanton, the fermion also has zero mode. More importantly, as we will show now, the (anti-)instanton simultaneously breaks the chiral symmetry in the vacuum, which is curicial for us to understand the QCD vacuum. First, we need to choose a gauge of the (anti-)instanton. In the author's works and other relating works [119, 120, 121, 122, 43, 46, 45, 44], the calculation is usually implemented in singular gauge, where the instanton configurations are more localized.

The massless Dirac equation in instanton background reads $\not{D}\psi = 0$. It is easy to show that in the presence of an instanton [116, 16],

$$\not{D}(1+\gamma^5)\psi = 0 \tag{3.31}$$

has no solution while

$$\not{D}(1-\gamma^5)\psi = 0 \tag{3.32}$$

has a normalizable left-handed zero mode. Let us explain it. In weyl basis, we have [119, 121, 122]

$$(\sigma_\mu)_{\alpha\beta}\left[\partial_\mu\delta_{ij} + \left(A_\mu^{\rm sin}\right)_{ij}\right]\xi_{\beta,j} = 0\,, \tag{3.33}$$

where we do not distinguish the upper and the lower indices for the Euclidean space. But the indices here are very important: α and β are spinor indices

while i and j are color indices. In perturbative QCD, they are independent, however, as we can see now, they are mixed in instanton background. In fact, one can find the solution:

$$\xi \sim (\bar{\sigma}_l)_{\beta\beta'} \epsilon_{\beta' j} \frac{(x-x_0)_l}{|x-x_0|} \frac{\rho^{\frac{3}{2}}}{[(x-x_0)^2+\rho^2]^{\frac{3}{2}}} , \tag{3.34}$$

where

$$\epsilon \equiv \begin{pmatrix} 0 & 1 \\ -1 & 0 \end{pmatrix} . \tag{3.35}$$

The important relation we need is

$$\epsilon \tau^a \epsilon = (\tau^a)^T . \tag{3.36}$$

To check it, let us assume $x_0 = 0$ for simplicity:

$$\begin{aligned} & (\sigma_\mu)_{\alpha\beta} \left[\partial_\mu \delta_{ij} + \left(A^{\rm sin}_\mu \right)_{ij} \right] \xi_{\beta,j} \\ = \; & (\sigma_\mu \bar{\sigma}_l \epsilon)_{\alpha i} \, \partial_\mu \left(\frac{x_l}{|x|} \frac{\rho^{\frac{3}{2}}}{[x^2+\rho^2]^{\frac{3}{2}}} \right) - \left(\sigma_\mu \bar{\sigma}_l \epsilon \sigma^T_{\mu\nu} \right)_{\alpha i} \left(\frac{\rho^2 x_\nu}{x^2(x^2+\rho^2)} \frac{x_l}{|x|} \frac{\rho^{\frac{3}{2}}}{[x^2+\rho^2]^{\frac{3}{2}}} \right) \end{aligned} \tag{3.37}$$

.

By using

$$\begin{aligned} \sigma_\mu \bar{\sigma}_l \epsilon \sigma^T_{\mu\nu} x_\nu x_l &= -\sigma_\mu \bar{\sigma}_l \sigma_{\mu\nu} \epsilon x_\nu x_l \\ &= 3x^2 \epsilon , \end{aligned} \tag{3.38}$$

we need to check

$$\begin{aligned} & \sigma_\mu \bar{\sigma}_l \partial_\mu \left(\frac{x_l}{|x|} \frac{1}{[x^2+\rho^2]^{\frac{3}{2}}} \right) - 3 \left(\frac{\rho^2}{x(x^2+\rho^2)^{\frac{5}{2}}} \right) \\ = \; & 0 . \end{aligned} \tag{3.39}$$

From which we can construct the zero mode propagator

$$S_0(x,y)_{\alpha,i\,;\beta,j} = \frac{\rho^2}{\pi^2 \lambda} \frac{(\bar{\sigma}_l \epsilon)_{\alpha i} \, (x-x_0)_l \, (\epsilon \sigma_\rho)_{j\beta} \, (y-y_0)_\rho}{[(x-x_0)^2+\rho^2]^{\frac{3}{2}} \, [(y-y_0)^2+\rho^2]^{\frac{3}{2}} \, |x-x_0||y-y_0|} , \tag{3.40}$$

where λ is the normalization factor. Instead of the instanton, in the presence of an anti-instanton, the zero mode reads

$$\bar{S}_0(x,y)_{\alpha,i\,;\beta,j} = \frac{\rho^2}{\pi^2\lambda}\frac{(\epsilon\sigma_l)_{i\alpha}\,(x-x_0)_l\;(\bar{\sigma}_\rho\epsilon)_{\beta j}\,(y-y_0)_\rho}{\left[(x-x_0)^2+\rho^2\right]^{\frac{3}{2}}\left[(y-y_0)^2+\rho^2\right]^{\frac{3}{2}}|x-x_0||y-y_0|}\,. \tag{3.41}$$

These two propagators are written in Euclidean space. Once we rotate them back to Minkowski space, we need to be careful with the upper and lower indices, also we need to define the $\epsilon^{\alpha i}$ accordingly.

One may argue that though one instanton selects left-handed fermion, the anti-instanton would select the right-handed one and in sum it should not result in any effect. However, as we will show later, it is not so. For example, if the incoming quark is polarized, then the instanton will be selected accordingly and thus the instanton and anti-instantons would be weighted differently in the ensemble. Other example is that, if the observant, instead of being the cross section of one particle, is the correlation of two outgoing particles. Then though the number of instantons equal the number of anti-instantons, the fluctuations will result in very important $\mathcal{P}$-odd effects.

3.1.3 Measure

The complete discussion of the measure for the zero modes is out of the scope of this paper. Here, let us explain how the bosonic zero modes we obtain before contribute to the Jacobian of the path integral. Notice, for QCD instanton instanton, the bosonic zero modes we listed before are not complete because we did not show the embedding of $SU(2)$ group in $SU(3)$ group. And also, the Fermionic zero modes are important in the measure.

Let us follow the logic in one of the author's papers [16]. To see the relation between the zero modes and the Jacobian, we write it in the quantum state language

$$\left|A_\mu^{\rm cl}\right\rangle = Z_\mu^{(1)}\left|\gamma^{(1)}\right\rangle \otimes Z_\mu^{(2)}\left|\gamma^{(2)}\right\rangle \otimes \cdots\,. \tag{3.42}$$

If $\left|\gamma^{(i)}\right\rangle$ is normalized, the norm of $\left|A_\mu^{\rm cl}\right\rangle$ is given by

$$\left\langle A_\mu^{\rm cl}|A_\mu^{\rm cl}\right\rangle = \det\left|U^{ij}\right|\,, \tag{3.43}$$

where

$$U^{ij} \equiv \langle Z_\mu^{(i)}\big|Z_\mu^{(j)}\rangle = -\frac{2}{g^2}\int d^4x\,{\rm Tr}\left[Z_\mu^{(i)}Z_\mu^{(j)}\right]\,. \tag{3.44}$$

If $\left|\gamma^{(i)}\right\rangle$ is orthogonal to each other as it is for results we obtained above, then U^{ij} should be a diagonal matrix. For simplicity, we adopt the approximation

$$\left|A_\mu^{\rm cl}\right\rangle \approx \sqrt{\det|U^{ij}|}\,\left|\gamma^{(1)}\right\rangle \otimes \left|\gamma^{(2)}\right\rangle \otimes \cdots\,, \tag{3.45}$$

where it has the same norm as Eq. (3.42). Hence,

$$[\mathrm{Jac}]_{\gamma^{(i)}} \approx \sqrt{\det|U^{ij}|}\,, \tag{3.46}$$

where the corrections come from two-loop diagrams or higher [116].

Now, let us calculate them one by one

- Translational ($\gamma^{(\nu)} = x_0^\nu$):

$$U^{\mu\nu} = \frac{8\pi^2}{g^2}\delta^{\mu\nu}\,. \tag{3.47}$$

- Gauge orientation ($\gamma^{(\alpha)} = \varphi^\alpha$):

$$U_{\alpha\beta}(\varphi) = e_\alpha{}^a(\varphi)\, e_\beta{}^a(\varphi)\, \frac{4\pi^2}{g^2}\rho^2\,, \tag{3.48}$$

  where $e_\alpha{}^a(\varphi)$ is the group vielbein.

- Dilatational (size ρ):

$$U^{\rho\rho}(\varphi) = \frac{16\pi^2}{g^2}\,. \tag{3.49}$$

In summary, for the 4D $SU(2)$ anti-instanton solution we obtain

$$\begin{aligned}
[\mathrm{Jac}]^{\rm cl}_{\rm transl} &= \left(\frac{8\pi^2}{g^2}\right)^2\,,\\
[\mathrm{Jac}]^{\rm cl}_{\rm gauge} &= \sqrt{\det g_{\alpha\beta}(\varphi)}\left(\frac{4\pi^2}{g^2}\right)^{\frac{3}{2}}\rho^3\,,\\
[\mathrm{Jac}]^{\rm cl}_{\rho} &= \frac{4\pi}{g}\,.
\end{aligned} \tag{3.50}$$

3.2 Non-zero mode

In this section, we will review the steps to derive the spin-0 propagator and spin-1/2 propagator in [119].

3.2.1 Spin-0

Our goal in this subsection is to solve the scalar propagator in instantons background. The calculation can be easily generalized to anti-instantons. The instantons solution in singular gauge reads

$$A_\mu = \frac{1}{2}\sigma_{\mu\nu}\partial_\nu \ln\Pi(x)\,, \tag{3.51}$$

where

$$\Pi(x) = 1 + \sum_{i=1}^{k} \frac{\rho_i^2}{(x-c_i)^2} \tag{3.52}$$

and c_i is the center of each instanton with size ρ_i. For only one instanton centering at $c_i = 0$, we have

$$\partial_\nu \ln\left(1+\frac{\rho^2}{x^2}\right) = \frac{-2x_\nu \frac{\rho^2}{x^4}}{1+\frac{\rho^2}{x^2}} = -2\frac{x_\nu}{x^2}\frac{\rho^2}{x^2+\rho^2}\,, \tag{3.53}$$

and hence

$$A_\mu = -\sigma_{\mu\nu}x_\nu \frac{\rho^2}{x^2(x^2+\rho^2)}\,, \tag{3.54}$$

which is indeed Eq. (2.60).

The scalar propagator $\Delta(x,y)$ satisfies

$$-D^2\Delta(x,y) = \delta(x-y)\,. \tag{3.55}$$

First

$$\begin{aligned} D^2 &= (\partial_\mu + A_\mu)^2 \\ &= \left(\partial_\mu + \frac{1}{2}\sigma_{\mu\nu}\partial_\nu \ln\Pi(x)\right)^2 \\ &= \partial^2 + \sigma_{\mu\nu}\left[\partial_\nu \ln\Pi(x)\right]\partial_\mu + \frac{1}{4}\sigma_{\mu\nu}\sigma_{\mu\rho}\left[\partial_\nu \ln\Pi(x)\right]\left[\partial_\rho \ln\Pi(x)\right] \\ &= \partial^2 + \sigma_{\mu\nu}\left[\partial_\nu \ln\Pi(x)\right]\partial_\mu - \frac{3}{4}\left[\partial_\mu \ln\Pi(x)\right]^2\,, \end{aligned} \tag{3.56}$$

where we used

$$\bar\sigma_\mu\sigma_{\nu\rho} = \delta_{\mu\nu}\bar\sigma_\rho - \delta_{\mu\rho}\bar\sigma_\nu - \epsilon_{\mu\nu\rho\sigma}\sigma_\sigma\,. \tag{3.57}$$

Second, let us calculate

$$\begin{aligned}
&\sqrt{\Pi(x)}(\sigma\partial)\frac{1}{\Pi(x)}(\bar{\sigma}\partial)\sqrt{\Pi(x)} \\
&= \sigma_\mu\bar{\sigma}_\nu\left[\frac{1}{2}\frac{(\partial_\mu\partial_\nu\Pi)}{\Pi}-\frac{3}{4}\frac{(\partial_\mu\Pi)(\partial_\nu\Pi)}{\Pi^2}+\frac{1}{2}\frac{(\partial_\nu\Pi)}{\Pi}\partial_\mu-\frac{1}{2}\frac{(\partial_\mu\Pi)}{\Pi}\partial_\nu+\partial_\mu\partial_\nu\right] \\
&= \partial^2+\sigma_{\mu\nu}\left[\partial_\nu \ln\Pi(x)\right]\partial_\mu-\frac{3}{4}\left[\partial_\mu \ln\Pi(x)\right]^2\,, \qquad (3.58)
\end{aligned}$$

where we denoted

$$(\sigma\partial)\doteq\sigma_\mu\partial_\mu \quad \text{and} \quad (\bar{\sigma}\partial)\doteq\bar{\sigma}_\mu\partial_\mu\,. \qquad (3.59)$$

Obviously, Eq. (3.56) equals Eq. (3.58), which would greatly simplify our calculation below. Also we would like to emphasize that

$$\begin{aligned}
\frac{1}{\Pi(x)}\partial^2\Pi(x) &= \frac{2}{\Pi(x)}\sum_{i=1}^{k}\rho_i^2\,\partial_\mu\frac{x^\mu-c_i^\mu}{(x-c_i)^4} \\
&= 0\,. \qquad (3.60)
\end{aligned}$$

Notice, the $\Pi^{-1}(x)$ in the equation above is necessary bcause

$$\frac{1}{4\pi^2}\partial^2\left(\frac{1}{x^2}\right)=-\delta(x)\,. \qquad (3.61)$$

Also because of Eq. (3.61) above, we expect that at the singular point, the propagator:

$$\Delta(x,y)\sim\frac{1}{4\pi^2}\frac{1}{(x-y)^2}\,. \qquad (3.62)$$

Therefore, we now write down the ansatz

$$\Delta(x,y)=\frac{1}{\sqrt{\Pi(x)}}\frac{f(x,y)}{4\pi^2(x-y)^2}\frac{1}{\sqrt{\Pi(y)}}\,, \qquad (3.63)$$

where

$$f(x,x)=\Pi(x)\,. \qquad (3.64)$$

Combining everything above, we obtain

$$\begin{aligned}
-\delta(x-y) &= D^2\Delta(x,y) \\
&= \sqrt{\Pi(x)}(\sigma\partial)\frac{1}{\Pi(x)}(\bar{\sigma}\partial)\frac{f(x,y)}{4\pi^2(x-y)^2}\frac{1}{\sqrt{\Pi(y)}}\,. \qquad (3.65)
\end{aligned}$$

It can be simplified as

$$(\sigma\partial)\frac{1}{\Pi(x)}(\bar{\sigma}\partial)\frac{f(x,y)}{4\pi^2(x-y)^2} = -\frac{1}{\sqrt{\Pi(x)}}\delta(x-y)\sqrt{\Pi(y)}$$
$$= -\delta(x-y)\,. \tag{3.66}$$

We also notice

$$(\sigma\partial)(\bar{\sigma}\partial)\frac{1}{4\pi^2(x-y)^2} = -\delta(x-y)\,. \tag{3.67}$$

Therefore

$$\frac{1}{\Pi(x)}(\bar{\sigma}\partial)\frac{f(x,y)}{4\pi^2(x-y)^2} - (\bar{\sigma}\partial)\frac{1}{4\pi^2(x-y)^2} = 0\,. \tag{3.68}$$

After simple algebra

$$(\bar{\sigma}\partial)f - 2\frac{\bar{\sigma}_\mu(x^\mu - y^\mu)}{(x-y)^2}[f-\Pi(x)] = 0\,. \tag{3.69}$$

The solution satisfies the equation above is not easy to obtain directly. Here we write it down and check if it solves the equation above. The solution reads

$$f(x,y) = 1 + \sum_{i=1}^{k}\rho_i^2\frac{\underline{(x-c_i)}}{(x-c_i)^2}\frac{\overline{(y-c_i)}}{(y-c_i)^2}\,, \tag{3.70}$$

where

$$\underline{(\cdots)} \equiv \sigma_\mu(\cdots)_\mu \quad \text{and} \quad \overline{(\cdots)} \equiv \bar{\sigma}_\mu(\cdots)_\mu\,. \tag{3.71}$$

First of all, the condition

$$f(x,x) = \Pi(x) \tag{3.72}$$

is satisfied. Second

$$[f-\Pi(x)] = \sum_{i=1}^{k}\frac{\rho_i^2}{(x-c_i)^2(y-c_i)^2}\left[\underline{(x-c_i)}\overline{(y-c_i)} - (y-c_i)^2\right]\,. \tag{3.73}$$

We can use

$$\begin{aligned}
&\overline{(x-y)}\left[\underline{(x-c_i)}\overline{(y-c_i)} - (y-c_i)^2\right] \\
=\;& \left[\overline{(x-c_i)} - \overline{(y-c_i)}\right]\left[\underline{(x-c_i)}\overline{(y-c_i)} - (y-c_i)^2\right] \\
=\;& (x-c_i)^2\overline{(y-c_i)} - \overline{(x-c_i)}(y-c_i)^2 + \overline{(y-c_i)}(y-c_i)^2 \\
& -\overline{(y-c_i)}\underline{(x-c_i)}\overline{(y-c_i)} \\
=\;& (x-c_i)^2\overline{(y-c_i)} - 2(x-c_i)_\mu(y-c_i)_\mu\overline{(y-c_i)} + \overline{(y-c_i)}(y-c_i)^2 \\
=\;& \left[(x-c_i)_\mu - (y-c_i)_\mu\right]^2\overline{(y-c_i)}\,,
\end{aligned} \tag{3.74}$$

where we used

$$\begin{aligned} & \overline{(y-c_i)}\overline{(x-c_i)}\overline{(y-c_i)} \\ = \; & 2(x-c_i)_\mu (y-c_i)_\mu \overline{(y-c_i)} - (y-c_i)^2 \overline{(x-c_i)} \,. \end{aligned} \tag{3.75}$$

In sum

$$\begin{aligned} 2\frac{\overline{x-y}}{(x-y)^2}[f-\Pi(x)] &= 2\sum_{i=1}^{k} \frac{\rho_i^2 \overline{(y-c_i)}}{(x-c_i)^2(y-c_i)^2} \\ &= (\bar{\sigma}\partial) f \,. \end{aligned} \tag{3.76}$$

In summary, we obtain the spin-0 propagator in multi-instantons background:

$$\Delta(x,y) = \frac{1}{\sqrt{\Pi(x)}} \frac{f(x,y)}{4\pi^2(x-y)^2} \frac{1}{\sqrt{\Pi(y)}} \,, \tag{3.77}$$

where

$$f(x,y) = 1 + \sum_{i=1}^{k} \rho_i^2 \frac{(x-c_i)}{(x-c_i)^2} \frac{\overline{(y-c_i)}}{(y-c_i)^2} \,. \tag{3.78}$$

For the spin-0 propagator in multi-anti-instantons, we have

$$f(x,y) = 1 + \sum_{i=1}^{k} \rho_i^2 \frac{\overline{(x-c_i)}}{(x-c_i)^2} \frac{(y-c_i)}{(y-c_i)^2} \,. \tag{3.79}$$

3.2.2 Spin-1/2

It is fairly easy to obtain the propagator once we have obtained the scalar propagator Eq. (3.77). The logic is the following: we need to find the propagator S satisfying:

$$\not{D} S = \hat{P} \,, \tag{3.80}$$

where $\hat{P}$ is the operator projecting to the nonzero mode subspace. Now let us show that

$$S = \not{D}\Delta \left(\frac{1+\gamma_5}{2}\right) + \Delta \not{D} \left(\frac{1-\gamma_5}{2}\right) \,. \tag{3.81}$$

First

$$\begin{aligned} \hat{P} &= \not{D} S \\ &= \left(\frac{1+\gamma_5}{2}\right) + \not{D}\Delta\not{D} \left(\frac{1-\gamma_5}{2}\right) \,, \end{aligned} \tag{3.82}$$

where we used

$$\not{D}\not{D} = D^2 \,. \tag{3.83}$$

Check

$$\begin{aligned}
\hat{P}^2 &= \left(\frac{1+\gamma_5}{2}\right) + \left(\frac{1+\gamma_5}{2}\right) \not{D}\Delta\not{D} \left(\frac{1-\gamma_5}{2}\right) + \not{D}\Delta\not{D} \left(\frac{1-\gamma_5}{2}\right)\left(\frac{1+\gamma_5}{2}\right) \\
&\quad + \not{D}\Delta\not{D} \left(\frac{1-\gamma_5}{2}\right) \not{D}\Delta\not{D} \left(\frac{1-\gamma_5}{2}\right) \\
&= \left(\frac{1+\gamma_5}{2}\right) + \not{D}\Delta\not{D} \left(\frac{1-\gamma_5}{2}\right) \\
&= \hat{P}
\end{aligned} \tag{3.84}$$

where we used

$$(1+\gamma_5)(1-\gamma_5) = 0 \,. \tag{3.85}$$

As we can see, $\hat{P}$ in indeed the projection operator.

By combining Eq. (3.81) and Eq. (3.77), we can obtain the spin-1/2 propagator in multi-(anti-)instantons background. Similar to Subsec-3.1.2, we need to be careful with the spinor and color indices since they are mixed. For simplicity, we only list the spin-1/2 propagator in single (anti-)instanton: [121]

- spin-1/2 propagator in one instanton

$$\begin{aligned}
S_{\rm NZ}(x,y)_{\alpha\beta;ij} &= \frac{1}{2\pi^2}\frac{1}{\sqrt{\Pi(x)}}\Big[\frac{\overline{(x-y)_{\alpha\beta}}}{(x-y)^4}\left(\delta_{ij} + \rho^2\frac{(\underline{x}\,\overline{y})_{ij}}{x^2y^2}\right) \\
&\qquad + \frac{\rho^2\ (\sigma_\mu)_{\alpha\beta}}{2(\rho^2+y^2)}\frac{\left(\underline{x}\,\overline{(x-y)}\,\sigma_\mu\,\overline{y}\right)_{ij}}{x^2(x-y)^2y^2}\Big]\frac{1}{\sqrt{\Pi(y)}} \,.
\end{aligned} \tag{3.86}$$

- spin-1/2 propagator in one anti-instanton

$$\begin{aligned}
\bar{S}_{\rm NZ}(x,y)_{\alpha\beta;ij} &= \frac{1}{2\pi^2}\frac{1}{\sqrt{\Pi(x)}}\Big[\frac{\overline{(x-y)_{\alpha\beta}}}{(x-y)^4}\left(\delta_{ij} + \rho^2\frac{(\underline{x}\,\overline{y})_{ij}}{x^2y^2}\right) \\
&\qquad + \frac{\rho^2\ (\bar{\sigma}_\mu)_{\alpha\beta}}{2(\rho^2+y^2)}\frac{\left(\underline{x}\,\bar{\sigma}_\mu\,\underline{(x-y)}\,\overline{y}\right)_{ij}}{x^2(x-y)^2y^2}\Big]\frac{1}{\sqrt{\Pi(y)}} \,.
\end{aligned} \tag{3.87}$$

  α and β are spinor indices while i and j are color indices.

Chapter 4

Spin Effects Through One Instanton

4.1 Spin physics and instanton

To best illustrate the important role played by instantons in QCD spin physics, consider a light quark in the fundamental color representation propagating in an external SU(2) colored Yang-Mills gauge field with a chromo-magnetic field $\mathbf{B}$ and a chromo-electric field $\mathbf{E}$ field [47]. Generically [123]

$$\left(-\nabla^2 + 4g_s\,\mathbf{S}\cdot(\mathbf{B}\mp\mathbf{E})\right)\varphi^{\pm} = 0 \tag{4.1}$$

with $i\nabla = i\partial + A$ and $\mathbf{S}^a$ the SU(2) spin generators. The signs in Eq. (4.1) refer to the chirality of the quark. Large quark amplitudes as polarized zero modes occur when the spin contribution (second term) balances the squared kinetic contribution (first term) in Eq. (4.1). For a self-dual instanton with $\mathbf{B} = \mathbf{E}$ the negative chirality quark produces a large zero mode state through the magnetic moment term

$$\left(-\nabla^2 + 4g_s\,\sigma\cdot\mathbf{B}\right)\varphi_D^{-} = 0 \tag{4.2}$$

and similarly for an anti-self-dual anti-instanton. Typically $\mathbf{E},\mathbf{B} \approx 1/g_s\rho^2$ with $\rho \approx 1/3$ fm the instanton or anti-instanton size in the vacuum and g_s the strong gauge coupling. So the induced and large magnetic moment in Eq. (4.2) is about $\mu_D \approx \mathbf{n}\rho^4$ where $\mathbf{n} \approx 1\,\mathrm{fm}^{-4}$ is the density of instantons in the vacuum [17, 118]. In contrast, perturbative QCD generates small magnetic moments or $\mu_{PT} \approx g_s$.

In a similar way, a propagating gluon in an external SU(2) colored gauge field acquires also an effective and large magnetic moment. Indeed, the analogue of Eq. (4.1) for a massless gluon in a covariant (Feynman) background gauge $\nabla^\mu \mathbf{a}_\mu = 0$ is

$$\left(-\nabla^2 \delta_{\mu\nu} - 2ig_s F_{\mu\nu}\right) \mathbf{a}^\nu = 0 \tag{4.3}$$

The colored gluon in Eq. (4.3) has two physical polarizations as both the longitudinal and time-like are gauge artifacts. Using the decomposition $\mathbf{a}_\mu = \mathbf{e}^a_\mu \mathbf{\Psi}^a$ with a transverse we have

$$\left(-\nabla^2 + \frac{g_s}{2}\Sigma^{\mu\nu} F_{\mu\nu}\right) \mathbf{\Psi}^a = 0 \tag{4.4}$$

with $i\Sigma_{\mu\nu} = 4\mathbf{e}^T_\mu \mathbf{e}_\nu$ playing the role of the spin in the gluon transverse polarization space. Eq. (4.4) is the analogue of Eq. (4.3) with an induced and large magnetic moment $\mu_G \approx \mathbf{n}\rho^4$ as well.

In the Appendix we give a quantitative derivation of these estimates. These semi-classical and large spin effects will now be explored in processes with polarized protons and in peripheral AA collisions sensitive to $\mathcal{P}$-odd fluctuations, in the framework of the instanton liquid model.

4.2 Single spin asymmetry in semi-inclusive deep inelastic scattering

To set up the notations for the semi-inclusive processes in deep inelastic scattering, we consider a proton at rest in the LAB frame with transverse polarization as depicted in Fig. 4.1 [47].

The incoming and outgoing leptons are unpolarized. The polarization of the target proton in relation to the DIS kinematics is shown in Fig. 4.2. Throughout, the spin dependent asymmetries will be evaluated at the partonic level. Their conversion to the hadronic level will follow the qualitative arguments presented in [41, 42, 43].

In general, the spin averaged leptonic tensor reads

$$L^{\mu\nu} = \frac{1}{2} \operatorname{tr}\left[\not{l}' \gamma_\mu \not{l} \gamma_\nu\right] \tag{4.5}$$

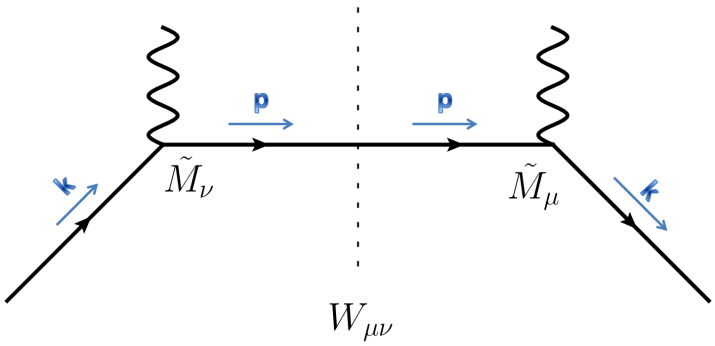

Figure 4.1: p and k are the momenta of the incoming and outgoing quark. The lepton and the quark exchange one photon in the single instanton background.

while the color averaged hadronic tensor in the one instanton background reads

$$W_{\mu\nu} = \sum_{\text{color}} \frac{1}{2} \text{tr} \left[\not{k} \tilde{M}_\mu \not{p} (1 + \gamma_5 \not{s}) \gamma_0 \left(\tilde{M}_\nu \right)^\dagger \gamma_0 \right] \tag{4.6}$$

with the constituent vertex

$$\tilde{M}_\mu = \gamma_\mu + \tilde{M}_\mu^{(1)} \tag{4.7}$$

that includes both the perturbative γ_μ and the non-perturbative insertion $M_\mu^{(1)}$.

Let us now derive the non-perturbative insertion $M_\mu^{(1)}$ following the original arguments in [121, 43, 44]: according to [119, 121, 122, 43], the zero mode quark propagator in the single instanton background after Fourier transformation with respect to the incoming momentum p is

$$S_0(x,p)_{\dot{\beta}}{}^{j}{}_{i\delta} = \frac{2\rho^2}{\lambda} \frac{x^l (\overline{\sigma}_l)_{\dot{\beta}\gamma} \varepsilon^{\gamma j} \varepsilon_{i\delta}}{(x^2 + \rho^2)^{\frac{3}{2}} |x|} \tag{4.8}$$

Note the chirality of the zero mode flips as $|L\rangle \langle R|$ as depicted in Fig. 4.3. The incoming quark is left-handed and has momentum p (on-shell). ρ is the size of instanton and λ is the mean virtuality. β and δ are spatial indices,

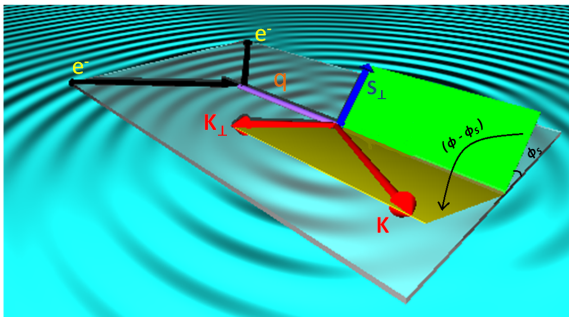

Figure 4.2: The lepton and photon are in the same plane. The angle between the transversely polarized spin $s_\perp$ and this plane is ϕ_s. The angle between the transversely spatial momentum $K_\perp$ of the outgoing pion and the plane is ϕ.

while j and i are color indices. In Euclidean space, $\sigma_\mu = (\vec{\sigma}, iI)$, $\bar{\sigma}_\mu = (\vec{\sigma}, iI)$ and $\epsilon^{01} = -\epsilon^{10} = -\epsilon_{01} = \epsilon_{10}$ [116]. The right-handed non-zero mode quark propagator in the single instanton after Fourier transformation with respect to the outgoing momentum k is [119, 121, 43]

$$S_{nz}(k,x)^{\beta i}{}_{j\alpha} = -\delta^\beta_\alpha \left(\delta^i_j + \frac{\rho^2}{x^2} \frac{(\sigma_\rho \overline{\sigma}_r)^i{}_j k^\rho x^r}{2k\cdot x} \left(1 - e^{-ik\cdot x}\right) \right) \frac{|x|}{\sqrt{x^2+\rho^2}} e^{ik\cdot x} \tag{4.9}$$

Consider the process depicted in Fig. 4.3: the incoming left-handed quark meets one instanton and flips its chirality (zero-mode), then exchanges one photon, and finally becomes an outgoing right-handed quark. As a result, the nonperturbative insertion $M^{(1)}_\mu$ reads

$$\left(\tilde{M}^{(1)}_\mu\right)^{\beta i}{}_{i'\delta} = \int d^4x\, e^{-iq\cdot x}\, S_{nz}(k,x)^{\beta i}{}_{j\alpha}\, \sigma^{\alpha\dot{\beta}}_\mu\, S_0(x,p)_{\dot{\beta}}{}^{j}{}_{i'\delta} \tag{4.10}$$

All the other parts of the diagram are trivial in color, therefore we take the trace of color indices i and i'. To further simplify the result, we need the following formula [116]

$$\delta^\beta_\alpha \delta^i_j (\sigma_\mu)^{\alpha\dot{\beta}} (\overline{\sigma}_l)_{\dot{\beta}\gamma} \varepsilon^{\gamma j} \varepsilon_{i\delta} = (\sigma_\mu \overline{\sigma}_l)^\beta{}_\delta \tag{4.11}$$

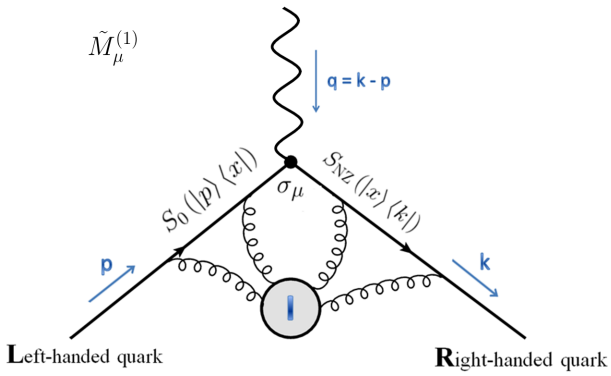

Figure 4.3: The incoming left-handed quark with momentum p meets one instanton and flips its chirality. The outgoing right-handed quark carries momentum k. The momentum of the photon is $q = p - k$. S_0 and S_{nz} stand for the zero-mode quark propagator and the non-zero mode quark propagator in the single instanton background respectively.

$$\delta_\alpha^\beta(\sigma_\rho\overline{\sigma}_r)^i{}_j(\sigma_\mu)^{\alpha\dot{\beta}}(\overline{\sigma}_l)_{\dot{\beta}\gamma}\varepsilon^{\gamma j}\varepsilon_{i\delta} = (\sigma_\mu\overline{\sigma}_l\sigma_r\overline{\sigma}_\rho)^\beta{}_\delta \tag{4.12}$$

Combining all the equations above, we obtain

$$\tilde{M}_\mu^{(1)} = -\int d^4x \quad \Big(\quad \frac{2\rho^2}{\lambda}\sigma_\mu\overline{\sigma}_l e^{ip\cdot x}\frac{x^l}{(x^2+\rho^2)^2} + \sigma_\mu\overline{\sigma}_\rho k^\rho\frac{\rho^4}{\lambda}(e^{ip\cdot x} - e^{-iq\cdot x})\frac{1}{(x^2+\rho^2)^2(k\cdot x)}\Big) \tag{4.13}$$

The d^4x integration in Eq. (4.13) can be done with the help of the following formula ($p^2 \longrightarrow 0$)

$$\int d^4x \;\; e^{ip\cdot x}\frac{x^l}{(x^2+\rho^2)^2} = i2\pi^2\frac{p^l}{p^2} \tag{4.14}$$

$$\begin{aligned}\int d^4x\frac{e^{ip\cdot x}}{(x^2+\rho^2)^2(k\cdot x)} &= -i\frac{\pi^2}{p\cdot k}\frac{\rho|p|}{\rho^2}K_1(\rho|p|) \\ &= i\frac{2\pi^2}{q^2}\frac{\rho|p|}{\rho^2}K_1(\rho|p|)\end{aligned} \tag{4.15}$$

where we used $-2p\cdot k = (k-p)^2 - k^2 - p^2 \approx q^2$. In our paper [44], we explicitly showed that all terms proportional to $\overline{\sigma}_l p^l$ vanish. Thus

$$\tilde{M}_\mu^{(1)} = -i\frac{4\pi^2\rho^2}{\lambda}\sigma_\mu\overline{\sigma}_l\frac{k^l}{q^2}[f(\rho|p|) - f(\rho|q|)] \tag{4.16}$$

where $f(a) = aK_1(a)$ As the incoming quark with momentum p is on-shell and the mass of the quark is small ($p^2 \longrightarrow 0$), we have

$$f(\rho|p|) = \rho|p|K_1(\rho|p|) \longrightarrow \rho|p|\frac{1}{\rho|p|} = 1 \tag{4.17}$$

Since $q^2 < 0$ in SIDIS, we define $Q^2 = -q^2 > 0$. Eq. (4.16) simplifies to

$$\tilde{M}_\mu^{(1)} = i\frac{4\pi^2\rho^2}{\lambda}\sigma_\mu\overline{\sigma}_l\frac{k^l}{Q^2}\left[1 - f(\rho Q)\right] \tag{4.18}$$

Here we note that Eq. (4.18) is derived from Eq. (4.10) which pictorially reads

- Left-handed quark ($\vec{p}$) $\xrightarrow{\text{Instanton}}$ Right-handed quark (zero mode) $\xrightarrow{\text{Photon}\,(\vec{q})}$ Right-handed quark ($\vec{k}$)

where $\vec{q} = \vec{k} - \vec{p}$. On the other hand, if we consider

- Right-handed quark ($\vec{k}$) $\xrightarrow{\text{Photon}\,(-\vec{q})}$ Right-handed quark (zero mode) $\xrightarrow{\text{Anti-instanton}}$ Left-handed quark ($\vec{p}$)

instead of Eq. (4.18), we would obtain

$$\tilde{M}_\mu^{(1)} = -i\frac{4\pi^2\rho^2}{\lambda^\dagger}\sigma_\mu\overline{\sigma}_l\frac{k^l}{Q^2}\left[1 - f(\rho Q)\right] \tag{4.19}$$

where we have taken the conjugate of Eq. (4.18) and replaced $p \leftrightarrow k$. Thus

$$M_\mu^{(1)} = 4\pi^2\rho^2\left(i\frac{\mathbf{P}_+}{\lambda}\sigma_\mu\overline{\sigma}_l k^l - i\frac{\mathbf{P}_-}{\lambda^\dagger}\sigma_l\overline{\sigma}_\mu p^l\right)\frac{\left[1 - f(\rho Q)\right]}{Q^2} \tag{4.20}$$

where $\mathbf{P}_\pm = 1/0$ denote one or no instanton/anti-instanton. Similarly, for the processes depicted pictorially as

- Right-handed quark ($\vec{p}$) $\xrightarrow{\text{Anti-Instanton}}$ Left-handed quark (zero mode) $\xrightarrow{\text{Photon}\,(\vec{q})}$ Left-handed quark ($\vec{k}$)
- Left-handed quark ($\vec{k}$) $\xrightarrow{\text{Photon}\,(-\vec{q})}$ Left-handed quark (zero mode) $\xrightarrow{\text{Instanton}}$ Right-handed quark ($\vec{p}$)

Thus the result combining both the instanton and anti-instanton contributions

$$M_\mu^{(1)} = 4\pi^2\rho^2 \left(i\frac{\mathbf{P}_+}{\lambda}\gamma_\mu \not{k} - i\frac{\mathbf{P}_-}{\lambda^\dagger}\not{p}\gamma_\mu \right) \frac{[1 - f(\rho Q)]}{Q^2} \tag{4.21}$$

Now, we need to average Eq. (4.21) using the instanton liquid model. The standard averaging in the vacuum is

$$\left\langle \frac{1}{\lambda} \right\rangle = \frac{1}{2N} \int \frac{d\lambda}{\lambda}\, n(\lambda) = -i\pi \frac{n(0)}{N} \tag{4.22}$$

where by Banks-Casher relation is used $\pi n(0)/N = -\left\langle q^\dagger q \right\rangle$. However, we note that $\mathbf{P}_\pm$ in Eq. (4.21) means that we fix an instanton or anti-instanton pertaining to the polarized hadron prior to the averaging. This means that the pertinent eigenvalue distribution instead is

$$n(\pm, \lambda) = n(\lambda) - \delta(\lambda \mp \lambda_*/N) \tag{4.23}$$

with λ_* a typical eigenvalue in the zero-mode-zone. Technically $n(\pm, \lambda)$ amounts to fixing an instanton or anti-instanton, and averaging over the remainder of the instanton-antiinstanton liquid by removing 1-row and 1-column in the $N \times N$ overlap matrix of zero-modes $\mathbf{T_{IJ}}$ for the fixed instanton or anti-instanton while averaging with det$\mathbf{T}$ in the instanton liquid model. Explicitly, this amounts to

$$\frac{\mathbf{P}_\pm}{\lambda} \xrightarrow{\text{fix an instanton/anti-instanton}} \left\langle \frac{\mathbf{P}_\pm}{\lambda} \right\rangle = \frac{1}{N} \int \frac{d\lambda}{\lambda}\, n(\pm, \lambda) = \mp \frac{1}{\lambda_*} - i\pi \frac{n(0)}{N} \tag{4.24}$$

Thus

$$\begin{aligned}\left\langle M_\mu^{(1)}\right\rangle = & \quad 4\pi^2\rho^2\frac{\pi n(0)}{N}\left(\gamma_\mu \not{k} + \not{p}\gamma_\mu\right)\frac{[1-f(\rho Q)]}{Q^2} \\ & - \; i\frac{4\pi^2\rho^2}{\lambda_*}\left(\gamma_\mu \not{k} + \not{p}\gamma_\mu\right)\frac{[1-f(\rho Q)]}{Q^2} \end{aligned} \tag{4.25}$$

The real part can be re-written as

$$\begin{aligned} & 4\pi^2\rho^2\frac{\pi n(0)}{N}\left(\gamma_\mu \not{k} + \not{p}\gamma_\mu\right)\frac{[1-f(\rho Q)]}{Q^2} \\ = \quad & 4\pi^2\rho^2\frac{\pi n(0)}{N}\frac{[1-f(\rho Q)]}{Q^2}q^\nu\sigma_{\mu\nu} + 4\pi^2\rho^2\frac{\pi n(0)}{N}\frac{[1-f(\rho Q)]}{Q^2}\left(\not{k}\gamma_\mu - \gamma_\mu\not{p}\right) \\ \longrightarrow \quad & 4\pi^2\rho^2\frac{\pi n(0)}{N}\frac{[1-f(\rho Q)]}{Q^2}q^\nu\sigma_{\mu\nu} \end{aligned} \tag{4.26}$$

where $\sigma_{\mu\nu} = [\gamma_\mu, \gamma_\nu]$. The parts proportional to $\not{k}\gamma_\mu$ and $\gamma_\mu\not{p}$ vanish as discussed in [124]. The imaginary part is

$$-i\frac{4\pi^2\rho^2}{\lambda_*}\left(\gamma_\mu \not{k} + \not{p}\gamma_\mu\right)\frac{[1-f(\rho Q)]}{Q^2} \tag{4.27}$$

and contributes to SSA in SIDIS as noted in [43, 44].

$$\mathrm{Im}\left(\left\langle \tilde{M}_\mu^{(1)}\right\rangle\right) = -\frac{4\pi^2\rho^2}{\lambda_* Q^2}[\gamma_\mu \not{k} + \not{p}\gamma_\mu](1-f(\rho Q)) \tag{4.28}$$

with $f(a) = aK_1(a)$ with K_1 a modified Bessel function. Here ρ is the instanton size and $\lambda_* \approx 1/(0.2\mathrm{GeV})^3$ [17, 118] is a typical near-mode in the zero-mode-zone as discussed. The electromagnetic gauge invariance in the hadronic tensor in the random instanton model of the vacuum is detailed in [120]. The normalized lepton-hadron cross section of Fig.4.1 follows in the form

$$\frac{d\sigma}{dxdydzd\phi} = y\frac{\alpha^2}{Q^6}L^{\mu\nu}W_{\mu\nu}\sum_i e_i^2 f_i(x,Q^2)D_i(z) \tag{4.29}$$

with $y = P\cdot q/P\cdot l$, where e_i is the i-parton electric charge, f_i its momentum fraction distribution and D_i its fragmentation function.

The perturbative contribution to the hadronic tensor follows from $M_\mu \to \gamma_\mu$,

$$W^{(0)}_{\mu\nu} = \frac{N_c}{2}\,\mathrm{tr}\,[\not{k}\gamma_\mu \not{p}\gamma_\nu] \tag{4.30}$$

Thus the leading perturbative contribution

$$\frac{d^{(0)}\sigma}{dxdydzd\phi} = 2N_c\frac{\alpha^2}{Q^2}\frac{1+(1-y)^2}{y}\sum_i e_i^2 f_i(x,Q^2)D_i(z) \tag{4.31}$$

with N_c the number of colors. The sum is over the charges e_i of the quarks. The non-perturbative instanton contribution to Eq. (4.29) is a cross contribution in the hadronic tensor in Eq. (4.29) after inserting the one-instanton vertex Eq. (4.28)

$$\begin{aligned}\left\langle W^{(1)}_{\mu\nu}\right\rangle &= i\frac{2\pi^2\rho^2}{\lambda_* Q^2}[1-f(\rho Q)]\big(\,\mathrm{tr}\,[\not{k}\gamma_\mu\not{p}\gamma_5\not{s}(\gamma_\nu\not{p}+\not{k}\gamma_\nu)] \\ &\qquad - \mathrm{tr}\,[\not{k}(\gamma_\mu\not{k}+\not{p}\gamma_\mu)\not{p}\gamma_5\not{s}\gamma_\nu]\big) \qquad (4.32)\\ &= -\frac{16\pi^2\rho^2}{\lambda_* Q^2}(1-f(\rho Q))(p+k)_{\{\mu}\epsilon_{\nu\}abc}s^a k^b p^c\end{aligned}$$

where $p\cdot s = 0$ and the short notation $(\cdots)_{\{\mu}\epsilon_{\nu\}abc} \equiv (\cdots)_\mu\epsilon_{\nu abc} + (\cdots)_\nu\epsilon_{\mu abc}$ is used. If we set $p = xP$ and $k = K/z$ and note that $p+k = 2p+q$, then Eq. (4.32) simplifies

$$\left\langle W^{(1)}_{\mu\nu}\right\rangle = -\frac{2^5\pi^2\rho^2}{\lambda_* Q^2}\frac{x^2}{z}(1-f(\rho Q))(P+\frac{q}{2x})_{\{\mu}\epsilon_{\nu\}abc}s^a K^b P^c \tag{4.33}$$

Combining Eq. (4.5) and Eq. (4.33) yields

$$\left\langle W^{(1)}_{\mu\nu}L^{\mu\nu}\right\rangle = -\frac{2^7\pi^2\rho^2}{\lambda_* Q^2}\frac{x^2}{z}(1-f(\rho Q))M\left(E\epsilon_{\nu abc}l'^\nu s^a K^b P^c + E'\epsilon_{\nu abc}l^\nu s^a K^b P^c\right) \tag{4.34}$$

where E (E') is the energy of the incoming (outgoing) (anti)electron. The leading instanton contribution to the total cross section Eq. (4.29) can be obtained by inserting Eq. (4.34) into Eq. (4.30). The result is

$$\frac{d^{(1)}\sigma}{dxdydzd\phi}$$
$$= \frac{\alpha^2}{yQ^2}\sum_q \Delta_\perp q_q \frac{64\pi^2\rho^2 e_q^2 D_q(z)}{\lambda_* Q}\frac{K_\perp}{zQ}(1-f(\rho Q))\frac{1-y-x^2y^2\frac{M^2}{Q^2}}{\sqrt{1+4\frac{M^2}{Q^2}x^2}}\sin(\phi-\phi_s) \tag{4.35}$$

where $\Delta_\perp q_q(x,Q^2) = s_\perp f_q(x)$ is the spin polarized distribution function for the quark in the transversely polarized proton. To compare with experiment and for simplicity, we will use the spin structure function [125]

$$g_1(x,Q^2) = \frac{1}{2}\sum_q e_q^2(\Delta q_q(x,Q^2) + \Delta\bar{q}_q(x,Q^2)) \tag{4.36}$$

where $g_1(x,Q^2)$ is the spin distribution function for a longitudinally polarized proton. In other words, we will assume for the sake of an estimate, that the proton has a similar spin distribution function whether polarized longitudinally, or transversely. As we note later, this assumption can be relaxed by calculating the specific instanton contributions to SIDID, $p_\uparrow p$ collisions etc. and then using the results to extract the spin polarization distribution from transversely polarized protons. However, this work is outside the scope of this work. Finally, as we are only interested in the SSA in hard scattering processes, we set $D_q(z) = 1$.

With this in mind, we now normalize Eq. (4.35) by dividing it by the regular zeroth order differential cross section. The result is

$$\frac{d^{(1)}\sigma}{d^{(0)}\sigma} = A_{UT}^{\sin(\phi-\phi_s)}\sin(\phi-\phi_s)\ , \tag{4.37}$$

where

$$A_{UT}^{\sin(\phi-\phi_s)} = \frac{32\pi^2\rho^2}{N_c Q\lambda_*}(1-f(\rho Q))\frac{K_\perp}{zQ}\frac{1}{1+(1-y)^2}\frac{1-y-x^2y^2\frac{M^2}{Q^2}}{\sqrt{1+4\frac{M^2}{Q^2}x^2}}\frac{g_1}{F_1} \tag{4.38}$$

with $F_1(x) = \frac{1}{2}\sum_q e_q^2 f_q(x)$. In Fig. 4.4 we compare Eq. (4.38) to the results reported by HERMES [1]. The mean quark zero mode virtuality $\bar{\lambda}$ is tied to the light quark condensate χ_{uu} through $\bar{\lambda} = 1/\chi_{uu}$. For two flavors we

have $\chi_{uu} \approx (200\,\mathrm{MeV})^3$. The average instanton size in the instanton liquid is $\rho_* \approx 1/3\,\mathrm{fm}$ (upper edge of the band). For comparison, we also show our results for smaller size instantons with $\rho \approx 0.3\,\mathrm{fm}$ (lower edge of the band). A better analysis could be done by averaging Eq. (4.38) over the instanton size distribution as measured say on the lattice. Overall, the instanton contribution through Eq. (4.38) appears to contribute sizably with the right magnitude and overall behavior. They should be considered in any analysis of the transversely polarized spin asymmetry, along with standard perturbative contributions.

4.3 Single spin asymmetry in pp

In this section we briefly review the SSA in semi-inclusive and polarized $p_\uparrow p \to \pi^{\pm,0} X$ experiments, following the recent analysis in [2, 46, 47].

4.3.1 Pauli form factor

The QCD vacuum is a random ensemble of instantons and anti-instantons interacting via the exchange of perturbative gluons and quasi-zero modes of light quarks and anti-quarks. In the dilute instanton approximation, a typical effective vertex with quarks and gluons attached to an instanton is shown in Fig. 4.5. The corresponding effective vertex is given by [13, 126, 127],

$$\begin{aligned}\mathcal{L} = \int \prod_q & \left[m_q \rho - 2\pi^2 \rho^3 \bar{q}_R \left(1 + \frac{i}{4} \tau^a \bar{\eta}^a_{\mu\nu} \sigma_{\mu\nu}\right) q_L \right] \\ \times & \exp\left(-\frac{2\pi^2}{g_s} \rho^2 \bar{\eta}^b_{\gamma\delta} G^b_{\gamma\delta} F_g(\rho Q)\right) d_0(\rho) \frac{d\rho}{\rho^5} d\bar{\sigma} + (L \leftrightarrow R)\end{aligned} \tag{4.39}$$

where $d\bar{\sigma}$ is the integration over the instanton orientation in color space and $\sigma_{\mu\nu} = [\gamma_\mu, \gamma_\nu]/2$. The incoming and outgoing quarks have small momenta p ($\rho p \ll 1$) and Q is the momentum transferred by the inserted gluon with a form-factor

$$F_g(x) \equiv \frac{4}{x^2} - 2K_2(x) \xrightarrow{x\to 0} 1 \tag{4.40}$$

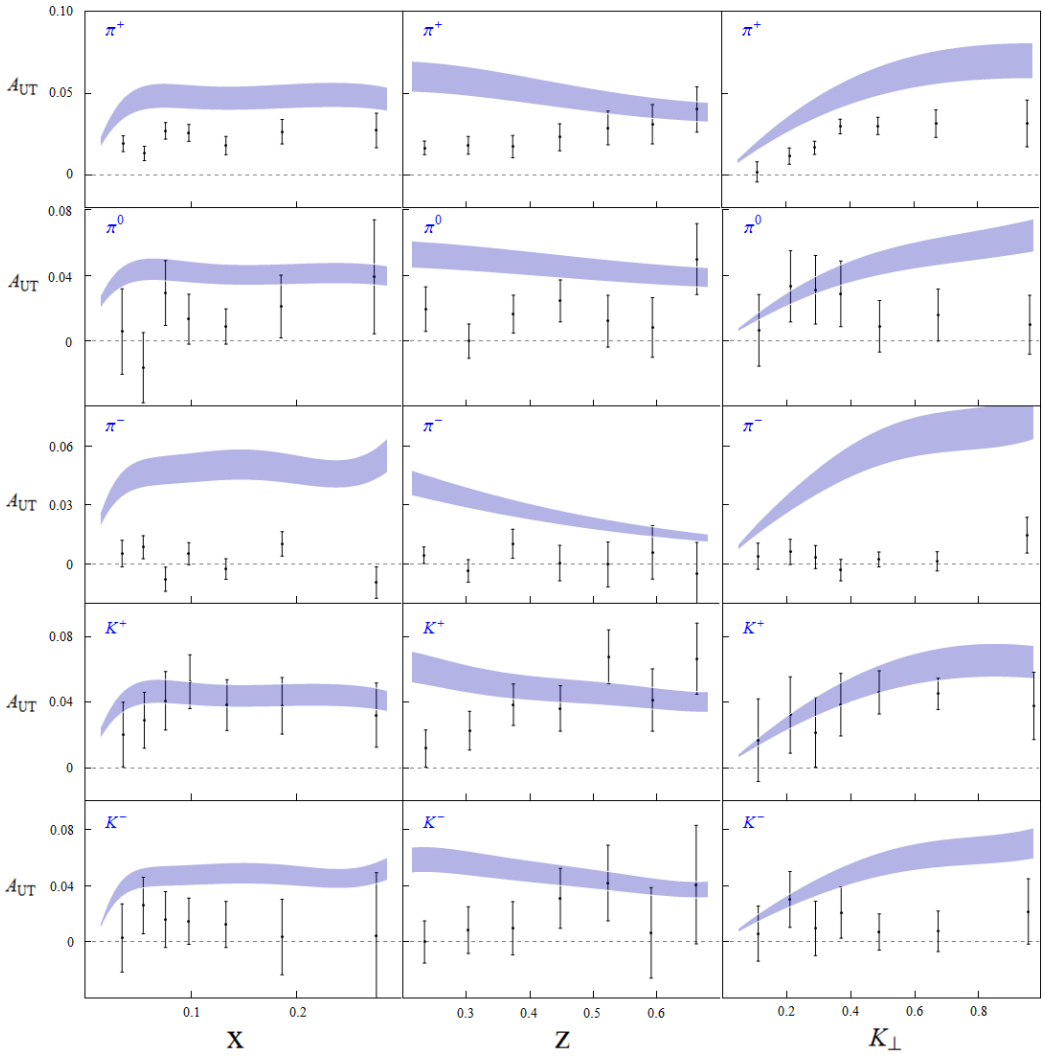

Figure 4.4: Transversely polarized spin asymmetry (solid line) versus data [1].

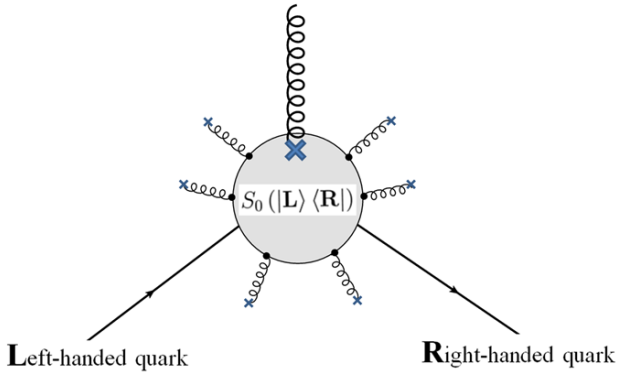

Figure 4.5: Effective Quark-Gluon vertex in the instanton vacuum.

By expanding Eq. (4.39) to leading order in the inserted gluon field of $G^b_{\gamma\delta}$ and integrating over the color indices, we obtain

$$\begin{aligned} & \frac{i}{g_s}F_g(\rho Q)\int \pi^4\rho^4\frac{\bar{q}_R t^a\sigma_{\mu\nu}q_L}{m_q^*}G^a_{\mu\nu}\times\left(\prod_q\left(\rho m_q^*\right)d_0(\rho)\frac{d\rho}{\rho^5}\right) \\ = \quad & \frac{i}{g_s}F_g(\rho Q)\int d\rho\ \pi^4\rho^4 n(\rho)\frac{\bar{q}_R t^a\sigma_{\mu\nu}q_L}{m_q^*}G^a_{\mu\nu} \end{aligned} \tag{4.41}$$

where $n(\rho)$ is the effective instanton density and m_q^* is the effective quark mass. In the dilute instanton approximation [21]

$$n(\rho) = n_I\delta(\rho-\rho_c) \tag{4.42}$$

where ρ_c is the average size of the instanton. Hence the induced instanton effective quark-gluon vertex

$$\frac{i}{g_s}F_g(\rho Q)\pi^4(n_I\rho_c^4)\frac{\bar{q}_R t^a\sigma_{\mu\nu}q_L}{m_q^*}G^a_{\mu\nu} \tag{4.43}$$

as illustrated in Fig. 4.5. In momentum space, the effective vertex is M^a_μ and reads

$$M^a_\mu = t^a\left[\gamma_\mu - \mathbf{P}_+\gamma_+\sigma_{\mu\nu}q^\nu\Psi - \mathbf{P}_-\gamma_-\sigma_{\mu\nu}q^\nu\Psi\right] \tag{4.44}$$

with $\gamma_\pm = (1 \pm \gamma_5)/2$ and

$$\Psi = \frac{F_g(\rho_c\, Q)\pi^4(n_I\rho_c^4)}{m_q^* g_s^2} \tag{4.45}$$

The averaging of Eq. (4.44) in the instanton liquid gives

$$\left\langle M_\mu^a \right\rangle = t^a \left[\gamma_\mu - \sigma_{\mu\nu} q^\nu \Psi\right] \tag{4.46}$$

where we used

$$\langle \mathbf{P}_+ \rangle = \langle \mathbf{P}_- \rangle = 1 \tag{4.47}$$

after the analytical continuation to Minkowski Space. Eq. (4.43) yields an anomalously large Quark Chromomagnetic Moment [127]

$$\mu_a = -\frac{2n_I\pi^4\rho_c^4}{g_s^2} \tag{4.48}$$

4.3.2 Single spin asymmetry in *pp*

In going through an instanton, the chirality of the light quark can be flipped as we noted in Eq. (4.2). The SSA follows from the diagrams of Fig. 4.6.

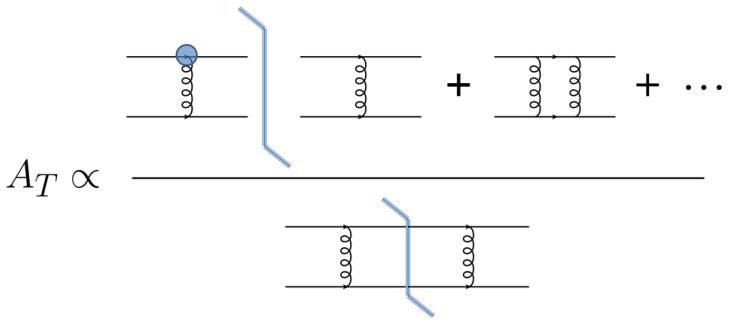

Figure 4.6: Schematically diagrammatic contributions to the SSA through the Pauli Form factor [2]

Using the Pauli form factor discussed before, the SSA follows from the diagrams of Fig. 4.6. As noted in [2], the leading diagram contributing to the SSA is displayed in Fig. 4.7.

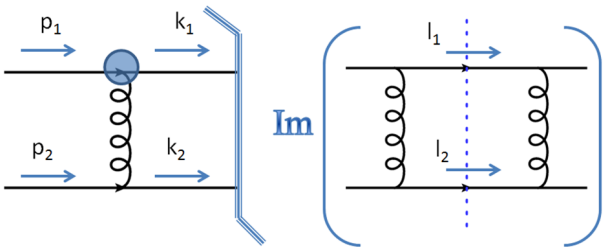

Figure 4.7: Leading diagrammatic contribution to the SSA through the Pauli form factor.

Note that Fig. 4.7 is of the same order in g_s as the zeroth order diagram in Fig. 4.6, since the chirality-flip effective vertex is semi-classical and of order $1/g_s^2$. The zeroth order differential cross section reads

$$d^{(0)}\sigma \sim \frac{64 g_s^4}{|p_1 - k_1|^4}[(k_1 \cdot p_2)(k_2 \cdot p_1) + (k_1 \cdot k_2)(p_1 \cdot p_2)] \tag{4.49}$$

The first order differential cross section for the chirality flip reads [128]

$$\begin{aligned} d^{(1)}\sigma \;\; \sim \;\; & i\frac{g_s^6}{(k_1 - p_1)^2}\frac{1}{16\pi}\frac{(4\pi)^\epsilon}{\Gamma(1-\epsilon)}\frac{\mu^{2\epsilon}}{s^\epsilon} \\ & \times \int_0^1 dy\; [y(1-y)]^{-\epsilon} \int_0^{2\pi} \frac{d\phi_l}{2\pi}\frac{1}{(l_1 - k_1)^2}\frac{1}{(p_1 - l_1)^2}\mathcal{G}(\Omega)\,, \end{aligned} \tag{4.50}$$

where $y = (1 + \cos\theta_l)/2$, $\pm\theta_l$ is the longitudinal angle of $l_{1/2}$ and

$$\mathcal{G}(\Omega) \equiv \mathrm{tr}\left[(M_\mu^a)^{(1)} \not{p}_1 \gamma_5 \not{s} \gamma_\nu t^b \not{l}_1 \gamma_\rho t^c \not{k}_1\right] \mathrm{tr}\left[\gamma^\mu t_a \not{p}_2 \gamma^\nu t_b \not{l}_2 \gamma^\rho t_c \not{k}_2\right] \tag{4.51}$$

We have obtained

$$\left\langle (M_\mu^a)^{(1)} \right\rangle = -t^a \sigma_{\mu\nu} q^\nu \Psi \tag{4.52}$$

where

$$\Psi = \frac{F_g(\rho_c Q)\pi^4 (n_I \rho_c^4)}{m_q^* g_s^2} \tag{4.53}$$

To simplify the analysis and compare to the existing semi-inclusive data,

we use the kinematics

$$\begin{aligned} p_{1/2} &= \frac{\sqrt{\tilde{s}}}{2}(1,0,0,\pm 1) \\ k_{1/2} &= \frac{\sqrt{\tilde{s}}}{2}(1,\pm\sin\theta\sin\phi,\pm\sin\theta\cos\phi,\pm\cos\theta) \\ s &= (0,0,s^{\perp},0) \end{aligned} \tag{4.54}$$

where $\sqrt{\tilde{s}}$ is the total energy of the colliding "partons". It is simple to show that $d^{(1)}\sigma \sim \vec{k}_1 \cdot (\vec{p}_1 \times \vec{s}) \sim \sqrt{\tilde{s}} s^{\perp} k_1^{\perp} \sin\phi$, which results in SSA. For simplicity, we calculate the first differential cross section $d^{(1)}\sigma$ with $\phi = \pi/2$, where the transverse momentum of the outgoing particle lines along the x axis. Straightforward algebra yields

$$\begin{aligned} \left\langle d^{(1)} \right\rangle \sigma \;\sim\; & s^{\perp} k_1^{\perp} \frac{2g_s^4}{3\pi} \frac{\Gamma(-\epsilon)}{\Gamma(2-2\epsilon)\Gamma(1-\epsilon)} \csc^2(\theta)(4\pi)^{\epsilon} \frac{\mu^{2\epsilon}}{s^{\epsilon}} \left(\Psi g_s^2\right) \\ & \times \Big[25\epsilon - 12 + \cos\theta(\epsilon(9+2\epsilon)-4)\,{}_2F_1\left(1, 1-\epsilon, 1-2\epsilon, \sec^2\frac{\theta}{2}\right) \\ & + \epsilon(1-\cos\theta)\,{}_2F_1\left(2, 1-\epsilon, 1-2\epsilon, \sec^2\frac{\theta}{2}\right) \Big] \end{aligned} \tag{4.55}$$

where ${}_2F(a,b,c;y)$ is a hypergeometric function. We note that $|{}_2F_1(1,1,1;y)|$ is much larger than $|{}_2F_1^{(0,1,0,0)}(1,1,1;y)|$ and $|{}_2F_1^{(0,0,1,0)}(1,1,1;y)|$ for $y \sim 1$. Therefore

$$\left\langle d^{(1)}\sigma \right\rangle \sim s^{\perp} k_1^{\perp} \frac{2g_s^4}{3\pi} \left(\Psi g_s^2\right) \csc^4\left(\frac{\theta}{2}\right) (3+\cos\theta) \left[-\frac{1}{\epsilon} + 2\gamma_{\mathrm{E}} + \ln\left(\frac{\tilde{s}}{4\pi\mu^2}\right) \right] \tag{4.56}$$

The divergence in Eq. (4.56) stems from the exchange of soft gluons in the box diagram. In [2] it was regulated using a constituent gluon mass m_g. For $\theta_l \sim 0$, $\vec{l}_1$ is parallel to $\vec{p}_1$, and this collinear divergence could be regulated by restricting $-(l_1 - p_1)^2 > m_g^2$ or equivalently setting $y_{\max} \sim 1 - c\, m_g^2/\tilde{s}$ with c an arbitrary constant of order 1. This regularization amounts to the substitution

$$\int_0^1 dy \longrightarrow \left(\int_0^{\frac{1+\cos\theta}{2} - c\frac{m_g^2}{\tilde{s}}} + \int_{\frac{1+\cos\theta}{2} + c\frac{m_g^2}{\tilde{s}}}^{1-c\frac{m_g^2}{\tilde{s}}} \right) dy \tag{4.57}$$

in Eq. (4.50), where we have also regulated the collinear divergence when $\vec{l}_1$ is parallel to $\vec{k}_1$. Thus

$$\left[-\frac{1}{\epsilon}+2\gamma_{\rm E}+\ln\left(\frac{\tilde{s}}{4\pi\mu^2}\right)\right]\longrightarrow\ln\left(c\frac{\tilde{s}}{m_g^2}\right)+\ln\left(\frac{1-\cos\theta}{1+\cos\theta}\right) \tag{4.58}$$

The regulated SSA is now given by

$$\begin{aligned} A_T^{\sin\phi} &\approx \left\langle\frac{d^{(1)}\sigma}{d^{(0)}\sigma}\right\rangle \\ &= s^\perp k_1^\perp\left(\frac{\Psi g_s^2}{\pi}\right)\frac{(3+\cos\theta)}{6(5+2\cos\theta+\cos^2\theta)}\left[\ln\left(c\frac{\tilde{s}}{m_g^2}\right)+\ln\left(\frac{1-\cos\theta}{1+\cos\theta}\right)\right] \end{aligned} \tag{4.59}$$

where the zeroth order cross section in Eq. (4.49) is used for normalization. We note that the single spin asymmetry A_T is sometimes referred to as A_N in other studies.

To compare with the semi-inclusive data on $p_\uparrow p\to\pi X$, we set $s^\perp u(x,Q^2)=\Delta_s u(x,Q^2)$ and $s^\perp d(x,Q^2)=\Delta_s d(x,Q^2)$, with $\Delta_s u(x,Q^2)$ and $\Delta_s d(x,Q^2)$ as the spin polarized distribution functions of the valence up-quarks and valence down-quarks in the proton respectively. For forward π^+, π^- and π^0 productions, the SSAs are

$$\begin{aligned} A_T^{\sin\phi}(\pi^+) &= k^\perp\frac{\Delta_s u(x_1,Q^2)}{u(x_1,Q^2)}\left(\frac{\Psi g_s^2}{\pi}\right)\frac{(3+\cos\theta)}{6(5+2\cos\theta+\cos^2\theta)} \\ &\quad\times\left[\ln\left(c\frac{\tilde{s}}{m_g^2}\right)+\ln\left(\frac{1-\cos\theta}{1+\cos\theta}\right)\right] \end{aligned} \tag{4.60}$$

$$\begin{aligned} A_T^{\sin\phi}(\pi^-) &= k^\perp\frac{\Delta_s d(x_1,Q^2)}{d(x_1,Q^2)}\left(\frac{\Psi g_s^2}{\pi}\right)\frac{(3+\cos\theta)}{6(5+2\cos\theta+\cos^2\theta)} \\ &\quad\times\left[\ln\left(c\frac{\tilde{s}}{m_g^2}\right)+\ln\left(\frac{1-\cos\theta}{1+\cos\theta}\right)\right] \end{aligned} \tag{4.61}$$

$$\begin{aligned} A_T^{\sin\phi}(\pi^0) &= k^\perp\frac{\Delta_s u(x_1,Q^2)+\Delta_s d(x_1,Q^2)}{u(x_1,Q^2)+d(x_1,Q^2)}\left(\frac{\Psi g_s^2}{\pi}\right)\frac{(3+\cos\theta)}{6(5+2\cos\theta+\cos^2\theta)} \\ &\quad\times\left[\ln\left(c\frac{\tilde{s}}{m_g^2}\right)+\ln\left(\frac{1-\cos\theta}{1+\cos\theta}\right)\right] \end{aligned} \tag{4.62}$$

According to [129, 130]

$$\begin{aligned}
\frac{\Delta_s u(x,Q^2)}{u(x,Q^2)} &= 0.959 - 0.588(1-x^{1.048}) \\
\frac{\Delta_s d(x,Q^2)}{d(x,Q^2)} &= -0.773 + 0.478(1-x^{1.243}) \\
\frac{u(x,Q^2)}{d(x,Q^2)} &= 0.624(1-x) \qquad (4.63)
\end{aligned}$$

These results can be compared to the experimental measurements in [3]. For simplicity, we assume the same fraction for each proton $\langle x_1\rangle = \langle x_2\rangle = \langle x\rangle$. This assumption will be revisited later. We set $\langle k^\perp\rangle \approx \langle K_\perp\rangle$ as the transverse momentum of the outgoing pion. We then have $\sqrt{s}\,\langle x\rangle\,\langle \sin\theta\rangle = 2\,\langle K_\perp\rangle$ and $\langle x\rangle\,\langle\cos\theta\rangle = \langle x_F\rangle$. For large $\sqrt{s}$, we also have $\langle Q\rangle \approx \langle K_\perp\rangle\,\sqrt{\langle x\rangle\,/\,\langle x_F\rangle}$. We set $c = 2$ and $\langle K_\perp\rangle = 2\,\text{GeV}$ for the outgoing pions. $n_I \approx 1/\text{fm}^4$ is the effective instanton density, $\rho \approx 1/3\text{fm}$ the typical instanton size and $m_q^* \approx 300\,\text{MeV}$ the constitutive quark mass in the instanton vacuum. $m_g \approx 420\,\text{MeV}$ is the effective gluon mass in the instanton vacuum[131].

In Fig. 4.8 we display the results Eq. (4.60)-Eq. (4.62) as a function of the parton fraction x_F for both the charged and uncharged pions at $\sqrt{s} = 19.4\,\text{GeV}$ [3].

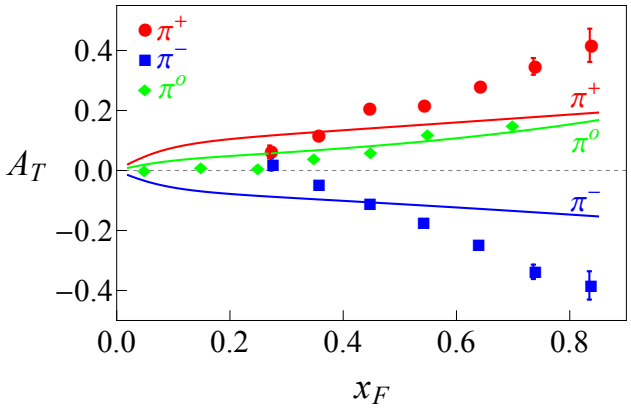

Figure 4.8: x_F dependent SSA in $p_\uparrow p \to \pi X$ collisions at $\sqrt{s} = 19.4\text{GeV}$ [3]. The solid lines are the analytical results in Eq. (4.60)- Eq. (4.62) with $c = 2$.

In Fig. 4.9, the divergence in Eq. (4.50) is now regulated by using a constituent gluon mass as in [2].

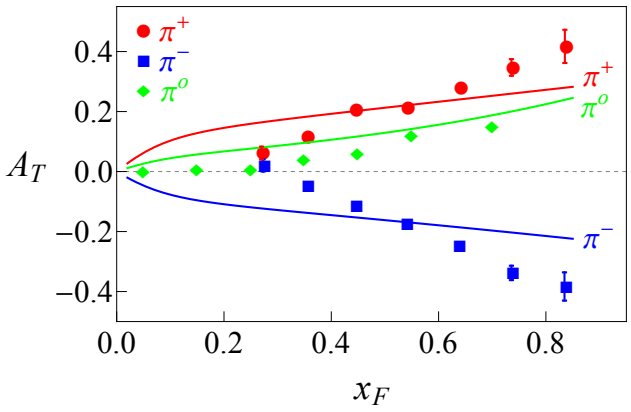

Figure 4.9: x_F dependent SSA in $p_\uparrow p \to \pi X$ collisions at $\sqrt{s} = 19.4$GeV [3]. The solid lines are the analytical results in Eq. (4.60)- Eq. (4.62) regulated by using a massive gluon propagator yields the results.

We also find that the instanton contribution is large with the right order of magnitude and trend. This contribution may not be complete but should be added to current perturbative estimates. Below we show that instantons also give large contributions to the Double Spin Asymmetry (DSA), in particular to DSA at $\sqrt{s} = 62.4\,\text{GeV}$ which is to be compared with RHIC's future measurement. Finally, we also compare our results with the data from [4] in Fig. 4.10 and with the data from [5] in Fig. 4.11.

In sum, the anomalous Pauli form factor can reproduce the correct magnitude of the observed SSA in polarized $p_\uparrow p \to \pi X$ for reasonable vacuum parameters.

At the end of this subsection, let us revisit the simple assumption $\langle x_1 \rangle = \langle x_2 \rangle$, which may appear to be unrealistic especially for large x_F. Here, we improve on this simplification and show that this amounts to a better fit to the data. In the lab frame, we define

$$\begin{aligned} p_1 &= x_1 \frac{\sqrt{s}}{2}(1,0,0,1) \\ p_2 &= x_2 \frac{\sqrt{s}}{2}(1,0,0,-1) \end{aligned} \tag{4.64}$$

set

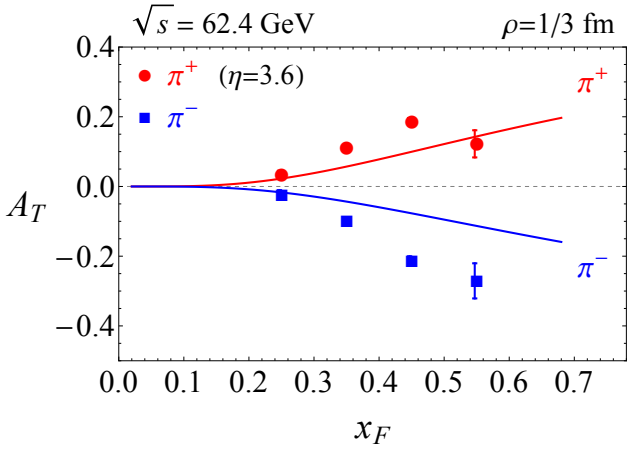

Figure 4.10: x_F dependent SSA in $p_\uparrow p \to \pi X$ collisions at $\sqrt{s} = 62.4\,\text{GeV}$. Data is from [4].

$$\tilde{s} = \frac{s}{4}\left[(x_1+x_2)^2 - (x_1-x_2)^2\right] = x_1 x_2 s \tag{4.65}$$

and identify the two Lorentz factors

$$\gamma = \frac{x_1+x_2}{2\sqrt{x_1 x_2}}, \quad \text{and} \quad \beta = \frac{x_1-x_2}{x_1+x_2}. \tag{4.66}$$

The longitudinal momentum of the outgoing particle k_1 is

$$k_L = \frac{\sqrt{s}}{2} x_F = \gamma(k_L^* + \beta E^*) \tag{4.67}$$

where k_L^* is the longitudinal momentum of the particle k_1 in the CM frame and E^* is the energy of particle k_1 in the CM frame. We have

$$k_L^* = \frac{\sqrt{\tilde{s}}}{2}\cos\theta, \quad \text{and} \quad E^* = \frac{\sqrt{\tilde{s}}}{2} \tag{4.68}$$

with

$$\cos\theta = \frac{2x_F - x_1 + x_2}{x_1 + x_2} \tag{4.69}$$

Also we have

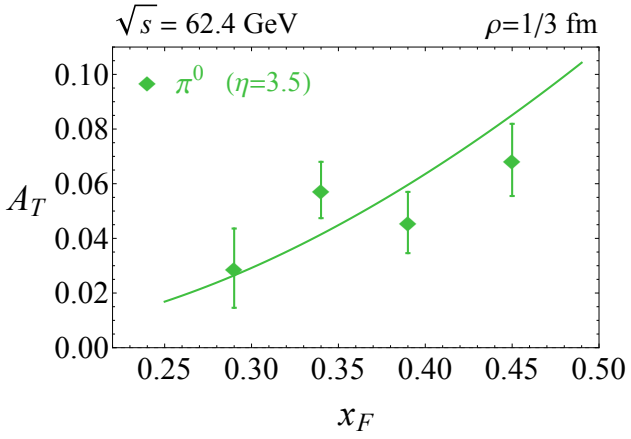

Figure 4.11: x_F dependent SSA in $p_\uparrow p \to \pi X$ collisions at $\sqrt{s} = 62.4\,\text{GeV}$. Data (right) is from [5].

$$k^\perp = \frac{\sqrt{\tilde{s}}}{2}\sin\theta\,, \quad \text{and} \quad Q = \sqrt{\tilde{s}}\,\sin\left(\frac{\theta}{2}\right) \tag{4.70}$$

With this in mind and for $x_F = 0.6$, we show

- the dependence of the SSA $A_T^{\sin\phi}(\pi^+)$ (Eq. (4.60)) in Fig. 4.12 on $x_1 \in (0.6, 0.9)$ and $x_2 \in (0.1, 0.3)$ for charged and uncharged pions.

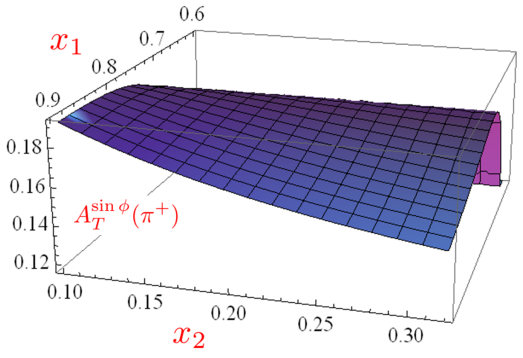

Figure 4.12: SSAs $A_T^{\sin\phi}(\pi^+)$ for $x_F = 0.6$.

- the dependence of the SSA $A_T^{\sin\phi}(\pi^-)$ (Eq. (4.61)) in Fig. 4.13 on $x_1 \in (0.6, 0.9)$ and $x_2 \in (0.1, 0.3)$ for charged and uncharged pions.

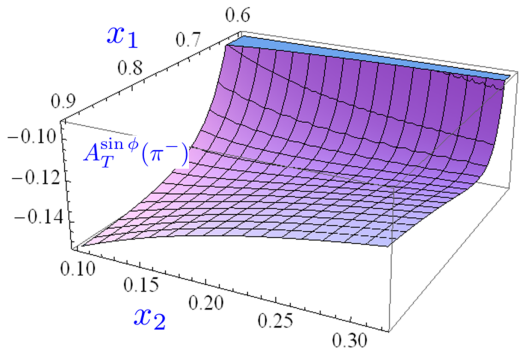

Figure 4.13: SSAs $A_T^{\sin\phi}(\pi^-)$ for $x_F = 0.6$.

- the dependence of the SSA $A_T^{\sin\phi}(\pi^0)$ (Eq. (4.62)) in Fig. 4.14 on $x_1 \in (0.6, 0.9)$ and $x_2 \in (0.1, 0.3)$ for charged and uncharged pions.

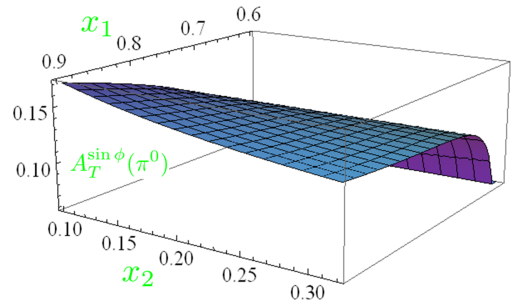

Figure 4.14: SSAs $A_T^{\sin\phi}(\pi^0)$ for $x_F = 0.6$.

Take $A_T^{\sin\phi}(\pi^+)$ for example, the SSA $A_T^{\sin\phi}(\pi^+)$ increases when x_1 increases and x_2 decreases. The simplifying assumption $\langle x_1 \rangle = \langle x_2 \rangle$, overestimates x_1 and underestimates x_2 for small x_F. Also, we underestimate x_1 and overestimate x_2 for large x_F. Instead of using $\langle x_1 \rangle = \langle x_2 \rangle$, a more careful calcution shows that $A_T^{\sin\phi}(\pi^+)$ is smaller for small x_F and larger for large x_F, and therefore fits the data better. Again, in this paper our aim was to

show that instanton do contribute sizably to SSA with the right magnitude and trend. They have to be included in any perturbative analysis of these effects.

Chapter 5

Spin Effects Through Two Instantons

5.1 Double spin asymmetry in pp

The same Pauli form factor and vacuum parameters can be used to assess the role of the QCD instantons on doubly polarized and semi-inclusive $p_\uparrow p_\uparrow \to \pi\pi X$ processes. The Double Spin Asymmetry (DSA) is defined as

$$A_{\rm DS} = \frac{\sigma^{\uparrow\uparrow+\downarrow\downarrow} - \sigma^{\downarrow\uparrow+\uparrow\downarrow}}{\sigma^{\uparrow\uparrow+\downarrow\downarrow} + \sigma^{\downarrow\uparrow+\uparrow\downarrow}} \tag{5.1}$$

with the proton beam polarized along the transverse direction. The valence quark from the polarized proton P_1 exchanges one gluon with the valence quark from the polarized proton P_2 as shown in Fig. 5.1. At large $\sqrt{s}$, Fig. 5.1-(a) is dominant in forward pion production and Fig. 5.1-(b) is dominant in backward pion production. For Fig. 5.1-(a), the differential cross section reads

$$\begin{aligned} d\sigma \sim \frac{g_s^4}{|p_1 - k_1|^4} \quad \sum\nolimits_{\rm color} \quad & {\rm tr}\left[M_\mu^a \not{p}_1 (1+\gamma_5 \not{s}_1)\gamma_0 (M_\nu^b)^\dagger \gamma_0 \not{k}_1\right] \\ & \times {\rm tr}\left[M_\mu^a \not{p}_2 (1+\gamma_5 \not{s}_2)\gamma_0 (M_\nu^b)^\dagger \gamma_0 \not{k}_2\right] \end{aligned} \tag{5.2}$$

where M_μ is proportional to $(\mathbf{P}_+ + \mathbf{P}_-)$ as detailed in 4.3.1. To second order, we approximately have

$$\left\langle d^{(2)}\sigma \right\rangle \sim (\cdots) \left\langle (\mathbf{P}_+ + \mathbf{P}_-)^2 \right\rangle \approx (\cdots) \left\langle \mathbf{P}_+ + \mathbf{P}_- \right\rangle^2 \tag{5.3}$$

since the instanton liquid is dilute. The contribution to the DSA then follows from simple algebra

$$\begin{aligned}\left\langle d^{(2)}\sigma\right\rangle \;\sim\; & \frac{256}{|p_1-k_1|^4}\left(\psi g_s^2\right)^2\left[(k_1\cdot s_1)(k_1\cdot s_2)(k_2\cdot p_1)(k_2\cdot p_2)\right.\\ & -(k_1\cdot p_1)(k_1\cdot s_2)(k_2\cdot p_2)(k_2\cdot s_1)-(k_1\cdot s_1)(k_1\cdot s_2)(k_2\cdot p_2)(p_1\cdot p_2)\\ & +(k_1\cdot k_2)(k_1\cdot p_1)(k_2\cdot p_2)(s_1\cdot s_2)-(k_1\cdot p_1)(k_1\cdot p_2)(k_2\cdot p_2)(s_1\cdot s_2)\\ & -(k_1\cdot p_1)(k_2\cdot p_1)(k_2\cdot p_2(s_1\cdot s_2)+(k_1\cdot p_1)(k_2\cdot p_2)(p_1\cdot p_2)(s_1\cdot s_2)\\ & -(k_1\cdot p_2)(k_1\cdot s_1)(k_2\cdot p_1)(k_2\cdot s_2)+(k_1\cdot p_1)(k_1\cdot p_2)(k_2\cdot s_1)(k_2\cdot s_2)\\ & \left.+(k_1\cdot k_2)(k_1\cdot s_1)(k_2\cdot s_2)(p_1\cdot p_2)-(k_1\cdot p_1)(k_2\cdot s_1)(k_2\cdot s_2)(p_1\cdot p_2)\right]\end{aligned} \tag{5.4}$$

after using the identity

$$\begin{aligned} & \mathrm{tr}\left[(\gamma_\mu \not{q}-\not{q}\gamma_\mu)\not{p}\gamma_5\not{s}\gamma_\nu\not{k}\right]+\mathrm{tr}\left[\gamma_\mu\not{p}\gamma_5\not{s}(\not{q}\gamma_\nu-\gamma_\nu\not{q})\not{k}\right]\\ = \;& \mathrm{tr}\left[(\gamma_\mu\not{k}+\not{p}\gamma_\mu)\not{p}\gamma_5\not{s}\gamma_\nu\not{k}\right]+\mathrm{tr}\left[\gamma_\mu\not{p}\gamma_5\not{s}(\not{k}\gamma_\nu+\gamma_\nu\not{p})\not{k}\right]\\ = \;& 8i\left[p_\mu\epsilon(\nu,k,p,s)-p_\nu\epsilon(\mu,k,p,s)+(k\cdot p)\epsilon(\mu,\nu,k,s)-(k\cdot s)\epsilon(\mu,\nu,k,p)\right]\end{aligned} \tag{5.5}$$

with $q=k-p$ and $p\cdot s=0$ because the protons are transversely polarized. For an empirical application of Eq. (5.4) we adopt the simple kinematical set up in Eq. (5.16). Thus

$$\begin{aligned}\left\langle d^{(2)}\sigma\right\rangle \;\sim\; & -\frac{4}{|p_1-k_1|^4}\left(\psi g_s^2\right)^2\tilde{s}^3 s_1^\perp s_2^\perp(1-\cos\theta)^2\\ & \times[4+\cos(\theta-2\phi)+2\cos(2\phi)+\cos(\theta+2\phi)]\end{aligned} \tag{5.6}$$

After adding the contribution of Fig. 5.1-(a) and Fig. 5.1-(b), and averaging over the transverse direction ϕ, we finally obtain

$$\frac{d^{(2)}\sigma}{d^{(0)}\sigma}\sim -4s_1^\perp s_2^\perp\left(\frac{\pi^4 n_I\rho_c^4}{m_q^* g_s^2}\right)^2\frac{F_g^2[\rho\sqrt{\frac{\tilde{s}(1-\cos\theta)}{2}}]\tilde{s}+F_g^2[\rho\sqrt{\frac{\tilde{s}(1+\cos\theta)}{2}}]\tilde{s}}{\frac{5+2\cos\theta+\cos^2\theta}{(1-\cos\theta)^2}+\frac{5-2\cos\theta+\cos^2\theta}{(1+\cos\theta)^2}} \tag{5.7}$$

Our DSA results can now be compared to future experiments at collider energies. Specifically, our DSA for dijet productions are

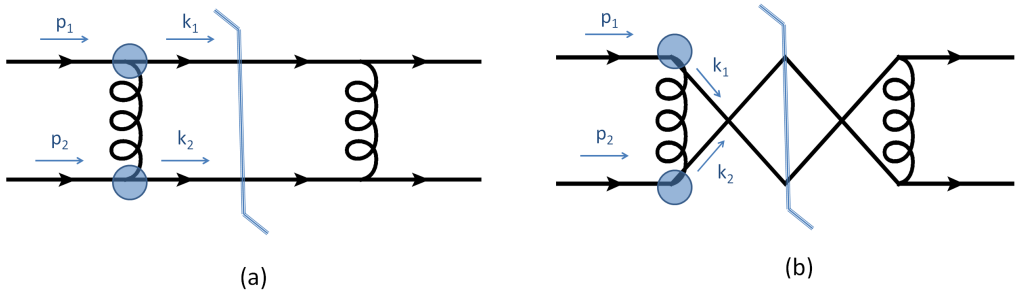

Figure 5.1: The valence quark in polarized proton p_1 exchange one gluon with the valence quark in the polarized proton p_2.

$$A_{\pi^+\pi^+} = -\frac{1}{8}\frac{\Delta_s u(x_1,Q^2)}{u(x_1,Q^2)}\frac{\Delta_s u(x_2,Q^2)}{u(x_2,Q^2)} \times \left(\frac{\pi^3 n_I \rho_c^4}{m_q^* \alpha_s}\right)^2 \frac{F_g^2[\rho\sqrt{\frac{\tilde{s}(1-\cos\theta)}{2}}]\tilde{s} + F_g^2[\rho\sqrt{\frac{\tilde{s}(1+\cos\theta)}{2}}]\tilde{s}}{(5+10\cos^2\theta+\cos^4\theta)\csc^4\theta} \quad (5.8)$$

$$A_{\pi^-\pi^-} = -\frac{1}{8}\frac{\Delta_s d(x_1,Q^2)}{d(x_1,Q^2)}\frac{\Delta_s d(x_2,Q^2)}{d(x_2,Q^2)} \times \left(\frac{\pi^3 n_I \rho_c^4}{m_q^* \alpha_s}\right)^2 \frac{F_g^2[\rho\sqrt{\frac{\tilde{s}(1-\cos\theta)}{2}}]\tilde{s} + F_g^2[\rho\sqrt{\frac{\tilde{s}(1+\cos\theta)}{2}}]\tilde{s}}{(5+10\cos^2\theta+\cos^4\theta)\csc^4\theta} \quad (5.9)$$

$$A_{\pi^+\pi^-} = -\frac{1}{8}\frac{\Delta_s u(x_1,Q^2)\Delta_s d(x_2,Q^2) + \Delta_s d(x_1,Q^2)\Delta_s u(x_2,Q^2)}{u(x_1,Q^2)d(x_2,Q^2) + d(x_1,Q^2)u(x_2,Q^2)} \times \left(\frac{\pi^3 n_I \rho_c^4}{m_q^* \alpha_s}\right)^2 \frac{F_g^2[\rho\sqrt{\frac{\tilde{s}(1-\cos\theta)}{2}}]\tilde{s} + F_g^2[\rho\sqrt{\frac{\tilde{s}(1+\cos\theta)}{2}}]\tilde{s}}{(5+10\cos^2\theta+\cos^4\theta)\csc^4\theta} \quad (5.10)$$

To compare our calculations with the future measurements at RHIC, we use the same kinematics in Fig. 4.9: $\sqrt{s} = 62.4$GeV and $\eta = 3.5$. The value of α_s is from [132]. Our estimates for charged di-jet production in semi-inclusive DSA are displayed in Fig. 5.2.

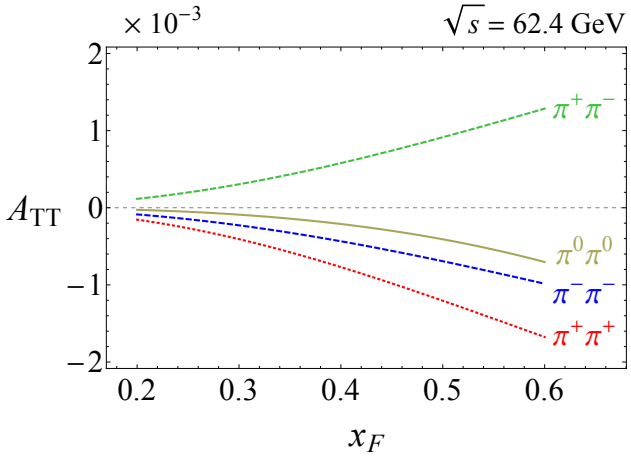

Figure 5.2: Predictions for charged di-jet production in semi-inclusive DSA.

5.2 $\mathcal{P}$-odd effects through instanton fluctuations

It is commonly accepted that in a typical non-central $AuAu$ collision at RHIC as illustrated in Fig. 5.3, the flying fragments create a large magnetic field that strongly polarizes the wounded or participant nucleons in the final state. The magnetic field is typically $eB/m_\pi^2 \approx 1$ at RHIC and $eB/m_\pi^2 \approx 15$ at the LHC and argued to last for about 1-3 fm/c [133]. We recall that in these units $m_\pi^2 \approx 10^{18}$ Gauss which is substantial. As a result, large $\mathcal{P}$-odd pion azimuthal charge correlations were predicted to take place in peripheral heavy ion collisions [134, 135, 136, 137].

In this section, we would review the analysis in [45] and show that a large contribution to the $\mathcal{P}$-odd pion azimuthal charge correlations may stem from the prompt part of the collision as each of the incoming nucleus polarizes strongly the participating nucleons from its partner nucleus during the collision process as illustrated in Fig. 5.4. The magnetic field is strong but short lived in the initial state, lasting for about $1/2\,\mathrm{fm}/c$ for a typical heavy ion collision at current collider energies. Polarized proton on proton scattering can exhibit large chirality flip effects through instanton and anti-instanton fluctuations as we now show.

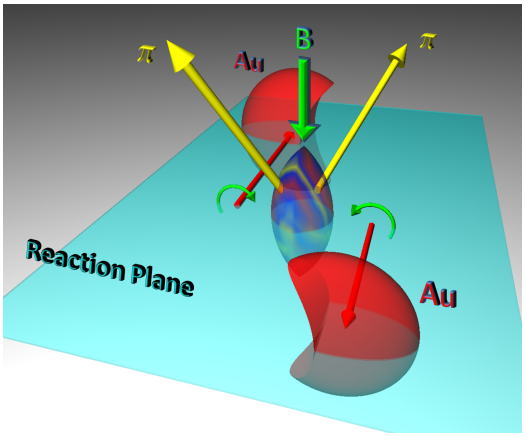

Figure 5.3: 2-pion correlations in $AuAu$ after the collision.

5.2.1 $\mathcal{P}$-odd effects in the instanton vacuum

Consider the typical parton-parton scattering amplitude of Fig. 5.5 with 2-gluon exchanges.

In each collision, the colliding "parton" p_i has spin s_i, and thus $u(p_i)\bar{u}(p_i) = \frac{1}{2}\not{p}_i(1+\gamma_5\not{s}_i)$. The parton p_1 from the A-nucleus encounters an instanton or anti-instanton as depicted by the gluonic form-factor. Rewrite the Eq. (4.44)

$$M^a_\mu = t^a\left[\gamma_\mu - \mathbf{P}_+\gamma_+\sigma_{\mu\nu}q^\nu\Psi - \mathbf{P}_-\gamma_-\sigma_{\mu\nu}q^\nu\Psi\right] \tag{5.11}$$

with $\mathbf{P}_+ = 1$ stands for an instanton insertion and $\mathbf{P}_- = 1$ for an anti-instanton insertion. In establishing Eq. (4.44), the instanton and anti-instanton zero modes are assumed to be undistorted by the prompt external magnetic field. Specifically, the chromo-magnetic field B_G is much stronger than the electro-magnetic field B, i.e. $|g_sB_G| \gg |eB| \approx$ or $m_\pi^2\rho_c^2 \approx 0.004 \ll 1$. The deformation of the instanton zero-modes by a strong magnetic field have been discussed in [138]. They will not be considered here.

In terms of Eq. (4.44), the contribution of Fig. 5.5 to the differential cross section is

$$d\sigma \sim \frac{g_s^4}{|p_1-k|^4}\,\mathrm{tr}\left[M^a_\mu\not{p}_1(1+\gamma_5\not{s}_1)\gamma_0(M^b_\nu)^\dagger\gamma_0\not{k}\right]\mathrm{tr}\left[\gamma^\mu t_a\not{p}_2(1+\gamma_5\not{s}_2)\gamma^\nu t_b\not{k}'\right] \tag{5.12}$$

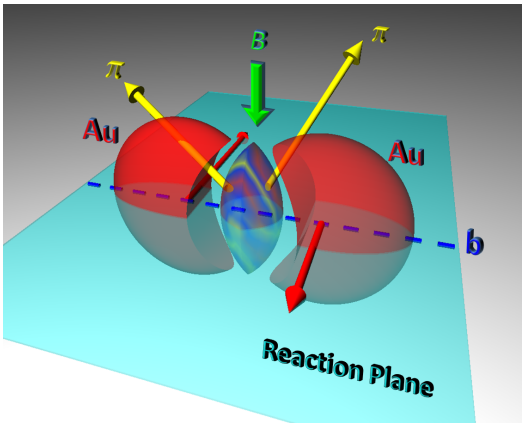

Figure 5.4: 2-pion correlations in $AuAu$ at the collision.

which can be decomposed into $d\sigma \approx d\sigma^{(0)} + d\sigma^{(1)}$ in the dilute instanton liquid. The zeroth order contribution is

$$d^{(0)}\sigma \sim \frac{64 g_s^4}{|p_1 - k|^4} \left[2(k \cdot p_2)(p_1 \cdot p_2) + (k \cdot p_1)(p_1 \cdot p_2 - k \cdot p_2)\right] \tag{5.13}$$

where we used $k' = p_1 + p_2 - k$. The first order contribution is

$$d^{(1)}\sigma \sim \frac{64 g_s^4}{|p_1 - k|^4} \left[(p_1 \cdot p_2)^2 + (k \cdot p_2)(p_1 \cdot p_2)\right] (k \cdot s_1)\Psi \left(\mathbf{P}_+ - \mathbf{P}_-\right) \tag{5.14}$$

after using $p_1 \cdot s_1 = 0$ and $p_1^2 = k^2 = 0$. Converting to standard parton kinematics with $p_1 \to x_1 P_1$, $p_2 \to x_2 P_2$ and $k \to K/z$, we obtain for the ratio of the $\mathcal{P}$-odd to $\mathcal{P}$-even contributions in the differential cross section

$$\frac{d^{(1)}\sigma}{d^{(0)}\sigma} = \frac{x_1 (P_1 \cdot P_2)^2 + \frac{1}{z}(K \cdot P_2)(P_1 \cdot P_2)}{2(K \cdot P_2)(P_1 \cdot P_2) + (K \cdot P_1)(\frac{x_1}{x2} P_1 \cdot P_2 - \frac{K \cdot P_2}{z x 2})} (K \cdot s_1)\Psi \left(\mathbf{P}_+ - \mathbf{P}_-\right) \tag{5.15}$$

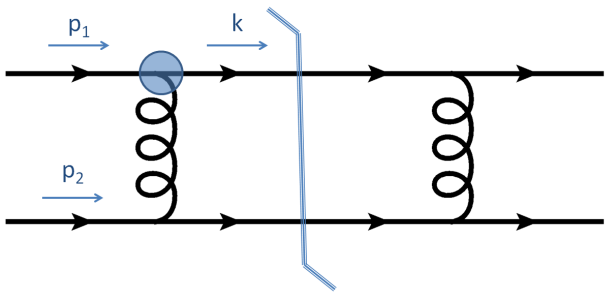

Figure 5.5: Gluon Exchange. The blob is an instanton or anti-instanton insertion. See text.

Now consider the kinematics appropriate for the collision set up in Fig. 5.4,

$$\begin{aligned} P_{1/2} &= \frac{\sqrt{s}}{2}(1,0,0,\pm 1) \\ K &= (E, K_\perp \cos\Delta\phi, K_\perp \sin\Delta\phi, \frac{\sqrt{s}}{2}x_F) \\ s_1 &= (0,0,s_1^\perp,0) \end{aligned} \tag{5.16}$$

where $K_\perp$ and $E^2 = K_\perp^2 + s x_F^2/4 + m_\pi^2$ are the transverse momentum and total squared energy of the outgoing pion respectively. x_F is the pion longitudinal momentum fraction. Thus

$$\begin{aligned} &\lim_{s\to\infty} \frac{d^{(1)}\sigma}{d^{(0)}\sigma} \\ &= (\sin\Delta\phi) s_1^\perp \frac{x_F + x_1 z}{x_F z} \frac{K_\perp}{m_q^*} \frac{\pi^3 (n_I \rho_c^4)}{8\alpha_s} F_g\left(\rho\sqrt{\frac{x_1}{x_F z}(K_\perp^2 + m_\pi^2)}\right)(\mathbf{P}_- - \mathbf{P}_+) \end{aligned} \tag{5.17}$$

We note that Eq. (5.17) vanishes after averaging over the instanton liquid background which is $\mathcal{P}$-even

$$\left\langle \frac{d^{(1)}\sigma}{d^{(0)}\sigma} \right\rangle = 0 \tag{5.18}$$

since on average $\langle \mathbf{Q} \rangle = \langle \mathbf{P}_+ - \mathbf{P}_- \rangle = 0$.

5.2.2 $\mathcal{P}$-odd effects in AA collisions

Now consider hard pp collisions in peripheral AA collisions as illustrated in Fig. 5.4. The Magnetic field is strong enough at the collision to partially polarize the colliding protons. Say $c\%$ of the wounded protons from a given nucleus get polarized by the partner colliding nucleus. For simplicity, we set $s_\perp u(x,Q^2) = c\%\Delta_s u(x,Q^2)$ and $s_\perp d(x,Q^2) = c\%\Delta_s d(x,Q^2)$, with $\Delta_s u(x,Q^2)$ and $\Delta_s d(x,Q^2)$ as the spin polarized distribution functions of the valence up-quarks and valence down-quarks in the proton respectively. We also assume that the outgoing u quark turns to π^+ and that the outgoing d quark turns to π^-. With this in mind, we may rewrite the ratio of differential contributions in Eq. (5.17) following [6, 139, 140, 7] as

$$\frac{d\mathbf{N}}{d\phi_\alpha} \sim 1 - 2a_\alpha \sin(\phi - \Psi_{RP}) \tag{5.19}$$

with $\alpha = \pm$ or

$$a_+ = \frac{\Delta_s u(x,Q^2)}{u(x,Q^2)} \Upsilon \mathbf{Q} \qquad a_- = \frac{\Delta_s d(x,Q^2)}{d(x,Q^2)} \Upsilon \mathbf{Q} \tag{5.20}$$

and

$$\Upsilon \equiv \frac{x_F + xz}{x_F z} \frac{K_\perp}{m_q^*} \frac{\pi^3 (n_I \rho_c^4)}{16\alpha_s} F_g \left(\rho \sqrt{\frac{x}{x_F z}(K_\perp^2 + m_\pi^2)} \right) \tag{5.21}$$

While on average $\langle a_\alpha \rangle = 0$ since $\langle \mathbf{Q} \rangle_V = 0$, in general $\langle a_\alpha a_\beta \rangle \neq 0$ for the 2-particle correlations. Explicitly

$$\begin{aligned}
-\langle a_{\pi^+} a_{\pi^-} \rangle &= -\left(\frac{\Delta_s u(x,Q^2)}{u(x,Q^2)} \frac{\Delta_s d(x,Q^2)}{d(x,Q^2)} \right) \Upsilon^2 \langle \mathbf{Q}^2 \rangle_V \\
-\langle a_{\pi^+} a_{\pi^+} \rangle &= -\left(\frac{\Delta_s u(x,Q^2)}{u(x,Q^2)} \right)^2 \Upsilon^2 \langle \mathbf{Q}^2 \rangle_V \\
-\langle a_{\pi^-} a_{\pi^-} \rangle &= -\left(\frac{\Delta_s d(x,Q^2)}{d(x,Q^2)} \right)^2 \Upsilon^2 \langle \mathbf{Q}^2 \rangle_V
\end{aligned} \tag{5.22}$$

For reasonable values of $\langle x \rangle$, $\langle a_{\pi^+} a_{\pi^+} \rangle \sim \langle a_{\pi^-} a_{\pi^-} \rangle \sim -\langle a_{\pi^+} a_{\pi^-} \rangle$ as expected [6, 139, 140, 7].

A more quantitative comparison to the reported data in [6, 7] can be carried out by estimating the fluctuations of the topological charge $\mathbf{Q}$ in the prompt collision 4-volume $V \approx (\tau^2/2)\Delta\eta V_\perp(b)$. In the latter, $\tau \approx 1/2$ fm/c

is the prompt proper time over which the induced magnetic field is active, $\Delta\eta$ is the interval in pseudo-rapidity and $V_\perp(b)$ the transverse collision area for fixed impact parameter b. Through simple geometry

$$V_\perp(b) = 2R^2 \left(\arccos\left(\frac{b}{2R}\right) - \frac{b}{2R}\sqrt{1-\left(\frac{b}{2R}\right)^2} \right) \tag{5.23}$$

where R is the radius of two identically colliding nuclei. $\mathbf{Q}^2$ involves a pair $\mathbf{P}, \mathbf{P}'$ of instanton-antiinstanton. Specifically,

$$\left\langle \mathbf{Q}^2 \right\rangle_V = \left\langle (\mathbf{P}_+ - \mathbf{P}_-)(\mathbf{P}'_+ - \mathbf{P}'_-) \right\rangle_V \tag{5.24}$$

If we denote by $N_\pm$ the number of instantons and antiinstantons in V, with $N = N_+ + N_-$ their total number, then in the instanton vacuum the pair correlation follows from

$$\left\langle \mathbf{Q}^2 \right\rangle_V \equiv \left\langle \left(\frac{N_+ - N_-}{N_+ + N_-}\right)^2 \right\rangle_V \approx \frac{\langle (N_+ - N_-)^2 \rangle_V}{\langle (N_+ + N_-)^2 \rangle_V} \tag{5.25}$$

Assuming $N_\pm$ to be large in V it follows that [141]

$$\left\langle \mathbf{Q}^2 \right\rangle_V \approx \frac{\langle N \rangle_V}{\langle N \rangle_V \left(\langle N \rangle_V + 4/\mathbf{b} \right)} \tag{5.26}$$

The deviation from the Poissonian distribution in the variance of the number average reflects on the QCD trace anomaly in the instanton vacuum or $\langle N^2 \rangle_V - \langle N \rangle_V^2 = 4/\mathbf{b} \langle N \rangle_V$ and vanishes in the large N_c limit [141]. Here $\mathbf{b} = 11N_c/3$ is the coefficient of the 1-loop beta function $\beta(\rho_c) \approx \mathbf{b}/\ln(\Lambda\rho_c)$ (quenched). Thus

$$\left\langle \mathbf{Q}^2 \right\rangle_V \approx \frac{1}{n_I(\tau^2 \Delta\eta V_\perp(b)/2) + 4/\mathbf{b}} \tag{5.27}$$

where we have used that the mean $\langle N \rangle_V = n_I V$ in the volume V. The topological fluctuations are suppressed by the collision 4-volume. Note that we have ignored the role of the temperature on the topological fluctuations in peripheral collisions. Temperature will cause these topological fluctuations to deplete and vanish at the chiral transition point following the instanton-antiinstanton pairing [142]. So our results will be considered as upper-bounds.

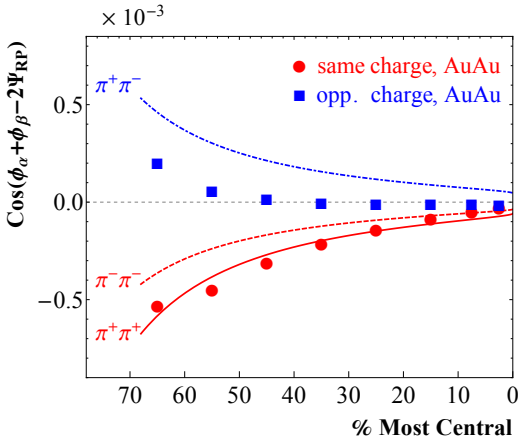

Figure 5.6: Pion azimuthal charge correlations of $AuAu$ versus the data [6] from STAR at $\sqrt{s} = 200\text{GeV}$.

For simplicity, we will set $\langle x \rangle \approx 0.01$ for each parton and $\langle z \rangle \approx 0.5$. The measured multiplicity spectra in [143] at different centralities suggest $m_\pi < \langle K_\perp \rangle < 3m_\pi$. We will set $\langle K_\perp \rangle = 2m_\pi$ in our analysis. We will assume a moderate polarization or $c\% = 15\%$ in the collision volume for a general discussion. We fix $\tau = 1/2\,\text{fm}$ to be the maximum duration of the magnetic field polarization, and set the pseudo-rapidity interval approximately $(-1, 1)$ for both STAR [6] and ALICE [7]. The radius of the colliding nuclei will be set to $R = 1\text{fm} \times \sqrt[3]{A}$ where A is the atomic number. The centrality is approximated as $n\% = b^2/(2R)^2$ [144]. We recall that [145]

$$\langle \cos(\phi_\alpha + \phi_\beta - 2\Psi_{\text{RP}}) \rangle \equiv - \langle a_\alpha a_\beta \rangle \tag{5.28}$$

and our results are displayed as

- $AuAu$ collisions at $\sqrt{s} = 200\text{GeV}$ (STAR) in Fig. 5.6
- $CuCu$ collisions at $\sqrt{s} = 200\text{GeV}$ (STAR) in Fig. 5.7
- $PbPb$ collisions at $\sqrt{s} = 2.76\text{TeV}$ (ALICE) in Fig. 5.8

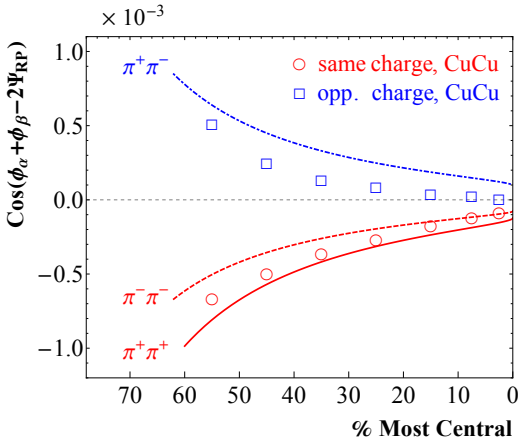

Figure 5.7: Pion azimuthal charge correlations of $CuCu$ versus the data [6] from STAR at $\sqrt{s} = 200$GeV.

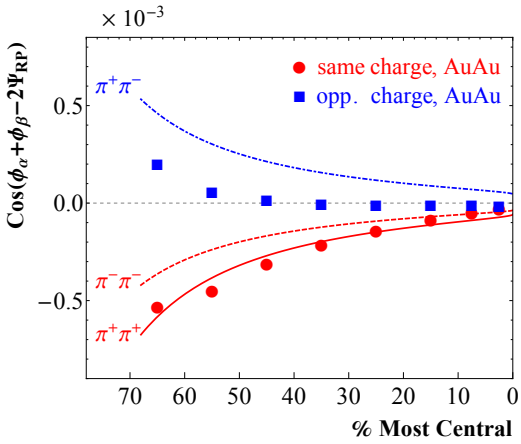

Figure 5.8: Pion azimuthal charge correlations of $PbPb$ versus the data from ALICE [7] at $\sqrt{s} = 2.76$TeV.

Chapter 6

Stringy Pomeron I

6.1 Dipole-dipole scattering I

In one of author's paper [74], we model the soft pomeron contribution to dipole-dipole scattering as a close string exchange in AdS_5 with a wall. The exchange of closed and long strings is characterized by an apparent Unruh temperature and entropy that are caused by the rapidity interval χ of the collision.

Let us now briefly review the basic formulation for the elastic dipole-dipole scattering amplitude through a Wilson loop correlator [74, 80, 76, 115, 146, 147, 148, 149] first in flat $D = 2 + D_\perp$ dimensions. Each dipole is described by a Wilson loop as shown in Fig. 6.1. The kinematics is captured by a fixed impact parameter $\mathbf{b}_\perp$, conjugate to the transferred momentum $\mathbf{q}_\perp$, and the rapidity interval χ related to the collisional energy.

At high energies, the T-matrix factorizes [150, 151, 147]

$$\mathcal{T}_{12\to 34}(s,t) = 2is \int du_1 du_2 \; \psi_4(u_1)\psi_3(u_1)\, \mathcal{T}_{DD}(\chi, \mathbf{q}_\perp, u_1, u_2) \; \psi_2(u_2)\psi_1(u_2) \; , \tag{6.1}$$

where u_i is related to the transverse size of the dipole element described by the wave function ψ_i. The dipole-dipole scattering amplitude is given by

$$\mathcal{T}_{DD}(\chi, \mathbf{q}_\perp, u_1, u_2) = \int d^{D_\perp - 1}\mathbf{b}_\perp \; e^{i\mathbf{q}_\perp \cdot \mathbf{b}_\perp} \, \mathbf{WW} \; , \tag{6.2}$$

with

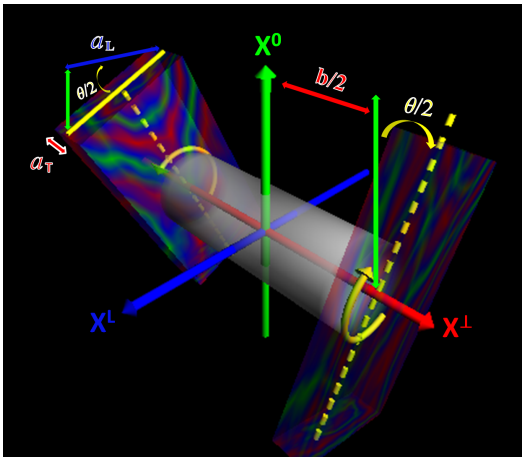

Figure 6.1: Twisted surface connecting the Wilson loops.

$$\mathbf{WW} \equiv 1 - \langle \mathbf{W}(C_1)\mathbf{W}(C_2)\rangle_G \tag{6.3}$$

The integration is taken over the $D_\perp - 1$ dimensional impact parameter space separating the two dipoles. For the results to follow and for simplicity, the dipole sizes will be fixed to a near the UV boundary. We use the normalization $\langle \mathbf{W}\rangle = 1$ and focus only on the connected part of the correlator. The Wilson loops are evaluated along the surfaces C_1, C_2 pictured in Fig. 6.1. The subscript G indicates that the expectation value of the Wilson loop correlator is taken over gauge fields. This is the pomeron limit.

We note that $\mathcal{T}_{DD}$ in (6.1-6.2) is the close string propagator attached to the 2 sourcing dipoles in 5-dimensions. It different is from the distorted (by curvature) spin-2 graviton exchange of [62, 63]. The graviton is massive in walled AdS. Our approach is similar to the one used initially in [58, 59, 70] with a key difference that $D_\perp = 5$ and not 10. In the eikonal approximation, the ultrarelativistic dipole is a scalar since it moves nearly on the light cone. In (6.2) we have suppressed a dependence on the individual momenta of the dipole constituents and assumed that the total momentum of each dipole is equally distributed between its constituents. The effective size of the dipole is at a maximum when the momentum is unequally distributed and, hence, we are restricting our analysis to small dipoles.

When the dipoles are small compared to the impact parameter and the

rapidity interval is large, the surface connecting the two dipoles is highly twisted and can be approximated by the world-sheet of a string with the appropriate boundary conditions, see Figure 6.1. The exchanged surface in Figure 6.1 is the world-sheet surface of a close string exchanged in the t-channel. The string is subjected to twisted (boosted) boundary conditions. The surface is best described in Euclidean space with a real twist angle θ and then analytically continued to Minkowski space through $\theta \to -i\chi$ [58, 59, 70, 152, 153].

At large N_c the surface can be thought as the worldsheet made of fishnet diagrams [55]. At strong coupling $\lambda = g^2 N_c$ the worldsheet can be sought in the context of holographic QCD. For that, we will use the bottom-up approach and assume the string to be exchanged in curved AdS_5 with a hard wall, i.e.

$$ds^2 = \frac{1}{z^2}\left((dx^0)^2 + (dx^1)^2 + (dx_\perp^2) + (dz)^2\right) \ , \tag{6.4}$$

with $0 \leq z \leq z_0$. So $D_\perp = 3$. The holographic z-direction will be identified with the size of the probing dipoles [71, 72]. Their evolution is captured by the conformal nature of the AdS_5 metric in the UV. Although the field theory corresponding to this truncated space is not exactly QCD, the idea is that it captures a key aspect of the QCD string evolution in the conformal limit. A similar idea was used in the light-front translation of the holographic wavefunctions [154].

For dipole sizes a small and near the boundary, at large impact parameters the exchanged string is long and lies mostly on the wall at $z \approx z_0$ whereby the metric is nearly flat [58, 59, 70]. In this limit the string action can be approximated by the flat Polyakov action

$$S[x] = \frac{\sigma_T}{2}\int_0^T d\tau \int_0^1 \left(\dot{x}^\mu \dot{x}_\mu + x'^\mu x'_\mu\right) \tag{6.5}$$

with $\dot{x} = \partial_\tau x$ and $x' = \partial_\sigma x$. The string tension is $\sigma_T = 1/(2\pi\alpha')$. The Regge slope α' is related to the fundamental string length by $\alpha' = l_s^2 \approx 1/(z_0^2\sqrt{\lambda})$. We have made the following gauge choice for the world-sheet metric $h_b^a = \delta_b^a$. With this in mind, the Wilson loop correlator is that of a close string exchange [70]

$$\mathbf{WW} = g_s^2 \int_0^\infty \frac{dT}{2T}\ \mathbf{K}(T)\ . \tag{6.6}$$

with the string partition function

$$\mathbf{K}(T) = \int_T d[x]\ e^{-S[x]+\text{ghosts}}\ . \tag{6.7}$$

The close string is parametrized by one parameter, the modulus ("circumference") T. The factor g_s^2 in (6.6) comes from the genus of the string configuration compared to the disconnected configuration.

Some details regarding the computation of the partition function (6.7) can be found at the end of this section where we derived the partition through both functional approach and canonical approach. The result is

$$\mathbf{K}(T) = i\frac{a^2}{\alpha'}\frac{e^{-\frac{\sigma_T}{2}Tb^2}}{2\sin(\frac{T}{2}\chi)} \times \prod_{n=1}^{\infty}\prod_{s=\pm}\frac{\sinh[\frac{T}{2}n\pi]}{\sinh[\frac{T}{2}(n\pi+is\chi)]} \times \eta^{-D_\perp}(\frac{iT}{2}) \tag{6.8}$$

or

$$\mathbf{WW} = \frac{ig_s^2a^2}{4\alpha'}\int_0^\infty \frac{dT}{T}\frac{e^{-\frac{\sigma_T}{2}Tb^2}}{\sin(\frac{T}{2}\chi)} \times \prod_{n=1}^{\infty}\prod_{s=\pm}\frac{\sinh[\frac{T}{2}n\pi]}{\sinh[\frac{T}{2}(n\pi+is\chi)]} \times \eta^{-D_\perp}(\frac{iT}{2}) \tag{6.9}$$

with $b^2 = \mathbf{b}_\perp^2$. The integral is dominated by the poles along the real T-axis or $T\chi/2 = k\pi$ with positive integer k. Thus

$$\mathbf{WW} = \pi g_s^2\frac{a^2}{4\alpha'}\sum_{k=1}^{\infty}\frac{\chi}{2k\pi}\frac{2}{\chi}(-1)^k e^{-k\frac{\pi\sigma_T b^2}{\chi}} \times \prod_{n=1}^{\infty}\prod_{s=\pm}\frac{\sinh(\frac{\pi^2nk}{\chi})}{\sinh[\frac{\pi^2nk}{\chi}+is\pi k]}\eta^{-D_\perp}(\frac{ik\pi}{\chi}) \tag{6.10}$$

Using the identity

$$\begin{aligned}\prod_{s=\pm}\frac{\sinh(\frac{\pi^2nk}{\chi})}{\sinh[\frac{\pi^2nk}{\chi}+is\pi k]} &= \frac{(e^{\frac{\pi^2nk}{\chi}}-e^{-\frac{\pi^2nk}{\chi}})^2}{(e^{\frac{\pi^2nk}{\chi}}e^{i\pi k}-e^{-\frac{\pi^2nk}{\chi}}e^{-i\pi k})(e^{\frac{\pi^2nk}{\chi}}e^{-i\pi k}-e^{-\frac{\pi^2nk}{\chi}}e^{i\pi k})} \\ &= 1\end{aligned} \tag{6.11}$$

we obtain

$$\mathbf{WW} = \frac{g_s^2 a^2}{4\alpha'} \sum_{k=1}^{[N_c/2]} \frac{(-1)^k}{k} e^{-k\frac{\pi\sigma_T \mathbf{b}^2}{\chi}} \eta^{-D_\perp}(\frac{ik\pi}{\chi}) \tag{6.12}$$

In [70], the sum over the successive poles labeled by k was identified with the N-ality of the Wilson-loop sourcing the close string exchange in Fig. 6.1. Specifically, $k = 1, .., [N_c/2]$ for the Wilson loops or $k = 1$ for $N_c = 3$. The switch from $[\infty/2]$ to $[N_c/2]$ can be inferred from the occurence of the k-string tension or $k\sigma_T$ in the exponent of (6.12) (see [70] for further arguments). Throughout only the $k = 1$ N-ality for $N_c = 3$ in the sum (6.12) will be retained, with

$$\mathbf{WW} \equiv -\frac{g_s^2 a^2}{4\alpha'} K_T(\beta, \mathbf{b}_\perp; k = 1) \tag{6.13}$$

Inserting (6.12-6.13) into (6.2) for fixed size dipoles $u_1 = u_2 = \ln(a/z_0)$ [71, 72], we obtain

$$\frac{1}{-2is}\mathcal{T}(s,t) \approx g_s^2 a^2 \int d^2\mathbf{b}_\perp \, e^{i\mathbf{q}_\perp\cdot\mathbf{b}_\perp} \, \mathbf{K}_T(\beta, \mathbf{b}_\perp; k = 1) \tag{6.14}$$

where $\mathbf{K}_T$ plays the role of a transverse partition function

$$\mathbf{K}_T\left(\beta, \mathbf{b}_\perp; k\right) = e^{-\sigma_k \beta b/2} \, \eta^{-D_\perp}\left(\frac{ik}{2}\frac{\beta}{b}\right) \tag{6.15}$$

Here $\sigma_k = k\sigma_T$ and σ_T is the fundamental string tension. It is important to note that the poles occur at (after restoring the dimension)

$$T = T_k \equiv 2k\pi/\chi \tag{6.16}$$

characterizing a periodic close loop exchange in Fig. 6.1. Also

$$\beta \equiv 2\pi b/\chi \tag{6.17}$$

where $1/\beta$ acts as the Unruh temperature for the close string exchange. Indeed, the string end-points are at a relative acceleration $\mathbf{a} = \chi/b$, so that the average Unruh temperature on the string world-sheet is $1/\beta = \mathbf{a}/2\pi$ [70].

For $N_c > \lambda > 1$, long strings and small Unruh temperatures in comparison to the Hagedorn temperature i.e. $\beta_H < \beta < b$, we will refer to $\mathbf{K}_T$ as the transverse propagator or partition function. In flat $5 = 2 + D_\perp$ dimensions it

follows from the scalar Polyakov action with twisted boundary conditions [70, 71]. The effects of AdS_5 curvature will be briefly discussed below. Using the modular identity for the Dedekind eta-function or $\eta(ix) = \eta(i/x)/\sqrt{x}$ [155], allows us to rewrite the eta-function in (6.15) as

$$\eta^{-D_\perp}\left(\frac{ik}{2}\frac{\beta}{b}\right) = \left(\frac{k\beta}{2b}\right)^{D_\perp/2} e^{\pi D_\perp b/6k\beta} \times \prod_{n=1}^{+\infty}\left(1-e^{-4\pi nb/k\beta}\right)^{-D_\perp} \tag{6.18}$$

effectively trading β/b with b/β which makes the string of exponents in (6.18) convergent. We note that large b corresponds to $\sqrt{-t} \ll \sqrt{s}$ pomeron exchange kinematics. Note that by inserting (6.18) into (6.15) and then in (6.14) the elastic amplitude rises with $(s/s_0)^{1+D_\perp/12k}$ for $\sqrt{s} \gg \sqrt{-t} = 0$. $D_\perp/12k$ is just the leading Luscher correction to the classical string contribution in flat space. Curvature corrections to this result will be discussed in next chapter.

We still need to derive the string partition function (Eq. 6.71) above using (**1**) the functional approach and (**2**) the canonical approach. Both approaches are complementary in illustrating the appearance of thermal effects. The string partition function reads

$$\mathbf{K}(T) = \int_T d[x]\; e^{-S[x]+\text{ghosts}} \tag{6.19}$$

where

$$S[x] = \frac{\sigma_T}{2}\int_0^T d\tau \int_0^1 d\sigma\left(\dot{x}^\mu\dot{x}_\mu + x'^\mu x'_\mu\right) \tag{6.20}$$

is the Polyakov string action. The collision set up is shown in Fig. 6.1, with the twisted boundary conditions

$$\begin{aligned}
&\cos\left(\frac{\theta}{2}\right)x^1 + \sin\left(\frac{\theta}{2}\right)x^0 \quad |_{\sigma=0} = 0, \qquad && x^\perp|_{\sigma=0} = -\frac{\mathbf{b}^\perp}{2} \\
&\cos\left(\frac{\theta}{2}\right)x^1 - \sin\left(\frac{\theta}{2}\right)x^0 \quad |_{\sigma=1} = 0, \qquad && x^\perp|_{\sigma=1} = +\frac{\mathbf{b}^\perp}{2}
\end{aligned} \tag{6.21}$$

with $\mathbf{b}^\perp = (0,\cdots,b,\cdots,0)$ and periodicity $x^\mu(\tau) = x^\mu(\tau+T)$. This latter property is at the origin of the thermal effects and the appearance of an Unruh temperature.

6.1.1 Functional approach

In Euclidean space, the twisted boundary condition (Eq. 6.21) can be simplified by the following transformation

$$\begin{pmatrix} x^0 \\ x^1 \end{pmatrix} = \begin{pmatrix} \cos\frac{\theta_\sigma}{2} & -\sin\frac{\theta_\sigma}{2} \\ \sin\frac{\theta_\sigma}{2} & \cos\frac{\theta_\sigma}{2} \end{pmatrix} \begin{pmatrix} \tilde{x}^0 \\ \tilde{x}^1 \end{pmatrix} \tag{6.22}$$

with $\theta_\sigma = \theta(2\sigma - 1)$ and leading to an ordinary Dirichlet boundary condition

$$\tilde{x}^1 \ |_{\sigma=0,1} = 0 \tag{6.23}$$

Note that (6.23) translates to

$$\partial_\tau \tilde{x}^1 \ |_{\sigma=0,1} = 0 \qquad \partial_\sigma \tilde{x}^0 \ |_{\sigma=0,1} = 0 \tag{6.24}$$

The second equation follows from the fact that the world-sheet $T^{\alpha\beta} = \delta S/\delta h_{\alpha\beta} = 0$. Thus, the mode decomposition

$$\begin{aligned} \tilde{x}^0(\tau,\sigma) &= \sum_{m=-\infty}^{\infty}\sum_{n=0}^{\infty} y^0_{m,n} \exp(i2\pi m\frac{\tau}{T})\cos(\pi n\sigma) \\ \tilde{x}^1(\tau,\sigma) &= \sum_{m=-\infty}^{\infty}\sum_{n=1}^{\infty} y^1_{m,n} \exp(i2\pi m\frac{\tau}{T})\sin(\pi n\sigma) \\ \tilde{x}^\perp(\tau,\sigma) &= x^\perp(\tau,\sigma) = (\sigma - \frac{1}{2})\mathbf{b}^\perp + \sum_{m=-\infty}^{\infty}\sum_{n=1}^{\infty} y^\perp_{m,n} \exp(i2\pi m\frac{\tau}{T})\sin(\pi n\sigma) \end{aligned} \tag{6.25}$$

Using the above results, we can recast (6.19) into

$$\mathbf{K} = \mathbf{K}_{0L} \times \mathbf{K}_{\varnothing L} \times \mathbf{K}_\perp \times \mathbf{K}_{\text{ghost}} \tag{6.26}$$

where $\mathbf{K}_{0L}$ and $\mathbf{K}_{\varnothing L}$ are the longitudinal zero and non-zero mode contributions respectively, $\mathbf{K}_\perp$ is the transverse contribution, and $\mathbf{K}_{\text{ghost}}$ is the ghost contribution. The explicit forms are given by

$$\mathbf{K}_{0L} = \prod_{m=-\infty}^{\infty} [\frac{\sigma_T T}{2\pi}(\theta^2 + \frac{4\pi^2 m^2}{T^2})]^{-\frac{1}{2}} \tag{6.27}$$

$$\mathbf{K}_{\emptyset L} = \prod_{n=1}^{\infty}\prod_{s=\pm}\prod_{m=-\infty}^{\infty}\{\frac{\sigma_T T}{4\pi}[\frac{4m^2\pi^2}{T^2}+(n\pi+s\theta)^2]\}^{-\frac{1}{2}} \tag{6.28}$$

$$\mathbf{K}_{\perp} = \exp[-\frac{\sigma_T}{2}Tb^2]\prod_{n=1}^{\infty}\prod_{m=-\infty}^{\infty}[\frac{\sigma_T T}{4\pi}(\frac{4\pi^2m^2}{T^2}+n^2\pi^2)]^{-\frac{D_\perp}{2}} \tag{6.29}$$

and the ghost contribution tags to the two longitudinal non-zero mode contribution

$$\mathbf{K}_{\rm ghost} = \prod_{n=1}^{\infty}\prod_{m=-\infty}^{\infty}\frac{\sigma_T T}{4\pi}(\frac{4m^2\pi^2}{T^2}+n^2\pi^2) \tag{6.30}$$

The products are divergent, but can be done with the help of ζ-function regularization and the product formula for sinh

$$\frac{\sinh x}{x} = \prod_{n=1}^{\infty}(1+\frac{x^2}{\pi^2n^2}) \tag{6.31}$$

The transverse-mode contribution $\mathbf{K}_\perp$ (Eq. 6.68) now reads

$$\begin{aligned}\mathbf{K}_{\perp} &= \exp[-\frac{\sigma_T}{2}Tb^2]\prod_{n=1}^{\infty}\prod_{m=-\infty}^{\infty}[m^2(1+\frac{(\frac{n\pi T}{2})^2}{m^2\pi^2})]^{-\frac{D_\perp}{2}} \\ &= \exp[-\frac{\sigma_T}{2}Tb^2]\prod_{n=1}^{\infty}[2\sinh(\frac{n\pi T}{2})]^{-D_\perp}\end{aligned} \tag{6.32}$$

where we used $\prod_{-\infty}^{\infty} c = 1$ and $\prod_{m=1}^{\infty} m = \sqrt{2\pi}$. We further notice

$$\begin{aligned}\prod_{n=1}^{\infty}2\sinh(\pi\frac{T}{2}n) &= \prod_{n=1}^{\infty}(e^{\pi n\frac{T}{2}}-e^{-\pi n\frac{T}{2}}) \\ &= e^{\sum_{n=1}^{\infty}\pi n\frac{T}{2}} * \prod_{n=1}^{\infty}(1-e^{-\pi nT}) \\ &= e^{-\pi\frac{T}{24}} * \prod_{n=1}^{\infty}(1-e^{-\pi nT}) \\ &= \eta(\frac{iT}{2})\end{aligned} \tag{6.33}$$

where $\eta(\tau)$ is Dedekind eta function after using $\zeta(0) = -1/12$. Similar arguments yield

$$\begin{aligned}\mathbf{K}_{0L} &= \frac{1}{2\sinh(\frac{T}{2}\theta)} \\ \mathbf{K}_{\emptyset L} &= \prod_{n=1}^{\infty}\prod_{s=\pm}\frac{1}{2\sinh[\frac{T}{2}(n\pi+s\theta)]}\end{aligned} \tag{6.34}$$

In sum, the string partition function is given by

$$\mathbf{K}(T) = \frac{a^2}{\alpha'}\frac{e^{-\frac{\sigma_T}{2}Tb^2}}{2\sinh(\frac{T}{2}\theta)} \times \prod_{n=1}^{\infty}\prod_{s=\pm}\frac{\sinh[\frac{T}{2}n\pi]}{\sinh[\frac{T}{2}(n\pi+s\theta)]} \times \eta^{-D_\perp}(\frac{iT}{2}) \tag{6.35}$$

with

$$a^2 \longrightarrow a_T^2 + \frac{a_L^2}{\sin^2(\frac{\theta}{2})} \approx a_T^2 \tag{6.36}$$

the transpose dipole size squared. The analytical continuation to Minkowski space or $\theta \longrightarrow -i\chi$, gives the final result

$$\mathbf{K}(T) = i\frac{a^2}{\alpha'}\frac{e^{-\frac{\sigma_T}{2}Tb^2}}{2\sin(\frac{T}{2}\chi)} \times \prod_{n=1}^{\infty}\prod_{s=\pm}\frac{\sinh[\frac{T}{2}n\pi]}{\sinh[\frac{T}{2}(n\pi+is\chi)]} \times \eta^{-D_\perp}(\frac{iT}{2}) \tag{6.37}$$

which is (6.71).

6.1.2 Canonical approach

In this subsection, we re-derive the string partition function (6.71) using the canonical approach. In Minkowski space, we recall the second quantized transverse coordinates

$$x_\perp^i(\tau,\sigma) = \mathbf{b}^i(\frac{\sigma}{\pi} - \frac{1}{2}) + i\sqrt{2\alpha'}\sum_{n\neq 0}\frac{a_n^i}{n}\sin(n\sigma)\, e^{-in\tau} \tag{6.38}$$

with the transverse oscillator algebra

$$\left[a_n^i, a_m^j\right] = n\,\delta^{ij}\delta_{n+m,0} \tag{6.39}$$

after rescaling $\sigma \to \sigma/\pi$. We have

$$P_\perp^i = \sigma_T \dot{x}_\perp^i = \sigma_T\sqrt{2\alpha'}\sum_{n\neq 0} a_n^i \sin(n\sigma)\, e^{-in\tau} \tag{6.40}$$

and the canonical commutation rule follows

$$
\begin{aligned}
[x^i_\perp(\tau,\sigma), P^j_\perp(\tau,\sigma')] &= i\sigma_T 2\alpha' \sum_{n\neq 0}\sum_{m\neq 0} \frac{\sin(n\sigma)e^{-in\tau}}{n}\sin(m\sigma')e^{-im\sigma'}[a^i_n, a^j_m] \\
&= i\delta_{\rm NM}(\sigma-\sigma') \qquad (6.41)
\end{aligned}
$$

The Nonzero-Mode delta function is defined as

$$
\delta_{NM}(\sigma-\sigma') = \sum_{n\neq 0}\sin(n\sigma)\sin(n\sigma')/\pi\,. \qquad (6.42)
$$

Thus

$$
\begin{aligned}
\int_0^T d\tau\int_0^\pi d\sigma\ \mathcal{H}_\perp &= \frac{\pi}{2}\int_0^T d\tau\int_0^\pi d\sigma\ (\frac{1}{\sigma_T}P^2 + \sigma_T(x')^2) \\
&= \frac{\sigma_T b^2 T}{2} + \frac{\pi T}{2}\sum_{n\neq 0}\sum_i^{D_\perp} a^i_n a^i_{-n} \qquad (6.43)
\end{aligned}
$$

We note that

$$
\begin{aligned}
< \exp(-\frac{\pi T}{2}\sum_{n\neq 0}\sum_i^{D_\perp} a^i_n a^i_{-n}) > &= < \exp\{-\frac{\pi T}{2}\sum_{n>0}\sum_i^{D_\perp}(a^i_n a^i_{-n} + a^i_{-n}a^i_n)\} > \\
&= < \exp\{-\frac{\pi T}{2}\sum_{n>0}\sum_i^{D_\perp}(2a^i_{-n}a^i_n + [a^i_n, a^i_{-n}])\} > \\
&= < \exp(-\pi T\mathbf{L}_0) > \exp(-\frac{\pi T}{2}\sum_{n>0}\sum_i^{D_\perp} n) \\
&= < \exp[-\pi T(\mathbf{L_0} - \frac{D_\perp}{24})] > \qquad (6.44)
\end{aligned}
$$

where

$$
\mathbf{L}_0 = \sum_{n>0}\sum_i^{D_\perp} a^i_{-n}a^i_n \qquad (6.45)
$$

is the temporal Virasoro generator. For arbitrary constant c, we have the

formula

$$\begin{aligned}\mathrm{Tr}\left[\exp(-c\mathbf{L}_0)\right] &= \prod_{i}^{D_\perp}\prod_{n=1}^{\infty}\prod_{N_i=0}^{\infty} e^{cnN_i} \\ &= (\prod_{n=1}^{\infty}\frac{1}{1-e^{-cn}})^{D_\perp} \\ &= \prod_{n=1}^{\infty}(1-e^{-cn})^{-D_\perp} \end{aligned} \tag{6.46}$$

where we used $< N_1, \cdots, N_{D_\perp}|a^i_{-n}a^i_n|N_1, \cdots, N_{D_\perp} >= N_i$. Combining these results, we reproduce the transverse propagator (6.32)

$$\begin{aligned}\mathbf{K}_\perp &= \mathrm{Tr}\left[\exp(-\int_0^T d\tau \int_0^\pi d\sigma\ \mathcal{H}_\perp)\right] \\ &= \exp(-\frac{\sigma_T}{2}Tb^2)\times e^{\frac{D_\perp}{24}\pi T}\prod_{n=1}^{\infty}(1-e^{-n\pi T})^{-D_\perp} \\ &= \exp(-\frac{\sigma_T}{2}Tb^2)\eta^{-D_\perp}(\frac{iT}{2}) \end{aligned} \tag{6.47}$$

Now, we derive the longitudinal propagator (Eq. 6.34). In Minkowski space $\theta \longrightarrow -i\chi$, the twisted boundary condition (Eq. 6.21) at $\sigma = 0$ reads

$$\sinh(\frac{\chi}{2})x^0 + \cosh(\frac{\chi}{2})x^1 = 0 \tag{6.48}$$

Apply ∂_τ to both sides of (6.48) and note again that $T^{\alpha\beta} = \delta S/\delta h_{\alpha\beta} = 0$. Thus

$$\begin{aligned}\sinh(\frac{\chi}{2})\partial_\tau x^0 + \cosh(\frac{\chi}{2})\partial_\tau x^1 &= 0 \\ \cosh(\frac{\chi}{2})\partial_\sigma x^0 + \sinh(\frac{\chi}{2})\partial_\sigma x^1 &= 0 \end{aligned} \tag{6.49}$$

Use T-duality along the direction x^1

$$\partial_\tau x^1 = \partial_\sigma y^1 \qquad \partial_\sigma x^1 = \partial_\tau y^1 \tag{6.50}$$

and denote $y^0 \doteq x^0$. The boundary condition is now given by

$$\begin{aligned}\sinh(\frac{\chi}{2})\partial_\tau y^0 + \cosh(\frac{\chi}{2})\partial_\sigma y^1 &= 0 \\ \cosh(\frac{\chi}{2})\partial_\sigma y^0 + \sinh(\frac{\chi}{2})\partial_\tau y^1 &= 0 \end{aligned} \tag{6.51}$$

To diagonalize the boundary conditions (Eq. 6.51), define

$$y^{\pm} = \frac{1}{\sqrt{2}}(y^0 \pm y^1) \tag{6.52}$$

We then obtain

$$\begin{aligned} \partial_\sigma y^{\pm} &= \mp \tanh(\frac{\chi}{2})\partial_\tau y^{\pm} \qquad (\sigma = 0) \\ \partial_\sigma y^{\pm} &= \pm \tanh(\frac{\chi}{2})\partial_\tau y^{\pm} \qquad (\sigma = 1) \end{aligned} \tag{6.53}$$

The canonical form of $y^{\pm}$ reads [156, 157]

$$y^{\pm} = Y^{\pm} + i\sqrt{2\alpha'}a_0^{\pm}\phi_0^{\pm} + i\sqrt{2\alpha'}\sum_{n>0}[a_n^{\pm}\phi_n^{\pm} - (a_n^{\pm})^*(\phi_n^{\pm})^*] \tag{6.54}$$

where

$$\phi_n^{\pm}(\tau,\sigma) = (n \pm i\frac{\chi}{\pi})^{-\frac{1}{2}} e^{-i(n\pm i\frac{\chi}{\pi})\tau}\cos[(n \pm i\frac{\chi}{\pi})\sigma \mp i\frac{\chi}{2}] \tag{6.55}$$

It follows readily that

$$\frac{\partial_\sigma \phi_n^{\pm}}{\partial_\tau \phi_n^{\pm}} = -i\tan[(n \pm i\frac{\chi}{\pi})\sigma \mp i\frac{\chi}{2}] = \begin{cases} \mp\tanh(\frac{\chi}{2}), & (\sigma = 0) \\ \pm\tanh(\frac{\chi}{2}), & (\sigma = 1) \end{cases} \tag{6.56}$$

which explicitly satisfy (6.53). Define the commutation relations

$$[a_n^{\pm}, (a_m^{\mp})^*] = \delta_{n,m} \tag{6.57}$$

where $(a_0^{\pm})^* = \pm i a_0^{\pm}$. The conjugate momentum is then

$$\begin{aligned} p^{\pm} &= \sigma_T \dot{y}^{\mp} \\ &= \sqrt{2\alpha'}\sigma_T(\mp i\frac{\chi}{\pi})a_0^{\mp}\phi_0^{\mp} + \sigma_T\sqrt{2\alpha'}\sum_{n>0}[(n \mp i\frac{\chi}{\pi})a_n^{\mp}\phi_n^{\mp} + (n \pm i\frac{\chi}{\pi})(a_n^{\mp})^*(\phi_n^{\mp})^*] \end{aligned} \tag{6.58}$$

The canonical commutation relation follows

$$\begin{aligned} [y^{\pm}, p^{\pm}] &= \frac{i}{\pi}\sum_n \{\cos[(n \pm i\frac{\chi}{\pi})\sigma \mp i\frac{\chi}{2}]\cos[(n \pm i\frac{\chi}{\pi})\sigma \mp i\frac{\chi}{2}]\} \\ &= i\delta(\sigma - \sigma') \end{aligned} \tag{6.59}$$

After simple algebra, we obtain

$$\begin{aligned}
&\int_0^T d\tau \int_0^\pi d\sigma\ \mathcal{H}_L \\
= &\frac{\pi}{2}\int_0^T d\tau \int_0^\pi d\sigma\ [\frac{1}{\sigma_T}(p^\pm p^\mp) + \sigma_T(\partial_\sigma y^\pm)(\partial_\sigma y^\mp)] \\
= &\frac{T}{2}\sum_{n>0}\{(n\pi - i\chi)[a_n^-(a_n^+)^* + (a_n^+)^* a_n^-] + h.c.\} + \chi(a_0^- a_0^+ + a_0^+ a_0^-)
\end{aligned} \tag{6.60}$$

where $n > 0$ are the nonzero modes and $a_0^\pm$ are zero modes. The zero mode propagator reads

$$\begin{aligned}
\mathbf{K}_{0L} &= \text{Tr } < \exp[-\int_0^T d\tau \int_0^\pi d\sigma\ \mathcal{H}_{0L}] > \\
&= \text{Tr } < \exp[-\frac{T}{2}\chi(a_0^- a_0^+ + a_0^+ a_0^-)] > \\
&= \text{Tr } < \exp[-iT\chi(a_0^-)^* a_0^+ - i\frac{T}{2}\chi[a_0^+, (a_0^-)^*]] > \\
&= e^{-i\frac{T}{2}\chi}\frac{1}{1-e^{-iT\chi}} \\
&= \frac{1}{2i\sin(\frac{\chi T}{2})}
\end{aligned} \tag{6.61}$$

Comparing with (6.34), we reproduce the zero mode propagator. A repeat of the same algebra yields

$$\mathbf{K}_{\emptyset L} = \prod_{n=1}^{\infty}\frac{1}{2\sinh(\frac{T}{2}(n\pi + i\chi))}\frac{1}{2\sinh(\frac{T}{2}(n\pi - i\chi))} \tag{6.62}$$

which is the nonzero mode propagator. In sum, we confirm the string partition function (6.71) through the canonical approach.

6.2 Dipole-dipole scattering II

In another one of author's paper [80], we model the soft pomeron in QCD using a scalar Polyakov string with extrinsic curvature in the bottom-up

approach of holographic QCD. The overall dipole-dipole scattering amplitude in the soft pomeron kinematics is shown to be sensitive to the extrinsic curvature of the string for finite momentum transfer. The characteristics of the diffractive peak in the differential elastic *pp* scatterings are affected by a small extrinsic curvature of the string.

Our approach here is similar to the previous section with the difference that $2 + D_\perp = 5$ and not 10 [71, 72, 73]. The analysis of the soft pomeron is different from the (distorted) spin-2 graviton exchange in [62, 63, 64, 65] as the graviton is massive in walled AdS_5. It is essentially an effective approach along the bottom-up scenario of AdS_5 with metric

$$ds^2 = \frac{R^2}{z^2}\left((dx^0)^2 + (dx^1)^2 + (dx_\perp)^2 + (dz)^2\right) \tag{6.63}$$

and $0 \leq z \leq z_0$. R is the size of the AdS space for $z_0 = \infty$. Although the dual field theory corresponding to this truncated version of AdS_5 metric is not QCD, it does capture some key aspects, i.e. conformality in the UV and confinement in the IR. A similar argument was made in [158] in calculating the light-front wave-functions from the AdS/CFT holographic correspondence.

There are many indications from lattice simulations that flux tubes in Yang-Mills theory can be described by an effective theory of strings of which the Nambu-Goto (NG) action is a good approximation in leading order [159]. Polyakov has suggested that the NG action must include an effective contribution that accounts for the extrinsic curvature of the world-sheet at next order. The extrinsic curvature favors smooth string configurations and penalizes strings with high curvature. Specifically, the scalar action in Polyakov form with extrinsic curvature is [160, 161]

$$\begin{aligned} S[x] &= \frac{\sigma_T}{2}\int_0^T d\tau \int_0^1 d\sigma\ (\dot{x}^\mu \dot{x}_\mu + x'^\mu x'_\mu) \\ &\quad + \frac{1}{2\kappa b^2}\int_0^T d\tau \int_0^1 d\sigma\ (\ddot{x}^\mu \ddot{x}_\mu + 2\dot{x'}^\mu \dot{x'}_\mu + x''^\mu x''_\mu) \end{aligned} \tag{6.64}$$

We have set the gauge on the world-sheet to be $h^a_b = \delta^a_b$ and used the nearly flat metric $g^{\mu\nu}(z \approx z_0) = \delta^{\mu\nu} R^2/z_0^2$ at the bottom of AdS_5 (long strings). Here $\dot{x} = \partial_\tau x$ and $x' = \partial_\sigma x$. The string tension is $\sigma_T = 1/(2\pi\alpha')$ with $\alpha' = z_0^2/\sqrt{\lambda}$, and the effective and dimensionless extrinsic curvature is $\kappa = e z_0^2/R^2$.

A similar calculation as before yields the closed string propagator $\mathbf{K}$ in the form

$$\mathbf{K} = \mathbf{K}_{0L} \times \mathbf{K}_{\varnothing L} \times \mathbf{K}_{\perp} \times \mathbf{K}_{\rm ghost} \tag{6.65}$$

$\mathbf{K}_{0L}$ and $\mathbf{K}_{\varnothing L}$ are the longitudinal zero and non-zero mode contributions respectively, $\mathbf{K}_{\perp}$ is the transverse contribution, and $\mathbf{K}_{\rm ghost}$ is the ghost contribution. Their explicit forms are

$$\mathbf{K}_{0L} = \{ \prod_{m=-\infty}^{\infty} [\frac{\sigma_T T}{2\pi}(\theta^2 + \frac{4\pi^2 m^2}{T^2}) + \frac{T}{2\kappa b^2 \pi}(\theta^2 + \frac{4\pi^2 m^2}{T^2})^2]\}^{-\frac{1}{2}} \tag{6.66}$$

$$\begin{aligned} \mathbf{K}_{\varnothing L} = \{\prod_{n=1}^{\infty}\prod_{s=\pm}\prod_{m=-\infty}^{\infty} & [\frac{\sigma_T T}{4\pi}(\frac{4m^2\pi^2}{T^2} + (n\pi + s\theta)^2) \\ & + \frac{T}{4\kappa b^2 \pi}(\frac{4m^2\pi^2}{T^2} + (n\pi + s\theta)^2)^2]\}^{-\frac{1}{2}} \end{aligned} \tag{6.67}$$

$$\begin{aligned} \mathbf{K}_{\perp} &= \{\prod_{n=1}^{\infty}\prod_{m=-\infty}^{\infty} [\frac{\sigma_T T}{4\pi}(\frac{4\pi^2 m^2}{T^2} + n^2\pi^2) + \frac{T}{4\kappa b^2\pi}(\frac{4\pi^2 m^2}{T^2} + n^2\pi^2)^2]\}^{-\frac{D_\perp}{2}} \\ &\quad \times \exp[-\frac{\sigma_T}{2} T b^2] \end{aligned} \tag{6.68}$$

$$\mathbf{K}_{\rm ghost} = \prod_{n=1}^{\infty}\prod_{m=-\infty}^{\infty} [\frac{\sigma_T T}{4\pi}(\frac{4m^2\pi^2}{T^2} + n^2\pi^2) + \frac{T}{4\kappa b^2\pi}(\frac{4m^2\pi^2}{T^2} + n^2\pi^2)^2] \tag{6.69}$$

which are seen to reduce to those in [70, 74] for $\kappa = \infty$. The ghost contribution beyond the scalar Polyakov action and for finite extrinsic curvature is assumed so as to cancel the $s = \pm 1$ spurious non-zero modes contribution from the longitudinal contribution for $\theta = 0$. This assumption while proved for $\kappa = \infty$ is now assumed for finite κ.

The string of diverging products can be regularized by standard zeta function regularization

$$\sinh(\pi x) = \pi x \prod_{m=1}^{\infty}\left(1 + \frac{x^2}{m^2}\right) \tag{6.70}$$

in terms of which the string partition function (6.65) now reads

$$\begin{aligned}
\mathbf{K}(T,\kappa) &= \frac{a^2}{\alpha'}\frac{e^{-\frac{\sigma_T}{2}Tb^2}}{2\sinh\left(\frac{\theta T}{2}\right)}\left[\prod_{n=1}^{\infty}\prod_{s=\pm}\frac{\sinh\left(\frac{n\pi T}{2}\right)}{\sinh\left(\frac{T(n\pi+s\theta)}{2}\right)}\right]\left[\prod_{n=1}^{\infty}2\sinh\left(\frac{n\pi T}{2}\right)\right]^{-D_\perp} \\
&\times\frac{1}{2\sinh\left(\frac{T}{2}\sqrt{\theta^2+\sigma_T\kappa b^2}\right)}\prod_{n=1}^{\infty}\prod_{s=\pm}\frac{1}{2\sinh\left[\frac{T(n\pi+s\theta)}{2}\sqrt{1+\frac{\sigma_T\kappa b^2}{(n\pi+s\theta)^2}}\right]} \\
&\times 2^{D_\perp}\left[2\prod_{n=1}^{\infty}\sinh\left(\frac{n\pi T}{2}\sqrt{1+\frac{\sigma_T\kappa b^2}{n^2\pi^2}}\right)\right]^{-D_\perp+2} \qquad (6.71)
\end{aligned}$$

with

$$a^2 \longrightarrow a_T^2+\frac{a_L^2}{\sin^2(\frac{\theta}{2})}\to a_T^2 \qquad (6.72)$$

as the longitudinal dipole size a_L is suppressed at large χ after analytical continuation. Note that for large transverse impact parameter b

$$\begin{aligned}
&\prod_{n=1}^{\infty}\prod_{s=\pm}\frac{1}{2\sinh\left(\frac{T(n\pi+s\theta)}{2}\sqrt{1+\frac{\sigma_T\kappa b^2}{(n\pi+s\theta)^2}}\right)} \\
&\approx \exp\left[-\sum_{n=1}^{\infty}\sum_{s=\pm}\frac{Tb\sqrt{\kappa\sigma_T}}{2}\left(1+\frac{1}{2}\frac{(n\pi+s\theta)^2}{\sigma_T\kappa b^2}+\cdots\right)\right] \\
&\approx \exp\left(-\zeta(0)Tb\sqrt{\kappa\sigma_T}\sqrt{1+\frac{\theta^2}{\sigma_T\kappa b^2}}\right) \\
&= \exp\left(\frac{T}{2}\sqrt{\sigma_T\kappa b^2+\theta^2}\right) \qquad (6.73)
\end{aligned}$$

and

$$\begin{aligned}
&\prod_{n=1}^{\infty}2\sinh\left(\frac{n\pi T}{2}\sqrt{1+\frac{\sigma_T\kappa b^2}{n^2\pi^2}}\right) \\
&\approx \exp\left[\sum_{n=1}^{\infty}\frac{Tb\sqrt{\kappa\sigma_T}}{2}\left(1+\frac{1}{2}\frac{n^2\pi^2}{\sigma_T\kappa b^2}+\cdots\right)\right] \\
&= \exp\left(-\frac{Tb\sqrt{\kappa\sigma_T}}{4}\right) \qquad (6.74)
\end{aligned}$$

where we used $\zeta(-2n)=0$ ($n=1,2,3,\cdots$). Thus (6.71) simplifies to

$$\mathbf{K}(T,\kappa)\approx\mathbf{K}_{\rm F}(T)\ \exp\left[\frac{(D_\perp-2)}{4}Tb\sqrt{\kappa\sigma_T}\right] \tag{6.75}$$

with $\mathbf{K}_{\rm F}(T)$ the closed string propagator without the extrinsic curvature κ,

$$\mathbf{K}_{\rm F}(T)=\frac{a^2}{\alpha'}\frac{e^{-\frac{\sigma_T}{2}Tb^2}}{2\sinh\left(\frac{\theta T}{2}\right)}\prod_{n=1}^{\infty}\prod_{s=\pm}\frac{\sinh\left(\frac{n\pi T}{2}\right)}{\sinh\left[\frac{T(n\pi+s\theta)}{2}\right]}\left[\prod_{n=1}^{\infty}2\sinh\left(\frac{n\pi T}{2}\right)\right]^{-D_\perp} \tag{6.76}$$

The resulting (6.75) is rather similar to the one derived in one-loop in [161] for a large and static Wilson loop. We now detail its impact on the scattering of two twisted dipoles with the soft Pomeron kinematics.

Now we can analytically continue $\theta\longrightarrow-i\chi$ and then obtain the twisted Wilson-loop correlator

$$\mathbf{WW}=\frac{g_s^2a^2}{4\alpha'}\sum_{k=1}^{\infty}\frac{(-1)^k}{k}e^{-k\frac{\pi\sigma_T\mathbf{b}^2}{\chi}}\eta^{-D_\perp}(\frac{ik\pi}{\chi})\ \exp\left[\frac{(D_\perp-2)k\pi}{2\chi}b\sqrt{\kappa\sigma_T}\right] \tag{6.77}$$

where $\eta(\tau)$ is Dedekind eta function and $\eta(ix)=\eta(i/x)/\sqrt{x}$ [70, 74]

$$\begin{aligned}\eta^{-D_\perp}(\frac{ik\pi}{\chi}) &= (\frac{k\pi}{\chi})^{\frac{D_\perp}{2}}e^{\frac{\chi D_\perp}{12k}}\prod_{n=1}^{\infty}(1-\exp[-\frac{2n\chi}{k}])^{-D_\perp}\\ &= (\frac{k\pi}{\chi})^{\frac{D_\perp}{2}}e^{\frac{\chi D_\perp}{12k}}\sum_{n=0}^{\infty}d(n)e^{-n\frac{2\chi}{k}}\end{aligned} \tag{6.78}$$

In momentum space, the scattering amplitude is

$$\begin{aligned}\frac{1}{-2is}\mathcal{T}_{DD}(\chi,q) &\approx \int d^2\mathbf{b}\ e^{i\mathbf{q}_\perp\cdot\mathbf{b}}\langle\mathbf{WW}\rangle\\ &\approx \frac{\pi^2g_s^2a^2}{2}\sum_{n=0}^{\infty}\sum_{k=1}^{\infty}\ d(n)\frac{(-1)^k}{k}\left(\frac{k\pi}{\chi}\right)^{\frac{D_\perp-2}{2}}\\ &\quad\times\exp\left(\chi\frac{D_\perp}{12k}-\chi\frac{2n}{k}-\chi\frac{\mathbf{q}_\perp^2}{4\sigma_Tk\pi}+\sqrt{\kappa}\frac{D_\perp-2}{4}\frac{|\mathbf{q}_\perp|}{\sqrt{\sigma_T}}\right)\end{aligned} \tag{6.79}$$

where we used $\chi \approx \ln s$ for large s. Recall that the sum over k runs over the N-ality of the gauge group which is up to $[N_c/2] = \infty$ in the AdS/CFT correspondence [74]. For QCD $N_c = 3$ and $[3/2] = 1$ which means only the $k = 1$ term contributes to the scattering of two dipoles in the fundamental representation of SU(N_c). The effect of the extrinsic curvature is a momentum dependent contribution to the exponent that is large but sub-leading at large χ.

6.3 *pp* scattering

For fixed impact parameter, $\langle \mathbf{WW} \rangle$ is the elastic amplitude of a dipole of size a onto a fixed dipole $a' = a$, both of which are fixed in the UV or on the boundary. In general, the dipole size in a given hadron, say p or $\bar{p}$ is scale dependent and identified with the holographic direction i.e. $a \to z = z_0 e^{-u(z)}$ and $a' \to z' = z_0 e^{-u'(z')}$ with $0 < u, u' < \infty$ [72]. With this in mind the elastic scattering amplitude for pp scattering $p_1 p_2 \to p_1 p_2$ reads in general

$$\mathcal{T}_{pp}(\chi, \mathbf{b}) = \int_0^\infty du \int_0^\infty du' \; \psi_1^*(u)\psi_2^*(u')\mathcal{T}_{DD}\left(\chi, \mathbf{b}, u, u'\right)\psi_1(u)\psi_2(u') \quad (6.80)$$

In our case $|\psi_{1,2}(u,u')|^2 \equiv \mathcal{N}_p \delta(u, u' - u(a))$ for equal and fixed size dipoles a and $\mathcal{T}_{DD}$ is the dipole-dipole scattering amplitude. In the eikonal approximation the elastic differential cross section reads

$$\begin{aligned} \frac{d\sigma}{dt} &= \frac{1}{16\pi s^2}\left|\mathcal{T}_{pp}(\chi, q)\right|^2 \\ &= \frac{1}{4\pi}\left| i \int d\mathbf{b}^2 \int du \int du' \; e^{i\mathbf{q}_\perp \cdot \mathbf{b}} |\psi_1(u)|^2 |\psi_2(u')|^2 \left(1 - e^{\mathbf{WW}}\right)\right|^2 \\ . \end{aligned} \quad (6.81)$$

An optimal analysis of the available elastic differential pp data follows by setting: $D_\perp = 3$, $N_c = 3$, $\lambda = g^2 N_c = 9.4$, $\kappa_g = 4\pi\, g_s/g^2 = 2.85$, $z_0 = R = 0.4$ fm, $\mathcal{N}_p = 1.5$ and $a = 0.25$ fm with a fixed rapidity interval $\chi = 6$. This parameter set is overall consistent with the one used in [72] for the analysis of the DIS data. The results are displayed in Fig 6.2 and compared to the elastic pp data for $\sqrt{s} = 30.7, 44.7, 52.8$ GeV from [162]. The solid curve is for

$\sqrt{s}$ [GeV]	t [GeV^2]	$\mathbf{B}(t)$ [GeV^{-2}] Experimental Data [162]	$\mathbf{B}(t)$ [GeV^{-2}]	
			$e = 0$	$e = 0.002$
30.7	0.015 - 0.055	13.0 ± 0.7	8.4	8.5
44.7	0.03 - 0.15	12.9 ± 0.4	8.4	8.5
52.8	0.04 - 0.16	13.0 ± 0.3	8.5	8.5

Table 6.1: Slope parameter $\mathbf{B}(t)$ for the elastic differential cross section.

no extrinsic curvature $e = \kappa = 0$ and the dashed curve is for $e = \kappa = 0.002$. The slope parameter $\mathbf{B}(t)$ for the elastic differential cross section

$$\mathbf{B}(t) = \frac{d}{dt}\left(\ln\left(\frac{d\sigma}{dt}\right)\right) \tag{6.82}$$

is tabulated in Table-6.1.

While $\mathbf{B}(t)$ does not change with a small change in the extrinsic curvature e, Fig 6.2 shows that the depth and somehow the position of the diffractive peak are affected by a small extrinsic curvature for a stringy description of the pomeron. The shaded region illustrates a possible range of extrinsic curvatures that are compatible with the measured diffractive peak.

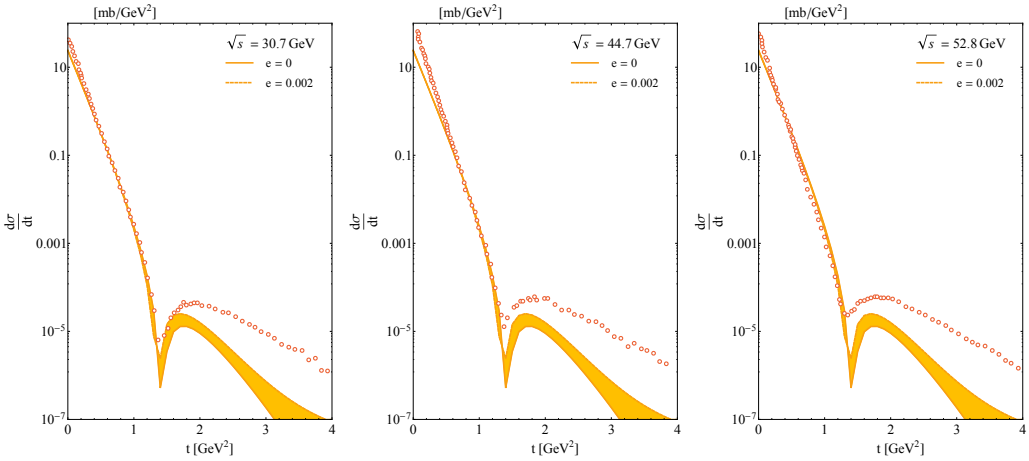

Figure 6.2: Elastic differential pp cross section: solid curve stringy pomeron with no extrinsic curvature $\kappa = e = 0$; dashed curve with $\kappa = e = 0.002$; the data is from [8].

While a more exhaustive analysis of the parameter space together with a better description of the dipole-dipole scattering amplitude at larger $|t|$

are needed, our estimates show an interesting interplay between the characteristics of the diffractive peak and the extrinsic curvature of the stringy pomeron. Is this expected within the range of our analysis? To answer this question, we recall that in dipole-dipole scattering the use of the leading scalar Polyakov action (first term in (6.64)) is justified for large impact parameters $\mathbf{b}$, when the induced Unruh temperature $1/\beta = 2\pi\mathbf{b}/\chi$ on the string world-sheet is small in comparison to the Hagedorn temperature $1/\beta_H = \sqrt{6/(D_\perp \alpha')}/2\pi$ [115, 75, 74, 163]

$$\frac{\beta}{\beta_H} \equiv \frac{2\pi\mathbf{b}}{\chi\beta_H} > \frac{1}{\sqrt{2}} \tag{6.83}$$

with the string length $\sqrt{\alpha'} = l_s \approx 0.1$ fm. For the above choice of parameters, this implies that $\mathbf{b} > 4l_s/\sqrt{2} \approx 0.28$ fm which puts the validity range at $\sqrt{-t} \approx 1/\mathbf{b} \approx 0.7$ GeV. The inclusion of the extrinsic curvature (second term in (6.64)) extends the validity range to smaller $\mathbf{b}$ or larger $\sqrt{-t}$. Our numerical analysis shows that these corrections are small with the exception of the region near the diffractive peak or $\sqrt{-t} \approx 1$ GeV. Clearly, next to next to leading corrections in the string effective action as discussed in [164] maybe needed to firm up the validity of this observation. Their analysis goes beyond the scope of this work. Finally, we note that if we were to relax the flat space approximation, the validity range can be somehow increased, as the effects of curvature on the stringy part of the dipole-dipole scattering can be schematically captured through an effective reduction in the transverse dimension $D_\perp = 3 \to D_\perp(\lambda) < 3$ [71, 72, 73, 75, 115, 76]. Thus, an effective increase in the Hagedorn temperature and a slightly lower bound on $\mathbf{b}$ through (6.83).

6.4 Static and stringy dipole-dipole interaction

At the end of this chapter, we detail the role of the extrinsic curvature on the correlator of two static but untwisted Wilson loops with $\theta = 0$, i.e. the interaction between two static dipoles. Instead of (6.25) we now have the mode decomposition

$$
\begin{aligned}
x^0(\tau,\sigma) &= \sum_{m=-\infty}^{\infty}\sum_{n=1}^{\infty} x^0_{m,n}\exp(i2\pi m\frac{\tau}{T})\cos(\pi n\sigma) + X + \frac{P}{\sigma_T}\tau \\
x^1(\tau,\sigma) &= \sum_{m=-\infty}^{\infty}\sum_{n=1}^{\infty} x^1_{m,n}\exp(i2\pi m\frac{\tau}{T})\sin(\pi n\sigma) \\
x^\perp(\tau,\sigma) &= (\sigma-\frac{1}{2})b^\perp + \sum_{m=-\infty}^{\infty}\sum_{n=1}^{\infty} x^\perp_{m,n}\exp(i2\pi m\frac{\tau}{T})\sin(\pi n\sigma) \quad (6.84)
\end{aligned}
$$

with P the number of windings in the temporal direction. The exchanged closed string is assumed to be infinitely thin in this case in the absence of the boosting kinematics for the two scattering dipoles in the text. This approximation is justified in the final result (6.91-6.93) below. With this in mind, a repeat of the algebra above, yields the string partition function

$$
\mathbf{K}(T,\kappa) = \mathbf{K}_{\rm F}(T)\ \exp\left(\frac{D_\perp}{4}Tb\sqrt{\kappa\sigma_T}\right) \quad (6.85)
$$

with $\mathbf{K}_{\rm F}(T)$ the string propagator propagator without the extrinsic curvature in 6.64

$$
\mathbf{K}_{\rm F}(T) = \frac{a^2}{\alpha'}\exp\left(-\frac{\sigma_T}{2}Tb^2 - \frac{TP^2}{2\sigma_T}\right)\left[\prod_{n=1}^{\infty}2\sinh\left(\frac{n\pi T}{2}\right)\right]^{-D_\perp} \quad (6.86)
$$

In comparing to the result in [161], we note the occurrence of the same zero-point energy (one loop)

$$
E_0^{\rm non} = -\frac{D_\perp}{4}\sqrt{\sigma_T\kappa} \quad (6.87)
$$

This is to be compared with our result (6.75) for the twisted dipoles, and shows the commonality between the untwisted and large Wilson loop and the twisted and far Wilson loops.

Now, we also notice that in our case

$$
x^0(\tau+T,\sigma) = x^0(\tau,\sigma) + \frac{P}{\sigma_T}T \quad (6.88)
$$

Thus $P = cW$ with $W = 0, \pm1, \pm2, ...$ with W the winding number and c a constant to be interpreted below. The propagators with different windings

can be re-summed using the Poisson summation formula

$$\begin{aligned}\sum_{W=-\infty}^{\infty}\mathbf{K}(T,\kappa) &= \sum_{W=-\infty}^{\infty}\frac{a^2}{\alpha'}\exp\left(-\frac{\sigma_T}{2}Tb^2-W^2\frac{Tc^2}{2\sigma_T}+\frac{D_\perp}{4}Tb\sqrt{\kappa\sigma_T}\right)\\ &\quad\times\left[\prod_{n=1}^{\infty}2\sinh\left(\frac{n\pi T}{2}\right)\right]^{-D_\perp}\\ &= \sqrt{\frac{2\pi\sigma_T}{Tc^2}}\frac{a^2}{\alpha'}\sum_{k=-\infty}^{\infty}\exp\left[-\frac{\sigma_T}{2}Tb^2\left(1-\frac{D_\perp\sqrt{\kappa}}{2b\sqrt{\sigma_T}}\right)-k^2\frac{2\pi^2\sigma_T}{Tc^2}\right]\\ &\quad\times\eta^{-D_\perp}\left(i\frac{T}{2}\right) \qquad (6.89)\end{aligned}$$

where $\eta(\tau)$ is Dedekind eta function [70, 74]

$$\eta(ix)=\eta(i/x)/\sqrt{x}\,. \qquad (6.90)$$

Obtain

$$\begin{aligned}\mathbf{WW} &= \frac{g_s^2a^2}{4\alpha'}\frac{\sqrt{\pi\sigma_T}}{|c|}\sum_{k=-\infty}^{\infty}\sum_{n=0}^{\infty}d(n)\int_0^\infty dT\ \left(\frac{T}{2}\right)^{\frac{D_\perp-3}{2}}\\ &\quad\times\exp\Big[-\frac{T}{2}\sigma_Tb^2\left(1-\frac{D_\perp\sqrt{\kappa}}{2b\sqrt{\sigma_T}}\right)\\ &\qquad-\frac{2}{T}k^2\frac{\pi^2\sigma_T}{c^2}\left(1+\frac{2n\pi c^2}{k^2\pi^2\sigma_T}-\frac{D_\perp c^2}{12k^2\pi\sigma_T}\right)\Big]\\ &= \frac{g_s^2a^2\sqrt{\sigma_T}}{\alpha'}\left(\frac{\pi}{|c|}\right)^{\frac{D_\perp}{2}}\sum_{k=-\infty}^{\infty}\sum_{n=0}^{\infty}d(n)\left(\frac{1+\frac{2n\pi c^2}{k^2\pi^2\sigma_T}-\frac{D_\perp c^2}{12k^2\pi\sigma_T}}{1-\frac{D_\perp\sqrt{\kappa}}{2b\sqrt{\sigma_T}}}\right)^{\frac{D_\perp-1}{4}}\\ &\quad\times\mathbf{K}_{\frac{D_\perp-1}{2}}\left(\frac{2bk\pi\sigma_T}{|c|}\sqrt{\left(1-\frac{D_\perp\sqrt{\kappa}}{2b\sqrt{\sigma_T}}\right)\left(1+\frac{2n\pi c^2}{k^2\pi^2\sigma_T}-\frac{D_\perp c^2}{12k^2\pi\sigma_T}\right)}\right)\\ &\quad\times\left(\frac{k}{b}\right)^{\frac{D_\perp-1}{2}} \qquad (6.91)\end{aligned}$$

which is the correlator between two static dipoles at large distances $b\gg D_\perp\sqrt{\kappa/4\sigma_T}$. The summation over k should be limited to $k=[N_c/2]=1$ for dipoles in the fundamental representation of SU(N_c) [74]. $d(n)$ is the

canonical string density of states with $d(0) = 1$. The static dipole-dipole potential following from the smooth string exchange, amounts to a tower of scalar exchanges with masses ($k = 1$)

$$m_n(b,c) = \frac{2\pi\sigma_T}{|c|}\sqrt{\left(1 - \frac{D_\perp\sqrt{\kappa}}{2b\sqrt{\sigma_T}}\right)\left(1 + \frac{2n\pi c^2}{\pi^2\sigma_T} - \frac{D_\perp c^2}{12\pi\sigma_T}\right)} \tag{6.92}$$

at large distances $b \gg D_\perp\sqrt{\kappa/4\sigma_T}$. Without the extrinsic curvature and setting $|c| \equiv 2\pi/\beta$, m_n is the mass spectrum for closed strings of (arbitrary) size $\beta > \beta_H$,

$$m_n(\infty, 2\pi/\beta) = \sigma_T\beta\sqrt{1 - \frac{\beta_H^2}{\beta^2} + \frac{8\pi n}{\sigma_T\beta^2}} \tag{6.93}$$

with the Hagedorn temperature $\beta_H = \sqrt{\pi D_\perp/3\sigma_T}$. Here $1/\beta = |c|/2\pi$ plays the role of an effective temperature associated with the exchange of a closed (periodic) string.

Chapter 7

Stringy Pomeron II

7.1 At high resolution

We model the (holographic) QCD Pomeron as a long and stretched (fixed impact parameter) transverse quantum string in flat $D_\perp = 3$ dimensions. After discretizing the string in N string bits, we analyze its length, mass and spatial distribution for large N or low-x ($x = 1/N$), and away from its Hagedorn point.

7.1.1 Discretized free transverse string

Scattering of dipoles in the pomeron kinematics with a large rapidity interval $\chi = \ln(s/s_0)$ and fixed impact parameter b is dominated by a closed t-channel string exchange. In leading order in χ, the exchange amplitude can be shown to be that of a free transverse string at fixed Unruh temperature $T = a/2\pi$ with the mean world-sheet acceleration $a = \chi/b$ [70, 71, 72, 73, 80]. For long strings the Unruh temperature is low. These strings will be referred to as cold strings. With this in mind, the free transverse string with fixed end-points in flat $D_\perp$ dimensions is characterized by

$$S_\perp = \frac{\sigma_T}{2} \int d\tau \int_0^\pi d\sigma \quad \left[(\dot{x}_\perp)^2 + (x'_\perp)^2 \right] \tag{7.1}$$

with the end-point condition

$$x^i_\perp(\sigma = 0, \tau) = 0 \qquad x^i_\perp(\sigma = \pi, \tau) = \mathbf{b}^i \tag{7.2}$$

The string tension is $\sigma_T = 1/(2\pi\alpha')$ with $\alpha' = l_s^2$. For simplicity, we will set $2l_s \equiv 1$ throughout and restore it by inspection when needed. The purpose of the present work is to show how the concept of saturation at low-x emerges from the string description and identify its key parameters in QCD through holography. We will also study the general geometrical structure of the transverse string, in particular its spatial size and deformation in the cold or pomeron regime both for a free and interacting string. Initial geometrical string deformations maybe the source of large prompt azimuthal deformations in the inelastic channels and for high multiplicity events.

The transverse free string (7.1) can be thought as a collection of N string bits connected by identical strings [83, 82] and discretized as follows

$$\mathcal{L}_\perp = \frac{1}{N}\sum_{k=0}^{N}\left(\dot{x}^i_\perp(k)\right)^2 - \frac{1}{N}\sum_{k=1}^{N}\left(\frac{x^i_\perp(k)-x^i_\perp(k-1)}{\frac{\pi}{N}}\right)^2 \tag{7.3}$$

with $S_\perp = \int d\tau \mathcal{L}_\perp$. For $N \to \infty$ the (7.1) is recovered. Using the mode decompostion for the amplitudes $x^i_\perp$

$$x^i_\perp(k,\tau) = \mathbf{b}^i\frac{k}{N} + \sum_{n=1}^{N-1} X^i_n(\tau)\sin\left(\frac{nk}{N}\pi\right) \qquad (k=0,1,\cdots,N) \tag{7.4}$$

and their conjugate momenta

$$p^i_\perp(k,\tau) = \frac{\partial\mathcal{L}}{\partial\dot{x}^i_\perp} = \frac{2}{N}\sum_{n=1}^{N-1}\dot{X}^i_n(\tau)\sin\left(\frac{nk}{N}\pi\right) \equiv \frac{2}{N}\sum_{n=1}^{N-1}P^i_n(\tau)\sin\left(\frac{nk}{N}\pi\right) \tag{7.5}$$

allow us to write the Hamiltonian

$$\begin{aligned}\mathcal{H}_\perp &= \frac{N}{4}\sum_{k=0}^{N}\left(p^i_k\right)^2 + \frac{1}{N}\sum_{k=1}^{N}\left(\frac{x^i_k - x^i_{k-1}}{\frac{\pi}{N}}\right)^2 \\ &= \frac{1}{2}\sum_{n=1}^{N-1}\left(P^i_n(\tau)P^i_n(\tau) + \Omega_n^2 X^i_n(\tau)X^i_n(\tau)\right) + \frac{b^2}{\pi^2}\end{aligned} \tag{7.6}$$

with free harmonic oscillators of frequencies

$$\Omega_n = \frac{2N}{\pi}\sin\left(\frac{n\pi}{2N}\right) \tag{7.7}$$

Each oscillator in (7.6) carries a small mass $m_N = 2/N$ and a large compressibility $k_N = 4/(\pi^2 m_N)$. The ground state of this dangling N-string bit Hamiltonian is a product of Gaussians [83]

$$\Psi[X] = \prod_{n,i} \Psi(X_n^i) = \prod_{n,i} \left(\frac{\Omega_n}{\pi}\right)^{\frac{1}{4}} \exp\left[-\frac{\Omega_n}{2}(X_n^i)^2\right] \tag{7.8}$$

leading to the ground state energy

$$\langle \mathcal{H}_\perp \rangle = \frac{D_\perp}{2} \sum_{n=1}^{N-1} \Omega_n + \frac{b^2}{\pi^2} = \frac{D_\perp}{2} \frac{N}{\pi} \left[\cot\left(\frac{\pi}{4N}\right) - 1\right] + \frac{b^2}{\pi^2} \tag{7.9}$$

The string transverse squared size is

$$R_\perp^2 = \frac{1}{N} \sum_{k=0}^{N} \left\langle \left(x_k^i - \mathbf{b}^i \frac{k}{N}\right)^2 \right\rangle = \frac{D_\perp}{4} \sum_{n=1}^{N-1} \frac{1}{\Omega_n}$$

while its transverse squared mass is

$$M_\perp^2 = \frac{1}{2} \langle \mathcal{H}_\perp \rangle = \frac{D_\perp}{4} \sum_{n=1}^{N-1} \Omega_n + \frac{b^2}{2\pi^2} = \frac{D_\perp}{4} \frac{N}{\pi} \left[\cot\left(\frac{\pi}{4N}\right) - 1\right] + \frac{b^2}{2\pi^2} \tag{7.10}$$

We note that back to the continuum $\Omega_n \to n$ with the ground state wave functions

$$\Psi(X_n^i) = \left(\frac{n}{\pi}\right)^{\frac{1}{4}} \exp\left[-\frac{n}{2}(X_n^i)^2\right] \tag{7.11}$$

so that

$$\langle \mathcal{H}_\perp \rangle \approx \frac{2D_\perp}{\pi^2} N^2 + \frac{b^2}{\pi^2} \tag{7.12}$$

The transverse squared radius of the string diverges logarithmically

$$R_\perp^2 \approx \frac{D_\perp}{4} \ln(N) \tag{7.13}$$

while its effectve squared mass diverges quadratically

$$M_\perp^2 \approx \frac{D_\perp}{\pi^2} N^2 + \frac{b^2}{2\pi^2} \tag{7.14}$$

with the number N of string bits.

A simple interpretation of N in relation to the holographic Pomeron follows from the diffusive equation for the tachyonic mode of the closed string exchange in [71],

$$\left(\partial_\chi - \frac{D_\perp}{12}\right)\mathbf{K} = \frac{\alpha'}{2}\Delta_\perp^2\mathbf{K} \equiv \frac{1}{8}\Delta_\perp^2\mathbf{K} \tag{7.15}$$

where $\mathbf{K}$ is the quantum propagator for long closed strings in flat $D_\perp + 2$ space. The last equality follows after setting $2l_s = 1$ in our current conventions. Thus the transverse diffusive size of the Pomeron is

$$R_\perp^2 = \frac{D_\perp}{4}\chi \equiv \frac{D_\perp}{4}\ln\left(\frac{Q^2}{s_0}\left(\frac{1}{x} - 1\right)\right) \tag{7.16}$$

where the last equality uses the DIS kinematics [71]. Thus, the identification

$$R_\perp^2 \approx \frac{D_\perp}{4}\ln\left(\frac{1}{x}\right) \tag{7.17}$$

for small x, which leads to

$$N \equiv \frac{1}{x} \tag{7.18}$$

as the string resolution as suggested earlier. The curvature of AdS_5 causes the leading Pomeron intercept $D_\perp/12 \to D_\perp(\lambda)/12$ in leading order in $\lambda = g_{YM}^2 N_c$ with $D_\perp(\lambda) < 3$ [71, 72, 73]. The string diffusion is reduced to a diffusion in a smaller effective dimension. We will return to this point below.

In its ground state, each of the discretized string bit coordinates X_n^i is normally distributed with probability $|\Psi(X_n^i)|^2$. This gives rise to a random walk of the string bits along the chain in the transverse direction with fixed end-points. This is also true for the continuum. In Fig. 7.1 and Fig. 7.2 we show the string shape for a fixed distance $\mathbf{b} = 5$ for two distinct resolutions $N = 10$ and $N = 50$ respectively. The left figure is the string projected in the transverse plane, while the right figure is the string in $D_\perp = 3$ dimensions. Fig. 7.3 (left) show the string bits in the transverse plane for an ensemble of 200 strings at a resolution of $N = 10$ with fixed $b = 5$. Fig. 7.3 (right) shows the same for 40 strings at a higher resolution $N = 50$.

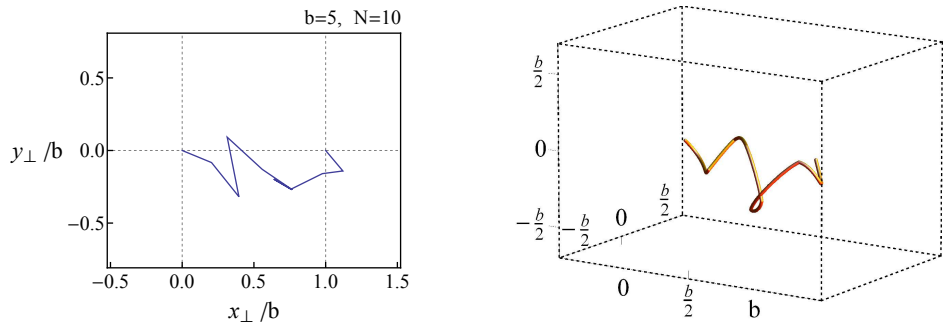

Figure 7.1: Free transverse string shape at a resolution $x = 1/10$ and $b = 5$.

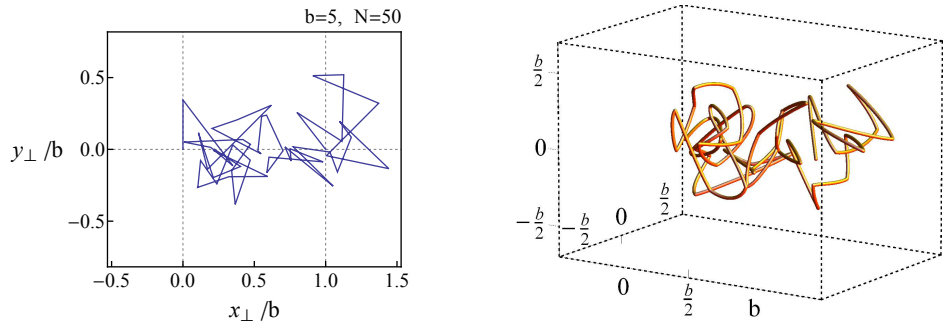

Figure 7.2: Free transverse string shape at a resolution of $x = 1/50$ and $b = 5$.

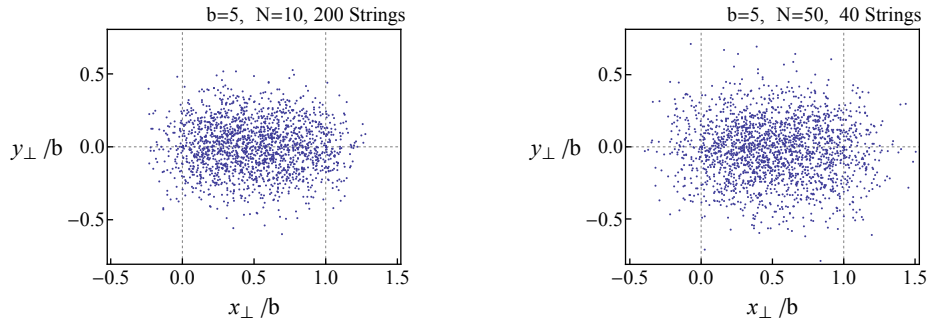

Figure 7.3: Transverse string bit distributions: at $x = 1/10$ sampling 200 strings (**Left**) and at $x = 1/50$ sampling 40 strings (**Right**).

7.1.2 Self-interacting string in the mean-field approximation

Attractive string self-interaction will cause the string to shrink transversely, while repulsive self-interactions will cause the transverse string to grow out-

ward, in a way pushing the string bits out. While string bits are held by confinement which is harmonic in our discretized case, self-string interactions are not well-known. We now postulate that for a sufficiently high resolution or large N we may average the inter-bit interactions in the string using two-body self-interactions

$$V = -\frac{g^2}{2}\sum_{k\neq k'}\int \frac{d^{D_\perp+1}p}{(2\pi)^{D_\perp+1}}\,\frac{M(\vec{x}_k)M(\vec{y}_k)}{p^2+m^2}\exp\left(i\vec{p}\cdot(\vec{x}_k-\vec{y}_k)\right) \tag{7.19}$$

where $M(\vec{x}_k)$ is the mass of the discrete point at $\vec{x}_k$. Here m is a finite mass in units of the string length that characterizes the range of the interaction. Most of our numerical analyses to follow will be for $m = 0$. Results at finite m may be mapped on $m = 0$ through a pertinent re-scaling of the bare coupling $g \to g(m)$. Note that the static interaction involves the virtual exchange in $D_\perp + 1$ as the holographic set up is in $D_\perp + 2$. The effect of the curvature of AdS_5 will be assessed phenomenologically below.

In holographic QCD m is typically the mass of the graviton in bulk which is dual to the glueball mass on the boundary. In the large number of colors limit, the value of m is large. However, for a finite number of colors and flavors mixing between the glueballs and the flavor scalars lead to a much lighter m [165, 166, 167]. Also, in a dense but cold gluon medium the glueball mass maybe lighter. In our case we will consider m a parameter that could be re-absorbed by redefining g. Throughout we will discuss in detail the attractive self-interactions or $g^2 > 0$. The repulsive case and results will only be quoted. Note that our analysis of the string ground state is quantum so that self-interactions do not result in a string collapse thanks to the quantum uncertainty principle.

For large N, the bit coordinates x_k and $x_{k'}$ are approximately independent. They are normally distributed with a probability distribution

$$\rho(\vec{x}_k) = \left(\frac{1}{\Sigma_k\sqrt{2\pi}}\right)^{D_\perp}\exp\left(-\frac{(\vec{x}_k-\vec{b}\frac{k}{N})^2}{2\Sigma_k^2}\right) \tag{7.20}$$

The squared variance is

$$\Sigma_k^2 = \sum_{n=1}^{N-1}\frac{\sin^2\left(\frac{nk}{N}\pi\right)}{2\omega_n} \approx \sum_{n=1}^{N-1}\frac{1}{4\omega_n} = \frac{R_\perp^2}{D_\perp} \tag{7.21}$$

We note that the normal frequencies ω_n differ from the free frequencies Ω_n. They are defined variationally below. (7.19) is a highly simplified two-body interaction as higher-order many-body interactions are also possible. We just note that $g \approx 1/N_c$ justifying the dominance of the two-body interactions.

Using (7.20) we may define the bit mass distribution on the string in the mean-field type approximation as

$$M(\vec{x}_k) \approx \frac{M_\perp}{N+1}\rho(\vec{x}_k) \tag{7.22}$$

Inserting (7.20-7.22) into (7.19) yield

$$V = -\frac{g^2}{2}\sum_{k\neq k'}\left(\frac{M_\perp}{N+1}\right)^2 \int \frac{d^{D_\perp+1}p}{(2\pi)^{D_\perp+1}}\ \rho(\vec{x}_k)\rho(\vec{y}_{k'})\frac{e^{i\vec{p}\cdot(\vec{x}_k-\vec{y}_k)}}{p^2+m^2} \tag{7.23}$$

In the large N limit, we may average (7.23) over x_k and y_k to obtain in the mean-field approximation

$$\begin{aligned}
\overline{V} &\equiv \frac{-g^2}{2}\sum_{k\neq k'}\left(\frac{M_\perp}{N+1}\right)^2 \int d^{D_\perp}x_k \int d^{D_\perp}y_k \int \frac{d^{D_\perp+1}p}{(2\pi)^{D_\perp+1}}\rho(\vec{x}_k)\rho(\vec{y}_{k'})\frac{e^{i\vec{p}\cdot(\vec{x}_k-\vec{y}_k)}}{p^2+m^2} \\
&= \frac{-g^2}{2}\sum_{k\neq k'}\left(\frac{M_\perp}{N+1}\right)^2 \int \frac{d^{D_\perp+1}p}{(2\pi)^{D_\perp+1}}\ \frac{1}{p^2+m^2} \\
&\qquad\qquad \times \exp\left[-\frac{p^2}{2}\left(\Sigma_k^2+\Sigma_{k'}^2\right)+i\vec{p}\cdot\vec{b}\frac{(k-k')}{N}\right]
\end{aligned} \tag{7.24}$$

Thus

$$\begin{aligned}
\overline{V} &\approx -\frac{g^2}{2}M_\perp^2 \int \frac{d^{D_\perp+1}p}{(2\pi)^{D_\perp+1}}\ \frac{1}{p^2+m^2}\int_0^1 dk \int_0^1 dk' \exp\left[-p^2\frac{R_\perp^2}{D_\perp}+i\vec{p}\cdot\vec{b}(k-k')\right] \\
&= -\frac{g^2}{2}M_\perp^2 \int \frac{d^{D_\perp+1}p}{(2\pi)^{D_\perp+1}}\ \frac{1}{p^2+m^2}\exp\left(-p^2\frac{R_\perp^2}{D_\perp}\right)\frac{4\sin^2\left(\frac{\vec{p}\cdot\vec{b}}{2}\right)}{\left(\vec{p}\cdot\vec{b}\right)^2}
\end{aligned} \tag{7.25}$$

For $m=0$ and $\vec{b}\to 0$, (7.23) simplifies

$$\overline{V} \approx -\mathbf{C}(D_\perp)\, g^2\, \frac{M_\perp^2}{R_\perp^{D_\perp - 1}} \tag{7.26}$$

with $\mathbf{C} \equiv (1/\sqrt{16\pi D_\perp})\,(D_\perp/4\pi)^{\frac{D_\perp}{2}}\,\Gamma(D_\perp/2 - 1/2)/\Gamma(D_\perp/2 + 1/2)$. In this limit, the self-interactions between the string bits reduce to a Newtonian potential acting as a mean-field approximation. The Newtonian constant is identified as $G_N = g^2 D_\perp^{(D_\perp - 1)/2}/(8\pi)$ through the bottom-up holographic setting in $D_\perp + 2$ dimensions [71]. Thus,

$$g^2 = 8\pi D_\perp^{\frac{1-D_\perp}{2}}\, l_P^{D\perp} = 8\pi D_\perp^{\frac{1-D_\perp}{2}}\, g_s^2 l_s^{D_\perp} \equiv 2^{3-D_\perp}\pi D_\perp^{\frac{1-D_\perp}{2}}\, g_s^2 \tag{7.27}$$

where in the last equality we reset $2l_s \equiv 1$ as per our current conventions. Recall that the curvature effects of AdS_5, which we are ignoring so far, amounts to an effective $D_\perp \to D_\perp(\lambda)$ in leading order on the transverse string propagator as we noted earlier. This observation will be used below to estimate the curvature corrections to the current analysis.

7.1.3 Variational analysis

For small perturbative interactions, we can modify the transverse Hamiltonian through

$$\mathcal{H}_\perp = 2M_\perp^2 + 2M_\perp \delta(2M_\perp) \equiv 2M_\perp^2 + 2M_\perp\, \overline{V} \tag{7.28}$$

$\mathcal{H}_\perp$ in Eq. 7.28 is difficult to analyze analytically in the presence of $\overline{V}$. We follow Thorn and Ogerman [82] and analyze it variationally by using a trial Gaussian distribution for each string bit

$$\Psi(X_n^i) = \left(\frac{\omega_n}{\pi}\right)^{\frac{1}{4}} \exp\left[-\frac{\omega_n}{2}(X_n^i)^2\right] \tag{7.29}$$

where the set of normal modes ω_n will be defined below by minimizing the energy of the string in the presence of V. In terms of (7.29) the scalar part is

$$\mathcal{H}_\perp^0 = \frac{D_\perp}{4}\sum_{n=1}^{N-1}\left(\omega_n + \frac{\Omega_n^2}{\omega_n}\right) + \frac{b^2}{\pi^2} \tag{7.30}$$

and reduces to (7.10) when $\omega_n = \Omega_n$ for $V = 0$. The effective mass of the string is

$$M_\perp^2[\omega_n] = \frac{1}{2}\mathcal{H}_\perp^0 = \frac{D_\perp}{8}\sum_{n=1}^{N-1}\left(\omega_n + \frac{\Omega_n^2}{\omega_n}\right) + \frac{b^2}{2\pi^2} \tag{7.31}$$

The squared effective transverse radius is

$$R_\perp^2[\omega_n] = \frac{1}{N}\sum_{k=0}^{N}\left\langle\left(x_k^i - \mathbf{b}^i\frac{k}{N}\right)^2\right\rangle = \frac{D_\perp}{4}\sum_{n=1}^{N-1}\frac{1}{\omega_n} \tag{7.32}$$

With our conventions the total string energy is $E[\omega_n] = 2M_\perp^2 + 2M_\perp\overline{V}$ depends on the set of variational parameters ω_n which are fixed through the minimum

$$\begin{aligned}
&\frac{\delta E}{\delta\omega_n}\\
&= \frac{\delta M_\perp^2}{\delta\omega_n}\left[2 - \frac{3g^2}{2}M_\perp\int\frac{d^{D_\perp+1}p}{(2\pi)^{D_\perp+1}}\,\frac{1}{p^2+m^2}\exp\left(-p^2\frac{R_\perp^2}{D_\perp}\right)\frac{4\sin^2\left(\frac{\vec{p}\cdot b}{2}\right)}{\left(\vec{p}\cdot\vec{b}\right)^2}\right]\\
&\quad + \frac{1}{D_\perp}\frac{\delta R_\perp^2}{\delta\omega_n}g^2M_\perp^3\int\frac{d^{D_\perp+1}p}{(2\pi)^{D_\perp+1}}\,\frac{p^2}{p^2+m^2}\exp\left(-p^2\frac{R_\perp^2}{D_\perp}\right)\frac{4\sin^2\left(\frac{\vec{p}\cdot b}{2}\right)}{\left(\vec{p}\cdot\vec{b}\right)^2}\\
&= 0\,.
\end{aligned} \tag{7.33}$$

The mass and size variations can be made explicit

$$\frac{\delta M_\perp^2}{\delta\omega_n} = \frac{D_\perp}{8}\left(1 - \frac{\Omega_n^2}{\omega_n^2}\right) \qquad \frac{1}{D_\perp}\frac{\delta R_\perp^2}{\delta\omega_n} = -\frac{1}{4\omega_n^2} \tag{7.34}$$

Inserting (7.34) into (7.33) and rearranging yield

$$\omega_n^2 = \Omega_n^2 + \frac{\frac{g^2M_\perp^3}{D_\perp}\int\frac{d^{D_\perp+1}p}{(2\pi)^{D_\perp+1}}\,\frac{p^2}{p^2+m^2}\exp\left(-p^2\frac{R_\perp^2}{D_\perp}\right)\frac{4\sin^2\left(\frac{\vec{p}\cdot b}{2}\right)}{\left(\vec{p}\cdot\vec{b}\right)^2}}{1 - \frac{3g^2}{4}M_\perp\int\frac{d^{D_\perp+1}p}{(2\pi)^{D_\perp+1}}\,\frac{1}{p^2+m^2}\exp\left(-p^2\frac{R_\perp^2}{D_\perp}\right)\frac{4\sin^2\left(\frac{\vec{p}\cdot b}{2}\right)}{\left(\vec{p}\cdot\vec{b}\right)^2}} \tag{7.35}$$

where both $M_\perp^2[\omega_n]$ and $R_\perp^2[\omega_n]$ depend on the variational parameters through (7.31-7.32). (7.35) define a highly non-linear set of equations for the variational parameters ω_n defining the Gaussian ansatz (7.29). The generic solution is of the form $\omega_n = \sqrt{\Omega_n^2 + \eta^2}$ with

$$\eta^2 = \frac{\frac{g^2 M_\perp^3}{D_\perp}\Phi_1}{2^{D_\perp}\pi^{\frac{D_\perp+2}{2}}\Gamma(\frac{D_\perp}{2}) - \frac{3g^2}{4}\Phi_2}\,, \tag{7.36}$$

where

$$\begin{aligned}
\Phi_1 &\equiv \int_0^\infty dp \int_0^\pi d\phi\ (\sin\phi)^{D_\perp-1}\,\frac{p^{D_\perp+2}}{p^2+m^2}\exp\left(-p^2\frac{R_\perp^2}{D_\perp}\right)\frac{4\sin^2\left(\frac{pb\cos\phi}{2}\right)}{p^2b^2\cos^2\phi} \\
\Phi_2 &\equiv \int_0^\infty dp \int_0^\pi d\phi\ (\sin\phi)^{D_\perp-1}\,\frac{p^{D_\perp}}{p^2+m^2}\exp\left(-p^2\frac{R_\perp^2}{D_\perp}\right)\frac{4\sin^2\left(\frac{pb\cos\phi}{2}\right)}{p^2b^2\cos^2\phi}
\end{aligned}$$

to be determined numerically. Note that for $b = 0$, (7.36) simplifies as

$$\eta^2 = \frac{M_\perp^2}{R_\perp^2}\frac{\mathbf{A}}{\mathbf{B}-\mathbf{C}}\,, \tag{7.37}$$

where

$$\begin{aligned}
\mathbf{A} &= \frac{1}{2}\frac{g^2 M_\perp}{R_\perp^{D_\perp-1}}\exp\left(\frac{m^2R_\perp^2}{D_\perp}\right)\Gamma\left(\frac{3+D_\perp}{2}\right)\left(\frac{m^2R_\perp^2}{D_\perp}\right)^{\frac{D_\perp+1}{2}} \\
&\quad\times\Gamma\left(-\frac{1+D_\perp}{2},\frac{m^2R^2}{D_\perp}\right) \\
\mathbf{B} &= 2^{D_\perp}\pi^{\frac{D_\perp+1}{2}}\,(D_\perp)^{\frac{1-D_\perp}{2}}\,\Gamma(\frac{D_\perp+1}{2}) \\
\mathbf{C} &= \frac{3}{8}\frac{g^2 M_\perp}{R_\perp^{D_\perp-1}}\exp\left(\frac{m^2R_\perp^2}{D_\perp}\right)\Gamma\left(\frac{1+D_\perp}{2}\right)\left(\frac{m^2R_\perp^2}{D_\perp}\right)^{\frac{D_\perp-1}{2}} \\
&\quad\times\Gamma\left(-\frac{D_\perp-1}{2},\frac{m^2R^2}{D_\perp}\right)\,.
\end{aligned} \tag{7.38}$$

For $m = 0$, Eq. 7.37 further simplifies as

$$\eta^2 = \frac{M_\perp^2}{R_\perp^2}\frac{\frac{1}{2}\frac{g^2M_\perp}{R_\perp^{D_\perp-1}}}{2^{D_\perp}\pi^{\frac{D_\perp+1}{2}}\,(D_\perp)^{\frac{1-D_\perp}{2}} - \frac{3}{4(D_\perp-1)}\frac{g^2M_\perp}{R_\perp^{D_\perp-1}}} \tag{7.39}$$

Note that for $b \neq 0$, (7.36) simplifies as

$$\eta^2 = \frac{M_\perp^2}{b^2} \frac{\frac{4}{D_\perp} \frac{g^2 M_\perp}{b^{D_\perp - 1}} \mathbf{I}[0]}{2^{D_\perp} \pi^{\frac{D_\perp + 2}{2}} \Gamma(\frac{D_\perp + 1}{2}) - 3 \frac{g^2 M_\perp}{b^{D_\perp - 1}} \mathbf{I}[2]} \,, \tag{7.40}$$

where

$$\mathbf{I}[a] \equiv \int_0^\infty dx \int_0^\pi d\phi \qquad (\sin\phi)^{D_\perp - 3} \tan^2\phi \; \frac{x^{D_\perp - a}}{x^2 + m^2 b^2} \times \exp\left(-\frac{x^2}{D_\perp} \frac{R_\perp^2}{b^2} \right) \sin^2\left(\frac{x \cos\phi}{2} \right) . \tag{7.41}$$

The repulsion will cause the string bits to expand. A rerun of the precedent arguments yields now $\omega_n = \sqrt{\Omega_n^2 - \eta^2}$ with

$$\eta^2 = \frac{M_\perp^2}{b^2} \frac{\frac{4}{D_\perp} \frac{\tilde{g}^2 M_\perp}{b^{D_\perp - 1}} \mathbf{I}[0]}{2^{D_\perp} \pi^{\frac{D_\perp + 2}{2}} \Gamma(\frac{D_\perp + 1}{2}) + 3 \frac{\tilde{g}^2 M_\perp}{b^{D_\perp - 1}} \mathbf{I}[2]} \tag{7.42}$$

The variational analysis will be now carried numerically for both the attractive and repulsive string interaction in the mean-field approximation.

7.1.4 Numerical results

The Gaussian variation ansatz (7.29) can be used to define a variational probability distribution $|\Psi(X_n^i)|^2$ for the string amplitudes X_n^i in the normal mode decomposition (7.54). Each string bit undergoes a Gaussian random walk which is free for $g = 0$ but constrained by the interaction through ω_n for $g \neq 0$. In Fig. 7.4 we show the spatial geometry of our discretized strings in $D_\perp = 3$ with a resolution $N = 200$ for the attractive interaction $g = 0.3$, no interaction and repulsive interaction $\tilde{g} = 0.3$. The string is stretched with $b = 5$. In Fig. 7.5 we show the transverse distribution of the string bits for an ensemble consisting of 40 stretched strings. The string bits are the dots and we have left out the string connection for a better visualization. The resolution is $N = 1/x = 200$. The attractive configurations are denser along b, while the repulsive configurations are spread out of b.

In Fig. 7.6 we show the growth of the transverse radius as measured by (7.32) versus the resolution N for different strengths of the attractive forces

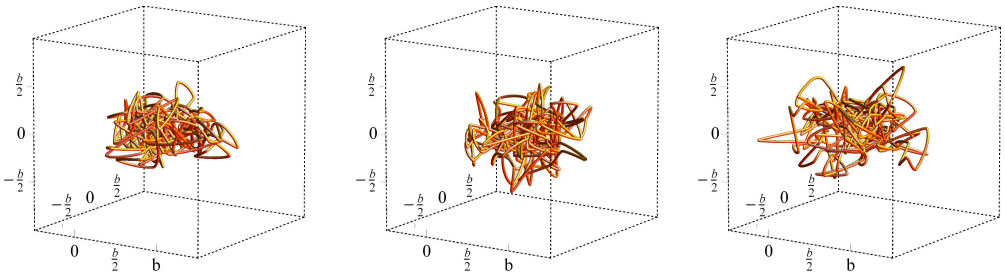

Figure 7.4: Attractive interaction: $g = 0.3$ (**Left**). No interaction: $g = \tilde{g} = 0$ (**Center**). Repulsive interaction: $\tilde{g} = 0.3$ (**Right**).

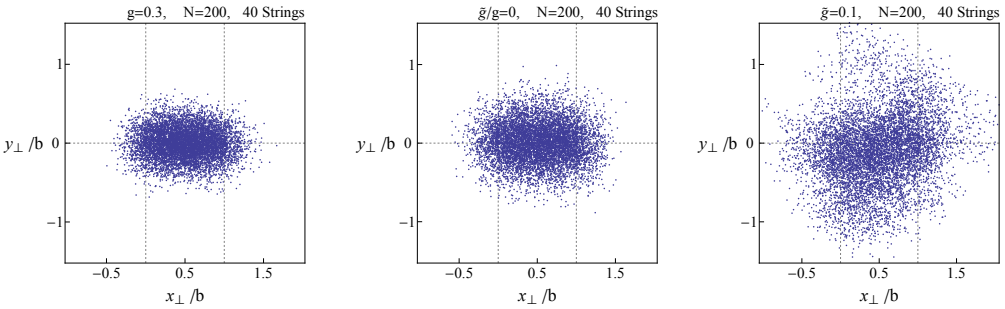

Figure 7.5: Attractive interaction: $g = 0.3$ (**Left**). No interaction: $g = \tilde{g} = 0$ (**Center**). Repulsive interaction: $\tilde{g} = 0.1$ (**Right**).

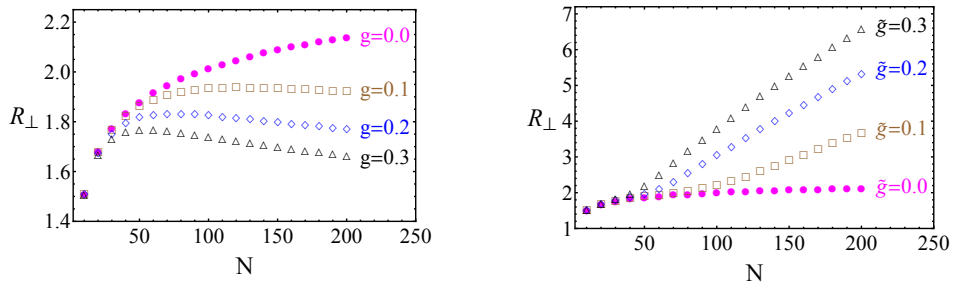

Figure 7.6: Attractive interaction: $g = 0.1, 0.2, 0.3$ (**Left**). Repulsive interaction: $\tilde{g} = 0.1, 0.2, 0.3$ (**Right**).

(left) and repulsive forces (right). For comparison, we also show the full length of the string

$$L \equiv \sum_{k=1}^{N} \sqrt{\left(x_k^i - x_{k-1}^i\right)^2} \tag{7.43}$$

The analogue change of the total length of the string with the resolution as defined in (7.43) and the mass of the string as defined in (7.31) are also shown in Fig. 7.7 and Fig. 7.8. While the length and mass scale linearly with N whatever the interaction, the transverse size of the string bit distribution shows sensitivity to N. For $g = \tilde{g} = 0$ the transverse radius grows logarithmically as expected. As the attraction is switched on, the transverse radius asymptotes a constant about the string length. In contrast, as the repulsion is switched on, the transverse radius asymptotes a linear rise with the resolution as also noted in [82] in their non-relativistic string bit models with a variety of repulsive string interactions of different ranges. This supports our earlier observation that at large resolution N the mean-field approximation is generic.

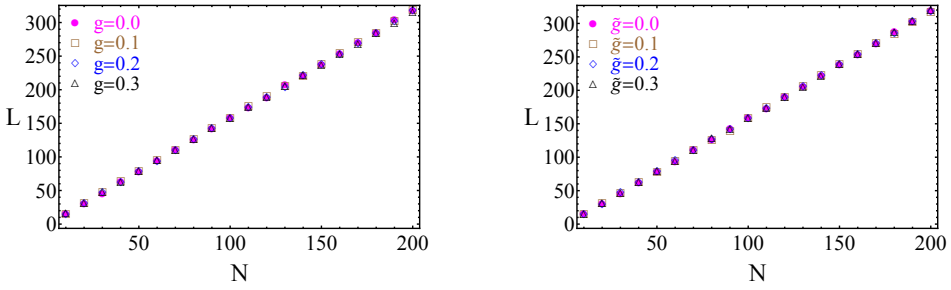

Figure 7.7: Attractive interaction: $g = 0.1, 0.2, 0.3$ (**Left**). Repulsive interaction: $\tilde{g} = 0.1, 0.2, 0.3$ (**Right**).

We note that all attractive string self-interactions result in transverse area that are less than or equal to the Froissart bound. In contrast, all repulsive string self-interactions result in a transverse area that upsets the Froissart bound at asymptotic N or asymptotically low-x. Thus our observation that saturation of the Bekenstein bound by the the string bits or wee gluons, follows from weakly attractive string-self interactions in conformity with the Froissart bound. We also note that our treatment of the interaction assumes weak self-interactions, or the smallness of the ratio

$$\frac{2M_\perp \overline{V}}{\mathcal{H}_\perp^0} = \frac{\overline{V}[g]}{M_\perp[g]} \tag{7.44}$$

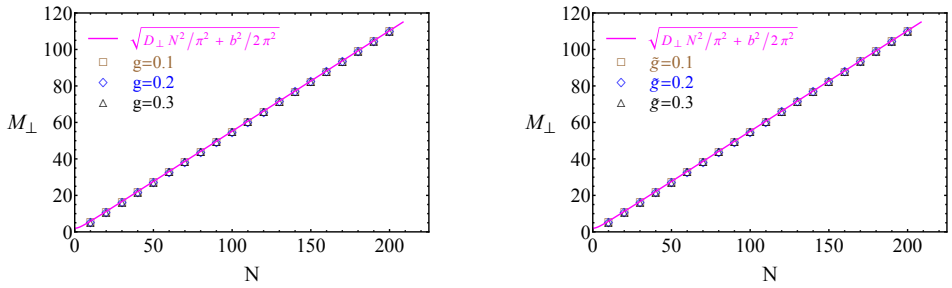

Figure 7.8: Solid line is the analytical result in (7.14). Numeric data is for attractive interaction: $g = 0.1, 0.2, 0.3$ (**Left**) and repulsive interaction: $\tilde{g} = 0.1, 0.2, 0.3$ (**Right**).

We show in Fig. 7.9 that this is indeed the case.

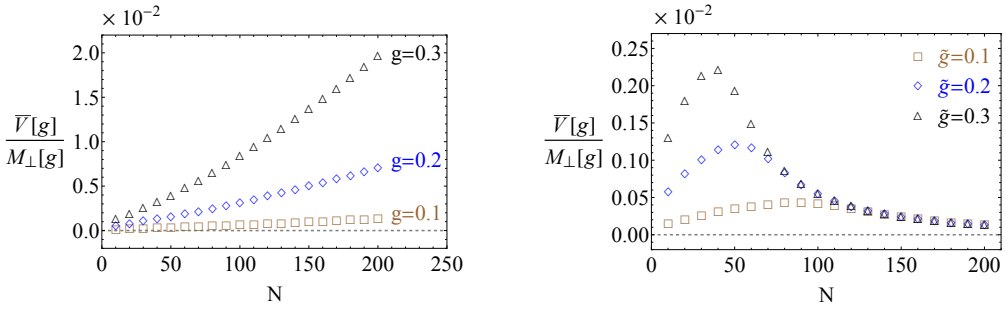

Figure 7.9: Attractive interaction: $g = 0.1, 0.2, 0.3$ (**Left**). Repulsive interaction: $\tilde{g} = 0.1, 0.2, 0.3$ (**Right**).

7.1.5 Saturation

At low-x or large N and $b = 0$, the transverse string density is high $\mathbf{n}_\perp(0, N) \approx N/R_\perp^{D_\perp}$ as $R_\perp$ shrinks under the effect of attractive self-interactions. For $0 < g < 0.3$ our numerical results yield $1.2 < R_\perp < 1.6$ in units where $2l_s = 1$, i.e. $2.4 < R_\perp/l_s < 3.2$. To understand the effects of the self-interaction on the string size configuration, we re-write schematically the squared mass $E = 2M_\perp^2 + 2M_\perp V$ of the self-interacting string in terms of N and $R_\perp$ dropping all numerical factors

$$E \approx N^2 \frac{1}{R_\perp^2} + N^2 \frac{R_\perp^2}{D_\perp^2 \ln^2 N} - N^2 \frac{g^2 N}{R_\perp^{D_\perp - 1}} \tag{7.45}$$

The first contribution in (7.45) follows from the kinetic contribution in (7.6) using the estimate $N^2 p_i^2$ and the uncertainty principle $p_i \approx 1/R_\perp$. The second contribution in (7.45) follows from the harmonic potential in (7.45) using the estimate $N^2 (\Delta x_i)^2$ with typically $\Delta x_i \approx R_\perp/(D_\perp \ln N)$ in the diffusive regime. The third contribution in (7.45) is the potential contribution $2M_\perp \overline{V}$ to the squared mass after using $M_\perp \approx N$. Note that for $g = 0$ the minimum of (7.45) yields the diffusive result $R_\perp^2 \approx D_\perp \ln N$ whatever $D_\perp$. For finite g, the minimum of (7.45) depends on the dimensionality $D_\perp$. A similar relation to (7.45) was found to hold for classical strings at hi high temperature by Damour and Veneziano [110] using different arguments.

Flat Space: $D_\perp = 3$

For our case $D_\perp = 3$ so the minimum of (7.45) occurs for

$$R_\perp \approx \left(1 - g^2 N\right)^{1/4} \sqrt{\ln N} \tag{7.46}$$

For a relatively small attraction $g^2 N \approx 1$, $R_\perp$ in (7.122) undergoes a numerical change from an increasingly large and diffusive string to a small and fixed size string of about few string lengths. Fig. 7.10 (left) shows that for $g = 0.1$ the transverse size flattens out at about $R_\perp \sim 1.85 \equiv 3.7 l_s \approx 0.3$ fm in the range $200 < N < 600$. For fixed b the transverse area is ellipsoidal with a transverse bit density

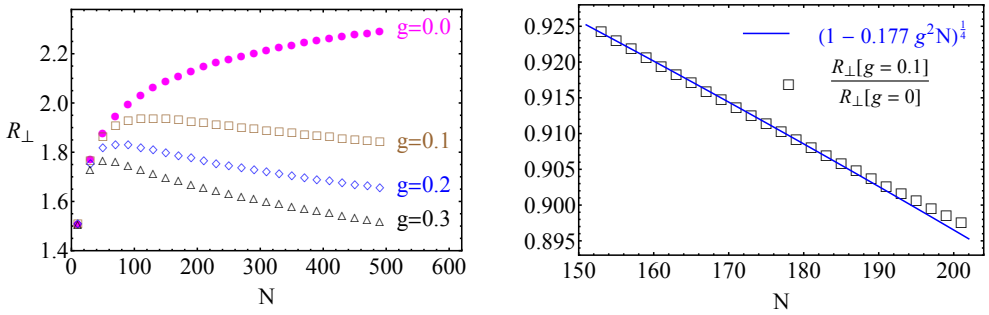

Figure 7.10: $R_\perp[g]$ for $g = 0.1, 0.2, 0.3$ (**Left**). $R_\perp[g = 0.1]/R_\perp[g = 0]$ for large N (**Right**).

$$\mathbf{n}_\perp(b,N) \approx \frac{N}{b\,(2R_\perp)^{D_\perp-1}} \equiv \frac{N}{N_c}\frac{1}{g^2 l_s^{D_\perp}}\frac{g^2 N_c}{\frac{b}{l_s}\left(2\frac{R_\perp}{l_s}\right)^{D_\perp-1}} \tag{7.47}$$

The critical resolution $x_c = 1/N_c$ at which this change takes place can be read from Fig. 7.10 (right)

$$x_c = \frac{1}{N_c} \approx 0.1^2 \times 0.177 = 1.77 \times 10^{-3} \tag{7.48}$$

for $g = 0.1$ with $D_\perp = 3$ and $b = 5 \equiv 10\, l_s \approx 1$ fm. We identify the onset $x \approx x_c$ as the pre-saturation phase of the string at high resolution whereby its transverse area contracts to the string scale under weak self-attraction. However, the transverse string bit density is still dilute at this resolution since

$$\mathbf{n}_\perp(5,x) \approx \frac{x_c}{x}\frac{1}{\frac{\pi}{3}l_p^3}\frac{1}{10\times(4\times 1.85)^2\times 0.177} = \frac{x_c}{x}\frac{0.01}{l_p^3} \equiv \frac{x_s}{x}\frac{1}{l_p^3} \tag{7.49}$$

or $n_\perp(5,x_c) \approx 0.01/l_P^3$. Recall that the Planck length $l_P^{D_\perp} = g_s^2 l_s^{D_\perp}$ and that $g^2 = (\pi/3)g_s^2$ from (7.27). At the saturation point or $x \equiv x_s = 0.01x_c \approx 10^{-5}$ the transverse density saturates the Bekenstein bound of one bit per transverse Planck area or $n_\perp(5,x_s) \approx 1/l_P^3$. We identify this point with the saturation scale or black hole regime. A schematic rendering of the pre-saturation and saturation phases in the low-x regime for $b = 5$ are shown in Fig. 7.11.

Curved Space: $D_\perp(\lambda) < 3$

An exact spatial analysis of the transverse string in curved AdS_5 space is beyond the scope of this work. In this section we will attempt to give simple estimates of the effects of the curvature of AdS_5 on some of our previous results. For that we first note that an aspect of the curved geometry on the Pomeron is to cause the string transverse degrees of freedom to effectively feel a reduced transverse spatial dimension [71, 72, 73, 75]

$$D_\perp \to D_\perp(\lambda) = D_\perp\left(1 - \frac{3(D_\perp-1)^2}{2D_\perp\sqrt{\lambda}} + \mathcal{O}\left(\frac{1}{\lambda}\right)\right) \tag{7.50}$$

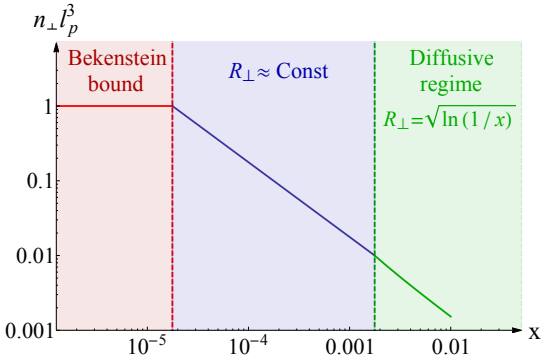

Figure 7.11: Saturation (red), pre-saturation (blue) and diffusive (green) regimes for a transverse string with decreasing resolution in $D_\perp = 3$.

with $\lambda = g_{YM}^2 N_c$. Indeed, (7.117) causes the Pomeron intercept to move from $D_\perp/12 = 0.25$ to $D_\perp(\lambda \approx 40) \approx 0.17$ closer to the empirical interceptt of 0.08 [168]. A phenomenological way to implement this effect is to add warping factors on the oscillators in (7.1) as we detail in the here and repeat the numerical analysis.

We introduce the rescalings $\tau \to \lambda_\tau \tau$ and $b \to \tilde{b}$, so that (7.1) now reads

$$S_\perp = \frac{\sigma_T}{2} \int d\tau \int_0^\pi d\sigma \quad \left[\frac{1}{\lambda_\tau^2} (\dot{x}_\perp)^2 + (x'_\perp)^2 \right] \tag{7.51}$$

with the end-point condition

$$x_\perp^i(\sigma = 0, \tau) = 0 \qquad x_\perp^i(\sigma = \pi, \tau) = \tilde{\mathbf{b}}^i \tag{7.52}$$

The Lagrangian for the discretized string is now

$$\mathcal{L}_\perp = \frac{1}{\lambda_\tau^2} \frac{1}{N} \sum_{k=0}^{N} \left(\dot{x}_\perp^i(k) \right)^2 - \frac{1}{N} \sum_{k=1}^{N} \left(\frac{x_\perp^i(k) - x_\perp^i(k-1)}{\frac{\pi}{N}} \right)^2 \tag{7.53}$$

The mode decomposition for the amplitudes $x_\perp^i$ reads

$$x_\perp^i(k, \tau) = \lambda_\tau \tilde{\mathbf{b}}^i \frac{k}{N} + \lambda_\tau \sum_{n=1}^{N-1} X_n^i(\tau) \sin\left(\frac{nk}{N} \pi \right) \qquad (k = 0, 1, \cdots, N) \tag{7.54}$$

and their conjugate momenta are

$$p^i_\perp(k,\tau)=\frac{\partial\mathcal{L}}{\partial\dot{x}^i_\perp}=\frac{1}{\lambda_\tau}\frac{2}{N}\sum_{n=1}^{N-1}\dot{X}^i_n(\tau)\sin\left(\frac{nk}{N}\pi\right)\equiv\frac{1}{\lambda_\tau}\frac{2}{N}\sum_{n=1}^{N-1}P^i_n(\tau)\sin\left(\frac{nk}{N}\pi\right) \tag{7.55}$$

Thus, the Hamiltonian

$$\mathcal{H}_\perp=\frac{1}{2}\sum_{n=1}^{N-1}\left(P^i_n(\tau)P^i_n(\tau)+\lambda_\tau^2\Omega_n^2X^i_n(\tau)X^i_n(\tau)\right)+\lambda_\tau^2\frac{\tilde{b}^2}{\pi^2} \tag{7.56}$$

The ground state of this dangling N-string is a product of warped Gaussians

$$\Psi[\lambda_\tau;X]=\prod_{n,i}\Psi(\lambda_\tau;X^i_n)=\prod_{n,i}\left(\frac{\lambda_\tau\Omega_n}{\pi}\right)^{\frac{1}{4}}\exp\left[-\frac{\lambda_\tau\Omega_n}{2}(X^i_n)^2\right] \tag{7.57}$$

leading to the ground state energy

$$\langle\mathcal{H}_\perp\rangle=\frac{D_\perp\lambda_\tau}{2}\sum_{n=1}^{N-1}\Omega_n+\frac{\lambda_\tau^2\tilde{b}^2}{\pi^2} \tag{7.58}$$

(7.9) is recovered for $\lambda_\tau=1$ as it should. If we set $\lambda_\tau=D_\perp(\lambda)/D_\perp$ and $\tilde{b}=b/\lambda_\tau$, (7.58) reads as

$$\langle\mathcal{H}_\perp\rangle=\frac{D_\perp(\lambda)}{2}\sum_{n=1}^{N-1}\Omega_n+\frac{b^2}{\pi^2} \tag{7.59}$$

The string transverse squared size (7.10) is now

$$R^2_\perp=\frac{1}{N}\sum_{k=0}^{N}\left\langle\left(x^i_k-\mathbf{b}^i\frac{k}{N}\right)^2\right\rangle=\frac{D_\perp(\lambda)}{4}\sum_{n=1}^{N-1}\frac{1}{\Omega_n}\approx\frac{D_\perp(\lambda)}{4}\ln(N) \tag{7.60}$$

with a Pomeron intercept $D_\perp(\lambda)/12$.

A simpler estimate follows from the substitution (7.117) in the interacting part of our variational analysis. Indeed, the schematic estimate (7.45) shows that the first contribution reflects on the uncertainty principle which probes short distances and thus is not sensitive to the curvature of AdS_5. The

second diffusive contribution is sensitive through $D_\perp$ but will turn out to be subleading as we will show below. The third contribution is long ranged and senses the curvature of AdS_5. Thus

$$E \to N^2 \frac{1}{R_\perp^2} + N^2 \frac{R_\perp^2}{D_\perp^2(\lambda) \ln^2 N} - N^2 \frac{g^2 N}{R_\perp^{D_\perp(\lambda)-1}} \tag{7.61}$$

For very small values of g the first two contributions in (7.118) are dominant and the string transverse size grows diffusively. The minimization of the first two dominant contributions in this regime yields $R_\perp^2 \approx D_\perp(\lambda) \ln N$. This is consistent with the growth of the Pomeron in curved AdS_5 noted in [71, 72, 73, 75]. However, for

$$g^2 > \frac{1}{N} (\ln N)^{\frac{D_\perp(\lambda)-3}{2}} \tag{7.62}$$

the string size shrinks and the transverse string size follows from balancing the first term with the last term due to the interaction. The balance between the self-interaction and the uncertainty principle, yields a continuously decreasing transverse string size

$$R_\perp \approx \left(\frac{1}{g^2 N} \right)^{\frac{2\sqrt{\lambda}}{3(D_\perp - 1)^2}} \tag{7.63}$$

in units of the string length. A typical configuration of the string with $N = 200$ using the string interaction (7.23-7.25) with the effective substitution $D_\perp \to D_\perp(\lambda)$ is displayed in Fig. 7.12.

For $\lambda = 40$, $D_\perp = 3$ and $g = 0.3$, the scaling regime (7.120) is observed to take place for our string samplings for $N_c \approx 400$ as shown in Fig. 7.13. As before, we identify the critical resolution $x_c = 1/N_c \approx 0.0025$ with the onset of the scaling regime (7.120).

The transverse density for fixed impact parameter b is now

$$\begin{aligned} \mathbf{n}_\perp(b, x = 1/N) &\approx \frac{N}{b\,(2R_\perp)^{D_\perp - 1}} \\ &\approx \left(\frac{(0.3)^2 \times 400}{x/x_c} \right)^{\frac{2\sqrt{\lambda}}{3(D_\perp-1)}+1} \left(\frac{l_s}{b} \right) \left(\frac{1}{2 \times 42.28} \right)^{D_\perp - 1} \frac{1}{l_p^{D_\perp}} \,. \end{aligned} \tag{7.64}$$

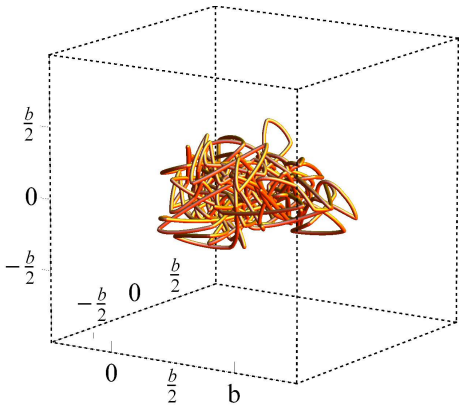

Figure 7.12: 3D configuration of the string with $N = 200$ and $g = 0.3$ using $D_\perp(\lambda)$ in the interaction. See text.

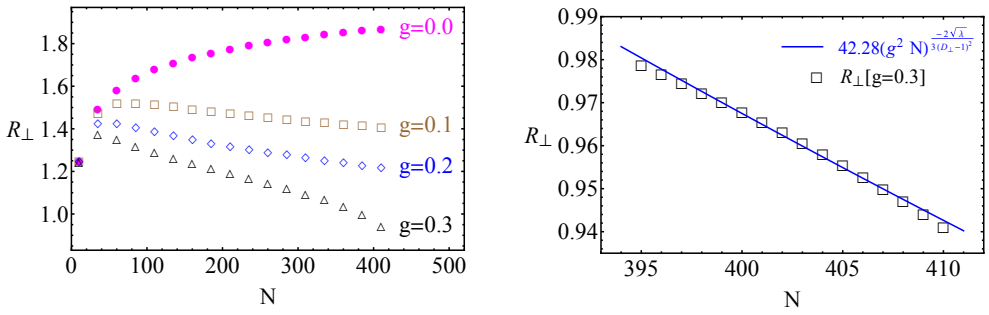

Figure 7.13: $R_\perp[g]$ for $g = 0.1, 0.2, 0.3$ (**Left**). $R_\perp[g = 0.3]$ and Eq. 7.120 (**Right**).

For a typical impact parameter of $b = 5l_s$, it saturates the Bekenstein bound for $x \equiv x_s \approx 0.6x_c$ $(1/x_s = N_s \approx 633)$

$$\mathbf{n}_\perp(5, x_s \approx 0.0016) \approx \frac{1}{l_p^{D_\perp}} \tag{7.65}$$

In Fig. 7.14 we give a schematic rendering of the diffusive (green, pre-saturation (blue) and saturation (red) regimes following from the effective $D_\perp \to D_\perp(\lambda)$ substitution.

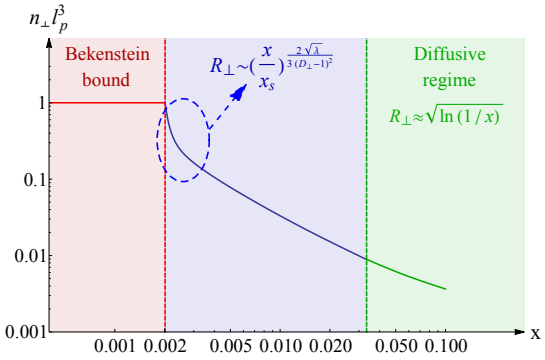

Figure 7.14: Saturation (red), pre-saturation (blue) and diffusive (green) regimes for a transverse string with decreasing resolution in $D_\perp(\lambda)$. See text.

Stringy Saturation

In flat $D_\perp = 3$ the transverse string size distribution remains diffusive or logarithmic in N for small self-attractive interactions in the range $0 < g^2N < 1$. However for $g^2N \approx 1 - 1/\ln^2 N$ the transverse string size shrinks to a fixed size comparable to the string length. The change sets in at weak coupling with $g^2 \approx 1/N$, for which the transverse density at $b = 0$ is now

$$\mathbf{n}_\perp(0, x = 1/N) \approx \frac{N}{R_\perp^{D_\perp}} \to (g^2N)\frac{1}{l_p^{D_\perp}} \tag{7.66}$$

after restoring the string length. The first transition occurs in a very narrow range of g and thus appears to be first order by our analysis in (7.45-7.122). It is a pre-saturation transition where the string size shrinks away from its diffusive growth and remains about fixed at a relatively dilute transverse string bit density. At much higher resolution or low-x a saturation transition takes place when the transverse string bit distribution reaches the Bekenstein bound of one string bit per Planck scale. This maybe intuitively understood by noting that low-x follows from large boosts a situation analogous to falling matter on a black-hole. For completeness, we note that self-repulsive strings increase in sizes following the substitution $g^2 \to -g^2$ in (7.66).

Using the estimates for the AdS curvature through the substitution (7.117) yields

$$\mathbf{n}_\perp(0, x = 1/N) \approx \frac{N}{R_\perp^{D_\perp}} \longrightarrow \left(g^2 N\right)^{\frac{2\sqrt{\lambda} D_\perp}{3(D_\perp - 1)^2}} \frac{1}{l_p^{D_\perp}} \tag{7.67}$$

instead of (7.66). (7.67) reaches more smoothly the Bekenstein bound as the string self-interaction satisfies $g^2 N \approx 1$. Alternatively, the effective density using the effective dimension $D_\perp(\lambda)$

$$\tilde{\mathbf{n}}_\perp(0, x = 1/N) \approx \frac{N}{R_\perp^{D_\perp(\lambda)}} \to \left(g^2 N\right)^{\frac{2\sqrt{\lambda} D_\perp(\lambda)}{3(D_\perp - 1)^2} + \frac{D_\perp(\lambda)}{D_\perp}} \left(\frac{1}{x}\right)^{\frac{3(D_\perp - 1)^2}{2 D_\perp \sqrt{\lambda}}} \frac{1}{l_p^{D_\perp(\lambda)}} \tag{7.68}$$

is seen to increase beyond the Bekenstein bound as the string self-interaction reaches $g^2 N \approx 1$. There is no black-hole to saturate in fractional dimension.

Relation to Saturation in DIS

The present observations on stringy saturation are consistent with the arguments presented in [71, 72, 73] whereby the stringy but eikonalized dipole-dipole cross section was found to saturate in the impact parameter space when $g_s^2 l_s^{D_\perp} n_\perp \equiv l_P^{D_\perp} n_\perp \approx 1$ (see their Eq. 47). Although the relationship between the string coupling and the gauge coupling depends on the holographic extension of QCD used, for the generic model of AdS_5 with a wall $g_s \approx C\, g_{YM}^2/4\pi \equiv C\, \alpha_s$ ($C = 1$ for AdS_5 without a wall). Our numerical analysis puts $g_s \approx 0.1 - 0.3$.

The 3-dimensional density $n_\perp$ was physically interpreted in [71, 72, 73] as the number of wee dipoles per unit transverse 2-dimensional space per unit dipole size z along the holographic direction. The latter enforces hyperbolic evolution of the dipole size through the AdS_5 metric (with a wall). At saturation $z_s \approx 1/Q_s$. The transverse 2-dimensional density is then defined as $Q_s^2 \equiv z_s n_\perp$.

For curved AdS_5, the Pomeron intercept is $D_\perp(\lambda \approx 40)/12 \approx= 0.17$, and (7.67) at saturation gives $l_s Q_s \approx l_s/l_p \approx 1/x^{\frac{1}{3}}$. This is to be compared with $l_s Q_s^{GW} \approx l_s/l_p \approx 1/x^{0.144}$ obtained empirically by Golec-Wustoff [169, 170], and $l_s Q_s^{SZ} \approx l_s/l_p \approx 1/x^{0.114}$ obtained by Stoffers and one of us [71, 72, 73]. For curved $D_\perp(\lambda)$, (7.68) yields at saturation

$$l_p Q_s(\lambda) \approx \left(\frac{1}{x}\right)^{\frac{3(D_\perp - 1)^2}{2 D_\perp \sqrt{\lambda} D_\perp(\lambda)}} \to \left(\frac{1}{x}\right)^{0.155} \tag{7.69}$$

using $D_\perp = 3$ and $\lambda \approx 40$ [71, 72, 73]. (7.69) is overall consistent with the full AdS_5 curved analysis carried in [71, 72, 73], and remarkably close to the empirical result [169, 170].

The saturation of the Bekenstein bound maybe viewed as the string dual to the gluon saturation description in the color glass condensate model for fixed impact parameter using the Pomeron or string slope as a scale [171, 172]. The large string bit density (7.66) may upset the integrity of the string. Perhaps a more appropriate description is in terms of a fluid of string bits. However, three generic stringy ingredients need to be retained: 1) the string provides for a key property of the wee partons namely their transverse (Gribov) diffusion with a diffusion constant $\mathbf{D} = l_s^2/2$ set by the string length; 2) the exponential rise in the string density of states with its mass, provides for the most efficient mechanism to scramble information and reach the Bekenstein bound and thus saturation; 3) the self-interacting string in the mean-field approximation maybe the dual of a Pomeron branching into multiple Pomerons or fan-diagrams in Reggeon calculus [173].

7.1.6 Angular deformations

The fluctuating string with fixed end-points exhibit azimuthal deformations in the transverse plane that can be characterized by the azimuthal moment [174, 165]

$$\epsilon_n = \frac{\frac{1}{N}\sum_i^N e^{in\phi_i}\left(r_i^\perp\right)^n}{r_\perp^n} \tag{7.70}$$

where

$$r_\perp^n = \frac{1}{N}\sum_i^N \left(r_i^\perp\right)^n \tag{7.71}$$

with ϕ the azimuthal angle as measured from the impact parameter line along $\mathbf{b}$. $r_\perp$ is the averaged size of the string on the transverse plane. For $b = 0$, we have $\langle r_\perp^2 \rangle /2 = R_\perp^2/D_\perp$, where $\langle \cdots \rangle$ is the average over string ensembles. Specifically, define $x \equiv x_\perp^{i=1}$ and $y \equiv x_\perp^{i=2}$ in the transverse plane, where x is

parallel to the impact parameter $\mathbf{b}$ and y perpendicular to it,

$$\begin{aligned} x_\perp(k,\tau) &= \sum_{n=1}^{N-1} X_n(\tau) \sin\left(\frac{nk}{N}\pi\right) + b\frac{k}{N} \\ y_\perp(k,\tau) &= \sum_{n=1}^{N-1} Y_n(\tau) \sin\left(\frac{nk}{N}\pi\right) \end{aligned} \tag{7.72}$$

Both X_n, Y_n are normally distributed with width $1/2\omega_n$ (7.29) or

$$X_n \sim \mathcal{N}\left(0, \frac{1}{2\omega_n}\right) \qquad Y_n \sim \mathcal{N}\left(0, \frac{1}{2\omega_n}\right) \tag{7.73}$$

satisfy the normal distributions. We obtain

$$x_\perp(k,\tau) \sim \mathcal{N}\left(b\frac{k}{N}, \Sigma_k^2\right) \qquad y_\perp(k,\tau) \sim \mathcal{N}\left(0, \Sigma_k^2\right) \tag{7.74}$$

where

$$\Sigma_k^2 = \sum_{n=1}^{N-1} \frac{\sin^2\left(\frac{nk}{N}\pi\right)}{2\omega_n} \tag{7.75}$$

For large N, each of the transverse coordinates $x_\perp(k,\tau)$ are almost independent. The azimuthal moments averaged over the independent transverse coordinates read

$$\begin{aligned} \langle \epsilon_n \rangle &= \left(\frac{1}{\langle r_T^n \rangle} \frac{1}{N+1} + \frac{i}{\langle r_T^n \rangle} \frac{1}{N+1} \right] \\ &\quad \times \sum_{k=1}^{N-1} \int_0^\infty dr \int_0^{2\pi} d\phi r^{n+1} \cos(n\phi) \rho\left(r\cos\phi + \frac{b}{2}, r\sin\phi, k\right) \\ &\quad + \frac{1}{\langle r_T^n \rangle} \frac{1+(-1)^n}{N+1} \left(\frac{b}{2}\right)^n , \end{aligned} \tag{7.76}$$

where

$$\langle r_T^n \rangle = \frac{1}{N+1} \sum_{k=1}^{N-1} \int_0^\infty dr \int_0^{2\pi} d\phi \, r^{n+1} \, \rho\left(r\cos\phi + \frac{b}{2}, r\sin\phi, k\right) + \frac{2}{N+1}\left(\frac{b}{2}\right)^n \tag{7.77}$$

and

$$\rho(x,y,k) = \frac{1}{2\pi}\frac{1}{\Sigma_k^2}\exp\left[-\frac{\left(x-b\frac{k}{N}\right)^2+y^2}{2\Sigma_k^2}\right] \tag{7.78}$$

The Gaussian integrations can be done leading to

$$\langle\epsilon_n\rangle = \frac{b^n}{\langle r_T^n\rangle}\left[\frac{1}{N+1}\sum_{k=1}^{N-1}\left(\frac{1}{2}-\frac{k}{N}\right)^n + \frac{1+(-1)^n}{N+1}\left(\frac{1}{2}\right)^n\right] \tag{7.79}$$

Note that the moments $\langle\epsilon_n\rangle$ are real and that all the odd moments vanish, i.e. $\langle\epsilon_n\rangle = 0$ for odd n. Simple algebra yields

$$\frac{\langle r_T^2\rangle}{b^2} = \frac{1}{N+1}\sum_{k=1}^{N-1}\left(\frac{1}{2}-\frac{k}{N}\right)^2 + \frac{2}{N+1}\sum_{k=1}^{N-1}\frac{\Sigma_k^2}{b^2} + \frac{2}{N+1}\left(\frac{1}{2}\right)^2 \tag{7.80}$$

and

$$\begin{aligned}\frac{\langle r_T^4\rangle}{b^4} &= \frac{1}{N+1}\sum_{k=1}^{N-1}\left(\frac{1}{2}-\frac{k}{N}\right)^4 + \frac{8}{N+1}\sum_{k=1}^{N-1}\frac{\Sigma_k^2}{b^2}\left(\frac{1}{2}-\frac{k}{N}\right)^2 \\ &\quad + \frac{8}{N+1}\sum_{k=1}^{N-1}\frac{\Sigma_k^4}{b^4} + \frac{2}{N+1}\left(\frac{1}{2}\right)^4\end{aligned} \tag{7.81}$$

In the limit $N \longrightarrow \infty$, the moments simplify

$$\Sigma_{\tilde{k}}^2 \approx \sum_{n=1}^{N}\frac{1}{4n} = \frac{R_\perp^2}{D_\perp} \tag{7.82}$$

so that (for even n)

$$\langle\epsilon_n\rangle \approx \frac{b^n}{\langle r_T^n\rangle}\int_0^1 d\tilde{k}\left(\frac{1}{2}-\tilde{k}\right)^n = \frac{b^n}{\langle r_T^n\rangle}\frac{1}{2^n(1+n)} \tag{7.83}$$

$$\frac{\langle r_T^2\rangle}{b^2} \approx \frac{1}{12} + \frac{2}{D_\perp}\frac{R_\perp^2}{b^2} \tag{7.84}$$

$$\frac{\langle r_T^4\rangle}{b^4} \approx \frac{1}{80} + \frac{2}{3}\frac{R_\perp^2}{b^2 D_\perp} + 8\frac{R_\perp^4}{D_\perp^2 b^4} \tag{7.85}$$

For small b, we obtain

$$\langle \epsilon_2 \rangle \approx \frac{D_\perp}{24} \frac{b^2}{R_\perp^2} \tag{7.86}$$

$$\langle \epsilon_4 \rangle \approx \frac{D_\perp^2}{640} \frac{b^4}{R_\perp^4} \tag{7.87}$$

For general b, the numerical results of $\langle \epsilon_2 \rangle$ and $\langle \epsilon_4 \rangle$ are displayed in Fig. 7.15 and Fig. 7.16 respectively.

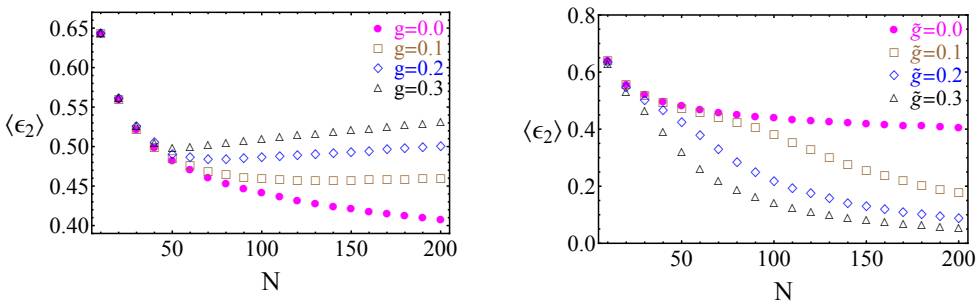

Figure 7.15: Attractive interaction: $g = 0.1, 0.2, 0.3$ (**Left**). Repulsive interaction: $\tilde{g} = 0.1, 0.2, 0.3$ (**Right**).

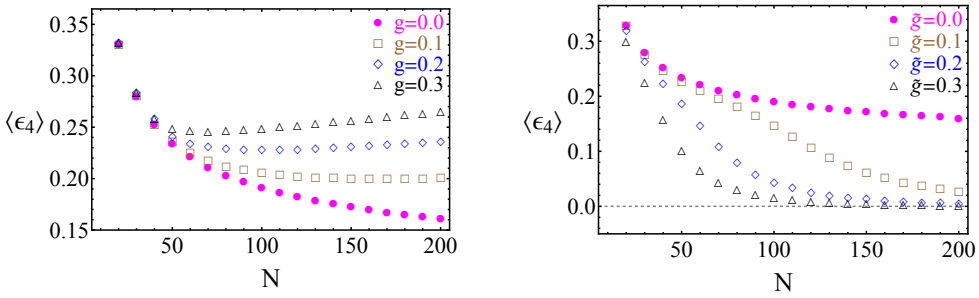

Figure 7.16: Attractive interaction: $g = 0.1, 0.2, 0.3$ (**Left**). Repulsive interaction: $\tilde{g} = 0.1, 0.2, 0.3$ (**Right**).

To show the transverse cross correlations it is also useful to use the cross

moments [174, 165]

$$
\begin{aligned}
(\epsilon_n\{2\})^2 &= \left\langle |\epsilon_n|^2 \right\rangle \\
(\epsilon_n\{4\})^4 &= -\left\langle |\epsilon_n|^4 \right\rangle + 2\left\langle |\epsilon_n|^2 \right\rangle^2 \\
(\epsilon_n\{6\})^6 &= \frac{1}{4}\left[\left\langle |\epsilon_n|^6 \right\rangle - 9\left\langle |\epsilon_n|^4 \right\rangle \left\langle |\epsilon_n|^2 \right\rangle + 12\left\langle |\epsilon_n|^2 \right\rangle^3\right] \\
(\epsilon_n\{8\})^8 &= \frac{1}{33}\Big[-\left\langle |\epsilon_n|^8 \right\rangle + 16\left\langle |\epsilon_n|^6 \right\rangle \left\langle |\epsilon_n|^2 \right\rangle + 18\left\langle |\epsilon_n|^4 \right\rangle^2 \\
&\qquad -144\left\langle |\epsilon_n|^4 \right\rangle \left\langle |\epsilon_n|^2 \right\rangle^2 + 144\left\langle |\epsilon_n|^2 \right\rangle^4 \Big] . \qquad (7.88)
\end{aligned}
$$

To characterize the initial azimuthal deformation of the string bits in the transverse collision plane, we show in Fig. 7.17 the pdf distributions of 1000 randomly generated strings at a resolution of $N = 200$ with no self-interactions $g/\tilde{g} = 0$.

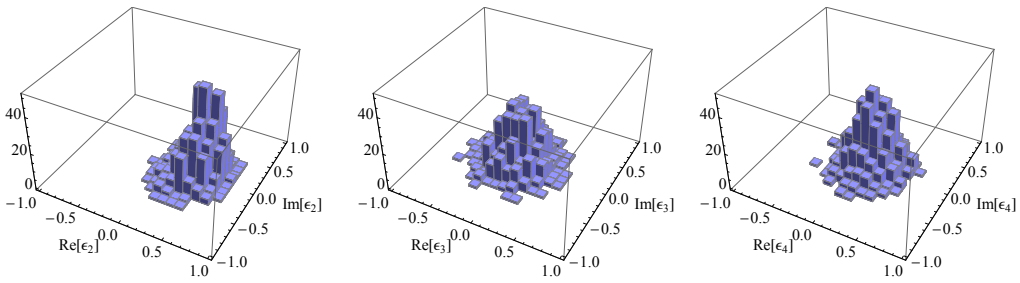

Figure 7.17: 3D Histograms, 1000 random generated strings. N=200.

The pdf shown are for the distributions in $\epsilon_{2,3,4}$ respectively. We also show in Fig. 7.18 the pdf distributions of 1000 randomly generated strings at a resolution of $N = 200$ undergoing string bit attractions with $g = 0.3$ in the mean-field approximation.

Note the strong dipole deformation in the leftmost figure. The same pdf for the repulsive case with $\tilde{g} = 0.3$ are shown in Fig. 7.19. The linear spreading of the string bits with the resolution N causes the azimuthal deformations to be relatively uniform.

For completeness we show the behavior of the cross moments with the resolution for attractive, non-interacting and repulsive strings in Fig. 7.20, Fig. 7.21 and Fig. 7.22 respectively by sampling 1000 times a single string stretched with $b = 5$.

The attraction is set at $g = 0.3$ while the repulsion at $\tilde{g} = 0.3$ for the infinite range case with $m = 0$. Recall that the realistic case of a massive

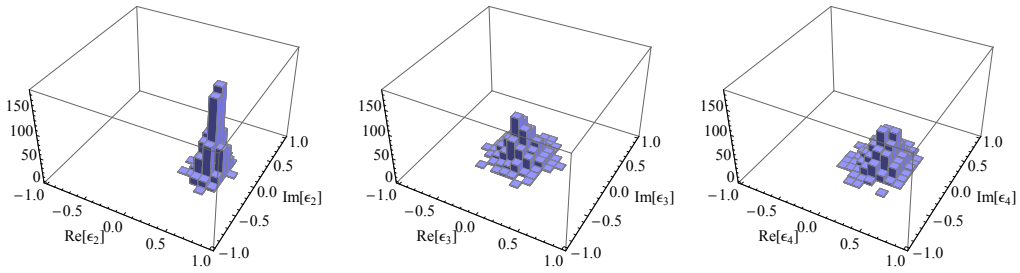

Figure 7.18: 3D Histograms, 1000 random generated strings. N=200. Attractive interaction $g = 0.3$.

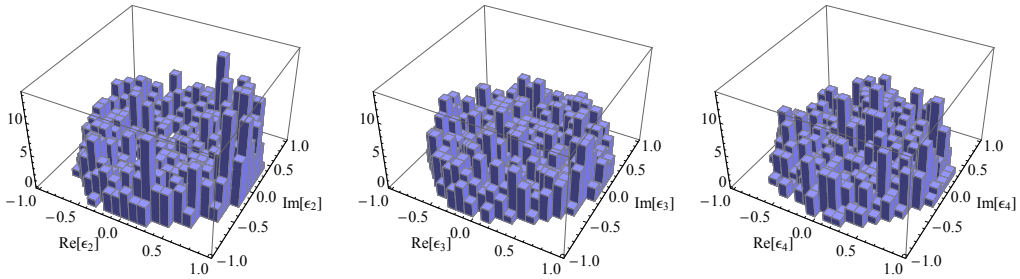

Figure 7.19: 3D Histograms, 1000 random generated strings. N=200. Repulsive interaction $\tilde{g} = 0.3$.

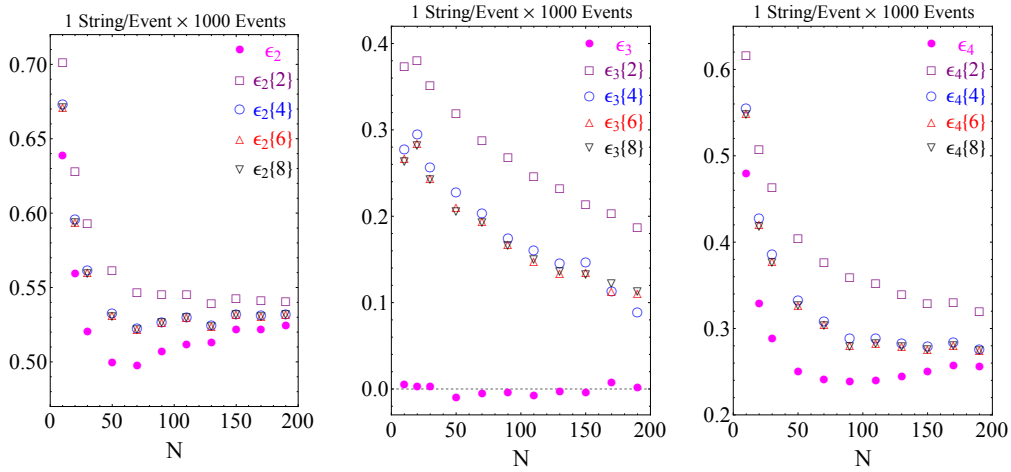

Figure 7.20: Attractive interaction $g = 0.3$.

glueball or scalar mass m is amenable to $m = 0$ by appropriately decreasing g or $\tilde{g}$. In a typical pp collision at collider energies, we expect to exchange

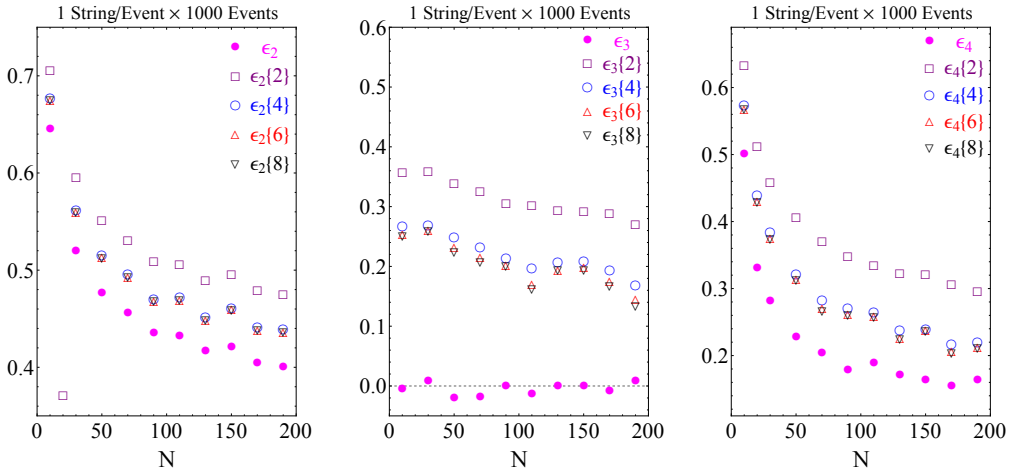

Figure 7.21: Non-interacting $g/\tilde{g} = 0$.

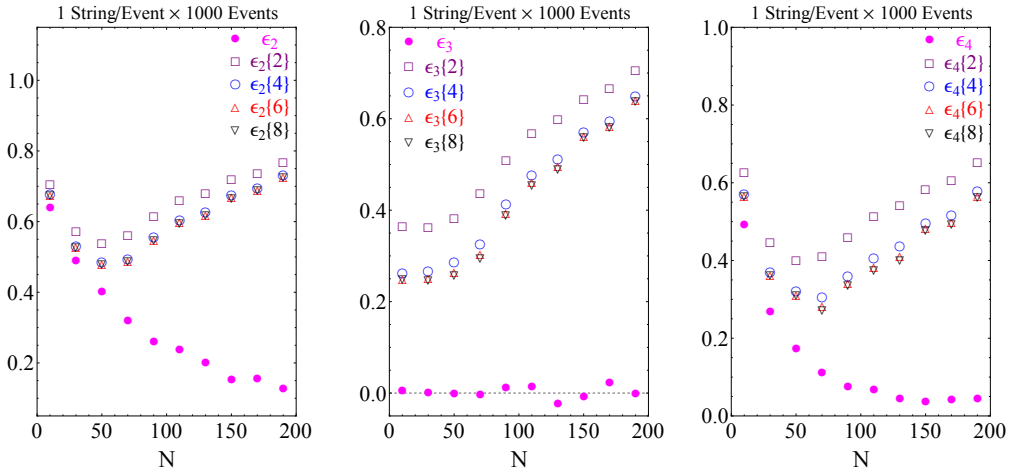

Figure 7.22: Repulsive interaction $\tilde{g} = 0.3$.

about 10 such long strings [71, 72, 73]. In Fig. 7.23, Fig. 7.24 and Fig. 7.25 we show the same cross moments following from the exchange of 5 typical strings stretched at $b = 5$ sampled 200 times for the attractive, non-interacting and repulsive case respectively.

The case where 10 string are exchanged is shown in Fig. 7.26, Fig. 7.27 and Fig. 7.28 for the same arrangements of parameters with each 10 string event sampled 100 times.

The critical moments for the pre-saturation coupling $g \approx 1/\sqrt{N} \approx 0.01$

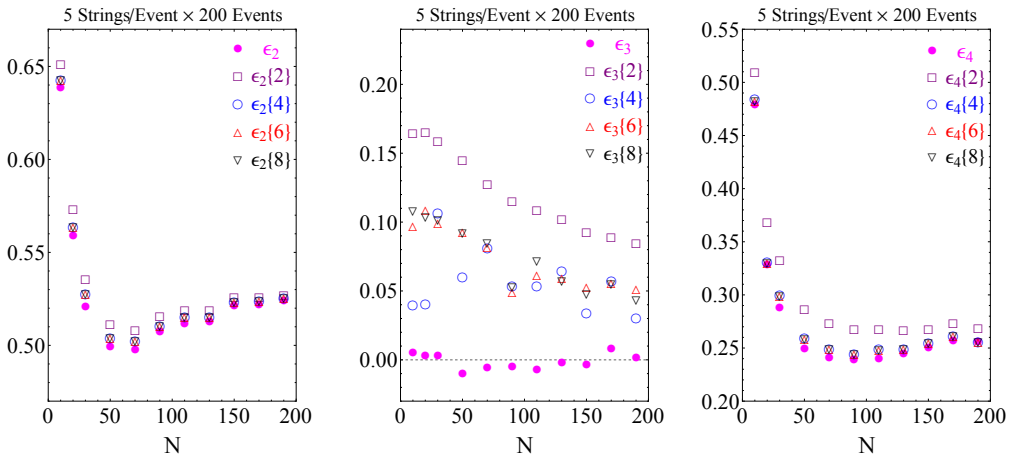

Figure 7.23: Attractive interaction $g = 0.3$.

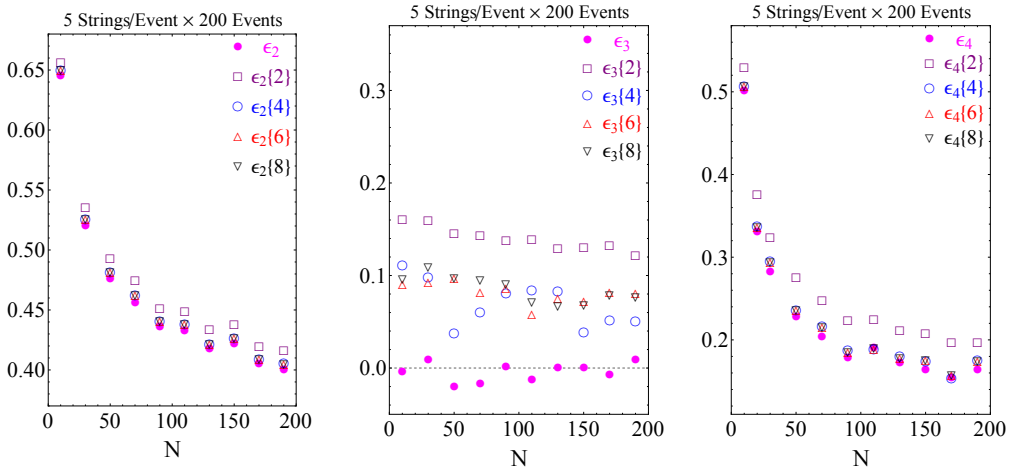

Figure 7.24: Non-interacting $g/\tilde{g} = 0$.

are not much different from the $g = 0$ presented here. We note that $\epsilon_n\{4\} \approx \epsilon_n\{6\} \approx \epsilon_n\{8\}$ in agreement with suggestion made in [174]. The more string exchanges, the denser and more symmetric the transverse string bit distribution for a fixed resolution N, the smaller the cross moments. Fig. 7.27 should represent typical cross moments in pp collisions at collider energies such as RHIC and LHC for minimum bias events. For the high multiplicity pp and pA events reported at LHC hot string configurations near the Hagedorn temperature are needed. They will be discussed in next subsection.

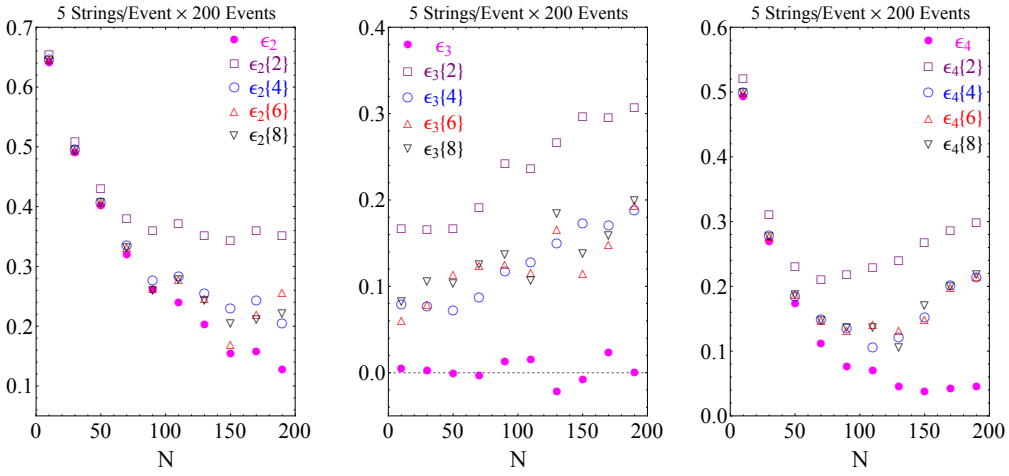

Figure 7.25: Repulsive interaction $\tilde{g} = 0.3$.

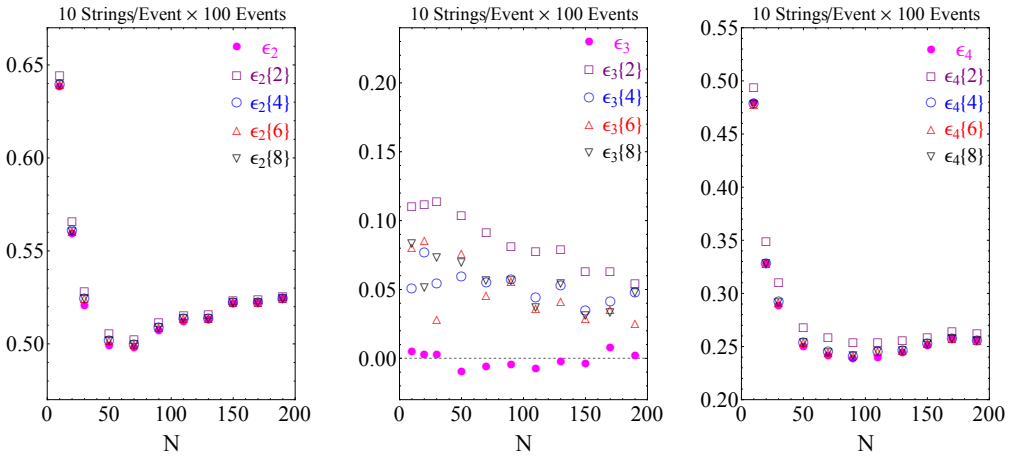

Figure 7.26: Attractive interaction $g = 0.3$.

7.2 At Hagedorn point

We analyze the length, mass and spatial distribution of a discretized transverse string in $D_\perp$ dimensions with fixed end-points near its Hagedorn temperature.

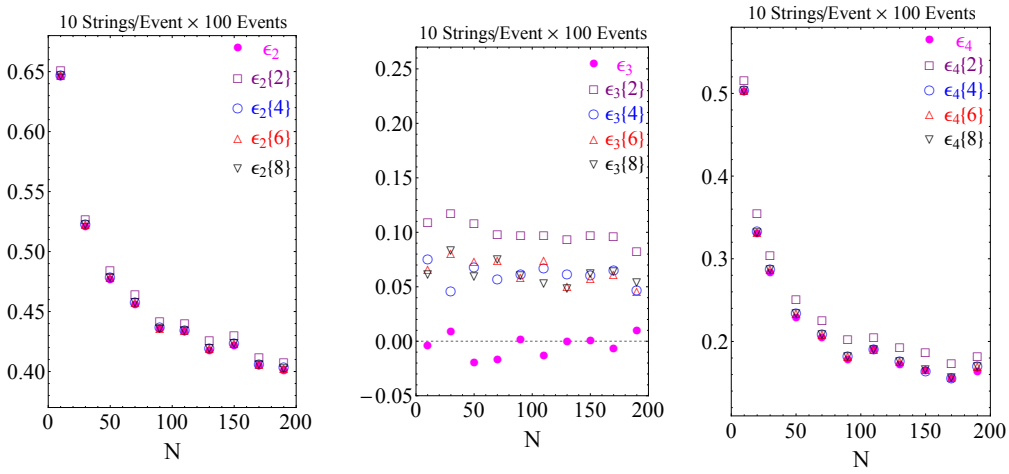

Figure 7.27: Non-interacting $g/\tilde{g} = 0$.

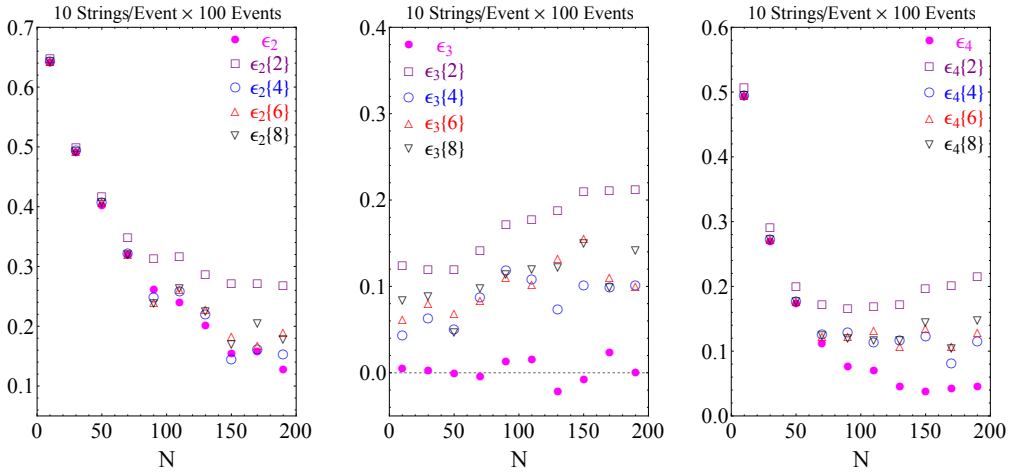

Figure 7.28: Repulsive interaction $\tilde{g} = 0.3$.

7.2.1 Free string at finite temperature

To describe the string close to its classical or Hagedorn point, we introduce an effective temperature $1/\beta$ which is conjugate of the squared and normal ordered mass operator [84, 85, 110],

$$: \mathcal{H}_\perp := \sum_{n=1}^{N-1} \Omega_n (a_n^i)^\dagger a_n^i + \frac{b^2}{\pi^2} \tag{7.89}$$

with the standard commutators $\left[a_n^i, (a_{n'}^{i'})^\dagger\right] = \delta_{nn'}\delta_{ii'}$. All expectation values at finite $1/\underline{\beta}$ will be carried using the density matrix $e^{-\underline{\beta}:\mathcal{H}_\perp:}/\mathcal{Z}_\perp$, with the transverse partition function

$$\mathcal{Z}_\perp = \left\langle e^{-\underline{\beta}:\mathcal{H}_\perp:} \right\rangle = \exp\left(-\underline{\beta}\frac{b^2}{\pi^2}\right) \prod_{i=1}^{D_\perp} \prod_{n=1}^{N-1} \frac{1}{1-e^{-\underline{\beta}\Omega_n}} \tag{7.90}$$

This is a micro-canonical description of a single thermal string. In practical terms, it corresponds to string bits X_n^i normally distributed with

$$X_n^i \sim \mathcal{N}\left(0, \frac{1}{\Omega_n\left(e^{\underline{\beta}\Omega_n}-1\right)}\right) \tag{7.91}$$

The squared mass is then $2M_\perp^2 \equiv -\partial\mathcal{Z}_\perp/\partial\underline{\beta}$ or

$$\begin{aligned}
2M_\perp^2 &= \langle\!\langle : \mathcal{H}_\perp : \rangle\!\rangle \\
&= D_\perp \sum_{n=1}^{N-1} \frac{\Omega_n}{e^{\underline{\beta}\Omega_n}-1} + \frac{b^2}{\pi^2} \\
&\longrightarrow \frac{D_\perp}{\underline{\beta}^2}\int_{\underline{\beta}}^{\infty} dx\ \frac{x}{e^x-1} + \frac{b^2}{\pi^2} \\
&\approx \frac{D_\perp}{6}\frac{\pi^2}{\underline{\beta}^2} + \frac{b^2}{\pi^2}
\end{aligned} \tag{7.92}$$

and its squared transverse size is

$$\begin{aligned}
R_\perp^2 &\equiv \frac{1}{N}\sum_{k=0}^{N}\left\langle\!\!\left\langle : \left(x_k^i - \mathbf{b}^i\frac{k}{N}\right)^2 : \right\rangle\!\!\right\rangle \\
&= \frac{D_\perp}{2}\sum_{n=1}^{N-1}\frac{1}{\Omega_n}\frac{1}{e^{\underline{\beta}\Omega_n}-1} \\
&\to \frac{D_\perp}{2}\int_{\underline{\beta}}^{\infty}\frac{dx}{x}\frac{1}{e^x-1} \\
&\approx \frac{D_\perp}{2\underline{\beta}},
\end{aligned} \tag{7.93}$$

where $\langle\langle \cdots \rangle\rangle$ is the expectation value carried using the density matrix. The effective entropy is

$$\begin{aligned} S_\perp &= -\underline{\beta}\frac{\partial \ln \mathcal{Z}_\perp}{\partial \underline{\beta}} + \ln \mathcal{Z}_\perp \\ &= D_\perp \sum_{n=1}^{N-1} \left[\frac{\underline{\beta}\Omega_n}{e^{\underline{\beta}\Omega_n} - 1} - \ln\left(1 - e^{-\underline{\beta}\Omega_n}\right) \right] \\ &\to \frac{D_\perp}{\underline{\beta}} \int_{\underline{\beta}}^{\infty} dx \ \left[\frac{x}{e^x - 1} - \ln\left(1 - e^{-x}\right) \right] \\ &\approx \frac{D_\perp}{3}\frac{\pi^2}{\underline{\beta}} \end{aligned} \tag{7.94}$$

which can be recasted using the Hagedorn temperature $1/\beta_H$

$$S_\perp \approx 2\pi\sqrt{\frac{D_\perp}{6}} M_\perp \to 2\pi\sqrt{\frac{D_\perp \alpha'}{6}} M_\perp \equiv \beta_H M_\perp \tag{7.95}$$

after re-instating the string unit with $M_\perp/l_s \to M_\perp$. Below the value of $1/\underline{\beta}$ will be fixed by fixing the mass or the entropy of the thermal string. We note that for large $1/\underline{\beta}$ the string behaves classically with dwarfed quantum or zero point contributions. Hence the normal ordering. To make contact with physical observables, we identify $S_\perp$ with the prompt multiplicity and approximate it with the final charge multiplicity $N_{\rm ch}$ (upper bound). For a single string exchange

$$S_\perp \approx \frac{D_\perp}{3}\frac{\pi^2}{\underline{\beta}} \approx 7.5\, N_{\rm ch} \tag{7.96}$$

Throughout, high temperature means $\underline{\beta} \ll 1$ and classical means $N\underline{\beta} \gg 1$. Analytically, we will take $N \to \infty$ and fix $\underline{\beta} \ll 1$. Numerically, the best we can do is set $N = 500$ which fixes the range $\underline{\beta} \approx (0.1, 0.02)$, since $\underline{\beta} \leq 0.1$ is small and $N\underline{\beta} \geq 10$ is large. For a single string this translates to a charge multiplicity N_{ch} in the range $(13, 66)$. In Fig. 7.29 and Fig. 7.30 we show a single string for a fixed distance $\mathbf{b} = 5 \equiv 10 l_s \approx 1\,\text{fm}$ with charge multiplicity $N_{ch} = 13$ and $N_{ch} = 66$ respectively. The left figure is the string projected in the transverse spatial plane, while the right figure is the string in the holographic but flat $D_\perp = 3$ dimensions. The effects of the warping in the holographic direction will be discussed below.

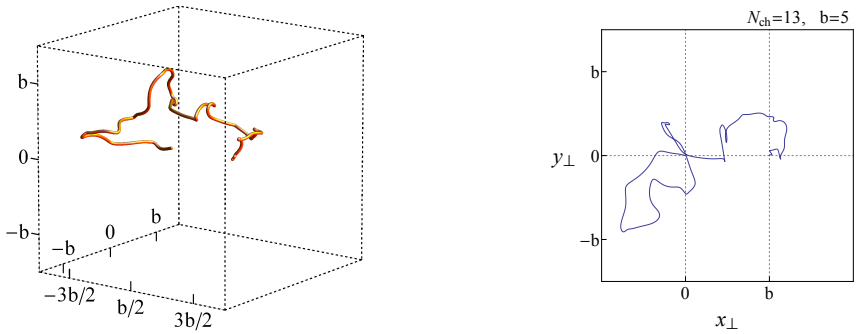

Figure 7.29: Streched string with fixed $\mathbf{b} = 5 = 10l_s$ and multiplicity $N_{ch} = 13$ in the holographic $D_\perp = 3$ (left) and projected onto the spatial 2-dimensional transverse space (right).

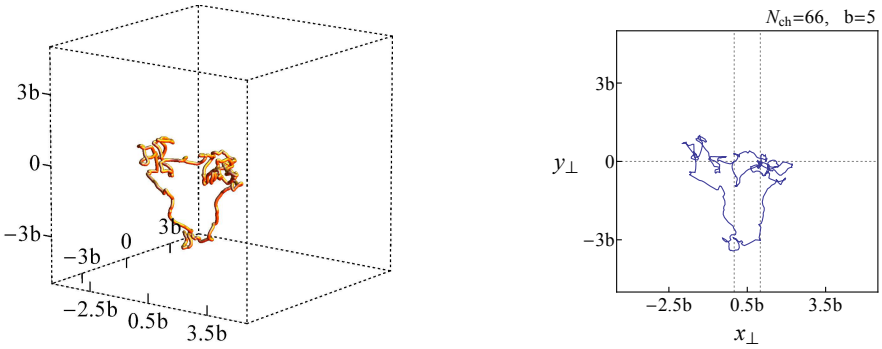

Figure 7.30: Streched string with fixed $\mathbf{b} = 5 = 10l_s$ and multiplicity $N_{ch} = 66$ in the holographic $D_\perp = 3$ (left) and projected onto the spatial 2-dimensional transverse space (right).

pp and *pA* scattering in the holographic context may involve more than a single string exchange [75, 175, 72]. Multiple string exchanges involve colder strings in their diffusive regime with a higher multiplicity. For 5 and 10 multiple string exchanges, the charge multiplicity N_{ch} is in the range $(66, 329)$ and $(132, 658)$ respectively. In Fig. 7.31 (left) we display 5 strings with $\underline{\beta} = 0.1$ or a charge multiplicity of $N_{ch} = 66$. In Fig. 7.31 (right) we display 10 strings with $\underline{\beta} = 0.1$ or a charge multiplicity of $N_{ch} = 132$.

Fig. 7.32 is the same as Fig. 7.31 but with $\underline{\beta} = 0.02$ or $N_{ch} = 329$ for 5 strings and $N_{ch} = 658$ for 10 strings.

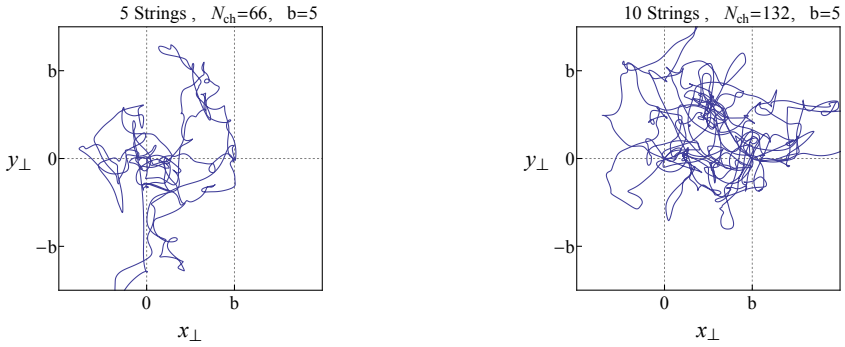

Figure 7.31: 5 string shapes (left) with a total multiplicity $N_{\rm ch} = 66$, and 10 string shapes (right) with a total multiplicity $N_{\rm ch} = 132$. The string end-points are fixed at $\mathbf{b} = 5 = 10\, l_s$

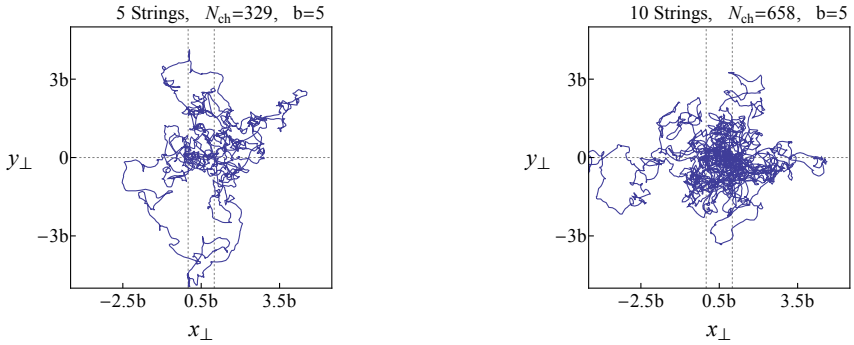

Figure 7.32: 5 string shapes (left) with a total multiplicity $N_{\rm ch} = 329$, and 10 string shapes (right) with a total multiplicity $N_{\rm ch} = 658$. The string end-points are fixed at $\mathbf{b} = 5 \equiv 10\, l_s$

7.2.2 Thermal string with self interactions

We now follow our recent analysis for the cold string in [76] and explicit the string self-interaction by assuming it to be dominated by the two-body string bits interactions mediated by a static exchange in $D_\perp + 2$ dimensions. Specifically,

$$V = -\frac{1}{2} g^2 \sum_{k \neq k'} \int \frac{d^{D_\perp+1} p}{(2\pi)^{D_\perp+1}} \frac{M(\vec{x}_k) M(\vec{x}_{k'})}{p^2 + m^2} \exp\left(i\vec{p} \cdot (\vec{x}_k - \vec{x}_{k'})\right) \qquad (7.97)$$

where $M(\vec{x}_k)$ is the mass of the discrete point at $\vec{x}_k$. The exchange is generic and is parameterized with an attractive coupling g and a mass m. In holographic QCD, the exchanged mass is that of the lowest scalar [165, 166, 167]. Throughout, we will set $m = 0$ as any finite m can be re-absorbed into a re-definition of the coupling and use g as a parameter.

The interacting Hamiltonian is now $\mathcal{H}_\perp \to \mathcal{H}^0_\perp + 2M_\perp V$. The partition function for the interacting string is now formally given by

$$\mathcal{Z} = \left\langle e^{-\underline{\beta}\mathcal{H}_\perp} \right\rangle = \left\langle e^{-\underline{\beta}\left(\mathcal{H}^0_\perp + 2M_\perp V\right)} \right\rangle \tag{7.98}$$

where the averaging is carried using a complete set of free harmonic oscillators with trial frequencies ω_n instead of the free frequencies Ω_n. This corresponds to the interacting string bits X^i_n normally distributed with

$$X^i_n \sim \mathcal{N}\left(0, \frac{1}{\omega_n\left[e^{\frac{\underline{\beta}}{2}\left(\omega_n + \frac{\Omega_n^2}{\omega_n}\right)} - 1\right]}\right) \tag{7.99}$$

Variational Analysis

To estimate (7.98) we will use the Feynman variational principle [141, 176]

$$\mathcal{Z} \geq \mathcal{Z}_0 \exp\left(-2\underline{\beta} M_\perp \left\langle\!\left\langle\, V \,\right\rangle\!\right\rangle\right) \tag{7.100}$$

with

$$\mathcal{Z}_0 = \left\langle e^{-\underline{\beta}\mathcal{H}^0_\perp} \right\rangle = \exp\left(-\underline{\beta}\frac{b^2}{\pi^2}\right) \prod_{i=1}^{D_\perp} \prod_{n=1}^{N-1} \frac{1}{1 - \exp\left[-\frac{\underline{\beta}}{2}\left(\omega_n + \frac{\Omega_n^2}{\omega_n}\right)\right]} \tag{7.101}$$

In leading order in the interaction the squared mass and size of the interacting string are given by

$$2M^2_\perp = \left\langle\!\left\langle\, \mathcal{H}^0_\perp \,\right\rangle\!\right\rangle = \frac{D_\perp}{2} \sum_{n=1}^{N-1} \frac{\omega_n + \frac{\Omega_n^2}{\omega_n}}{\exp\left[\frac{\underline{\beta}}{2}\left(\omega_n + \frac{\Omega_n^2}{\omega_n}\right)\right] - 1} + \frac{b^2}{\pi^2} \tag{7.102}$$

$$R_\perp^2 \;= \frac{1}{N}\sum_{k=0}^{N}\left\langle\!\!\left\langle \left(x_k^i - \mathbf{b}^i\frac{k}{N}\right)^2 \right\rangle\!\!\right\rangle = \frac{D_\perp}{2}\sum_{n=1}^{N-1}\frac{1}{\omega_n}\frac{1}{\exp\left[\frac{\beta}{2}\left(\omega_n + \frac{\Omega_n^2}{\omega_n}\right)\right]-1} \tag{7.103}$$

The discretized string mass distribution $M(\vec{x}_k) \longrightarrow M_\perp/N + 1$ so that the averaged pair-interaction reads

$$\begin{aligned}
\langle\!\langle\, V \,\rangle\!\rangle \approx -\frac{g^2}{2}\frac{M_\perp^2}{N^2} \quad & \sum_{k\neq k'} \quad \int \frac{d^{D_\perp+1}p}{(2\pi)^{D_\perp+1}}\frac{e^{i\vec{p}\cdot\vec{b}\frac{(k-k')}{N}}}{p^2+m^2} \\
& \times \exp\left(-\frac{p^2}{2D_\perp}\left\langle\!\!\left\langle \left(\vec{x}_k - \mathbf{b}^i\frac{k}{N} - \vec{x}_{k'} + \mathbf{b}^i\frac{k'}{N}\right)^2 \right\rangle\!\!\right\rangle\right) \\
\approx -\frac{g^2}{2}\frac{M_\perp^2}{N^2} \quad & \sum_{k\neq k'} \quad \int \frac{d^{D_\perp+1}p}{(2\pi)^{D_\perp+1}}\frac{e^{i\vec{p}\cdot\vec{b}\frac{(k-k')}{N}}}{p^2+m^2} \\
& \times \exp\left(-\frac{p^2}{2D_\perp}\left\langle\!\!\left\langle \left(\vec{x}_k - \mathbf{b}^i\frac{k}{N}\right)^2 + \left(\vec{x}_{k'} - \mathbf{b}^i\frac{k'}{N}\right)^2 \right\rangle\!\!\right\rangle\right)
\end{aligned} \tag{7.104}$$

where we have exponentiated the averaging and then used the quadratic nature of the distributions. Since the position of the string bits are normally distributed, we can carry the averaging in the exponent explicitly. The result is

$$\begin{aligned}
\langle\!\langle\, V \,\rangle\!\rangle \;\approx\; & -\frac{1}{2}g^2\frac{M_\perp^2}{N^2}\sum_{k\neq k'}\int \frac{d^{D_\perp+1}p}{(2\pi)^{D_\perp+1}}\frac{e^{i\vec{p}\cdot\vec{b}\frac{(k-k')}{N}}}{p^2+m^2} \\
& \times \exp\left(-\frac{p^2}{2}\sum_{n=1}^{N-1}\frac{\left[\sin^2\left(\frac{nk}{N}\pi\right) + \sin^2\left(\frac{nk'}{N}\pi\right)\right]}{\omega_n\left(e^{\frac{\beta}{2}\left(\omega_n + \frac{\Omega_n^2}{\omega_n}\right)} - 1\right)}\right) \\
\approx\; & -\frac{1}{2}g^2 M_\perp^2 \int \frac{d^{D_\perp+1}p}{(2\pi)^{D_\perp+1}}\frac{1}{p^2+m^2}\frac{4\sin^2\left(\frac{\vec{p}\cdot\vec{b}}{2}\right)}{(\vec{p}\cdot\vec{b})^2}\exp\left(-p^2\frac{R_\perp^2}{D_\perp}\right)
\end{aligned} \tag{7.105}$$

We note that (7.104) is overall similar to the result established in [76], except that now both $M_\perp, R_\perp$ are implicit functions of the effective temperature $1/\underline{\beta}$. Inserting (7.105) back into (7.100) shows that for the interacting string the free energy is bounded from below

$$\begin{aligned} F &\geq -g^2 M_\perp^3 \int \frac{d^{D_\perp+1}p}{(2\pi)^{D_\perp+1}} \frac{1}{p^2+m^2} \frac{4\sin^2\left(\frac{\vec{p}\cdot\vec{b}}{2}\right)}{(\vec{p}\cdot\vec{b})^2} \exp\left(-p^2\frac{R_\perp^2}{D_\perp}\right) \\ &\quad + \frac{D_\perp}{\underline{\beta}} \sum_{n=1}^{N-1} \ln\left(1-\exp\left[-\frac{\underline{\beta}}{2}\left(\omega_n + \frac{\Omega_n^2}{\omega_n}\right)\right]\right) + \frac{b^2}{\pi^2}\,. \end{aligned} \tag{7.106}$$

The bound in 7.106 is parametrized by the set of frequencies ω_n which are fixed variationally through

$$\begin{aligned} \frac{\delta F}{\delta \omega_n} &\geq \frac{D_\perp}{2}\left(1-\frac{\Omega_n^2}{\omega_n^2}\right) \frac{1}{\exp\left[\frac{\underline{\beta}}{2}\left(\omega_n+\frac{\Omega_n^2}{\omega_n}\right)\right]-1} \\ &\quad - \frac{\delta M_\perp^2}{\delta\omega_n}\frac{3g^2M_\perp}{2}\int \frac{d^{D_\perp+1}p}{(2\pi)^{D_\perp+1}}\frac{1}{p^2+m^2}\frac{4\sin^2\left(\frac{\vec{p}\cdot\vec{b}}{2}\right)}{(\vec{p}\cdot\vec{b})^2}\exp\left(-p^2\frac{R_\perp^2}{D_\perp}\right) \\ &\quad + \left(\frac{1}{D_\perp}\frac{\delta R_\perp^2}{\delta\omega_n}\right) g^2 M_\perp^3 \int \frac{d^{D_\perp+1}p}{(2\pi)^{D_\perp+1}}\frac{p^2}{p^2+m^2}\frac{4\sin^2\left(\frac{\vec{p}\cdot\vec{b}}{2}\right)}{(\vec{p}\cdot\vec{b})^2}\exp\left(-p^2\frac{R_\perp^2}{D_\perp}\right) \\ &= 0 \end{aligned} \tag{7.107}$$

High Temperature Limit

To find the lower bound in (7.107) is in general involved. However, at high temperature the contributions simplify

$$\begin{aligned} \frac{\delta M_\perp^2}{\delta\omega_n} &= \frac{D_\perp\left(1-\frac{\Omega_n^2}{\omega_n^2}\right)}{\left(2\exp\left[\frac{\underline{\beta}}{2}\left(\omega_n+\frac{\Omega_n^2}{\omega_n}\right)\right]-1\right)^2}\Bigg(\exp\left[\frac{\underline{\beta}}{2}\left(\omega_n+\frac{\Omega_n^2}{\omega_n}\right)\right]-1 \\ &\quad -\frac{\underline{\beta}}{2}\left(\omega_n+\frac{\Omega_n^2}{\omega_n}\right)\exp\left[\frac{\underline{\beta}}{2}\left(\omega_n+\frac{\Omega_n^2}{\omega_n}\right)\right]\Bigg) \\ &\approx 0\left(\frac{1}{\underline{\beta}}\right) \end{aligned} \tag{7.108}$$

$$
\begin{aligned}
-\frac{1}{D_\perp}\frac{\delta R_\perp^2}{\delta\omega_n} &= \frac{1}{2\omega_n^2}\frac{1}{\exp\left[\frac{\beta}{2}\left(\omega_n+\frac{\Omega_n^2}{\omega_n}\right)\right]-1} \\
&\quad +\frac{\underline{\beta}}{4\omega_n}\left(1-\frac{\Omega_n^2}{\omega_n^2}\right)\frac{\exp\left[\frac{\beta}{2}\left(\omega_n+\frac{\Omega_n^2}{\omega_n}\right)\right]}{\left(\exp\left[\frac{\beta}{2}\left(\omega_n+\frac{\Omega_n^2}{\omega_n}\right)\right]-1\right)^2} \\
&\approx \frac{2\omega_n}{\underline{\beta}\left(\omega_n^2+\Omega_n^2\right)^2}\,. \qquad (7.109)
\end{aligned}
$$

So in leading order in $1/\underline{\beta}$ or close to the Hagedorn temperature, the lower bound in (7.107) is reduced to finding ω_n which are solutions to

$$
\begin{aligned}
\frac{\delta F}{\delta\omega_n} &\approx \frac{D_\perp}{\underline{\beta}\omega_n}\frac{\omega_n^2-\Omega_n^2}{\omega_n^2+\Omega_n^2} \\
&\quad -\frac{2\omega_n}{\underline{\beta}\left(\omega_n^2+\Omega_n^2\right)^2}g^2M_\perp^3\int\frac{d^{D_\perp+1}p}{(2\pi)^{D_\perp+1}}\frac{p^2}{p^2+m^2}\frac{4\sin^2\left(\frac{\vec{p}\cdot\vec{b}}{2}\right)}{(\vec{p}\cdot\vec{b})^2}\exp\left(-p^2\frac{R_\perp^2}{D_\perp}\right) \\
&= 0 \qquad (7.110)
\end{aligned}
$$

Thus $\omega_n^2=\eta^2+\sqrt{\eta^4+\Omega_n^4}$ with

$$
\eta^2=\frac{g^2M_\perp^3}{D_\perp}\int\frac{d^{D_\perp+1}p}{(2\pi)^{D_\perp+1}}\frac{p^2}{p^2+m^2}\frac{4\sin^2\left(\frac{\vec{p}\cdot\vec{b}}{2}\right)}{(\vec{p}\cdot\vec{b})^2}\exp\left(-p^2\frac{R_\perp^2}{D_\perp}\right) \qquad (7.111)
$$

Since $M_\perp, R_\perp$ in (7.111) involve ω_n implicitly, the evaluation of η follows iteratively using numerical analysis.

Numerical Results: $D_\perp=3$

In Fig. 7.33 we show the string shape for an interacting string with fixed end-points $\mathbf{b}=5=10l_s$, an effective temperature parameter $1/\underline{\beta}=1/0.1$ or a charge multiplicity of $N_{ch}=66$, and a coupling $g=0.6$. On the right the string is displaced in $D_\perp=3$ dimensions with a flat holographic direction. On the left, we show the same string projected on the 2 transverse spatial directions only. Fig. 7.34 is the same as Fig. 7.33 with the exchange of 5 strings and 10 strings with $g=0.6$.

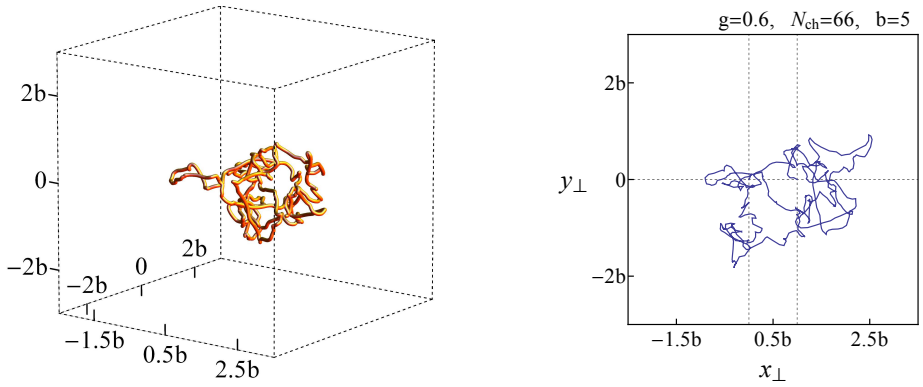

Figure 7.33: Interacting string with $g = 0.6$ and $N_{ch} = 66$ for a separation of $b = 5 = 10l_s$ in $D_\perp = 3$ (left) and projected onto the 2-spatial dimensions (right).

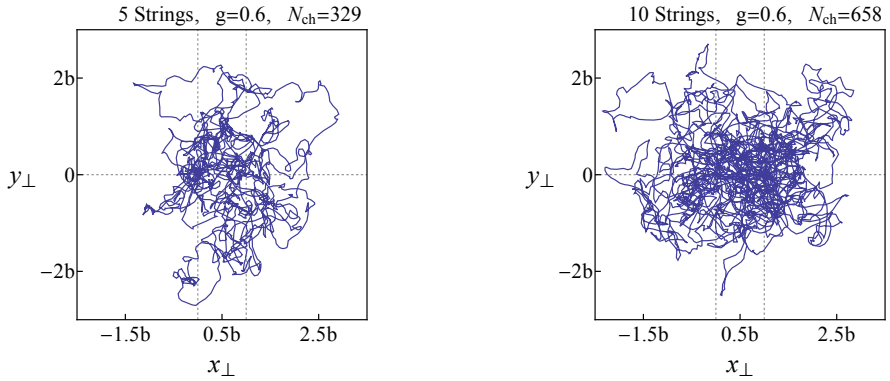

Figure 7.34: 5 interacting strings with $g = 0.6$ and $N_{ch} = 329$ for a separation of $b = 5 = 10l_s$ in $D_\perp = 3$ (left) and the same for 10 interacting strings and $N_{ch} = 658$ (right).

In Fig. 7.35 (right) the single string mass versus the charge multiplicity $N_{\rm ch}$ following from (7.102) is shown for a string at high resolution with $N = 500$ and different attractive couplings. In Fig. 7.35 (left) the transverse size $R_\perp$ versus $\sqrt{N_{ch}}$ following from (7.103) for the same string parameters. We note that the attraction does not change the mass or entropy, but does cause the string to contract transversally away from its free diffusive thermal expansion.

In Fig. 7.36 we show the transverse size versus the string mass (also entropy) or $R_\perp$ as given by (7.103) versus $M_\perp$ as defined in (7.102). The

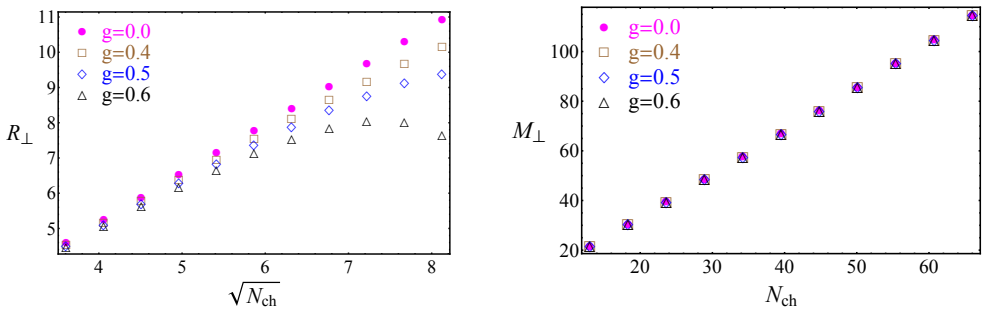

Figure 7.35: Transverse size (left) and mass (right) of the string versus its multiplicity for $N = 500$ string bits and different attractive self-couplings g.

lines in Fig. 7.36 (right) corresponds to

$$R_\perp^2 \approx 1.5\sqrt{\frac{3D_\perp}{2\pi^2}}\sqrt{1-0.012g^2M_\perp}\,M_\perp \tag{7.112}$$

and in overall agreement with the schematic analysis of the variational result in (7.116). The latter suggests a first order transmutation to a black-hole for sufficiently strong and attractive self-string interactions. (7.112) shows that weak coupling but high temperature means $0.012g^2M_\perp < 1$. Since for most of our analyses we use $M_\perp < 100$, this corresponds to $g < 1$, hence our choices of $g = 0.4, 0.5, 0.6$.

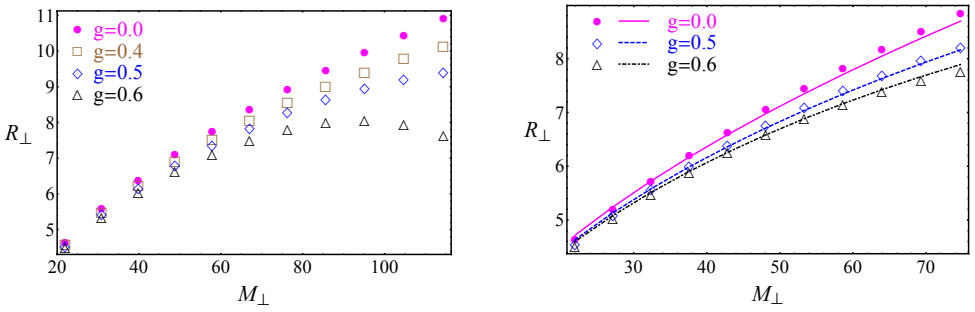

Figure 7.36: Transverse size of the interacting string for $N = 500$ string bits and attractive self-coupling coupling g versus its mass (left). The solid curves are analytical results (right).

For completeness, the length of the string L defined as

$$L = \left\langle\!\!\left\langle \sum_{k=1}^{N} \sum_{i=1}^{D_\perp} \left| x_k^i - x_{k-1}^i \right| \right\rangle\!\!\right\rangle \tag{7.113}$$

versus $M_\perp$ (7.102) and $R_\perp$ (7.103) with the resolution $N = 100$ for different coupling strengths g are displayed in Fig. 7.37 (left) and Fig. 7.37 (right).

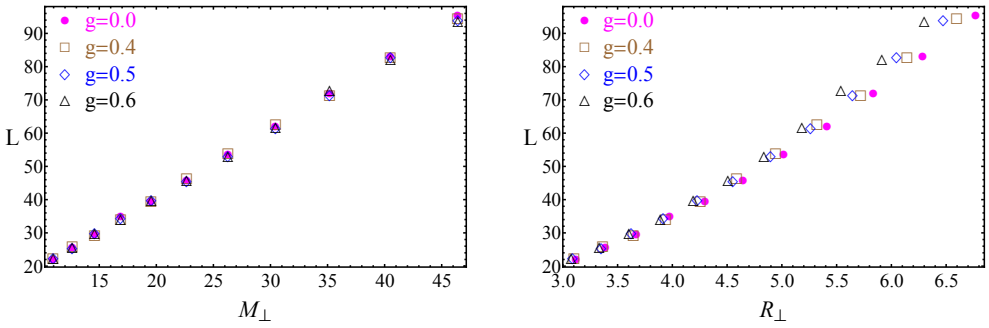

Figure 7.37: Total length of the interacting string versus its mass (left) and its transverse size (right) for different attractive self-coupling coupling g. The number of string bits is $N = 100$.

Schematic Analysis

An understanding of the self-interacting string in the Hagedorn regime follows from the variational minimization of the free energy above. Here we note, that for no self-interaction or $g = 0$, the classical diffusive growth noted in (7.93) follows from the fact that the kinetic term in the transverse Hamiltonian (7.6) scales like $1/R^2$ by the uncertainty principle and does not favor short strings, while the confining harmonic term in (7.6) does not favor long strings and scales like R^2. This trade-off is captured by minimizing the schematic free energy

$$\mathcal{F}_{0\perp} = M_\perp^2 \left(\frac{1}{R^2} + \frac{R^2}{M_\perp^2} \right) \tag{7.114}$$

$d\mathcal{F}_{0\perp}/dR = 0$ yields (7.93). Self-interactions in $2 + D_\perp$ are holographically dual to the exchange of light excitations in bulk. As a result, (7.114) now reads

$$\mathcal{F}_\perp \equiv \mathcal{F}_{0\perp} + M_\perp V = M_\perp^2 \left(\frac{1}{R^2}(1 - g_s^2 M_\perp) + \frac{R^2}{M_\perp^2} \right) \tag{7.115}$$

after dropping terms of order 1. $d\mathcal{F}_\perp/dR = 0$ now occurs for

$$R_\perp^2 \approx \sqrt{1 - g_s^2 M_\perp}\, M_\perp \tag{7.116}$$

which is (7.112) for $g^2 M_\perp \ll 1$. However, for $g^2 M_\perp \approx 1 - 1/M_\perp^2$ (7.116) undergoes a first order change into a fixed size string of few string lengths. The self-interacting string described variationally above begins its transmutation to a black-hole as illustrated by the present schematic analysis.

Numerical Results: $2 < D_\perp(\lambda) < 3$

An exact treatment of the transverse string in curved AdS_5 space is beyond the scope of this work. In this section we will give simple estimates of the effects of the curvature of AdS_5 on some of our previous results. One of the main effect of the curved geometry on the Pomeron is to cause the string transverse degrees of freedom to effectively feel a reduced transverse spatial dimension [71, 72, 73, 75]

$$D_\perp \to D_\perp(\lambda) = D_\perp \left(1 - \frac{3(D_\perp - 1)^2}{2D_\perp \sqrt{\lambda}} + \mathcal{O}\left(\frac{1}{\lambda}\right) \right) \tag{7.117}$$

with $\lambda = g_{YM}^2 N_c$. (7.117) causes the Pomeron intercept to move from $D_\perp/12 = 0.25$ to $D_\perp(\lambda \approx 40) \approx 0.17$ closer to the empirical intercept of 0.08 [168]. A phenomenological way to implement this effect is to add warping factors on the oscillators in (7.1) as we noted in our recent analysis [80]. This will be used in our numerical results to follow. A simple estimate follows from the substitution (7.117) in the schematic analysis. Indeed, the estimate in (7.115) shows that the first contribution reflects on the uncertainty principle which probes short distances and thus is not sensitive to the curvature of AdS_5. The second diffusive contribution is sensitive through $D_\perp$ but will turn out to be sub-leading as we will show below. The third contribution is long ranged and senses the curvature of AdS_5. Thus

$$\mathcal{F}_{0\perp} \to M_\perp^2 \left(\frac{1}{R_\perp^2} + \frac{R_\perp^2}{D_\perp(\lambda)\, M_\perp^2} - \frac{g^2 M_\perp}{R_\perp^{D_\perp(\lambda)-1}} \right) \tag{7.118}$$

For very small values of g the first two contributions in (7.118) are dominant and the string transverse size grows diffusively. The minimization of the first two dominant contributions in this regime yields $R_\perp^2 \approx \sqrt{D_\perp(\lambda)}\, M_\perp$, in agreement with (7.93). However, for

$$g^2 M_\perp > M_\perp^{\frac{D_\perp(\lambda)-3}{2}} \tag{7.119}$$

the string size shrinks and the transverse string size follows from balancing the first term with the last term due to the interaction. The balance between the self-interaction and the uncertainty principle, yields a continuously decreasing transverse string size

$$R_\perp \approx \left(\frac{1}{g^2 M_\perp}\right)^{\frac{2\sqrt{\lambda}}{3(D_\perp-1)^2}} \tag{7.120}$$

in units of the string length. A black-hole with a transverse string size emerges for $g^2 M_\perp \approx 1$. In Fig. 7.38 we display the interacting string in the effectively curved space for $\lambda = 40$, $D_\perp = 3$ and $g = 0.6$. In Fig. 7.39 we display the transverse size of the interacting string in the effectively curved space versus $M_\perp$. The dots are from the numerically simulated string, while the line is a fit to the schematic result (7.119) with $R_\perp \approx 209(1/g^2 M_\perp)^{2\sqrt{\lambda}/3(D_\perp-1)^2}$ in a narrow range of $M_\perp$.

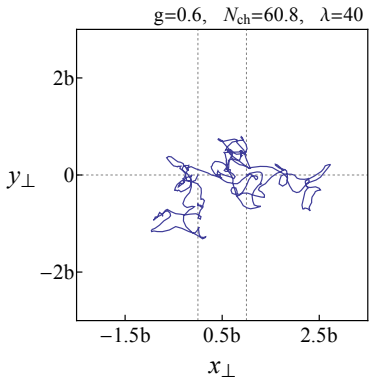

Figure 7.38: A typical string with multiplicity $N_{ch} = 60.8$.

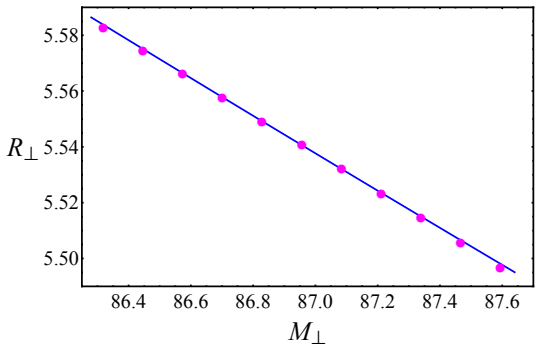

Figure 7.39: Solid line is $R_\perp \sim 209(1/g^2 M_\perp)^{2\sqrt{\lambda}/3(D_\perp-1)^2}$ and the dots are numerical results.

7.2.3 Angular deformations

The fluctuating string with fixed end-points exhibits large azimuthal deformations in the transverse plane that can be characterized by the azimuthal moment [174, 165]

$$\epsilon_n = \frac{\frac{1}{N}\sum_i^N e^{in\phi_i}\left(r_i^\perp\right)^n}{r_\perp^n} \tag{7.121}$$

with $Nr_\perp^n = \sum_i^N \left(r_i^\perp\right)^n$. Here ϕ is the azimuthal angle as measured from the impact parameter line along $\mathbf{b}$. $r_\perp$ is the averaged size of the string in the transverse plane. For $\mathbf{b} = 0$, we have $\langle r_\perp^2 \rangle /2 = R_\perp^2/D_\perp$, where $\langle \cdots \rangle$ is the average over string ensembles. Specifically, define $x \equiv x_\perp^{i=1}$ and $y \equiv x_\perp^{i=2}$ in the transverse plane, where x is parallel to the impact parameter $\mathbf{b}$ and y perpendicular to it,

$$x_\perp(k,\tau) = \sum_{n=1}^{N-1} X_n(\tau)\sin\left(\frac{nk}{N}\pi\right) + b\frac{k}{N} \qquad y_\perp(k,\tau) = \sum_{n=1}^{N-1} Y_n(\tau)\sin\left(\frac{nk}{N}\pi\right) \tag{7.122}$$

where both string bit coordinates X_n, Y_n are normally distributed according to

$$X_n \sim \mathcal{N}\left(0, \frac{1}{\omega_n\left[e^{\frac{\beta}{2}\left(\omega_n+\frac{\Omega_n^2}{\omega_n}\right)}-1\right]}\right) \qquad Y_n \sim \mathcal{N}\left(0, \frac{1}{\omega_n\left[e^{\frac{\beta}{2}\left(\omega_n+\frac{\Omega_n^2}{\omega_n}\right)}-1\right]}\right) \tag{7.123}$$

Since (7.122) are themselves sum of random walks, they are both normally distributed according to

$$x_\perp(k,\tau) \sim \mathcal{N}\left(b\frac{k}{N}, \Sigma_k^2\right) \qquad y_\perp(k,\tau) \sim \mathcal{N}\left(0, \Sigma_k^2\right) \tag{7.124}$$

with the squared variance

$$\Sigma_k^2 = \sum_{n=1}^{N-1} \frac{\sin^2\left(\frac{nk}{N}\pi\right)}{\omega_n\left[e^{\frac{\beta}{2}\left(\omega_n+\frac{\Omega_n^2}{\omega_n}\right)}-1\right]} \tag{7.125}$$

For $N \to \infty$, the squared variance is $\Sigma_{\tilde{k}}^2 \approx R_\perp^2/D_\perp$ and the moments simplify (even n)

$$\langle \epsilon_n \rangle \approx \frac{b^n}{\langle r_T^n \rangle} \int_0^1 d\tilde{k} \left(\frac{1}{2} - \tilde{k}\right)^n = \frac{b^n}{\langle r_T^n \rangle} \frac{1}{2^n(1+n)} \tag{7.126}$$

$$\frac{\langle r_T^2 \rangle}{b^2} \approx \frac{1}{12} + \frac{2}{D_\perp}\frac{R_\perp^2}{b^2} \qquad \frac{\langle r_T^4 \rangle}{b^4} \approx \frac{1}{80} + \frac{2}{3}\frac{R_\perp^2}{b^2 D_\perp} + 8\frac{R_\perp^4}{D_\perp^2 b^4} \tag{7.127}$$

For small b, the lowest moments reduce to

$$\langle \epsilon_2 \rangle \approx \frac{D_\perp}{24}\frac{b^2}{R_\perp^2} \qquad \langle \epsilon_4 \rangle \approx \frac{D_\perp^2}{640}\frac{b^4}{R_\perp^4} \tag{7.128}$$

The numerical results of $\langle \epsilon_2 \rangle$ and $\langle \epsilon_4 \rangle$ with a maximum resolution of $N = 500$ are displayed in Fig. 7.40.

For the cross moments (flow), we can only do $N = 100$ (randomly generated strings). We use $\underline{\beta} \sim (0.2, 0.05)$ such that $\underline{\beta} \leq 0.2$ and $N\underline{\beta} \geq 5$. For a single string exchange, the multiplicity range is $N_{ch} \sim (7, 26)$, while for 5 strings $N_{ch} \sim (35, 130)$ and 10 strings $N_{ch} \sim (70, 260)$. To characterize

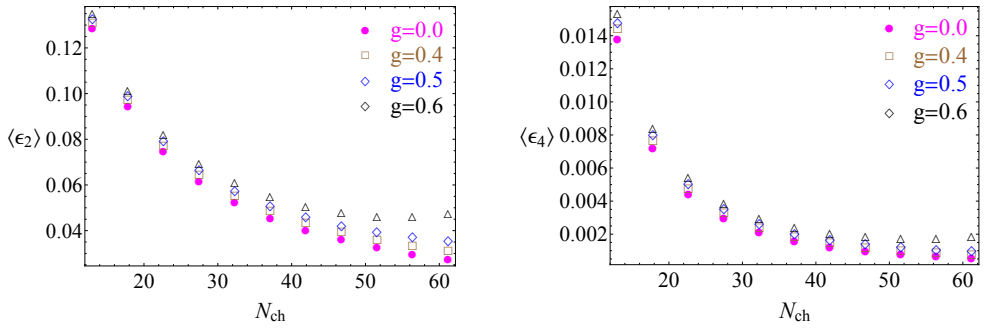

Figure 7.40: The azimuthal moments $\langle \epsilon_{2,4} \rangle$ versus multiplicity for a single string with attractive self-coupling g.

the initial azimuthal deformation of the string bits in the transverse collision plane, we show in Fig. 7.41 the pdf distributions of 1000 randomly generated single strings at a resolution of $N = 100$ and a multiplicity of $N_{ch} = 7$ with no self-interactions $g = 0$. The pdf shown are for the distributions in $\epsilon_{2,3,4}$ respectively.

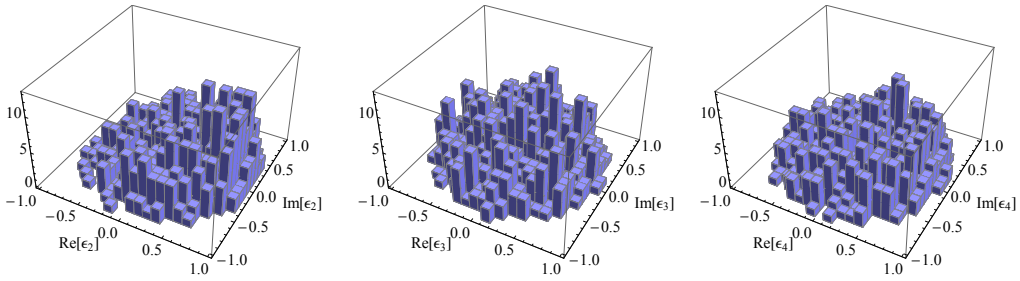

Figure 7.41: 3D Histograms, 1000 random generated strings. N=100 and $N_{ch} = 7$.

We also show in Fig. 7.42 the pdf distributions of 1000 randomly generated single strings at a resolution of $N = 100$ with a multiplicity $N_{ch} = 7$ undergoing string bit attractions with $g = 0.6$ in the mean-field approximation. Note the strong dipole deformation in the leftmost figure.

For completeness we show the behavior of the cross moments with the resolution $N = 100$ for a non-interacting and for an attractive string, in Fig. 7.43 and Fig. 7.44 respectively by sampling 1000 times a single string stretched with $b = 5 = 10 l_s$. The attraction is set at $g = 0.6$.

In a typical pp collision at collider energies, we expect to exchange about

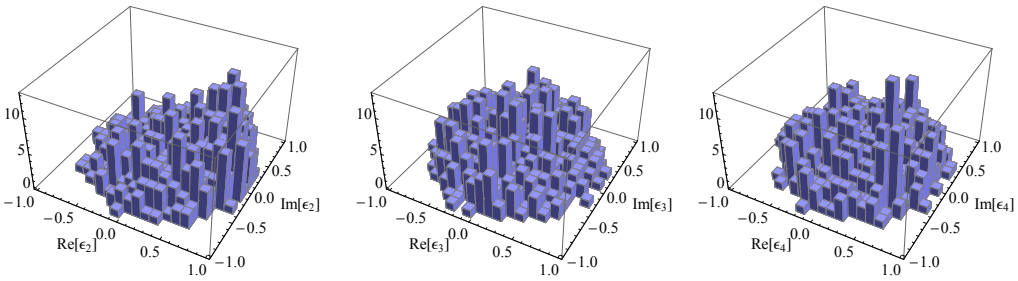

Figure 7.42: 3D Histograms, 1000 random generated strings. N=100 and $N_{ch} = 7$ with attractive interaction $g = 0.3$.

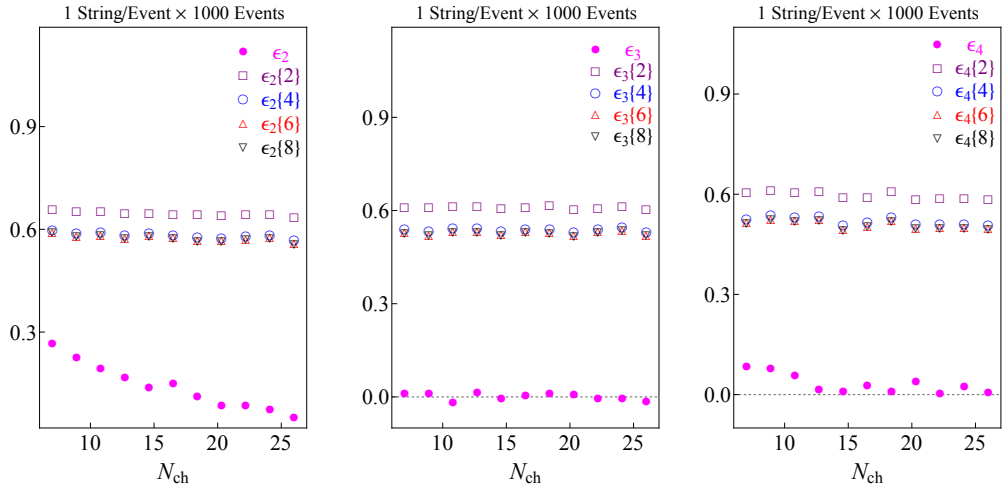

Figure 7.43: Non-interacting.

10 such long strings [71, 72, 73]. In Fig. 7.45 and Fig. 7.46 we show the same cross moments following from the exchange of 5 typical strings stretched at $b = 5$ sampled 200 times for non-interacting and attractive case respectively.

The case where 10 string are exchanged is shown in Fig. 7.47 and Fig. 7.48 for the same arrangements of parameters with each 10 string event sampled 100 times.

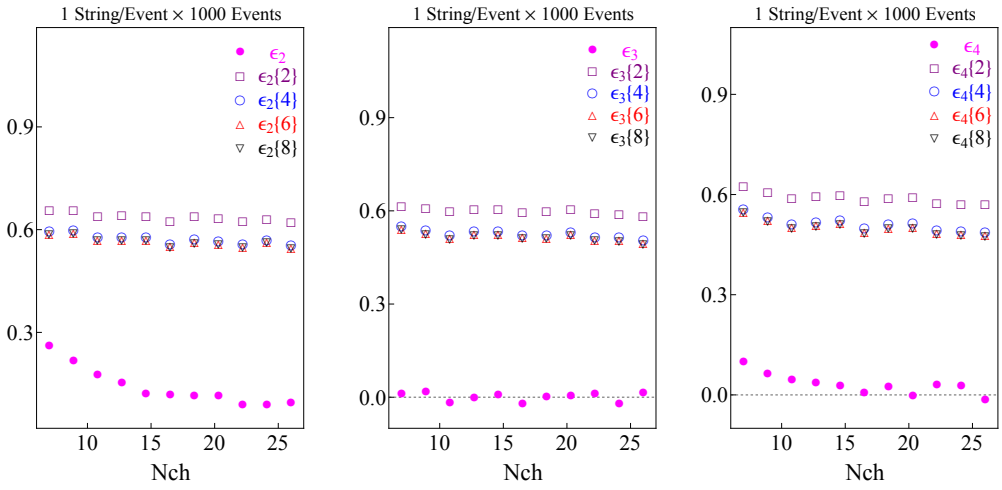

Figure 7.44: Attractive interaction $g = 0.6$.

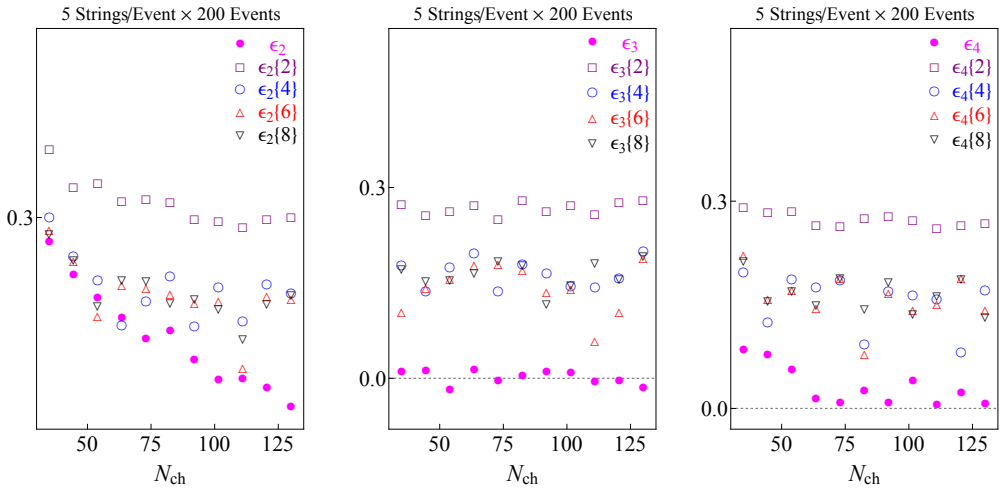

Figure 7.45: Non-interacting.

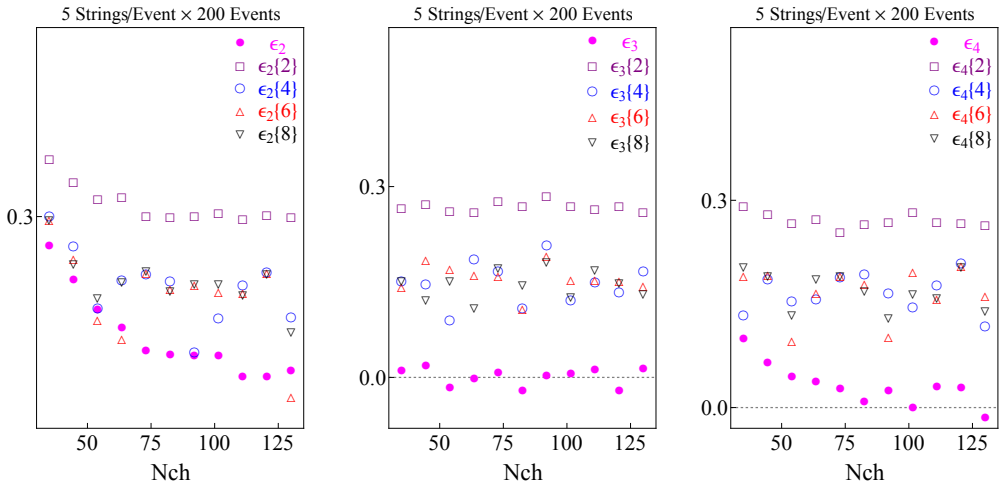

Figure 7.46: Attractive interaction $g = 0.6$.

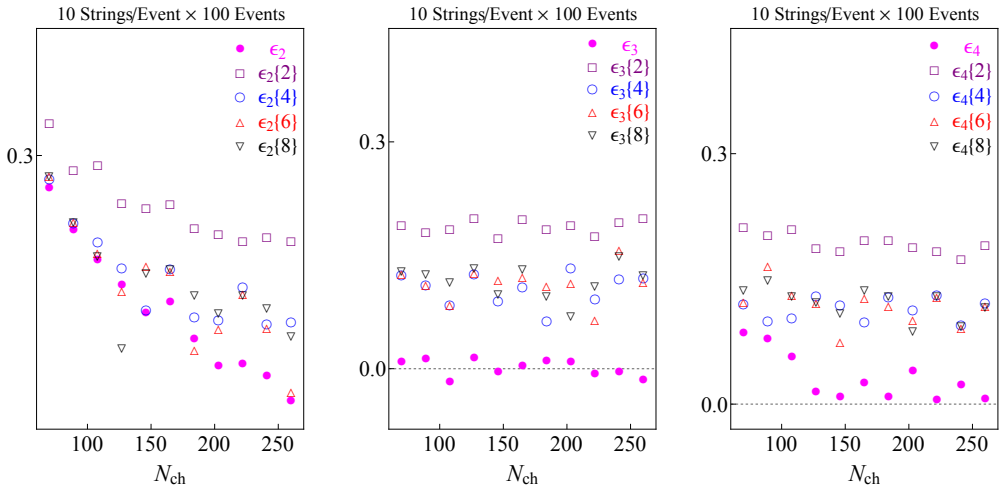

Figure 7.47: Non-interacting.

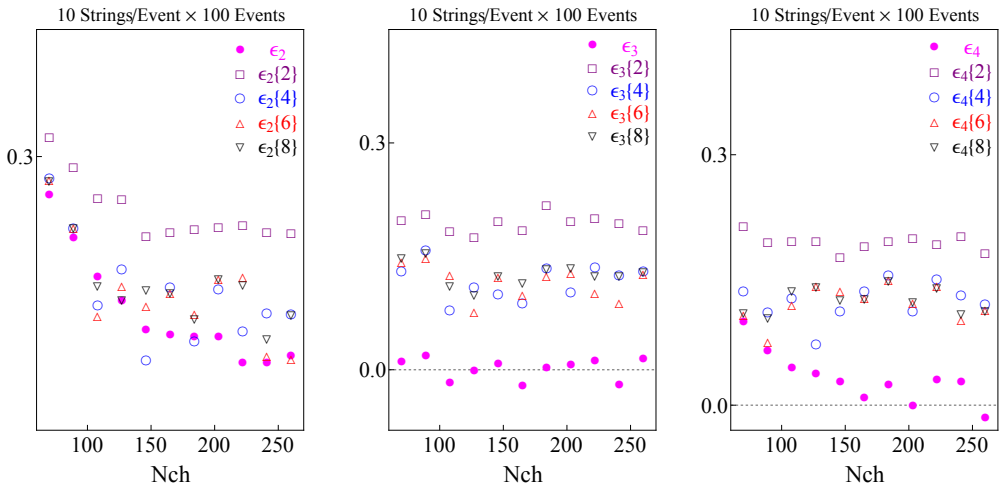

Figure 7.48: Attractive interaction $g = 0.6$.

Chapter 8

Conclusion

8.1 Spin physics through QCD instantons

Instantons and anti-instantons provide the key building blocks of the instanton liquid model. The latter offers a detailed framework for understanding aspects of the spontaneous breaking of chiral symmetry and the resolution of the U(1) problem. Key to this is the appearance of light quark zero modes of fixed chirality and their de-localization through the formation of an interacting liquid. Some aspects of this model are supported by lattice simulations upon cooling [177, 178, 22].

In light of the many phenomenological successes of the instanton liquid model, it is natural to ask about the role of instantons in scattering processes, in particular on spin physics. An essential aspect of the light quark zero modes is the emergence of large constituent masses and (chromo) magnetic moments. Also instantons and anti-instantons correlate strongly the spin with color leading to sizable contributions in spin polarized processes involving light quarks.

We give a brief summary of recent advances in the emerging field of spin physics where the induced effects by instantons and anti-instantons in a semi-classical analysis, are sizable in comparison to those usually parametrized using perturbation theory. We stress that the effects we have reported both in polarized electron-proton or proton-proton semi-inclusive scattering, rely solely on the instanton liquid parameters in the vacuum without additional changes. The effects are large and comparable in size with those reported experimentally. We also show that the large spin effects induced by instan-

tons and anti-instantons in polarized experiments may also be present in peripheral AA collisions where a prompt and large magnetic field can induce a prompt and large polarization although on a short time scale. A simple analysis of the correlated fluctuations between target and projectile protons shows that the effects is of the same magnitude and sign are those reported in the peripheral charged pion azimuthal correlations at collider energies. Again it is important to stress that only the fluctuations expected from instanton vacuum configurations were used. The study of the spin effects induced by instanton is not exhaustive as many new effects can be explored using this framework. One important shortcoming of the instanton liquid model is the lack of confinement as described by an ordering of the eigenvalues of the Polyakov line at low temperature. Some important amendments to the instanton liquid model have been proposed, suggesting that instantons and anti-instantons split into dyons in the confined phase [179]. It was recently shown that the key chiral effects and U(1) effects in the standard instanton liquid model are about similar to those emerging from the new instanton-dyon liquid model [180, 181, 182, 183, 184, 185, 186]. It would be important to revisit the spin effects in this context.

8.2 Stringy pomeron

Holographic strings in walled AdS_5 provide a non-perturbative description of diffractive scattering, production as well as low-x DIS [71]. Although a key aspect of AdS_5 is its conformality which translates to the conformal character of QCD in the UV, the essentials of the walled AdS_5 construction for the holographic string with a large rapidity interval can be captured by a string with an effective transverse dimension $2 < D_\perp < 3$. The holographic Pomeron intercept follows from the zero-point motion or Luscher term of the free transverse string with $D_\perp/12$, and the Pomeron slope is fixed by the string tension.

Long color flux tubes in QCD are smooth. In leading order, the Nambu-Goto effective theory is corrected by a term that depends on the extrinsic curvature to allow for smooth string configurations [160]. The extrinsic curvature affects the zero-point energy of large Wilson loops to one loop [161] and is amenable to lattice simulations. We have shown that a similar contribution affects the scattering amplitude of two dipoles.

In leading order, the extrinsic curvature induces an overall momentum

dependent contribution to the scattering amplitude. Detailed comparison with accurate but differential proton on proton measurements at large $\sqrt{s}$ but fixed $t = -\mathbf{q}_\perp^2$ show sensitivity of the diffractive peak to changes in the extrinsic curvature. pp scattering may provide for an empirical estimate of the extrinsic curvatures of smooth QCD strings, besides the current measurement estimates for the slope (string tension) and intercept (Luscher contribution) of the Pomeron.

Low-x physics in the holographic string set up corresponds to a string with higher zero-point resolution, whereby the string bits play the non-perturbative analogue of the wee partons in perturbative QCD. A key aspect of the partonic description is Gribov transverse diffusion which arises naturally in the quantum string description as emphasized by Susskind and others [84, 85, 110, 111]. A new aspect of our recent study of the holographic string at low-x consists in the role played by the interactions between the string bits in $2 < D_\perp < 3$ and their role in producing a stringy mechanism for saturation [76].

For strings exchanged at smaller impact parameters, the exponential increase in the string excited states dwarf the zero point fluctuations making the string essentially classical. We have used this observation to construct a micro-canonical description of a holographic string by introducing an effective temperature. Close to its Hagedorn temperature, the string carries large entropy and multiplicity and provides a possible and generic mechanism for large multiplicity events in hadronic collisions in the Pomeron kinematics.

In flat $D_\perp = 3$ dimensions the free string close to its Hagedorn temperature carries large multiplicities and exhibits large transverse geometrical deformations mostly due to its transverse and classical diffusion [115]. The large outgrowth of the string bits makes it ideal for a mean-field analysis of the string self-interactions. We have used the variational analysis to put a lower bound on the interacting string free energy and use it to detail its geometrical content. Self-interactions cause the effectively thermal string to contract, a process typical of string-black-hole transmutation in fundamental string theory [75, 163, 87, 88, 89, 81, 84, 85].

The geometry of the string bit distributions emerging from stretched strings for small impact parameters is rich in structure and transverse deformation. We have presented a detailed study of its transverse moments and distributions for single and multiple string exchanges. These prompt and deformed distributions can be used to initialize the prompt parton distributions in current pp and pA collisions for the recently reported high multiplic-

ity events by the LHC [112, 113, 114]. Our azimuthal and cross-moments provide a specific measure of the prompt asymmetries versus multiplicity. The holographic string close to its Hagedorn temperature maybe at the origin of the fire ball mechanism underlying the relevance of a hydrodynamical description in hot but small hadronic volumes [163, 187, 188, 189, 165].

Bibliography

[1] **HERMES** Collaboration, A. Airapetian *et al.*, "Observation of the Naive-T-odd Sivers Effect in Deep-Inelastic Scattering," *Phys. Rev. Lett.* **103** (2009) 152002, arXiv:0906.3918 [hep-ex].

[2] N. Kochelev and N. Korchagin, "Anomalous Quark Chromomagnetic Moment and Single-Spin Asymmetries," arXiv:1308.4857 [hep-ph].

[3] **E704 Collaboration** Collaboration, J. Skeens, "Analyzing power in inclusive pi+, pi-, and Lambda production at high x(F) with 200-GeV polarized protons," *AIP Conf.Proc.* **243** (1992) 1008–1011.

[4] **BRAHMS** Collaboration, I. Arsene *et al.*, "Single Transverse Spin Asymmetries of Identified Charged Hadrons in Polarized p+p Collisions at s**(1/2) = 62.4-GeV," *Phys. Rev. Lett.* **101** (2008) 042001, arXiv:0801.1078 [nucl-ex].

[5] **PHENIX** Collaboration, A. Adare *et al.*, "Measurement of transverse-single-spin asymmetries for midrapidity and forward-rapidity production of hadrons in polarized p+p collisions at $\sqrt{s}$ =200 and 62.4 GeV," *Phys. Rev.* **D90** no. 1, (2014) 012006, arXiv:1312.1995 [hep-ex].

[6] **STAR Collaboration** Collaboration, B. Abelev *et al.*, "Azimuthal Charged-Particle Correlations and Possible Local Strong Parity Violation," *Phys.Rev.Lett.* **103** (2009) 251601, arXiv:0909.1739 [nucl-ex].

[7] **ALICE Collaboration** Collaboration, I. Selyuzhenkov, "ALICE probes of local parity violation with charge dependent azimuthal

correlations in Pb-Pb collisions," *PoS* **WPCF2011** (2011) 044, arXiv:1203.5230 [nucl-ex].

[8] U. Amaldi and K. R. Schubert, "Impact Parameter Interpretation of Proton Proton Scattering from a Critical Review of All ISR Data," *Nucl.Phys.* **B166** (1980) 301.

[9] C.-N. Yang and R. L. Mills, "Conservation of Isotopic Spin and Isotopic Gauge Invariance," *Phys. Rev.* **96** (1954) 191–195.

[10] S. L. Glashow, "Partial Symmetries of Weak Interactions," *Nucl. Phys.* **22** (1961) 579–588.

[11] S. Weinberg, "A Model of Leptons," *Phys. Rev. Lett.* **19** (1967) 1264–1266.

[12] A. Salam, "Weak and Electromagnetic Interactions," *Conf. Proc.* **C680519** (1968) 367–377.

[13] G. 't Hooft, "Computation of the Quantum Effects Due to a Four-Dimensional Pseudoparticle," *Phys.Rev.* **D14** (1976) 3432–3450.

[14] A. A. Belavin, A. M. Polyakov, A. S. Schwartz, and Yu. S. Tyupkin, "Pseudoparticle Solutions of the Yang-Mills Equations," *Phys. Lett.* **B59** (1975) 85–87.

[15] T. T. Wu and C.-N. Yang, "SOME SOLUTIONS OF THE CLASSICAL ISOTOPIC GAUGE FIELD EQUATIONS,".

[16] Y. Qian and J. Nian, "Form Invariance, Topological Fluctuations and Mass Gap of Yang-Mills Theory," arXiv:1605.08425 [hep-th].

[17] T. Schfer and E. V. Shuryak, "Instantons in QCD," *Rev.Mod.Phys.* **70** (1998) 323–426, arXiv:hep-ph/9610451 [hep-ph].

[18] R. Jackiw and C. Rebbi, "Vacuum Periodicity in a Yang-Mills Quantum Theory," *Phys. Rev. Lett.* **37** (1976) 172–175.

[19] C. G. Callan, Jr., R. F. Dashen, and D. J. Gross, "The Structure of the Gauge Theory Vacuum," *Phys. Lett.* **B63** (1976) 334–340.

[20] A. M. Polyakov, "Quark Confinement and Topology of Gauge Groups," *Nucl. Phys.* **B120** (1977) 429–458.

[21] E. V. Shuryak, "Hadrons Containing a Heavy Quark and QCD Sum Rules," *Nucl.Phys.* **B198** (1982) 83.

[22] M. C. Chu, J. M. Grandy, S. Huang, and J. W. Negele, "Evidence for the role of instantons in hadron structure from lattice QCD," *Phys. Rev.* **D49** (1994) 6039–6050, arXiv:hep-lat/9312071 [hep-lat].

[23] E. V. Shuryak and I. Zahed, "Instanton induced effects in QCD high-energy scattering," *Phys. Rev.* **D62** (2000) 085014, arXiv:hep-ph/0005152 [hep-ph].

[24] M. A. Nowak, E. V. Shuryak, and I. Zahed, "Instanton induced inelastic collisions in QCD," *Phys. Rev.* **D64** (2001) 034008, arXiv:hep-ph/0012232 [hep-ph].

[25] E. V. Shuryak and I. Zahed, "Understanding the nonperturbative deep inelastic scattering: Instanton induced inelastic dipole dipole cross-section," *Phys. Rev.* **D69** (2004) 014011, arXiv:hep-ph/0307103 [hep-ph].

[26] D. Kharzeev and E. Levin, "Scale anomaly and 'soft' pomeron in QCD," *Nucl. Phys.* **B578** (2000) 351–363, arXiv:hep-ph/9912216 [hep-ph].

[27] A. Dorokhov and I. Cherednikov, "QCD instantons in high energy diffractive scattering: Instanton model of Pomeron," *Nucl.Phys.Proc.Suppl.* **146** (2005) 140–142, arXiv:hep-ph/0412082 [hep-ph].

[28] A. Ringwald and F. Schrempp, "Zooming in on instantons at HERA," *Phys. Lett.* **B503** (2001) 331–340, arXiv:hep-ph/0012241 [hep-ph].

[29] F. Schrempp and A. Utermann, "QCD instantons and saturation at small x," in *5th Internationa Conference on Strong and Electroweak Matter (SEWM 2002) Heidelberg, Germany, October 2-5, 2002.* 2003. arXiv:hep-ph/0301177 [hep-ph].

[30] M. Giordano and E. Meggiolaro, "Instanton effects on Wilson-loop correlators: a new comparison with numerical results from the lattice," *Phys.Rev.* **D81** (2010) 074022, arXiv:0910.4505 [hep-ph].

[31] M. Giordano and E. Meggiolaro, "Hadron-Hadron Total Cross Sections and Soft High-Energy Scattering on the Lattice," *PoS* **LATTICE2011** (2011) 155, arXiv:1110.5188 [hep-lat].

[32] **HERMES** Collaboration, A. Airapetian *et al.*, "Single-spin asymmetries in semi-inclusive deep-inelastic scattering on a transversely polarized hydrogen target," *Phys. Rev. Lett.* **94** (2005) 012002, arXiv:hep-ex/0408013 [hep-ex].

[33] **CLAS** Collaboration, H. Avakian *et al.*, "Measurement of Single and Double Spin Asymmetries in Deep Inelastic Pion Electroproduction with a Longitudinally Polarized Target," *Phys. Rev. Lett.* **105** (2010) 262002, arXiv:1003.4549 [hep-ex].

[34] **STAR Collaboration** Collaboration, B. Abelev *et al.*, "Forward Neutral Pion Transverse Single Spin Asymmetries in p+p Collisions at s**(1/2) = 200-GeV," *Phys.Rev.Lett.* **101** (2008) 222001, arXiv:0801.2990 [hep-ex].

[35] **PHENIX Collaboration** Collaboration, K. Eyser, "Transverse single-spin asymmetries at mid-rapidity at s**(1/2) = 200-GeV in p + p collisions," *AIP Conf.Proc.* **842** (2006) 404–406.

[36] **FNAL-E704** Collaboration, D. L. Adams *et al.*, "Analyzing power in inclusive pi+ and pi- production at high x(F) with a 200-GeV polarized proton beam," *Phys. Lett.* **B264** (1991) 462–466.

[37] D. W. Sivers, "Single Spin Production Asymmetries from the Hard Scattering of Point-Like Constituents," *Phys. Rev.* **D41** (1990) 83.

[38] D. W. Sivers, "Hard scattering scaling laws for single spin production asymmetries," *Phys. Rev.* **D43** (1991) 261–263.

[39] J. C. Collins, "Fragmentation of transversely polarized quarks probed in transverse momentum distributions," *Nucl. Phys.* **B396** (1993) 161–182, arXiv:hep-ph/9208213 [hep-ph].

[40] J. C. Collins, S. F. Heppelmann, and G. A. Ladinsky, "Measuring transversity densities in singly polarized hadron hadron and lepton - hadron collisions," *Nucl. Phys.* **B420** (1994) 565–582, arXiv:hep-ph/9305309 [hep-ph].

[41] N. Kochelev, "A new mechanism for single spin asymmetries in strong interactions," *JETP Lett.* **72** (2000) 481–485, arXiv:hep-ph/9905497 [hep-ph].

[42] A. E. Dorokhov, N. I. Kochelev, and W. D. Nowak, "Single Spin Asymmetries in High Energy Reactions and Nonperturbative QCD Effects," *Phys. Part. Nucl. Lett.* **6** (2009) 440–445, arXiv:0902.3165 [hep-ph].

[43] D. Ostrovsky and E. Shuryak, "Instanton-induced azimuthal spin asymmetry in deep inelastic scattering," *Phys.Rev.* **D71** (2005) 014037, arXiv:hep-ph/0409253 [hep-ph].

[44] Y. Qian and I. Zahed, "Single Spin Asymmetry through QCD Instantons," *Phys.Rev.* **D86** (2012) 014033, arXiv:1112.4552 [hep-ph].

[45] Y. Qian and I. Zahed, "$\mathcal{P}$-Odd Pion Azimuthal Charge Correlations in Heavy Ion Collisions," *Nucl. Phys.* **A940** (2015) 227–234, arXiv:1205.2366 [hep-ph].

[46] Y. Qian and I. Zahed, "Double Spin Asymmetries through QCD Instantons," arXiv:1404.6270 [hep-ph].

[47] Y. Qian and I. Zahed, "Spin Physics through QCD Instantons," arXiv:1512.08172 [hep-ph].

[48] L. Gribov, E. Levin, and M. Ryskin, "Semihard Processes in QCD," *Phys.Rept.* **100** (1983) 1–150.

[49] E. A. Kuraev, L. N. Lipatov, and V. S. Fadin, "Multi - Reggeon Processes in the Yang-Mills Theory," *Sov.Phys.JETP* **44** (1976) 443–450.

[50] L. N. Lipatov, "Reggeization of the Vector Meson and the Vacuum Singularity in Nonabelian Gauge Theories," *Sov. J. Nucl. Phys.* **23** (1976) 338–345. [Yad. Fiz.23,642(1976)].

[51] G. F. Sterman, "Recent progress in QCD," arXiv:hep-ph/9905548 [hep-ph].

[52] V. S. Fadin, E. Kuraev, and L. Lipatov, "On the Pomeranchuk Singularity in Asymptotically Free Theories," *Phys.Lett.* **B60** (1975) 50–52.

[53] I. Balitsky and L. Lipatov, "The Pomeranchuk Singularity in Quantum Chromodynamics," *Sov.J.Nucl.Phys.* **28** (1978) 822–829.

[54] G. Veneziano, "Construction of a crossing - symmetric, Regge behaved amplitude for linearly rising trajectories," *Nuovo Cim.* **A57** (1968) 190–197.

[55] J. Greensite, "Monte Carlo Meets the Fishnet: String Formation in a Gas of Feynman Diagrams," *Nucl.Phys.* **B249** (1985) 263.

[56] J. M. Maldacena, "Wilson loops in large N field theories," *Phys.Rev.Lett.* **80** (1998) 4859–4862, arXiv:hep-th/9803002 [hep-th].

[57] M. Rho, S.-J. Sin, and I. Zahed, "Elastic parton-parton scattering from AdS / CFT," *Phys.Lett.* **B466** (1999) 199–205, arXiv:hep-th/9907126 [hep-th].

[58] R. Janik and R. B. Peschanski, "Minimal surfaces and Reggeization in the AdS / CFT correspondence," *Nucl.Phys.* **B586** (2000) 163–182, arXiv:hep-th/0003059 [hep-th].

[59] R. A. Janik, "String fluctuations, AdS / CFT and the soft pomeron intercept," *Phys.Lett.* **B500** (2001) 118–124, arXiv:hep-th/0010069 [hep-th].

[60] J. Polchinski and M. J. Strassler, "Hard scattering and gauge / string duality," *Phys.Rev.Lett.* **88** (2002) 031601, arXiv:hep-th/0109174 [hep-th].

[61] J. Polchinski and M. J. Strassler, "Deep inelastic scattering and gauge / string duality," *JHEP* **0305** (2003) 012, arXiv:hep-th/0209211 [hep-th].

[62] R. C. Brower, J. Polchinski, M. J. Strassler, and C.-I. Tan, "The Pomeron and gauge/string duality," *JHEP* **0712** (2007) 005, arXiv:hep-th/0603115 [hep-th].

[63] R. C. Brower, M. J. Strassler, and C.-I. Tan, "On The Pomeron at Large 't Hooft Coupling," *JHEP* **0903** (2009) 092, arXiv:0710.4378 [hep-th].

[64] R. C. Brower, M. Djuric, I. Sarcevic, and C.-I. Tan, "String-Gauge Dual Description of Deep Inelastic Scattering at Small-x," *JHEP* **1011** (2010) 051, arXiv:1007.2259 [hep-ph].

[65] R. C. Brower, M. Djuric, I. Sarcevic, and C.-I. Tan, "The AdS Graviton/Pomeron Description of Deep Inelastic Scattering at Small x," arXiv:1106.5681 [hep-ph].

[66] Y. Hatta, E. Iancu, and A. Mueller, "Deep inelastic scattering off a N=4 SYM plasma at strong coupling," *JHEP* **0801** (2008) 063, arXiv:0710.5297 [hep-th].

[67] Y. Hatta, E. Iancu, and A. Mueller, "Deep inelastic scattering at strong coupling from gauge/string duality: The Saturation line," *JHEP* **0801** (2008) 026, arXiv:0710.2148 [hep-th].

[68] J. L. Albacete, Y. V. Kovchegov, and A. Taliotis, "DIS on a Large Nucleus in AdS/CFT," *JHEP* **0807** (2008) 074, arXiv:0806.1484 [hep-th].

[69] J. L. Albacete, Y. V. Kovchegov, and A. Taliotis, "DIS in Ads," *AIP Conf.Proc.* **1105** (2009) 356–360, arXiv:0811.0818 [hep-th].

[70] G. Basar, D. E. Kharzeev, H.-U. Yee, and I. Zahed, "Holographic Pomeron and the Schwinger Mechanism," *Phys.Rev.* **D85** (2012) 105005, arXiv:1202.0831 [hep-th].

[71] A. Stoffers and I. Zahed, "Holographic Pomeron: Saturation and DIS," *Phys.Rev.* **D87** (2013) 075023, arXiv:1205.3223 [hep-ph].

[72] A. Stoffers and I. Zahed, "Diffractive and deeply virtual Compton scattering in holographic QCD," arXiv:1210.3724 [nucl-th].

[73] A. Stoffers and I. Zahed, "Diffractive proton-proton scattering in holographic QCD," *Acta Phys.Polon.Supp.* **6** (2013) 7–12.

[74] Y. Qian and I. Zahed, "Holographic Pomeron and Primordial Viscosity," `arXiv:1211.6421 [hep-ph]`.

[75] E. Shuryak and I. Zahed, "New Regimes of Stringy (Holographic) Pomeron and High Multiplicity pp and pA Collisions," *Phys.Rev.* **D89** (2014) 094001, `arXiv:1311.0836 [hep-ph]`.

[76] Y. Qian and I. Zahed, "Stretched String with Self-Interaction at High Resolution: Spatial Sizes and Saturation," *Phys. Rev.* **D91** no. 12, (2015) 125032, `arXiv:1411.3653 [hep-ph]`.

[77] L. Cornalba, M. S. Costa, and J. Penedones, "AdS black disk model for small-x DIS," *Phys.Rev.Lett.* **105** (2010) 072003, `arXiv:1001.1157 [hep-ph]`.

[78] L. Cornalba, M. S. Costa, and J. Penedones, "Deep Inelastic Scattering in Conformal QCD," *JHEP* **1003** (2010) 133, `arXiv:0911.0043 [hep-th]`.

[79] L. Cornalba and M. S. Costa, "Saturation in Deep Inelastic Scattering from AdS/CFT," *Phys.Rev.* **D78** (2008) 096010, `arXiv:0804.1562 [hep-ph]`.

[80] Y. Qian and I. Zahed, "A Stringy (Holographic) Pomeron with Extrinsic Curvature," `arXiv:1410.1092 [nucl-th]`.

[81] J. Polchinski and L. Susskind, "String theory and the size of hadrons," `arXiv:hep-th/0112204 [hep-th]`.

[82] O. Bergman and C. B. Thorn, "The Size of a polymer of string bits: A Numerical investigation," *Nucl.Phys.* **B502** (1997) 309–324, `arXiv:hep-th/9702068 [hep-th]`.

[83] M. Karliner, I. R. Klebanov, and L. Susskind, "Size and Shape of Strings," *Int.J.Mod.Phys.* **A3** (1988) 1981.

[84] L. Susskind and P. Griffin, "Partons and black holes," `arXiv:hep-ph/9410306 [hep-ph]`.

[85] L. Susskind, "The World as a hologram," *J.Math.Phys.* **36** (1995) 6377–6396, arXiv:hep-th/9409089 [hep-th].

[86] M. Froissart, "Asymptotic behavior and subtractions in the Mandelstam representation," *Phys.Rev.* **123** (1961) 1053–1057.

[87] J. D. Bekenstein, "Black holes and entropy," *Phys.Rev.* **D7** (1973) 2333–2346.

[88] J. Bekenstein, "Black holes and the second law," *Lett.Nuovo Cim.* **4** (1972) 737–740.

[89] J. D. Bekenstein, "Generalized second law of thermodynamics in black hole physics," *Phys.Rev.* **D9** (1974) 3292–3300.

[90] S. Hawking, "Black hole explosions," *Nature* **248** (1974) 30–31.

[91] S. Hawking, "Particle Creation by Black Holes," *Commun.Math.Phys.* **43** (1975) 199–220.

[92] L. D. McLerran, "The Color glass condensate and small x physics: Four lectures," *Lect.Notes Phys.* **583** (2002) 291–334, arXiv:hep-ph/0104285 [hep-ph].

[93] **ALICE** Collaboration, J. Tapia Takaki, "The colour glass condensate framework in p + p and Pb + p interactions at the ALICE experiment," *J.Phys.* **G37** (2010) 094050.

[94] E. Iancu and R. Venugopalan, "The Color glass condensate and high-energy scattering in QCD," arXiv:hep-ph/0303204 [hep-ph].

[95] E. Iancu, A. Leonidov, and L. McLerran, "The Color glass condensate: An Introduction," arXiv:hep-ph/0202270 [hep-ph].

[96] H. Navelet and R. B. Peschanski, "Conformal invariant saturation," *Nucl.Phys.* **B634** (2002) 291–308, arXiv:hep-ph/0201285 [hep-ph].

[97] E. Iancu, "Gluon saturation at small x," arXiv:hep-ph/0111400 [hep-ph].

[98] E. Levin, "Saturation at low x," arXiv:hep-ph/0105205 [hep-ph].

[99] L. D. McLerran and R. Venugopalan, "Gluon distribution functions for very large nuclei at small transverse momentum," *Phys.Rev.* **D49** (1994) 3352–3355, arXiv:hep-ph/9311205 [hep-ph].

[100] F. Gelis, E. Iancu, J. Jalilian-Marian, and R. Venugopalan, "The Color Glass Condensate," *Ann.Rev.Nucl.Part.Sci.* **60** (2010) 463–489, arXiv:1002.0333 [hep-ph].

[101] C. Marquet, A. Mueller, A. Shoshi, and S. Wong, "On the projectile-target duality of the color glass condensate in the dipole picture," *Nucl.Phys.* **A762** (2005) 252–271, arXiv:hep-ph/0505229 [hep-ph].

[102] E. Iancu and A. Mueller, "From color glass to color dipoles in high-energy onium onium scattering," *Nucl.Phys.* **A730** (2004) 460–493, arXiv:hep-ph/0308315 [hep-ph].

[103] E. Iancu, "Color Glass Condensate and its relation to HERA physics," *Nucl.Phys.Proc.Suppl.* **191** (2009) 281–294, arXiv:0901.0986 [hep-ph].

[104] F. Gelis, "Color Glass Condensate and Glasma," *Int.J.Mod.Phys.* **A28** (2013) 1330001, arXiv:1211.3327 [hep-ph].

[105] P. Tribedy and R. Venugopalan, "QCD saturation at the LHC: comparisons of models to p+p and A+A data and predictions for p+Pb collisions," *Phys.Lett.* **B710** (2012) 125–133, arXiv:1112.2445 [hep-ph].

[106] P. Tribedy and R. Venugopalan, "Inclusive hadron distributions in p+p collisions from saturation models of HERA DIS data," arXiv:1101.5922 [hep-ph].

[107] P. Tribedy and R. Venugopalan, "Saturation models of HERA DIS data and inclusive hadron distributions in p+p collisions at the LHC," *Nucl.Phys.* **A850** (2011) 136–156, arXiv:1011.1895 [hep-ph].

[108] S. Fubini, D. Gordon, and G. Veneziano, "A general treatment of factorization in dual resonance models," *Phys. Lett.* **B29** (1969) 679–682.

[109] S. Fubini and G. Veneziano, "Level structure of dual-resonance models," *Nuovo Cim.* **A64** (1969) 811–840.

[110] T. Damour and G. Veneziano, "Selfgravitating fundamental strings and black holes," *Nucl.Phys.* **B568** (2000) 93–119, arXiv:hep-th/9907030 [hep-th].

[111] G. T. Horowitz and J. Polchinski, "A Correspondence principle for black holes and strings," *Phys.Rev.* **D55** (1997) 6189–6197, arXiv:hep-th/9612146 [hep-th].

[112] **CMS** Collaboration, S. Chatrchyan *et al.*, "Observation of long-range near-side angular correlations in proton-lead collisions at the LHC," *Phys. Lett.* **B718** (2013) 795–814, arXiv:1210.5482 [nucl-ex].

[113] **ALICE Collaboration** Collaboration, B. Abelev *et al.*, "Long-range angular correlations on the near and away side in p-Pb collisions at $\sqrt{s_{NN}} = 5.02$ TeV," *Phys.Lett.* **B719** (2013) 29–41, arXiv:1212.2001 [nucl-ex].

[114] **ATLAS Collaboration** Collaboration, G. Aad *et al.*, "Observation of Associated Near-side and Away-side Long-range Correlations in $\sqrt{s_{NN}}$=5.02 TeV Proton-lead Collisions with the ATLAS Detector," *Phys.Rev.Lett.* **110** (2013) 182302, arXiv:1212.5198 [hep-ex].

[115] Y. Qian and I. Zahed, "Stretched string with self-interaction at the Hagedorn point: Spatial sizes and black holes," *Phys. Rev.* **D92** no. 10, (2015) 105001, arXiv:1508.03760 [hep-ph].

[116] S. Vandoren and P. van Nieuwenhuizen, "Lectures on instantons," arXiv:0802.1862 [hep-th].

[117] I. Zahed and G. E. Brown, "The Skyrme Model," *Phys. Rept.* **142** (1986) 1–102.

[118] M. Nowak, M. Rho, and I. Zahed, *Chiral Nuclear Dynamics*. No. v. 1. World Scientific, 1996. https://books.google.com/books?id=zhd2QgAACAAJ.

[119] L. S. Brown, R. D. Carlitz, D. B. Creamer, and C.-k. Lee, "Propagation Functions in Pseudoparticle Fields," *Phys. Rev.* **D17** (1978) 1583.

[120] N. Andrei and D. J. Gross, "The Effect of Instantons on the Short Distance Structure of Hadronic Currents," *Phys. Rev.* **D18** (1978) 468.

[121] S. Moch, A. Ringwald, and F. Schrempp, "Instantons in deep inelastic scattering: The Simplest process," *Nucl.Phys.* **B507** (1997) 134–156, arXiv:hep-ph/9609445 [hep-ph].

[122] P. Faccioli and E. V. Shuryak, "Systematic study of the single instanton approximation in QCD," *Phys. Rev.* **D64** (2001) 114020, arXiv:hep-ph/0106019 [hep-ph].

[123] E. V. Shuryak and I. Zahed, "Towards a theory of binary bound states in the quark gluon plasma," *Phys. Rev.* **D70** (2004) 054507, arXiv:hep-ph/0403127 [hep-ph].

[124] N. Kochelev, "The Pauli form-factor of the quark induced by instantons," *Phys.Lett.* **B565** (2003) 131–136, arXiv:hep-ph/0304171 [hep-ph].

[125] **HERMES** Collaboration, A. Airapetian *et al.*, "Measurement of the proton spin structure function g1(p) with a pure hydrogen target," *Phys. Lett.* **B442** (1998) 484–492, arXiv:hep-ex/9807015 [hep-ex].

[126] A. Vainshtein, V. I. Zakharov, V. Novikov, and M. A. Shifman, "ABC's of Instantons," *Sov.Phys.Usp.* **25** (1982) 195.

[127] N. Kochelev, "Anomalous quark chromomagnetic moment induced by instantons," *Phys.Lett.* **B426** (1998) 149–153, arXiv:hep-ph/9610551 [hep-ph].

[128] B. Potter, "Calculational Techniques in Perturbative QCD: The Drell-Yan Process,".

[129] M. Hirai, S. Kumano, and N. Saito, "Determination of polarized parton distribution functions with recent data on polarization asymmetries," *Phys.Rev.* **D74** (2006) 014015, arXiv:hep-ph/0603213 [hep-ph].

[130] **Fermilab E704 Collaboration** Collaboration, D. Adams *et al.*, "Measurement of single spin asymmetry in eta meson production in p

(polarized) p and anti-p (polarized) p interactions in the beam fragmentation region at 200-GeV/c," *Nucl.Phys.* **B510** (1998) 3–11.

[131] M. Hutter, "Gluon mass from instantons," `arXiv:hep-ph/9501335 [hep-ph]`.

[132] **Particle Data Group** Collaboration, J. Beringer *et al.*, "Review of Particle Physics (RPP)," *Phys. Rev.* **D86** (2012) 010001.

[133] V. Skokov, A. Y. Illarionov, and V. Toneev, "Estimate of the magnetic field strength in heavy-ion collisions," *Int.J.Mod.Phys.* **A24** (2009) 5925–5932, `arXiv:0907.1396 [nucl-th]`.

[134] D. Kharzeev, R. Pisarski, and M. H. Tytgat, "Possibility of spontaneous parity violation in hot QCD," *Phys.Rev.Lett.* **81** (1998) 512–515, `arXiv:hep-ph/9804221 [hep-ph]`.

[135] D. Kharzeev, "Parity violation in hot QCD: Why it can happen, and how to look for it," *Phys.Lett.* **B633** (2006) 260–264, `arXiv:hep-ph/0406125 [hep-ph]`.

[136] D. E. Kharzeev, L. D. McLerran, and H. J. Warringa, "The Effects of topological charge change in heavy ion collisions: 'Event by event P and CP violation'," *Nucl.Phys.* **A803** (2008) 227–253, `arXiv:0711.0950 [hep-ph]`.

[137] K. Fukushima, D. E. Kharzeev, and H. J. Warringa, "The Chiral Magnetic Effect," *Phys.Rev.* **D78** (2008) 074033, `arXiv:0808.3382 [hep-ph]`.

[138] G. Basar, G. V. Dunne, and D. E. Kharzeev, "Electric dipole moment induced by a QCD instanton in an external magnetic field," *Phys.Rev.* **D85** (2012) 045026, `arXiv:1112.0532 [hep-th]`.

[139] **STAR Collaboration** Collaboration, B. Abelev *et al.*, "Observation of charge-dependent azimuthal correlations and possible local strong parity violation in heavy ion collisions," *Phys.Rev.* **C81** (2010) 054908, `arXiv:0909.1717 [nucl-ex]`.

[140] P. Christakoglou, "Charge dependent azimuthal correlations in Pb–Pb collisions at $\sqrt{s_{NN}} = 2.76$ TeV," *J.Phys.* **G38** (2011) 124165, `arXiv:1106.2826 [nucl-ex]`.

[141] D. Diakonov and V. Y. Petrov, "Instanton Based Vacuum from Feynman Variational Principle," *Nucl.Phys.* **B245** (1984) 259.

[142] R. A. Janik, M. A. Nowak, G. Papp, and I. Zahed, "U(1) problem at finite temperature," *AIP Conf.Proc.* **494** (1999) 408–422, arXiv:hep-lat/9911024 [hep-lat].

[143] P. K. Khandai, P. Shukla, and V. Singh, "Meson spectra and m_T scaling in $p+p$, d+Au, and Au + Au collisions at $\sqrt{s_{NN}} = 200$ GeV," *Phys. Rev.* **C84** (2011) 054904, arXiv:1110.3929 [hep-ph].

[144] C. Aguiar, T. Kodama, R. Andrade, F. Grassi, Y. Hama, *et al.*, "Comparison between classification using impact parameter and using number of participants in relativistic nuclear collisions," *Braz.J.Phys.* **34** (2004) 319–321.

[145] S. A. Voloshin, "Parity violation in hot QCD: How to detect it," *Phys.Rev.* **C70** (2004) 057901, arXiv:hep-ph/0406311 [hep-ph].

[146] O. Nachtmann, "Considerations concerning diffraction scattering in quantum chromodynamics," *Annals Phys.* **209** (1991) 436–478.

[147] O. Nachtmann, "High-energy collisions and nonperturbative QCD," arXiv:hep-ph/9609365 [hep-ph].

[148] G. P. Korchemsky, "On Near forward high-energy scattering in QCD," *Phys.Lett.* **B325** (1994) 459–466, arXiv:hep-ph/9311294 [hep-ph].

[149] A. Shoshi, F. Steffen, and H. Pirner, "S matrix unitarity, impact parameter profiles, gluon saturation and high-energy scattering," *Nucl.Phys.* **A709** (2002) 131–183, arXiv:hep-ph/0202012 [hep-ph].

[150] A. Kramer and H. G. Dosch, "High-energy scattering and vacuum properties," *Phys.Lett.* **B252** (1990) 669–675.

[151] H. G. Dosch, E. Ferreira, and A. Kramer, "Nonperturbative QCD treatment of high-energy hadron hadron scattering," *Phys.Rev.* **D50** (1994) 1992–2015, arXiv:hep-ph/9405237 [hep-ph].

[152] E. Meggiolaro, "The High-energy quark quark scattering: From Minkowskian to Euclidean theory," *Z. Phys.* **C76** (1997) 523–535, arXiv:hep-th/9602104 [hep-th].

[153] E. Meggiolaro, "The Analytic continuation of the high-energy quark quark scattering amplitude," *Eur. Phys. J.* **C4** (1998) 101–106, arXiv:hep-th/9702186 [hep-th].

[154] S. J. Brodsky, "Hadron Spectroscopy and Structure from AdS/CFT," *Eur. Phys. J.* **A31** (2007) 638–644, arXiv:hep-ph/0610115 [hep-ph].

[155] T. Apostol, *Modular Functions and Dirichlet Series in Number Theory*. Graduate Texts in Mathematics. Springer Verlag, 2012. http://books.google.com/books?id=byrEkgEACAAJ.

[156] C. Bachas and M. Porrati, "Pair creation of open strings in an electric field," *Phys.Lett.* **B296** (1992) 77–84, arXiv:hep-th/9209032 [hep-th].

[157] A. Abouelsaood, C. G. Callan, Jr., C. R. Nappi, and S. A. Yost, "Open Strings in Background Gauge Fields," *Nucl. Phys.* **B280** (1987) 599–624.

[158] S. J. Brodsky, G. F. de Tramond, and H. G. Dosch, "Conformal Symmetry, Confinement, and Light-Front Holographic QCD," *Nuovo Cim.* **C036** (2013) 265–273, arXiv:1302.5399 [hep-ph].

[159] J. Kuti, "Lattice QCD and string theory," *PoS* **LAT2005** (2006) 001, arXiv:hep-lat/0511023 [hep-lat].

[160] A. M. Polyakov, "Fine Structure of Strings," *Nucl.Phys.* **B268** (1986) 406–412.

[161] Y. Hidaka and R. D. Pisarski, "Zero Point Energy of Renormalized Wilson Loops," *Phys.Rev.* **D80** (2009) 074504, arXiv:0907.4609 [hep-ph].

[162] U. Amaldi, R. Biancastelli, C. Bosio, G. Matthiae, J. Allaby, *et al.*, "Measurements of small angle proton proton elastic scattering at the cern intersecting storage rings," *Phys.Lett.* **B36** (1971) 504–508.

[163] E. Shuryak and I. Zahed, "High-multiplicity pp and pA collisions: Hydrodynamics at its edge," *Phys.Rev.* **C88** no. 4, (2013) 044915, arXiv:1301.4470 [hep-ph].

[164] O. Aharony and Z. Komargodski, "The Effective Theory of Long Strings," *JHEP* **05** (2013) 118, arXiv:1302.6257 [hep-th].

[165] T. Kalaydzhyan and E. Shuryak, "Self-interacting QCD strings and string balls," *Phys.Rev.* **D90** (2014) 025031, arXiv:1402.7363 [hep-ph].

[166] Y. Liu and I. Zahed, "Probing Wilson Loops in the QCD Instanton Vacuum," arXiv:1408.3331 [hep-ph].

[167] Y. Liu and I. Zahed, "Probing Wilson Loops in AdS/QCD," arXiv:1407.0384 [hep-ph].

[168] A. Donnachie and P. Landshoff, "Total cross-sections," *Phys.Lett.* **B296** (1992) 227–232, arXiv:hep-ph/9209205 [hep-ph].

[169] K. J. Golec-Biernat and M. Wusthoff, "Saturation effects in deep inelastic scattering at low Q**2 and its implications on diffraction," *Phys.Rev.* **D59** (1998) 014017, arXiv:hep-ph/9807513 [hep-ph].

[170] K. J. Golec-Biernat and M. Wusthoff, "Saturation in diffractive deep inelastic scattering," *Phys.Rev.* **D60** (1999) 114023, arXiv:hep-ph/9903358 [hep-ph].

[171] A. H. Rezaeian, M. Siddikov, M. Van de Klundert, and R. Venugopalan, "Analysis of combined HERA data in the Impact-Parameter dependent Saturation model," *Phys.Rev.* **D87** no. 3, (2013) 034002, arXiv:1212.2974.

[172] H. Kowalski and D. Teaney, "An Impact parameter dipole saturation model," *Phys.Rev.* **D68** (2003) 114005, arXiv:hep-ph/0304189 [hep-ph].

[173] V. N. Gribov, *The Theory of Complex Angular Momenta*. Cambridge University Press, 2003. http://dx.doi.org/10.1017/CBO9780511534959. Cambridge Books Online.

[174] A. Bzdak, P. Bozek, and L. McLerran, "Fluctuation induced equality of multi-particle eccentricities for four or more particles," *Nucl.Phys.* **A927** (2014) 15–23, arXiv:1311.7325 [hep-ph].

[175] A. Stoffers and I. Zahed, "Holographic Pomeron and Entropy," *Phys.Rev.* **D88** no. 2, (2013) 025038, arXiv:1211.3077 [nucl-th].

[176] R. P. Feynman, "Slow Electrons in a Polar Crystal," *Phys. Rev.* **97** (1955) 660–665.

[177] M. C. Chu, J. M. Grandy, S. Huang, and J. W. Negele, "Lattice calculation of point-to-point hadron current correlation functions in the QCD vacuum," *Phys. Rev. Lett.* **70** (1993) 255–258, arXiv:hep-lat/9211019 [hep-lat].

[178] M. C. Chu, J. M. Grandy, S. Huang, and J. W. Negele, "Correlation functions of hadron currents in the QCD vacuum calculated in lattice QCD," *Phys. Rev.* **D48** (1993) 3340–3353, arXiv:hep-lat/9306002 [hep-lat].

[179] D. Diakonov and V. Petrov, "Confining ensemble of dyons," *Phys. Rev.* **D76** (2007) 056001, arXiv:0704.3181 [hep-th].

[180] E. Shuryak and T. Sulejmanpasic, "The Chiral Symmetry Breaking/Restoration in Dyonic Vacuum," *Phys. Rev.* **D86** (2012) 036001, arXiv:1201.5624 [hep-ph].

[181] E. Shuryak, "On Chiral Symmetry Breaking, Topology and Confinement," *Nucl. Phys.* **A928** (2014) 138–143, arXiv:1401.2032 [nucl-th].

[182] R. Larsen and E. Shuryak, "Classical interactions of the instanton-dyons with antidyons," arXiv:1408.6563 [hep-ph].

[183] R. Larsen and E. Shuryak, "Interacting ensemble of the instanton-dyons and the deconfinement phase transition in the SU(2) gauge theory," *Phys. Rev.* **D92** no. 9, (2015) 094022, arXiv:1504.03341 [hep-ph].

[184] R. Larsen and E. Shuryak, "Instanton-dyon Ensemble with two Dynamical Quarks: the Chiral Symmetry Breaking," arXiv:1511.02237 [hep-ph].

[185] Y. Liu, E. Shuryak, and I. Zahed, "Confining dyon-antidyon Coulomb liquid model. I.," *Phys. Rev.* **D92** no. 8, (2015) 085006, arXiv:1503.03058 [hep-ph].

[186] Y. Liu, E. Shuryak, and I. Zahed, "Light quarks in the screened dyon-antidyon Coulomb liquid model. II.," *Phys. Rev.* **D92** no. 8, (2015) 085007, arXiv:1503.09148 [hep-ph].

[187] P. Bozek and W. Broniowski, "Collective dynamics in high-energy proton-nucleus collisions," *Phys.Rev.* **C88** no. 1, (2013) 014903, arXiv:1304.3044 [nucl-th].

[188] R. D. de Souza, T. Koide, and T. Kodama, "Hydrodynamic Approaches in Relativistic Heavy Ion Reactions," arXiv:1506.03863 [nucl-th].

[189] T. Kalaydzhyan and E. Shuryak, "Collective interaction of QCD strings and early stages of high multiplicity pA collisions," *Phys. Rev.* **C90** no. 1, (2014) 014901, arXiv:1404.1888 [hep-ph].